# DESIGN OF TWO-DIMENSIONAL DIGITAL FILTERS HAVING MONOTONIC AMPLITUDE-FREQUENCY RESPONSES USING DARLINGTON-TYPE GYRATOR NETWORKS

Muhammad Tariqus Salam

A thesis

in

The Department

of

Electrical and Computer Engineering

Presented in Partial Fulfillment of the Requirements
For the Degree of Master of Applied Science (Electrical and Computer Engineering)
Concordia University
Montréal, Québec, Canada

September 2007

*Your file Votre référence*
*ISBN: 978-0-494-34772-0*
*Our file Notre référence*
*ISBN: 978-0-494-34772-0*

# Abstract

## Design of Two-Dimensional Digital Filters Having Monotonic Amplitude-Frequency Responses Using Darlington-type Gyrator Networks

Muhammad Tariqus Salam

A design of two-dimensional (2D) digital filter with monotonic amplitude-frequency responses using Darlington-type gyrator networks by the application of Generalized Bilinear Transformation is discussed. The proposed design provides the stable monotonic amplitude-frequency responses and the desired cutoff frequency of the 2D digital filters. This 2D recursive digital filter design includes 2D digital low-pass, high-pass, band-pass and band-elimination filters.

The proposed design shows that the impedances of doubly terminated RLC networks are integrated into the Darlington-type gyrator networks and the coefficients of the resultant 2D analog transfer functions are function of gyrator constant ($g$). The behavior of the filter is changed not only for the values of resistance, capacitance and inductance of the filter, but also for the value and sign of $g$. The proposed design uses the Generalized Bilinear Transformation to obtain the digital filter and it provides six parameters to regulate in order to design the desired digital filters. The several constraints are obtained for the monotonic amplitude-frequency responses of the filters. The ranges of $g$ of the each type filter are defined for attaining the monotonic characteristics of the digital filter, because the $g$ has control on the frequency response of the filter.

A digital filter transformation method is proposed and the digital filters are transformed by regulating the value or sign of $g$. A new realization of 2D digital polynomial is given, which is suitable to implement any 2D polynomial with finite order. The performances of the designed 2D digital filters in the image processing applications are discussed and significant improvements in the reconstructed images are obtained by the filters.

# Acknowledgments

First of all, I would like to express my deepest sense of gratitude to my supervisor Venkat Ramachandran for his supervision, advice, and guidance from the very early stage of this research as well as giving me extraordinary experiences through out the work. Above all and the most needed, he provided me unflinching encouragement and support in various ways. His truly scientist intuition has made him as a constant oasis of ideas and passions in science, which exceptionally inspire and enrich my growth as a student and a researcher.

I would like to express my thanks to the various professors from whom I took courses during my Master's program. I would like to thank the members of the examining committe M. Zahangir Kabir, Rabin Raut and A. K. Waizuddin Ahmed for their suggestions to improve the quality of the presentation of the thesis.

I would also like to express my sincere thanks to M. I. H. Bhuiyan and S. A. Fattah for their invaluable experience and advice. I am thankful to my colleagues and my friends (IUT and SCC) for their collaboration and valuable assistance in the research.

Finally, I wish to thank my parents and brother for their continuous support and encouragement.

# Contents

# List of Figures

# List of Tables

# List of Important Symbols and Abbreviations

| | |
|---|---|
| $s$ | Laplace domain parameter in one dimension |
| $z$ | z domain parameter in one dimension |
| $2D$ | Two dimension |
| $z_1$, $z_2$ | z domain parameter in first and second dimensions |
| $s_1$, $s_2$ | Laplace domain parameter in first and second dimensions |
| $H_a$ | Transfer function of a filter in analog domain |
| $H_d$ | Transfer function of a filter in digital domain |
| $M, N$ | Order of a filter in analog domain |
| $M_d, N_d$ | Order of a filter in digital domain |
| $Z_1, Z_2, Z_3$ | Impedances of the gyrator networks |
| $g$ | Gyrator constant of the gyrator networks |
| $H_1$ | Transfer function of the gyrator filter1 in analog domain |
| $H_2$ | Transfer function of the gyrator filter2 in analog domain |
| $\sum$ | Summation |

| | |
|---|---|
| $k_i, a_i, b_i$ | Parameters of generalized bilinear transformation |
| $R, L, C$ | Resistanc, inductance, capacitance |
| $b_{ii}$ | Coefficient of the numerator of digital transfer function |
| $a_{ii}$ | Coefficient of the denominator of digital transfer function |
| $\triangle$ | Determinant of a matrix |
| SHP | Stricty Hurwitz Polynomial |
| VSHP | Very Stricty Hurwitz Polynomial |
| GBT | Generalized Bilinear Transformation |
| FIR | Finite Impulse Response |
| IIR | Infinite Impulse Response |
| RLC | Resistor, Inductor, Capacitor |
| DFF | D-flipflop |
| MSE | Mean Square Error |
| dB | Decible |
| PSNR | Peak Signal-to-Noise Ratio |
| MRI | Magnetic Resonance Imaging |

# Chapter 1

# Introduction

## 1.1 General

Two dimensional (2-D) Digital signal processing is a rapidly evolving field with growing applications in medical science, geographical science and environment, space and robotic engineering [1]. For example, medical applications are concerned with processing of chest X-Ray, cine angiogram, projection of frame axial tomography and other medical images that occurs in radiology, nuclear magnetic resonance (NMR) ultrasonic scanning and magnetic resonance imaging (MRI) etc. and the restoration and enhancement of these images are done by 2D digital filters. Due to the increasing requirements of this particular area, researchers have focused considerable attention on the design and implementation of multidimensional filters and conduct research on advanced and newly emerging topics.

## 1.2 Applications

Applications of 2D signal processing are described in the following.

### 1.2.1 High Definition Television

A large amount of research is being conducted now in the 2D filters because of increased interest in High definition television. For example researchers have found that a 2D Digital comb filter helps reducing video noise by comparing each horizontal scanning line with the line above and below and with the corresponding line on

the previous subsequent video frames. It can create higher picture clarity and reduce dot crawl by analyzing and correcting color transitions in the each video frame. It can separate chrominance (color) from luminance (brightness) information in the video signal for independent processing to improve picture resolution and minimize distortion like- Magnavox 15MF605T HD flat panel LCD TV.

### 1.2.2 X-Ray Tomography

X-ray tomography is a series of projection images and generally it contains 2D data. It is useful in the materials science, biology and biomedicine, microelectronics, geographical science etc. For analyzing a structure like bones, microchip etc, accurately it is necessary to remove noise from the image data by 2D filters [2].

### 1.2.3 Seismic Signal Processing

2D filters play important roles to improve seismic discontinuity data for interpretation. Reflected seismic wave can be obtained by recording earthquakes or large explosions and analyzing the wave. Modern computer software can analyze digital seismic data and can find out other earthquakes information. The physical structure and composition of the interior of a planet seismic topology utilizes information obtained by recording the arrival times of the seismic wave at different points on the earth surface from a known epicenter [3]. It is possible to model the interior of the earth using seismic data. That can show the boundary between earth's core and mantle as well as between the solid inner core and fluid outer core. In the seismic reflection method, frequency of the ground surface is lower than the reflection from the surface and the same can be removed by 2D fan filter having specific angle [4].

### 1.2.4 Sonar

Sonar image is important for an underwater vehicle, but it is also necessary to remove geometric distortion and radiometric errors from the sonar image in order to analyze the image and digital mosaicking. 2D low-pass filter is generally used to remove the noise. During the data acquisition of sonar data, some noise comes with real data because of vehicle instability or noise in the water. Such stripped noise can also be

removed by 2D filter and 2D low-pass filter is used to obtain smooth sonar image. Forward-looking sonar data is obtained from an underwater vehicle where tracking object of vehicle's environment is an essential requirement of obstacles avoidance systems. Vehicle is needed to track different obstacles including stationary object in the sea bed and moving object in the water, like- marine animal and others underwater vehicles. The number of targets and their locations are needed to be estimated from the noisy measurements obtained from sonar data. Using low-pass filters, multiple objects can be tracked by forward-looking sonar images [5].

### 1.2.5 Radio Astronomy

Radio waves can penetrate in the gas and dust in the space as well as the clouds of the planetary atmospheres and pass through the terrestrial atmosphere with little distortion [6]. So radio astronomers can obtain a much clearer image of the stars and galaxies. But the levels of interference are billions of times stronger than the radio astronomy signal. The effective technique to remove interference is filtering by 2D low-pass filter.

### 1.2.6 2D image resizing

2D image resizing is an important issue for pixel oriented displays with variable input formats. Low-resolution pictures look bad on high-resolution screens, especially when only simple up-conversion method like pixel and line repletion or bilinear interpolation are used. Even when applying separable polyphase up-conversion filters, the problem of jagged lines (staircase) remains. For high-quality resizing with suitable post-filtering such as 2D low-pass filter can make the jagged lines smoothen perfectly [7].

### 1.2.7 Image encoding

Pre-filtering is necessary for efficient image encoding, specially when digital transmission and storage of image is needed and the amount of bits required is huge [8]. The recent interest of efficient coding is in broadcast television and teleconferencing. In the broadcasting tv, color video signal is needed to sample with high frequency and

after quantization we get high bit rate. Using different coding techniques, broadcast quality system is constructed with less bit rate. In the teleconferencing, because of less motion, more degradation can be tolerated and low bit rate can be achieved. In the multi-spectral, efficient coding is necessary for storage and transmission of the image. A large compression factor is needed for the high-resolution image to handle and the degradation of data makes some difficulties [8].

### 1.2.8 Image restoration and enhancement

Image restoration work has been done using 2D filter, when artificial satellite takes images of moon, Mars and other planets, various image degradations occur because of random noise, interference, geographical distortion, field non-uniformity, contrast loss and blurring etc., Another research is in image restoration because of image of planets, stars are taken through the atmosphere and image becomes blurring due to atmospheric turbulence [8].

## 1.3 Distinction between Finite Impulse Response and Infinite Impulse Response filter

FIR filters have precisely (generalized) linear phase. 2D FIR filter can be characterized by the transfer function in the analog continuous time domain as

$$H_a(s_1, s_2) = \sum_{m=0}^{M} \sum_{n=0}^{N} a_{mn} s_1^m s_2^n \tag{1.3.1}$$

or in the discrete time domain as

$$H_d(z_1, z_2) = \sum_{m=0}^{M_d} \sum_{n=0}^{N_d} a_{mn} z_1^{-m} z_2^{-n} \tag{1.3.2}$$

Problems of stability of FIR filter do not occur because the impulse response sequence is bounded and exists only for a finite time. High selectivity of prescribed specification can be achieved by higher order of transfer function. In such condition

the order of the filter would be quite high and implementation could be difficult. But generally FIR filter are simple to implement. All DSP processors have architectures that are suited to FIR filtering and moreover FIR filters suffer less from the effects of finite word-length than those of IIR.

IIR filters are advantageous when different frequency-selective filters are designed. IIR filters can be characterized by the transfer function in the analog domain as

$$H_a(s_1, s_2) = \frac{N_a(s_1, s_2)}{D_a(s_1, s_2)} \tag{1.3.3}$$

$$= \frac{\sum_{m=0}^{M} \sum_{n=0}^{N} a_{mn} s_1^m s_2^n}{\sum_{i=0}^{K} \sum_{j=0}^{L} a_{ij} s_1^i s_2^j} \tag{1.3.4}$$

or in the discrete domain as

$$H_d(z_1, z_2) = \frac{N_d(z_1, z_2)}{D_d(z_1, z_2)} \tag{1.3.5}$$

$$= \frac{\sum_{m=0}^{M_d} \sum_{n=0}^{N_d} a_{mn} z_1^{-m} z_2^{-n}}{\sum_{i=0}^{K_d} \sum_{j=0}^{L_d} a_{ij} z_1^{-i} z_2^{-j}} \tag{1.3.6}$$

The order of IIR filters can be found from the prescribed specifications in term of appropriate functions for a given approximation (Butterworth, Chebyshev or elliptic etc.). Simplicity of design procedure makes it easy to design IIR filter. However IIR could be unstable, so any IIR filter should ensure first that designed filter is stable. Limitation in the frequency-selective filter that permits only the magnitude response to be specified, sometimes prescribed phase-response or group delay response is required, and in each case different algorithm is needed to design the filter.

## 1.4 Stability in Infinite Impulse Response Filter

Feedback mechanism is inherent in any IIR structure and feedback occurs when a scaled version of the output is fedback to the input, and this is responsible for the infinite number of impulse response. The output of IIR filter could depend on the both previous inputs and outputs and this causes instability. One might argue that mathematically the response can go on for ever, getting smaller and smaller, but in the digital world below a certain level, the signal becomes zero. Stability of the IIR

filters is not guaranteed as in the case of the FIR filter and tests have to be carried out to ensure that the filter obtained by the approximation is stable.

## 1.5 Very Stricty Hurwitz Polynomial (VSHP) ensures stability

The design of 2D IIR filters is difficult due to the non-existence of the fundamental theorem of algebra in the factorization of 2D polynomials into lower order polynomials. Because of this problem, the testing for stability of a 2D IIR transfer function requires a large number of computations. One way to ensure a 2D transfer function is stable is if the denominator of the transfer function is satisfied to be a Very Strict Hurwitz Polynomial (VSHP) [9] and that can ensure a transfer function that there is no singularity in the right half of the biplane, which can make a system unstable. Before proceeding further few definitions are given below:

$H_a(s_1, s_2)$ possesses the non-essential singularity of first kind at $(s_1, s_2) = (\alpha, \beta)$ if $D_a(\alpha, \beta) = 0$ and $N_a(\alpha, \beta) \neq 0$ . So the denominator of transfer function may become simultaneously zero at a specific sets of points, but not in their neighborhood.

$H_a(s_1, s_2)$ possesses the non-essential singularity of second kind at $(s_1, s_2) = (\alpha, \beta)$ if $D_a(\alpha, \beta) = 0$ and $N_a(\alpha, \beta) = 0$ . Both the numerator and denominator of transfer function may become zero simultaneously at a given set of points.

Similarly in discrete time domain, $H_d(z_1, z_2)$ posses the non-essential singularity of first kind at $(z_1, z_2) = (\alpha, \beta)$ if $D_d(\alpha, \beta) = 0$ and $N_d(\alpha, \beta) \neq 0$.

$H_d(z_1, z_2)$ posses the non-essential singularity of second kind at $(z_1, z_2) = (\alpha, \beta)$ if $D_d(\alpha, \beta) = 0$ and $N_d(\alpha, \beta) = 0$.

$D_a(s_1, s_2)$ is known to be a strictly Hurwitz polynomial(SHP), if $\frac{1}{D_a(s_1, s_2)}$does not possess any singularities in the right half of $s_1, s_2$-plane. Otherwise it will be unstable. The define region which does not possess any singularity is given by-
$\{(s_1, s_2) | Re[s_1] \geq 0, Re[s_2] \geq 0, |s_1| < \infty \text{ and } |s_2| < \infty\}$.

$D_a(s_1, s_2)$ is a Very Strictly Hurwitz Polynomial(VSHP), if $\frac{1}{D_a(s_1,s_2)}$does not possess any singularities in the region-
$\{(s_1, s_2)|Re[s_1] \geq 0, Re[s_2] \geq 0, |s_1| \leq \infty \text{ and } |s_2| \leq \infty\}$.

## 1.6 Properties of VSHP

Some of the important properties of VSHP [9] are discussed in the following.

1. A 2D transfer function does not possess any singularity in the closed right half of the biplane, if and only if the denominator is VSHP.

2. Multiplication of two 2D functions is a VSHP, if and only if each of 2D functions is individually VSHP.

3. A 2D function is VSHP and partial derivative of the function with the respect of any variable will be VSHP.

4. A 2D VSHP polynomial can be represented a single variable polynomial considering the coefficients function of other variable and each coefficients are SHP in their own domain.

   Example: A VSHP polynomial, $D_a(s_1, s_2)$ can be represented by,

$$D_a(s_1, s_2) = \sum_{i=0}^{P} E_i(s_2) s_1^i \tag{1.6.1}$$

   or

$$D_a(s_1, s_2) = \sum_{i=0}^{P} F_i(s_1) s_2^i \tag{1.6.2}$$

   The polynomials $E_i(s_2)$ and $F_i(s_1)$ are SHPs in $s_2$ and $s_1$ respectively.

5. A 2D VSHP polynomial can be represented by a single variable polynomial considering the coefficients of the function of the other variable and division of two consecutive coefficients is a minimum reactive positive real function in the their own domain.

Example: The polynomials $E_i(s_2)$ and $F_i(s_1)$ are defined in the equation 1.6.1 and 1.6.2, and each of the functions $\frac{E_i(s_2)}{E_{i-1}(s_2)}$ and $\frac{F_i(s_1)}{F_{i-1}(s_1)}$ are minimum reactive positive real functions in $s_2$ and $s_1$ respectively.

## 1.7 Generation of VSHP

VSHP can be generated using different properties of VSHPs. A few methods [9] are discussed in the following to generate a VSHP.

### 1.7.1 Method I:

A SHP in 2 or n-variables can be generated from a k-variable physically realizable network, because the input immittance (impedance or admittance) of the network always represents an even or an odd part of a SHP in the corresponding number of variables. In the following, some of the possibilities of generation of VSHP are shown.

**(a)** The starting network is a n-port gyrator terminated in n-variable reactances, each of degree unity. The determinant of the immittance matrix yields an even or an odd part of an n-variable Hurwitz polynomial. A SHP results by the addition of this determinant to its derivatives with the respect to the n-variables. The resulting SHP in n-variables can be converted to a 2-variable VSHP. A large number of possibilities exist.

**(b)** Instead of taking the derivatives of the determinant of the terminated n-port gyrator, by judicious choices of n-variables as positive real constants, VSHP can be generated.

**(c)** A positive definite or positive semidefinite matrix is physically realizable. Consider,

$$\begin{aligned} D_n &= A\psi A^t s_1 + B\Lambda B^t s_2 + R\Gamma R^t + G \\ &= A_1 s_1 + B_1 s_2 + R_1 + G \end{aligned} \tag{1.7.1}$$

where $A$, $B$, $R$ are lower triangular matrices; $\psi, \Lambda, \Gamma$ are diagonal matrices and G is a skew-symmetric matrix.

The matrices $A$, $B$ and $R$ can be upper-triangular. If all the components of $\psi, \Lambda, \Gamma$ are positive, $A_1, B_1, R_1$ are positive-definite matrices and they are physically realizable. It can be realized even if some of the components of $\psi, \Lambda, \Gamma$ are equal to zero and in such a case $A_1, B_1, R_1$ become positive semi-definite matrices. If $\Gamma$ is a null matrix, determinant of $D_n$ becomes a strictly even or strictly odd polynomial depending on the value of n. In such case, by the use of derivatives a suitable VSHP can be obtained.

### 1.7.2 Method II

The desired VSHP can be generated from a simple VSHP,

$$D(s_1, s_2) = a_{11}s_1s_2 + a_{10}s_1 + a_{01}s_2 + a_{00} \tag{1.7.2}$$

For the reactance function obtained as

$$G_1(s_1, s_2) = \frac{P_1(s_1, s_2)}{Q_1(s_1, s_2)} \tag{1.7.3}$$

$$= \frac{a_{11}s_1s_2 + a_{00}}{a_{10}s_1 + a_{01}s_2} \tag{1.7.4}$$

applying the transformation,

$$s_1 \longrightarrow \frac{b_{11}s_1s_2 + b_{00}}{b_{10}s_1 + b_{01}s_2} \tag{1.7.5}$$

(where $b_{11} > 0, b_{10} > 0, b_{01} > 0$ and $b_{00} > 0$)

one gets the function

$$G_2(s_1, s_2) = \frac{P_2(s_1, s_2)}{Q_2(s_1, s_2)} \tag{1.7.6}$$

The resultant polynomial $P_2(s_1, s_2) + Q_2(s_1, s_2)$ is a VSHP. To obtain desired degree of $s_1$ and $s_2$, the following transformation can be applied again.

$$s_2 \longrightarrow \frac{c_{11}s_1s_2 + c_{00}}{c_{10}s_1 + c_{01}s_2} \tag{1.7.7}$$

(where $c_{11} > 0, c_{10} > 0, c_{01} > 0$ and $c_{00} > 0$)

To obtain desire higher order of VSHP, these transformation can be repeated.

### 1.7.3 Method III

In the case of product-separable denominators $D_a(s_1).D_b(s_2)$, it is necessary that $D_a(s_1)$ and $D_b(s_2)$ are SHPs in $s_1$ and $s_2$ respectively. Such denominator can be generated by substituting $s_1 = s_2 = s$ in the equation 1.7.2 or making either $A_1 = 0$ or $B_1 = 0$ in the equation 1.7.2.

## 1.8 Scope of the thesis

In the thesis, two new filter designs and filter transformation method are proposed for 2D recursive filter design which has variable monotonic magnitude characteristic. The monotonic amplitude-frequency response of a filter can be achieved and in the case transition bands are increased rapidly [10]. Most of the works of such area have done in one dimensional domain, but vast area of signal processing applications are in two dimension domain, so researchers have started to work on 2D filters with monotonic frequency response.

Darlington-synthesis is an attractive technique for the realization of a driving-point function. The extension of Darlington-synthesis for the realization of single-variable positive real function's to two-variable positive real function's is described in [11] and [12]. Darlington-type realization of two-variable driving-point impedance of lossless two-port network is described and as an extension form of the theorem to n-variable driving-point impedance is realized in [11]. In [13], necessary and sufficient conditions for the realization of the classes of two-variable positive real function's as doubly-terminated lossless two-variable lossless ladder networks are obtained. In this thesis, two filter structures are proposed from Darlingotn-synthesis [14] which are doubly-terminated gyrator networks and impedances of the network are replaced by doubly-terminated RLC networks whose response has monotonic characteristics. The objective of this thesis is to obtain monotonic amplitude-frequency responses of the doubly-terminated gyrator networks by regulating the value/sign of gyrator constant and the parameters of the generalized bilinear transformation [15].

In Chapter 2, the doubly-terminated gyrator networks are introduced and transfer functions of each filter are derived. For the frequency transformation and filter response modification, generalized bilinear transformation [15] is introduced and the

relation between analog domain with digital domain as well as digital domain with modified analog domain [16] are obtained. For the generation of VSHPs, second-order filters are replaced with the impedances of the doubly terminated gyrator networks and properties of the overall filters are outlined.

In Chapter 3, two methods are proposed for 1D and 2D low-pass filter design and several numerical examples are illustrated. The 1D and 2D low-pass filter design provides frequency responses containing monotonic amplitude-frequency response in the pass-band [17]. Generalized bilinear transformation and the magnitude of gyrator constant of the filter are used together to obtain desired digital filter response. In the section 3.3, the proposed method is applied on the doubly terminated networks when the impedances are replaced with different second order filters. A realization of a second order two-dimensional filter is shown.

In Chapter 4, another design is proposed to design high-pass filter which has monotonic amplitude-frequency response in the passband. In the section 4.2, the method is applied to the doubly terminated networks when impedances are replaced with different combinations of second order filters and corresponding high-pass filter responses are shown. Another important method is proposed for the frequency transformation and the method ensures the monotonic amplitude-frequency response and stability of resultant filter, if the original filter contains monotonic amplitude-frequency response. In the section 4.4, the proposed method is applied to the doubly terminated networks as before and low-pass to high-pass filter transformations as well as band-pass to band-eliminated filter transformations are shown.

In Chapter 5, some applications of image processing are shown using the various filters designed by the proposed method. The 2D low-pass filters are used for the image restoration purposes. The 2D high-pass filters are used for the enhancement purpose. The 2D band-pass and band-eliminated filters are used to attenuate some frequencies from the Fourier transformation of the image.

Overall, some designs and methods are proposed for various kinds of filter design and these methods are very useful in the case of image processing applications. For the frequency transformation, the generalized bilinear transformation is used, as a result, the proposed method is obtain more flexibilities in the transformation. Two

methods are proposed to design analog and digital filters and a realization of the digital filter is shown. A method is proposed for the digital filter transformation and this method depends on the value/sign of gyrator constant and parameters of generalized bilinear transformation.

# Chapter 2

# Filter Structures

## 2.1 Introduction

Two filter structures are considered in this chapter for 2D digital recursive filters design and both structures are taken from Darlington-synthesis [14]. The 2D digital filters are designed by Darlington-type networks containing gyrators. Gyrator was introduced as new network element in 1948 and an ideal gyrator has been shown as passive component, non-reciprocal two port network [18]. A gyrator can convert an impedance into its inverse and a gyrator is represented as an active device and a gyrator with an inductor is replaced by a capacitor, a couple of operational amplifiers and some resistors [19]. Coil with large inductance is needed in telecommunication system and filter, but large inductances are hard to achieve in VLSI or modern small electronic circuit. To overcome the problem, there is one solution which can be used in many applications [20], and that is to simulate the behavior of coil using gyrator. This is a very handy gadget to put large value inductors into very small package, because the inductance value is proportional to the capacitance value [20].

In this chapter, the value and sign of gyrator constant (g) of the Darlington-type gyrator networks are used to design the 2D digital filters. Transfer functions of the networks are generated by replacing the impedances of the Darlington-type gyrator networks with the doubly terminated RLC networks and the overall 2D analog transfer functions are stable in analog domain, if the denominators of the transfer functions are satisfied to be VSHPs (section 1.5).

Transfer functions of the doubly terminated gyrator networks are derived in section 2.2 and 2D VSHPs are generated by replacing impedances of the gyrator networks

with second-order doubly terminated RLC networks (section 2.4). In this chapter, second-order Butterworth and Gargour&Ramachandran filters [16] are considered as doubly terminated RLC networks. Some properties of both doubly terminated gyrator filters are pointed out in the section 2.5, when two impedances of the filters are replaced by the doubly terminated RLC circuits (second-order Butterworth and Gargour&Ramachandran filters).

Generalized bilinear transformation (GBT) [15] is applied to the overall analog filter, and as a result the reactive components of the filter are changed to the desired ones (equations (2.3.12) and (2.3.14)). For example, impedances of the gyrator network are replaced by second-order doubly terminated Butterworth filters and generalized bilinear transformation is applied to the overall transfer function in order to obtain the desired filter and the corresponding modified analog filter is obtained by inverse bilinear transformation(equation(2.3.5)). In this case, the GBT modifies the reactive properties of the Butterworth filter as shown in the section 2.3. Properties of the GBT on second-order Butterworth filter are described in detail in the section 2.3.6. Stability of the designed filter is ensured [21] and also the monotonic amplitude-frequency response in the pass-band of the desired filter. In this chapter, it shows that a sufficient condition of the overall transfer function in order to obtain monotonic response is that the denominator of the transfer function contains roots where magnitude of the real-part is greater than or equal to the magnitude of the imaginary-part. The same also hold for the transfer functions of the doubly terminated RLC network.

## 2.2 Transfer Function

The transfer function of the doubly terminated gyrator networks which are taken from Darlington synthesis [14] are derived in the following:

### 2.2.1 Transfer Function of filter 1 (Figure 2.1)

According to the principle of gyrator [22] in Figure 2.1(b), $I_a = gV_b$ and $I_b = -gV_a$.

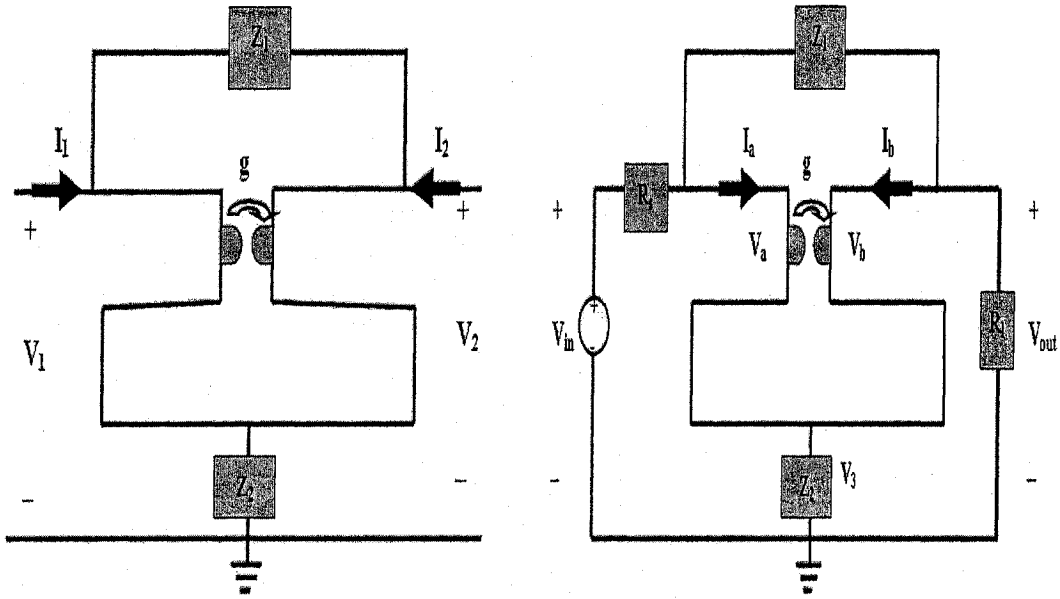


(a)Two port gyrator network (b) Doubly terminated gyrator network

Figure 2.1: Filter 1

Two port circuit analysis in Figure 2.1(a) gives,

$$Z_{11} = \frac{1 + g^2 Z_1 Z_2}{g^2 Z_1} \tag{2.2.1}$$

$$Z_{12} = \frac{1 - gZ_1 + g^2 Z_1 Z_2}{g^2 Z_1} \tag{2.2.2}$$

$$Z_{21} = \frac{1 + gZ_1 + g^2 Z_1 Z_2}{g^2 Z_1} \tag{2.2.3}$$

$$Z_{22} = \frac{1 + g^2 Z_1 Z_2}{g^2 Z_1} \tag{2.2.4}$$

In Figure 2.1(b), If $R_s = R_l = 1$, the transfer function of the doubly terminated network will be

$$H_1 = \frac{1 + gZ_1 + g^2 Z_1 Z_2}{2 + Z_1 + g^2 Z_1 + 2g^2 Z_1 Z_2} \tag{2.2.5}$$

### 2.2.2 Transfer Function of filter 2 (Figure 2.2)

According to the principles of the gyrator theory [22] in Figure 2.2(b), $I_a = gV_b$ and $I_b = -gV_a$.

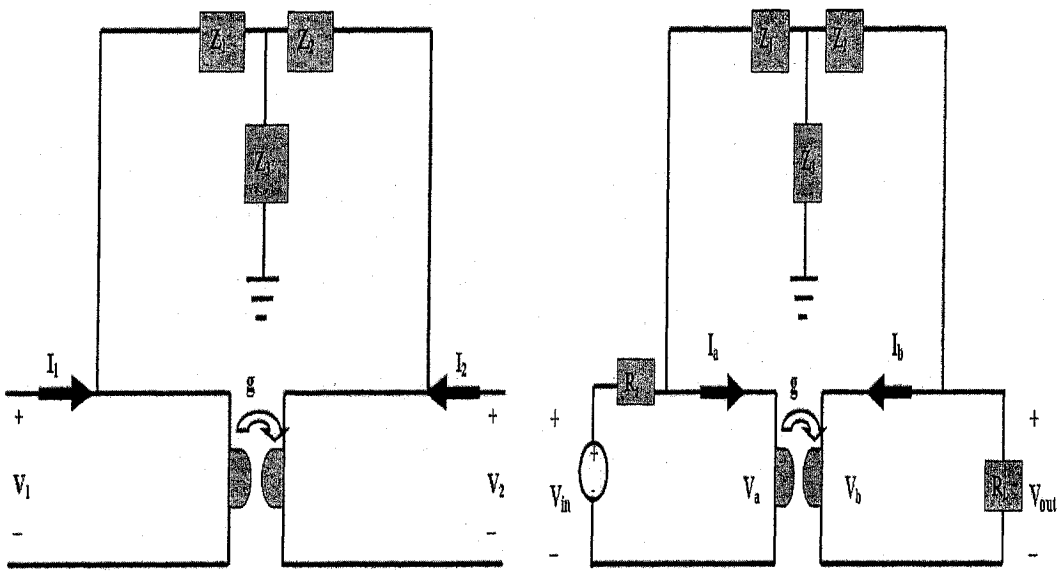


(a)Two port gyrator network (b) Doubly terminated gyrator network

Figure 2.2: Filter 2

Two port circuit analysis in Figure 2.2(a) gives

$$Z_{11} = \frac{Z_1 + Z_3}{1 + g^2 Z_1 Z_3 + g^2 Z_3 Z_2 + g^2 Z_1 Z_2} \tag{2.2.6}$$

$$Z_{12} = \frac{Z_3 - gZ_1 Z_3 - gZ_3 Z_2 - gZ_1 Z_2}{1 + g^2 Z_1 Z_3 + g^2 Z_3 Z_2 + g^2 Z_1 Z_2} \tag{2.2.7}$$

$$Z_{21} = \frac{Z_3 + gZ_1 Z_3 + gZ_3 Z_2 + gZ_1 Z_2}{1 + g^2 Z_1 Z_3 + g^2 Z_3 Z_2 + g^2 Z_1 Z_2} \tag{2.2.8}$$

$$Z_{22} = \frac{Z_2 + Z_3}{1 + g^2 Z_1 Z_3 + g^2 Z_3 Z_2 + g^2 Z_1 Z_2} \tag{2.2.9}$$

In Figure 2.2(b), If $R_s = R_l = 1$, the overall transfer function of doubly terminated gyrator network will be

$$H_2 = \frac{gZ_2 Z_3 + gZ_1 Z_3 + gZ_1 Z_2 + Z_3}{Z_2 Z_3 + Z_1 Z_3 + Z_1 Z_2 + 2Z_3 + Z_1 + Z_2 + 1 + g^2 Z_2 Z_3 + g^2 Z_1 Z_3 + g^2 Z_2 Z_1} \tag{2.2.10}$$

From this transfer function, it can be readily seen that if $Z_1$ and $Z_2$ are replaced by doubly terminated RLC filters, it is essential to replace $Z_3$ by a resistive component, otherwise denominator of the transfer function will not satisfy to be the VSHPs which is proved in section 2.4.5. Even, $Z_3$ is replaced by inductor or capacitor, denominator of the resultant transfer function will not satisfy to be the VSHPs. In this thesis Generalized Bilinear Transformation is applied to the stable overall analog transfer

function to design desired digital filter as well as corresponding modified analog filter, details are discussed in the bellow.

## 2.3 Generalized Bilinear Transformation (GBT)

Desired digital filter responses are obtained using generalized bilinear transformation. The transformation is applied to a transfer function of an analog circuit and this generalized bilinear transformation [16] modifies the analog circuit according to the desired filter response. The generalized bilinear transformation in the case of one dimension (1D) is shown bellow.

$$s = k\frac{(z+a)}{(z+b)} \tag{2.3.1}$$

where, s is Laplace domain parameter and z is discrete domain parameter. To obtain a stable transfer function by applying this transformation, stability conditions for $k > 0$ are:

$$|\, a \,| \leq 1 \tag{2.3.2}$$

$$|\, b \,| \leq 1 \tag{2.3.3}$$

$$ab < 0 \tag{2.3.4}$$

Different filter responses are achieved from an analog transfer function by varying the values of $k$, $a$ and $b$, such as low-pass, high-pass, band-pass and band-elimination filter.

It has been seen that the effect of the GBT on a second-order Butterworth filter provides a modified low-pass filter, when $a$ is negative and $b$ is positive; high-pass filter is obtained when $a$ is positive and $b$ is negative; band-pass filter is obtain when the transformation is the sum of low-pass and high-pass transformation and band-elimination filter is the reciprocal of band-pass transformation. Modified analog transfer function are obtained from discrete transfer function by applying inverse bilinear transformation [23],

$$z = \frac{(1+s)}{(1-s)} \tag{2.3.5}$$

The relations between analog frequency and modified digital frequency are obtained. Similarly the relation between modified analog frequency and digital frequency is shown in below.

$$\begin{aligned} s_a &= k\frac{z+a}{z+b} \\ s_a &= k\frac{(cos\omega+a)(cos\omega+b)+(sin\omega)^2+i*sin\omega(b-a)}{1+b^2+2bcos\omega} \end{aligned} \tag{2.3.6}$$

where, $\omega$ is digital frequency. Equating the imaginary terms from the above equation, The following relation is obtained.

$$\Omega = k\frac{(b-a)sin\omega}{1+b^2+2bcos\omega} \tag{2.3.7}$$

where, $\Omega$ is analog frequency. The frequency relation is obtained from the modified analog to digital domain by using inverse bilinear transformation [23], is in following.

$$\begin{aligned} s_{mod} &= \frac{z-1}{z+1} \\ &= \frac{(cos\omega-1)(cos\omega+1)+(sin\omega)^2+i*2sin\omega}{2(1+cos\omega)} \end{aligned} \tag{2.3.8}$$

Equating the imaginary terms from the above equation, The following relation is obtained in between modified analog domain and modified digital domain.

$$\begin{aligned} \Omega_{mod} &= \frac{2sin\omega}{2(1+cos\omega)} \\ &= tan(\omega/2) \end{aligned} \tag{2.3.9}$$

where, $\Omega_{mod}$ is the modified analog frequency. In the following, generalized bilinear transformation is applied on second order Butterworth filter and designed various kinds of filter, such as low-pass, high-pass, band-pass and band-elimination filter and frequency mapping can be made in between original analog domain, modified digital domain and modified analog domain using corresponding frequency relationships in the equations (2.3.7) and (2.3.9). Applying the relationships, desired cutoff frequencies are obtained which are shown in the following:

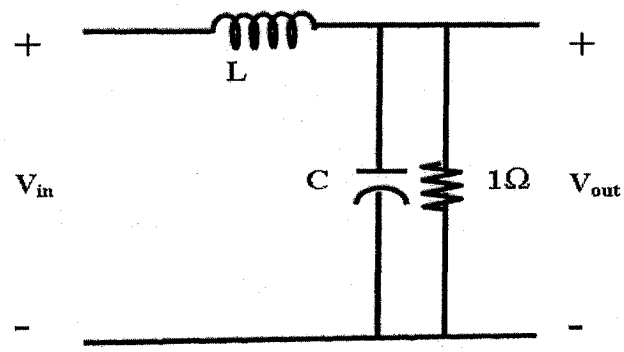


Figure 2.3: Second order Butterworth Low-pass filter.

### 2.3.1 Filters design using generalized bilinear transformation

A second order Butterworth transfer function can be realized as a doubly-terminated RLC low-pass filter with cutoff frequency 1 radian/sec [24]. Circuit diagram of Butterworth filter is shown in Figure 2.3. The transfer function is obtained as

$$T(s) = \frac{1}{LC(s^2 + \frac{1}{C}s + \frac{1}{LC})} \tag{2.3.10}$$

$$\tag{2.3.11}$$

Where, $L = 1.4142$ and $C = 0.7071$.

The GBT is applied to the reactances of the circuit and the reactances are modified depending on the parameters of the transformation and desired cutoff frequency can be achieved using equation (2.3.7).

$$Z_L = sL \tag{2.3.12}$$

$$= \frac{(1+a)kL}{(1+b)+(1-b)s} + \frac{(sLk)(1-a)}{(1+b)+(1-b)s} \tag{2.3.13}$$

Similarly admittance of capacitor is modified in the following way,

$$Y_C = sC \tag{2.3.14}$$

$$= \frac{(k+a)C}{(1+b)+(1-b)s} + \frac{(sC)(k-a)}{(1+b)+(1-b)s} \tag{2.3.15}$$

Table 2.1: The parameters of Figure 2.4

| | | | |
|---|---|---|---|
| $R_{sp1} = \frac{Lk(1-a)}{1-b}$ | $L_{sp} = \frac{Lk(1-a)}{1+b}$ | $R_{sp2} = \frac{Lk(1+a)}{1+b}$ | $C_{sp} = \frac{(1-b)}{(1+a)kL}$ |
| $R_{ps1} = \frac{(1+b)}{Ck(1+a)}$ | $L_{ps} = \frac{(1-b)}{Ck(1+a)}$ | $R_{ps2} = \frac{(1-b)}{Ck(1-a)}$ | $C_{ps} = \frac{Ck(1-a)}{(1+b)}$ |

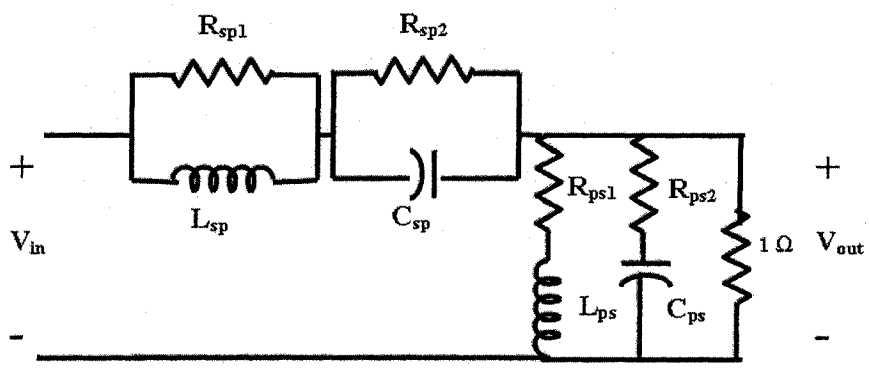


Figure 2.4: The modified Butterworth Low-pass filter.

The modified filter is shown in Figure 2.4 and the components' values are in Table 2.1.

Depending on the components' value of the modified filter, desired frequency response is obtained [16]. However, $R_{sp1}$, $L_{sp}$, $R_{ps2}$ and $C_{ps}$ could have negative values, if and only $a > k$ and physically, it is possible to have negative values of resistor and capacitor [25]. Applying the proposed method, low-pass, high-pass, band-pass and band-elimination filter design are shown in the following.

### 2.3.2 Low-pass filter design

Second order Butterworth filter is basically low pass filter having 1 rad/sec cutoff frequency and the cutoff frequency can be changed applying the transformation and the desired cutoff is achieved by varying the parameters' value of the transformation. The GBT is used to design a low-pass filter in the following:

$$s = k\frac{(z+a)}{(z+b)} \tag{2.3.16}$$

The limitations of the transformation depend on the stability criteria of modified filter [15]. To obtain stable low-pass, stability conditions for k > 0 are-

$$-1 \leq a < 0$$
$$0 < b \leq 1$$
$$ab < 0$$

Applying the GBT to be Butterworth filter, three types of low-pass filters are designed. First low-pass filter is obtained replacing the inductor of Butterworth filter to a parallel branch of a resistor and an inductor and the capacitor of the Butterworth filter is replaced by a series branch of a resistor with a capacitor. Second low-pass filter is obtained replacing the inductor of Butterworth filter to series combination of a resistor and a inductor and capacitor of Butterworth filter is replaced by a parallel branch of a resistor and a capacitor. Third low-pass filter is same as Butterworth filter but parameters' values are different.

Consider, ideal parameters' values are unit magnitude of all parameters. In the following tables the parameters of the transformation are varied one parameter at a time keeping rest of the parameters to ideal values.

Tables 2.2, 2.3, 2.4 give various low-pass filter designs. In Table 2.2, parameters of the GBT, $k$ and $a$ are kept constant and $b$ is the variable. As a result, band-width of the modified low-pass filter is decreased when b decreases. In Table 2.3, parameters of the GBT, $k$ and $b$ are kept constant and $a$ is variable. As a result, bandwidth of the modified low-pass filter is increased when the magnitude of $a$ decreases. In Table 2.4, parameters of the GBT, $a$ and $b$ are kept constant and $k$ is variable. As a result, bandwidth of the modified low-pass filter is decreased when $k$ increases.

Table 2.2: The low-Pass Filter designs corresponding to Figure 2.5

| a | b | $R_{sp}$ | $L_{sp}$ | $R_{ps}$ | $C_{ps}$ | Transfer Function | Cutoff (rad/sec) |
|---|---|---|---|---|---|---|---|
| $-1$ | 0.8 | 10L | $\frac{10L}{9}$ | $\frac{1}{10C}$ | $\frac{10C}{9}$ | $\frac{(s+9)^2}{s^2+1.26s+0.7035}$ | 0.81 |
| $-1$ | 0.5 | 4L | $\frac{4L}{3}$ | $\frac{1}{4C}$ | $\frac{4C}{3}$ | $\frac{(s+3)^2}{s^2+1.0139s+0.3972}$ | 0.58 |
| $-1$ | 0.1 | $\frac{20L}{9}$ | $\frac{20L}{11}$ | $\frac{10}{C}$ | $\frac{3C}{4}$ | $\frac{(9s+11)^2}{s^2+0.6922s+0.1645}$ | 0.32 |

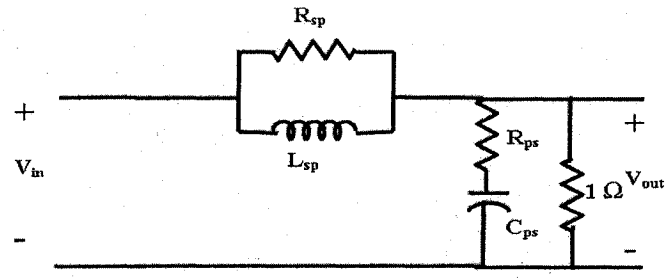


Figure 2.5: The modified low-pass filter when '$b$' is variable and the rest of the parameters are constant.

Table 2.3: The low-Pass Filter designs corresponding to Figure2.6

| a | b | $R_s$ | $L_s$ | $R_p$ | $C_p$ | Transfer Function | Cutoff (rad/sec) |
|---|---|---|---|---|---|---|---|
| $-0.8$ | 1 | $\frac{1}{10L}$ | $\frac{9L}{10}$ | $\frac{10}{C}$ | $\frac{9C}{10}$ | $\frac{1}{s^2+1.7936s+1.4215}$ | 1.13 |
| $-0.5$ | 1 | $\frac{L}{4}$ | $\frac{3L}{4}$ | 4C | $\frac{3C}{4}$ | $\frac{1}{s^2+2.5523s+2.5175}$ | 1.38 |
| $-0.1$ | 1 | $\frac{9L}{20}$ | $\frac{11L}{20}$ | $\frac{20}{9C}$ | $\frac{11C}{20}$ | $\frac{1}{s^2+4.2077s+6.0791}$ | 2 |

### 2.3.3 High-pass filter design

High-pass filter can be designed applying the GBT to the Butterworth filter and in the modified circuit inductive reactance is replaced by capacitive reactance and capacitive reactance is replaced by inductive reactance.

The GBT is used to design a high-pass filter in the following

$$s = k\frac{(z+a)}{(z+b)} \tag{2.3.17}$$

The limitations of the transformation depend on the stability criteria of modified filter. To obtain stable high-pass filter, the conditions for $k > 0$ are-

$$0 < a \leq 1$$
$$-1 \leq b < 0$$
$$ab < 0$$

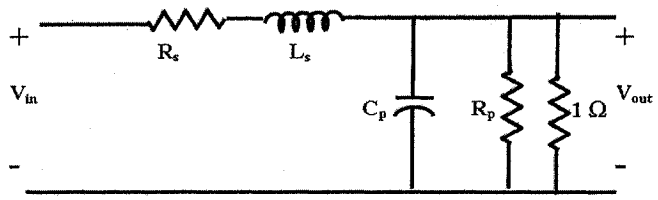


Figure 2.6: The modified low-pass filter when '$a$' is variable and the rest of the parameters are constant.

Table 2.4: The low-Pass Filter designs corresponding to the Butterworth filter

| k | $L_s$ | $C_p$ | Transfer Function | Cutoff (rad/sec) |
|---|---|---|---|---|
| 1 | 0.7071 | 1.4142 | $\frac{1}{s^2+1.4142s+1}$ | 1.00 |
| 2 | 1.4142 | 2.8284 | $\frac{1}{s^2+0.8757s+0.3096}$ | 0.51 |
| 3 | 2.1213 | 4.2426 | $\frac{1}{s^2+0.4714s+0.1111}$ | 0.34 |
| 4 | 2.8284 | 5.6568 | $\frac{1}{s^2+0.4381s+0.0774}$ | 0.26 |

Applying the GBT to the Butterworth filter, three type of high-pass filters are designed. First high-pass filter is obtained replacing inductor of Butterworth filter by a parallel branch containing a resistor and a capacitor and the capacitor of Butterworth filter is replaced by a series branch of a resistor with an inductor. The second high-pass filter is obtained replacing the inductor of Butterworth filter by a series combination of a resistor and a capacitor and the capacitor of Butterworth filter is replaced by a parallel branch of a resistor and an inductor. The third high-pass filter is achieved by replacing an inductor by a capacitor and the capacitor by an inductor.

Similarly, in the following tables the parameters of the transformation are varied one parameter at a time keeping the rest of the parameters to ideal values.

Tables 2.5, 2.6, 2.7 give various high-pass filter designs. In Table 2.5, parameters of the GBT, $k$ and $a$ are kept constant and $b$ is the variable. As a result, the bandwidth of the high-pass filter is decreased when the magnitude of $b$ decreases. In Table 2.6,

Table 2.5: The high-Pass Filter designs corresponding to Figure 2.7

| a | b | $R_{sp}$ | $C_{sp}$ | $R_{ps}$ | $L_{ps}$ | Transfer Function | Cutoff (rad/sec) |
|---|---|---|---|---|---|---|---|
| 1 | $-1$ | $\infty$ | $\frac{1}{L}$ | 0 | $\frac{1}{C}$ | $\frac{s^2}{s^2+1.4142s+1}$ | 1.04 |
| 1 | $-0.8$ | 10L | $\frac{9}{10L}$ | $\frac{1}{10C}$ | $\frac{9}{10C}$ | $\frac{(1+9s)^2}{s^2+1.7936s+1.4215}$ | 1.23 |
| 1 | $-0.5$ | 4L | $\frac{3}{4L}$ | $\frac{1}{4C}$ | $\frac{3}{4C}$ | $\frac{(1+3s)^2}{s^2+2.5523s+2.5174}$ | 1.61 |
| 1 | $-0.1$ | $\frac{20L}{9}$ | $\frac{11}{20L}$ | $\frac{9}{20C}$ | $\frac{11}{20C}$ | $\frac{(9+11s)^2}{s^2+4.2076s+6.0789}$ | 2.01 |

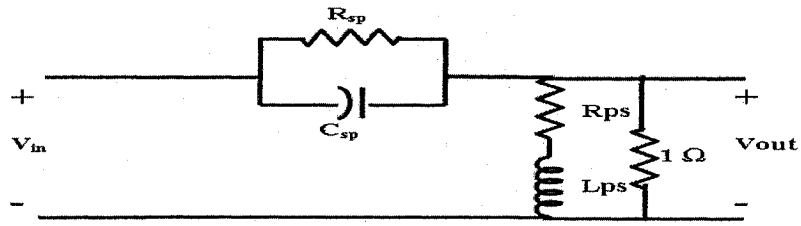


Figure 2.7: The modified High-pass filter when '$b$' is variable and the rest of the parameters are constant.

parameters of the GBT, $k$ and $b$ are kept constant and $a$ is variable. As a result, band-width of the high-pass filter is increased when $a$ decreases. In the Table 2.7, parameters of the GBT, $a$ and $b$ are kept constant and $k$ is variable. As a result, bandwidth of the high-pass filter is increased when $k$ increases.

### 2.3.4 Band-pass filter design

The GBT is used to design a band-pass filter by the following transformation:

$$s = K_1 \frac{(z + a_1)}{(z + b_1)} + K_2 \frac{(z + a_2)}{(z + b_2)} \tag{2.3.18}$$

The transformation is a combination of the low-pass and the high-pass of the GBT (section 2.3.2, 2.3.3). The limitations of the transformation depend on the stability criteria of band-pass filter. To obtain stable band-pass filter, the conditions for $K_1 > 0$ and $K_2 > 0$ are $-1 \leq a_1 < 0$, $0 < b_1 \leq 1$, $a_1 b_1 < 0$, $0 < a_2 \leq 1$, $-1 \leq b_1 < 0$, $a_2 b_2 < 0$.

Table 2.6: The high-Pass Filter designs corresponding to Figure 2.8

| a | b | $R_s$ | $C_s$ | $R_p$ | $L_p$ | Transfer Function | Cutoff (rad/sec) |
|---|---|---|---|---|---|---|---|
| 0.8 | $-1$ | $\frac{L}{10}$ | $\frac{10}{9L}$ | $\frac{10}{C}$ | $\frac{10}{9C}$ | $\frac{s^2}{s^2+1.2617s+0.7035}$ | 0.89 |
| 0.5 | $-1$ | $\frac{L}{4}$ | $\frac{4}{3L}$ | $\frac{4}{C}$ | $\frac{4}{3C}$ | $\frac{s^2}{s^2+1.0138s+0.3972}$ | 0.72 |
| 0.1 | $-1$ | $\frac{9}{20L}$ | $\frac{20}{11L}$ | $\frac{20}{9C}$ | $\frac{20}{11C}$ | $\frac{s^2}{s^2+0.6922s+0.1645}$ | 0.51 |

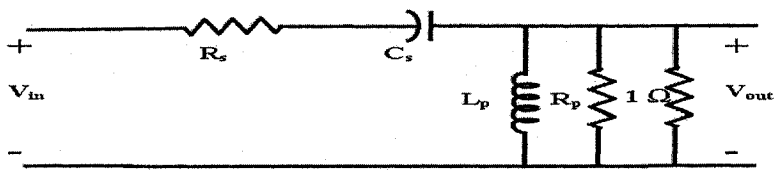


Figure 2.8: The modified High-pass filter when '$a$' is variable and the rest of the parameters are constant.

Band-width of the modified band-pass filter can be changed to the desired value and the center frequency can be moved choosing appropriate parameters' values of the transformation.

Applying the GBT to the Butterworth filter, two band-pass filters are achieved. First band-pass filter is obtained by replacing the inductor of Butterworth filter to series combination of a resistor, an inductor and a capacitor and the capacitor of Butterworth filter is replaced by a parallel combination of a resistor, an inductor and a capacitor. The second band-pass filter is obtained by replacing the inductor of Butterworth filter to parallel combination of a resistor and an inductor and a capacitor and the capacitor of Butterworth filter is replaced by a series combination of a resistor, an inductor and a capacitor.

Consider, the ideal values of the parameters of the transformation are $a_1 = -1, b_1 = 1, K_1 = 1, a_2 = 1, b_2 = -1, K_2 = 1$.

In Tables 2.8, 2.9 and 2.10, the parameters of the transformation are varied one parameter at a time keeping the rest of the parameters to ideal values. They represent the band-pass filter designs and $W_{cen}$ is center frequency of band-pass filter (rad/sec)

Table 2.7: The high-Pass Filter designs corresponding to Figure 2.9

| k | $C_s$ | $L_p$ | Transfer Function | Cutoff (rad/sec) |
|---|---|---|---|---|
| 1 | 1.4142 | 0.7071 | $\frac{s^2}{s^2+1.4142s+1}$ | 1.00 |
| 2 | 0.7071 | 0.3536 | $\frac{s^2}{s^2+2.8281s+3.9995}$ | 1.87 |
| 3 | 0.4714 | 0.2357 | $\frac{s^2}{s^2+4.2427s+9}$ | 2.36 |
| 4 | 0.3536 | 0.1768 | $\frac{s^2}{s^2+5.6561s+16}$ | 2.54 |

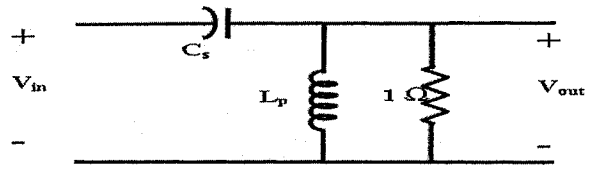


Figure 2.9: The modified High-pass filter when '$k$' is variable and the rest of the parameters are constant.

and $BW$ is bandwidth of band-pass filter.

In Table 2.8, the parameters of the GBT, $k_i$ and $b_i$ are kept constant and $a_i$ is variable. As a result, the bandwidth of the band-pass filter is increased when the magnitude of $a_1$ or $a_2$ decreases. The center frequency of the filter is moved to high frequency scale and low frequency scale when magnitude of $a_1$ and $a_2$ decrease respectively. The parameters of Table 2.8 are given corresponding to band-pass filter (Figure 2.10).

Table 2.8: The band-pass filter designs corresponding to Figure 2.10

| i | $a_i$ | $R_s$ | $L_s$ | $C_s$ | $R_p$ | $L_p$ | $C_p$ | $W_{cen}$ | BW |
|---|---|---|---|---|---|---|---|---|---|
| 1 | $-1$ | 0 | $L$ | $\frac{1}{L}$ | $\infty$ | $\frac{1}{C}$ | $C$ | 1.05 | 1.1 |
| 1 | $-0.5$ | $\frac{L}{4}$ | $\frac{3L}{4}$ | $\frac{1}{L}$ | $\frac{4}{C}$ | $\frac{1}{C}$ | $\frac{3C}{4}$ | 1.2 | 1.25 |
| 1 | $-0.1$ | $\frac{9L}{20}$ | $\frac{11L}{20}$ | $\frac{1}{L}$ | $\frac{20}{9C}$ | $\frac{1}{C}$ | $\frac{11C}{20}$ | 1.4 | 1.75 |
| 2 | 0.5 | $\frac{L}{4}$ | $L$ | $\frac{4}{3L}$ | $\frac{4}{C}$ | $\frac{4}{3C}$ | $C$ | 0.9 | 0.95 |
| 2 | 0.1 | $\frac{9L}{20}$ | $L$ | $\frac{20}{11L}$ | $\frac{20}{9C}$ | $\frac{20}{11C}$ | $C$ | 0.8 | 1.00 |

Table 2.9: The band-pass filter designs corresponding to Figure 2.11

| i | $b_i$ | $R_{sp1}$ | $L_{sp}$ | $R_{sp2}$ | $C_{sp}$ | $R_{ps1}$ | $L_{ps}$ | $R_{ps2}$ | $C_{ps}$ | $W_{cen}$ | $BW$ |
|---|---|---|---|---|---|---|---|---|---|---|---|
| 1 | 0.5 | $4L$ | $\frac{4L}{3}$ | $\infty$ | $\frac{1}{L}$ | 0 | $\frac{1}{C}$ | $\frac{1}{4C}$ | $\frac{4C}{3}$ | 0.75 | 0.5 |
| 1 | 0.1 | $\frac{20L}{9}$ | $\frac{20L}{11}$ | $\infty$ | $\frac{1}{L}$ | 0 | $\frac{1}{C}$ | $\frac{9}{20C}$ | $\frac{20C}{11}$ | 0.7 | 0.55 |
| 2 | $-0.5$ | $\infty$ | L | $4L$ | $\frac{3}{4L}$ | $\frac{1}{4C}$ | $\frac{3}{4C}$ | 0 | $C$ | 1.45 | 0.9 |
| 2 | $-0.1$ | $\infty$ | L | $\frac{20L}{9}$ | $\frac{11}{20L}$ | $\frac{9}{20C}$ | $\frac{11}{20C}$ | 0 | $C$ | 1.65 | 1.05 |

Table 2.10: The band-pass filter design corresponding to Figure 2.10

| i | $K_i$ | $R_s$ | $L_s$ | $C_s$ | $R_p$ | $L_p$ | $C_p$ | $W_{cen}$ | $BW$ |
|---|---|---|---|---|---|---|---|---|---|
| 1 | 2 | 0 | $2L$ | $\frac{1}{L}$ | $\infty$ | $\frac{1}{C}$ | $2C$ | 0.75 | 0.5 |
| 1 | 5 | 0 | $5L$ | $\frac{1}{L}$ | $\infty$ | $\frac{1}{C}$ | $5C$ | 0.5 | 0.2 |
| 2 | 2 | 0 | $L$ | $\frac{1}{2L}$ | $\infty$ | $\frac{1}{2C}$ | $C$ | 1.45 | 1.00 |
| 2 | 5 | 0 | $L$ | $\frac{1}{5L}$ | $\infty$ | $\frac{1}{5C}$ | $C$ | 2.3 | 0.95 |

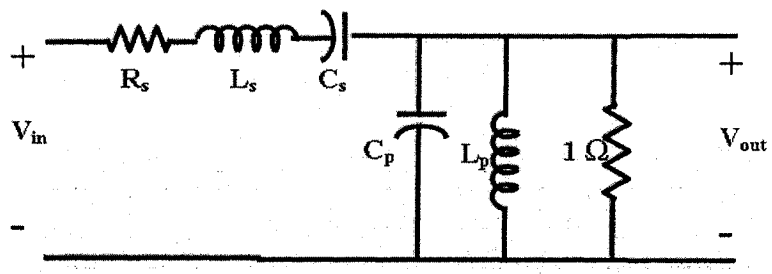


Figure 2.10: The band-pass filter when $a_i$ and $k_i$ change.

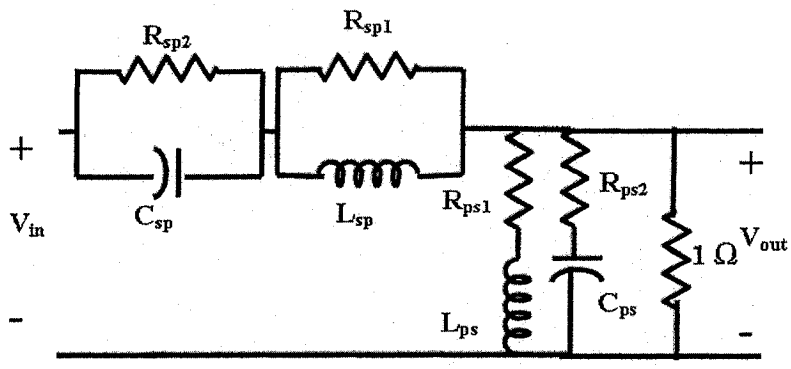


Figure 2.11: The band-pass filter when $b_i$ changes.

In the parameters of the GBT in Table 2.9, $k_i$ and $a_i$ are kept constant and $b_i$ is variable. As a result, the band-width of the band-pass filter is increased when the magnitude of $b_1$ or $b_2$ decreases. The center frequency of the filter is moved to low frequency scale and high frequency scale when magnitude of $b_1$ and $b_2$ decrease respectively. Table 2.9 shows the elements' values of the band-pass filter (Figure 2.11).

Table 2.10 represents another band-pass filter which has same filter structure of Figure 2.10. In Table 2.10, the parameters of the GBT, $a_i$ and $b_i$ are kept constant and $k_i$ is variable. As a result, the band-width of the bandpass filter is decreased when the magnitude of $K_1$ or $K_2$ increases. The center frequency of the filter is moved to low frequency scale and high frequency scale when magnitude of $K_1$ and $K_2$ increase respectively.

### 2.3.5 Band-elimination filter design

The GBT is used to design a band-elimination filter by the following transformation:

$$s = \frac{1}{K_1 \frac{(z+a_1)}{(z+b_1)} + K_2 \frac{(z+a_2)}{(z+b_2)}} \tag{2.3.19}$$

Table 2.11: The band-elimination filter designs corresponding to Figure 2.12

| i | $a_i$ | $R_{sp}$ | $L_{sp}$ | $C_{sp}$ | $R_{ps}$ | $L_{ps}$ | $C_{ps}$ | $W_{cen}$ | BW |
|---|---|---|---|---|---|---|---|---|---|
| 1 | $-1$ | $\infty$ | $L$ | $\frac{1}{L}$ | 0 | $\frac{1}{C}$ | $C$ | 1.05 | 1.05 |
| 1 | $-0.5$ | $4L$ | $L$ | $\frac{3}{4L}$ | $\frac{1}{4C}$ | $\frac{3}{4C}$ | $C$ | 1.2 | 1.8 |
| 1 | $-0.1$ | $\frac{20L}{9}$ | $L$ | $\frac{11}{20L}$ | $\frac{9}{20C}$ | $\frac{11}{20C}$ | $C$ | 1.4 | 2.45 |
| 2 | 0.5 | $4L$ | $\frac{4L}{3}$ | $\frac{1}{L}$ | $\frac{1}{4C}$ | $\frac{1}{C}$ | $\frac{4C}{3}$ | 0.9 | 1.35 |
| 2 | 0.1 | $\frac{20L}{9}$ | $\frac{20L}{11}$ | $\frac{1}{L}$ | $\frac{9}{20C}$ | $\frac{1}{C}$ | $\frac{20C}{11}$ | 0.8 | 1.4 |

Table 2.12: The band-elimination filter designs corresponding to Figure 2.13

| i | $b_i$ | $R_{sp1}$ | $L_{sp}$ | $R_{sp2}$ | $C_{sp}$ | $R_{ps1}$ | $L_{ps}$ | $R_{ps2}$ | $C_{ps}$ | Cutoff | Filter response |
|---|---|---|---|---|---|---|---|---|---|---|---|
| 1 | 0.5 | 0 | $L$ | $\frac{L}{4}$ | $\frac{4}{3L}$ | $\frac{4}{C}$ | $\frac{4}{3C}$ | $\infty$ | C | 0.55,3.15 | Band-elimination |
| 1 | 0.1 | 0 | $L$ | $\frac{9L}{20}$ | $\frac{20}{11L}$ | $\frac{20}{9C}$ | $\frac{20}{11C}$ | $\infty$ | $C$ | 0.5 | Low-pass |
| 2 | $-0.5$ | $\frac{L}{4}$ | $\frac{3L}{4}$ | 0 | $\frac{1}{L}$ | $\infty$ | $\frac{1}{C}$ | $\frac{4}{C}$ | $\frac{3C}{4}$ | 0.05, 1.95 | Band-elimination |
| 2 | $-0.1$ | $\frac{9L}{20}$ | $\frac{11L}{20}$ | 0 | $\frac{1}{L}$ | $\infty$ | $\frac{1}{C}$ | $\frac{20}{9C}$ | $\frac{11C}{20}$ | $\omega = 2.1$ | High-pass |

This is the inverse transformation of the band-pass of GBT (section 2.3.4)and the limitation of the transformation is similar to that of the band-pass transformation.

Applying the GBT to the Butterworth filter, two types of band-elimination filters are achieved and the circuit diagrams are shown in Figures 2.12 and 2.13. The first band-elimination filter is obtained by replacing the inductor of Butterworth filter by a series combination of two parallel branches, one contains a resistor and inductor and another contains a resistor and capacitor. The capacitor of Butterworth filter is replaced by two parallel branches, one branch contains the series combination of a resistor and an inductor and another contains a series connection of a resistor and capacitor. The second band-elimination filter is obtained by replacing the inductor of Butterworth filter by a parallel branch, one contains a series combination of resistor with inductor and another contains a series of resistor with capacitor. The capacitor of Butterworth filter is replaced by a series combination of two parallel branches, one branch contains a resistor and an inductor and another contains a resistor and capacitor.

Similar to the previous design, the parameters of the GBT are varied one parameter at a time keeping the rest of the parameters to the ideal values.

Tables 2.11, 2.12, 2.13 represent band-pass filter designs and $W_{cen}$ is the center frequency of band-pass filter (rad/sec) and BW is bandwidth of band-pass filter. In

Table 2.13: The band-elimination filter designs corresponding to Figure 2.12

| i | $K_i$ | $R_{sp}$ | $L_{sp}$ | $C_{sp}$ | $R_{ps}$ | $L_{ps}$ | $C_{ps}$ | $W_{cen}$ | BW |
|---|---|---|---|---|---|---|---|---|---|
| 1 | 2 | $\infty$ | $L$ | $\frac{2}{L}$ | 0 | $\frac{2}{C}$ | $C$ | 0.75 | 0.5 |
| 1 | 5 | $\infty$ | $L$ | $\frac{5}{L}$ | 0 | $\frac{5}{C}$ | $C$ | 0.5 | 0.2 |
| 2 | 2 | $\infty$ | $\frac{L}{2}$ | $\frac{1}{L}$ | 0 | $\frac{1}{C}$ | $\frac{C}{2}$ | 1.05 | 0.45 |
| 2 | 5 | $\infty$ | $\frac{L}{5}$ | $\frac{1}{L}$ | 0 | $\frac{1}{C}$ | $\frac{C}{5}$ | 1.65 | 0.5 |

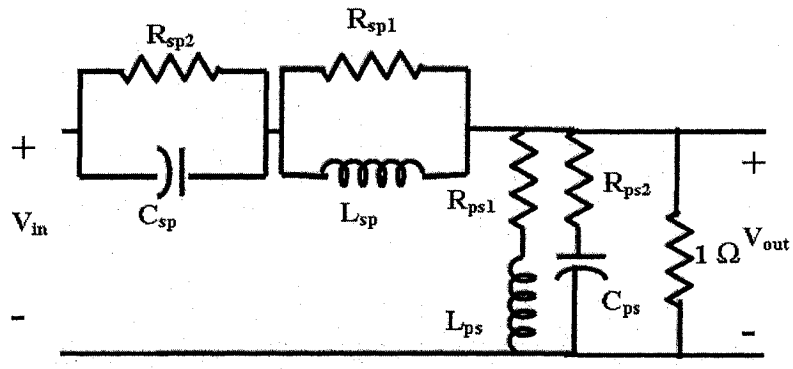


Figure 2.12: The Band-elimination filter designs when $a_i$ and $k_i$ change.

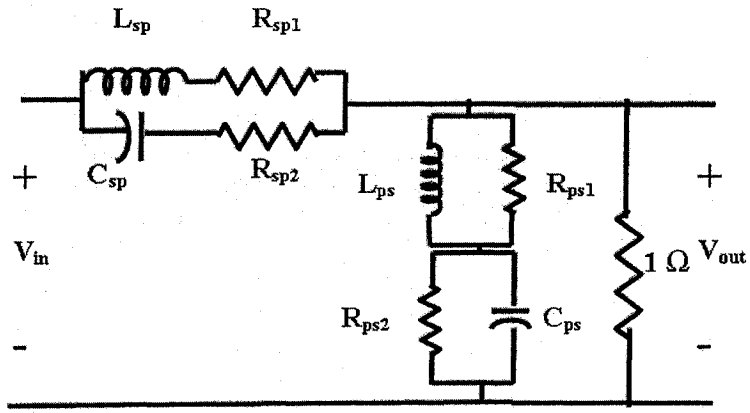


Figure 2.13: The band-elimination filter designs when $b_i$ changes.

the Table 2.11, parameters of the GBT, $k_i$ and $b_i$ are kept constant and $a_i$ is variable. As a result, the rejected-band width of the filter is increased when the magnitude of $a_1$ or $a_2$ decreases. The center frequency of the rejected-band width is moved to high frequency scale and low frequency scale when magnitude of $a_1$ and $a_2$ deceases respectively. The parameters of the Table 2.11 are given corresponding to Figure 2.12.

In the parameters of the GBT in Table 2.12, $k_i$ and $a_i$ are kept constant and $b_i$ is varied. As a result, the band-elimination filter is turned to low-pass and high-pass filter when the magnitude of $b_1$ and $b_2$ decreases respectively. The parameters of the Table 2.12 is corresponding to Figure 2.13.

In Table 2.13, the parameters of the GBT, $a_i$ and $b_i$ are kept constant and $k_i$ is variable. As a result, the rejected-band width of the filter is decreased when $K_1$ increases or $K_2$ decreases. The center frequency of the rejected band is moved to low frequency scale and high frequency scale when magnitude of $K_1$ and $K_2$ increases respectively. The parameters of the Table 2.13 are corresponding to Figure 2.12.

### 2.3.6 Properties of the GBT as applied to second-order Butterworth low-pass filters

Generalized bilinear transformation is applied to a second order Butterworth filter and the various designed filters are shown in sections 2.3.2, 2.3.3, 2.3.4 and 2.3.5. Depending on the values of the parameters of the transformation, different filter responses can be achieved. From the above discussion, some properties of the GBT on second order Butterworth filter are figured out which are discussed below-

(a) Low pass filter: This is obtained by putting '$a$' as negative and '$b$' positive in the Generalized Bilinear Transformation.

- Bandwidth of filter is decreased when '$b$' decreases.
- Bandwidth of filter is increased when '$a$' increases.
- Bandwidth of filter is decreased when '$k$' increases.

(b) High pass filter: This is obtained putting '$a$' is positive and '$b$' negative in the Generalized Bilinear Transformation.

- Bandwidth of filter is increased when '$b$' increases.
- Bandwidth of filter is decreased when '$a$' decreases.
- Bandwidth of filter is decreased when '$k$' increases.

(c) Band pass filter: The transformation of band pass filter is the combination of the transformations of those used for low pass and high pass filters.

- Bandwidth of the filter is increased when the magnitude of '$a_1$' or '$a_2$' decreases.
- Bandwidth of the filter is decreased when the magnitude of '$b_1$' or '$b_2$' decreases.
- Bandwidth of the filter is decreased when '$K_1$' or '$K_2$' increases.
- Bandwidth of the filter is moved to high frequency when '$a_1$' or '$b_2$' decreases or '$K_2$' increases.
- bandwidth of the filter is moved to low frequency when '$a_2$' or '$b_1$' decreases or '$K_1$' increases.

(d) Band elimination filter: The transformation of the band-elimination filter is the reciprocal of the transformation of band pass filter.

- Rejected bandwidth of the filter is increased when $|a_1|$ or $|a_2|$ decreases.
- Band-elimination filter turns to low pass filter when $|b_1|$ decreases.
- Band-elimination filter turns to high pass filter when $|b_2|$ decreases.
- Rejected bandwidth starts decreasing and rejected band moves to low frequency when '$K_1$' increases.
- Rejected bandwidth starts decreasing and rejected band moves to high frequency when '$K_2$' increases.

## 2.4 Generation of VSHP by the gyrator networks

The stability is one of the main concerns in 2D filter design and a 2D transfer function is guaranteed to be stable if the denominator of the transfer function is satisfied to be Very Strict Hurwitz Polynomial (VSHP) [9] which can ensure that there is no singularity in the right half of the biplane. To generate VSHPs from the doubly terminated gyrator networks (Figures 2.1 and 2.2), two second order RLC filters are replaced with the impedances of the gyrator filters. Details are discussed below:

### 2.4.1 VSHP generated from filter 1 using the Butterworth polynomials

Second-order Butterworth filters are replaced by $Z_1$ and $Z_2$ in the transfer function of filter 1, equation (2.2.5) to generate VSHP. In the transfer function $Z_1$ in terms of $s_1$ and $Z_2$ in terms of $s_2$. Impedance of the doubly terminated second-order Butterworth filter is in the following.

$$Z_1 = \frac{L_B C_B s_1^2 + L_B s_1 + 1}{1 + C_B s_1} \tag{2.4.1}$$

$$Z_2 = \frac{L_B C_B s_2^2 + L_B s_2 + 1}{1 + C_B s_2} \tag{2.4.2}$$

where, $L_B = 1.4142$ and $C_B = 0.7071$.

The overall transfer function of filter 1 is obtained in 2D domain as

$$H_{a1B2D}(s_1, s_2) = \frac{N_{a1B2D}(s_1, s_2)}{D_{a1B2D}(s_1, s_2)} \tag{2.4.3}$$

where,

$$\begin{aligned} N_{a1B2D}(s_1, s_2) &= \{g^2 s_2^2 + (g^2 L_B^2 C_B + g L_B C_B^2) s_2 + g^2 L_B C_B + g L_B C_B\} s_1^2 \\ &+ \{g^2 s_2^2 L_B^2 C_B + (L_B^2 C_B^4 + g^2 L_B^4 C_B^2 + g L_B^3 C_B^3) s_2 \\ &+ g^2 L_B^3 C_B^2 + L_B^2 C_B^3 + g L_B^3 C_B^2\} s_1 + g^2 s_2^2 L_B C_B \\ &+ (g^2 L_B^3 C_B^2 + g L_B^2 C_B^3 + L_B^2 C_B^3) s_2 + L_B^2 C_B^2 + g^2 L_B^2 C_B^2 \\ &+ g L_B^2 C_B^2 \end{aligned} \tag{2.4.4}$$

$$\begin{aligned} D_{a1B2D}(s_1, s_2) &= \{2g^2 s_2^2 + (2L_B^2 g^2 C_B + L_B C_B^2 + L_B g^2 C_B^2) s_2 \\ &+ 3L_B g^2 C_B + L_B C_B\} s_1^2 + \{2g^2 s_2^2 L_B^2 C_B + (2g^2 L_B^4 C_B^2 \\ &+ L_B^3 g^2 C_B^3 + L_B^3 C_B^3 + 2L_B^2 C_B^4) s_2 + 3L_B^3 g^2 C_B^2 + L_B^3 C_B^2 \\ &+ 2L_B^2 C_B^3\} s_1 + \{2g^2 s_2^2 L_B C_B + (3L_B^2 C_B^3 + 2L_B^3 g^2 C_B^2 \\ &+ L_B^2 g^2 C_B^3) s_2 + 3L_B^2 C_B^2 + 3L_B^2 g^2 C_B^2\} \end{aligned} \tag{2.4.5}$$

Equation (2.4.5) can be expressed as following.

$$D_{a1B2D}(s_1, s_2) = A_{1B} s_1^2 s_2^2 + B_{1B} s_1^2 s_2 + C_{1B} s_1 s_2^2 + D_{1B} s_1^2 + E_{1B} s_2^2 + F_{1B} s_1 s_2 + G_{1B} s_1 + H_{1B} s_2 + I_{1B} \tag{2.4.6}$$

where,

$$A_{1B} = 2g^2 \tag{2.4.7}$$

$$B_{1B} = 2L_B^2 g^2 C_B + L_B C_B^2 + L_B g^2 C_B^2 \tag{2.4.8}$$

$$C_{1B} = 2g^2 L_B^2 C_B \tag{2.4.9}$$

$$D_{1B} = 3L_B g^2 C_B + L_B C_B \tag{2.4.10}$$

$$E_{1B} = 2g^2 L_B C_B \tag{2.4.11}$$

$$F_{1B} = 2g^2 L_B^4 C_B^2 + L_B^3 g^2 C_B^3 + L_B^3 C_B^3 + 2L_B^2 C_B^4 \tag{2.4.12}$$

$$G_{1B} = 3L_B^3 g^2 C_B^2 + L_B^3 C_B^2 + 2L_B^2 C_B^3 \tag{2.4.13}$$

$$H_{1B} = 3L_B^2 C_B^3 + 2L_B^3 g^2 C_B^2 + L_B^2 g^2 C_B^3) \tag{2.4.14}$$

$$I_{1B} = 3L_B^2 C_B^2 + 3L_B^2 g^2 C_B^2 \tag{2.4.15}$$

If $s_2 = 1$ in equation (2.4.5), $D_{a1B2D}$ should be strictly Hurwitz polynomial in $s_1$ domain.

$$\begin{aligned} D_{a1B2D}(s_1, 1) &= (A_{1B} + B_{1B} + D_{1B})s_1^2 + (C_{1B} + F_{1B} + G_{1B})s_1 + (E_{1B} + H_{1B} + I_{1B}) \\ &= a_{1B}s_1^2 + b_{1B}s_1 + c_{1B} \end{aligned} \tag{2.4.16}$$

where,

$$a_{1B} = (A_{1B} + B_{1B} + D_{1B}) \tag{2.4.17}$$

$$b_{1B} = (C_{1B} + F_{1B} + G_{1B}) \tag{2.4.18}$$

$$c_{1B} = (E_{1B} + H_{1B} + I_{1B}) \tag{2.4.19}$$

Step 1: Roots of $D_{a1B2D}(s_1, 1)$ are $T_{1B}(g) = \frac{-b_{1B} \pm \sqrt{(b_{1B}^2 - 4a_{1B}c_{1B})}}{2a_{1B}}$.

For the all values of gyrator constant $D_{a1B2D}(s_1, 1)$ is strictly Hurwitz polynomial in $s_1$ domain is shown in the Figure 2.14.

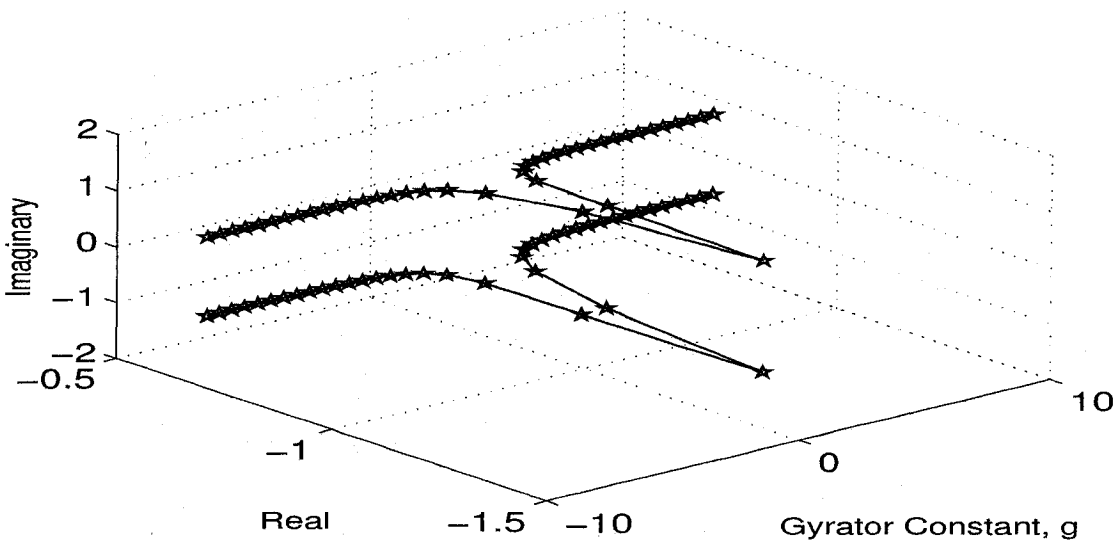


Figure 2.14: 3D plot of the roots of $D_{a1B2D}(s_1, 1)$ with respect of g.

Step 2: In the equation (2.4.6), substituting $s_1 = j\Omega_1$, $s_2 = j\Omega_2$, where, $j = \sqrt{-1}$. The resultant equation (2.4.20) is arranged in the form of Inners [26] as follows.

$$\begin{aligned} D_{a1B2D}(j\Omega_1, j\Omega_2) &= A_{1B}(\Omega_1^2\Omega_2^2) - jB_{1B}(\Omega_1^2\Omega_2) - jC_{1B}(\Omega_1\Omega_2^2) - D_{1B}(\Omega_1^2) - E_{1B}(\Omega_2^2) \\ &- F_{1B}(\Omega_1\Omega_2) + jG_{1B}\Omega_1 + jH_{1B}\Omega_2 + I_{1B} \end{aligned} \tag{2.4.20}$$

Equation (2.4.20) is expressed as following.

$$D_{a1B2D}(j\Omega_1, j\Omega_2) = (A_{1B}\Omega_2^2 - D_{1B})\Omega_1^2 - (F_{1B}\Omega_2)\Omega_1 + (-E_{1B}\Omega_2^2 + I) + j\{(-B_{1B}\Omega_2)\Omega_1^2 + (G_{1B} - C_{1B}\Omega_2^2)\Omega_1 + H_{1B}\Omega_2\} \quad (2.4.21)$$

$$\triangle_{a1B2D} = \begin{bmatrix} (-B_{1B}\Omega_2) & (-C_{1B}\Omega_2^2 + G_{1B}) & H_{1B} & 0 \\ 0 & (-B_{1B}\Omega_2) & (-C_{1B}\Omega_2^2 + G_{1B}) & H_{1B} \\ 0 & (A_{1B}\Omega_2^2 - D_{1B}) & -(F_{1B}\Omega_2) & (-E_{1B}\Omega_2^2 + I_{1B}) \\ (A_{1B}\Omega_2^2 - D_{1B}) & -(F_{1B}\Omega_2) & (-E_{1B}\Omega_2^2 + I_{1B}) & 0 \end{bmatrix}$$

$$\triangle_{1_{a1B2D}} = A_{1B}C_{1B}\Omega_2^4 + (B_{1B}F_{1B} - A_{1B}G_{1B} - C_{1B}D_{1B})\Omega_2^2 + D_{1B}G_{1B} \quad (2.4.22)$$

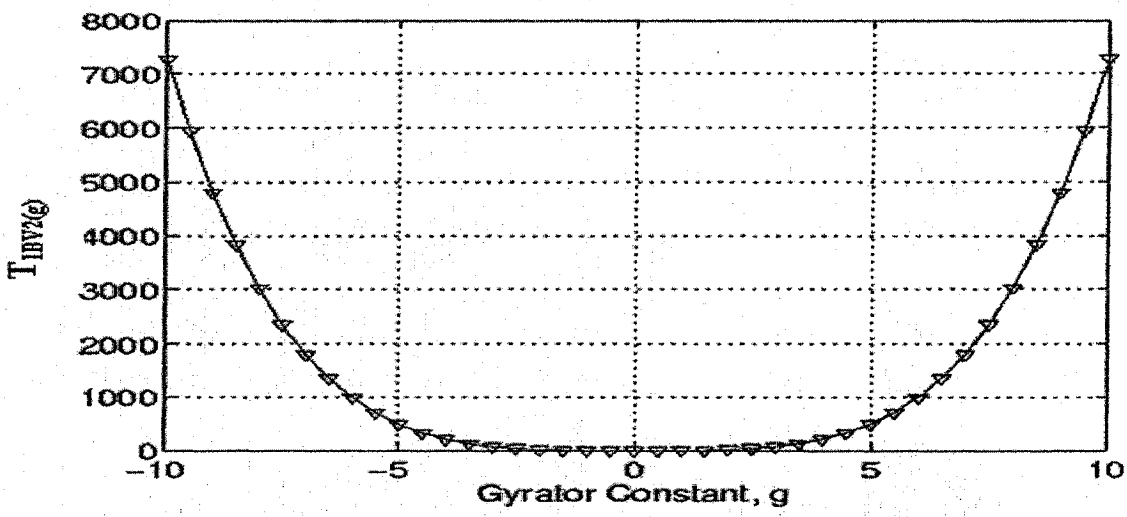


Figure 2.15: Plot of $T_{1BV2}(g)$ vs g .

Let, $T_{1BV2}(g) = (B_{1B}F_{1B} - A_{1B}G_{1B} - C_{1B}D_{1B})$. In the equation 2.4.22, it is observed that $\triangle_1 \geq 0$ for all the values of $\Omega_2$ and g, if $T_{1BV2}(g) \geq 0$ or $A_{1B}C_{1B}\Omega_2^4 + D_{1B}G_{1B} \geq T_{1BV2}(g)\Omega_2^2$. Figure 2.15 shows that $T_{1BV2}$ is always positive for all the values of g.

Step 3: $D_{a1B2D}$ is satisfied to be VSHP, which is shown in the following:

$$\begin{aligned} D_{a1B2D}(s_1,s_2) &= A_{1B}s_1^2s_2^2 + B_{1B}s_1^2s_2 + C_{1B}s_1s_2^2 + D_{1B}s_1^2 + E_{1B}s_2^2 \\ &+ F_{1B}s_1s_2 + G_{1B}s_1 + H_{1B}s_2 + I_{1B} \end{aligned} \tag{2.4.23}$$

$$\begin{aligned} D_{a1B2D}(\frac{1}{s_1},s_2) &= A_{1B}\frac{1}{s_1^2}s_2^2 + B_{1B}\frac{1}{s_1^2}s_2 + C_{1B}\frac{1}{s_1}s_2^2 + D_{1B}\frac{1}{s_1^2} + E_{1B}s_2^2 \\ &+ F_{1B}\frac{1}{s_1}s_2 + G_{1B}s_1 + H_{1B}s_2 + I_{1B} \end{aligned} \tag{2.4.24}$$

$$\begin{aligned} D_{a1B2D}(s_1,\frac{1}{s_2}) &= A_{1B}s_1^2\frac{1}{s_2^2} + B_{1B}s_1^2\frac{1}{s_2} + C_{1B}s_1\frac{1}{s_2^2} + D_{1B}s_1^2 + E_{1B}\frac{1}{s_2^2} \\ &+ F_{1B}s_1\frac{1}{s_2} + G_{1B}s_1 + H_{1B}\frac{1}{s_2} + I_{1B} \end{aligned} \tag{2.4.25}$$

$$\begin{aligned} D_{a1B2D}(\frac{1}{s_1},\frac{1}{s_2}) &= A_{1B}\frac{1}{s_1^2}\frac{1}{s_2^2} + B_{1B}\frac{1}{s_1^2}\frac{1}{s_2} + C_{1B}\frac{1}{s_1}\frac{1}{s_2^2} + D_{1B}\frac{1}{s_1^2} + E_{1B}\frac{1}{s_2^2} \\ &+ F_{1B}\frac{1}{s_1}\frac{1}{s_2} + G_{1B}\frac{1}{s_1} + H_{1B}\frac{1}{s_2} + I_{1B} \end{aligned} \tag{2.4.26}$$

So the denominator of the transfer function, $H_{a1B2D}$ is generated from filter1 using second-order butterworth polynomials, that satisfies to be VSHP.

### 2.4.2 VSHP generated from filter 1 using Gargour&Ramachadran polynomials

$Z_1$ and $Z_2$ in the transfer function of filter 1, equation(2.2.5) are replaced the Gargour&Ramachadran filters by to generate VSHP. In equation(2.2.5) $Z_1$ and $Z_2$ are expressed in term of $s_1$ and $s_2$ respectively.

$$Z_1 = \frac{L_GC_Gs_1^2 + L_Gs_1 + 1}{1 + C_Gs_1} \tag{2.4.27}$$

$$Z_2 = \frac{L_GC_Gs_2^2 + L_Gs_2 + 1}{1 + C_Gs_2} \tag{2.4.28}$$

For Gargour&Ramachadran filter, $L_G = 2.103$ and $C_G = 0.3362$.

The resultant transfer function is obtained in 2D domain as

$$H_{a1G2D}(s_1, s_2) = \frac{N_{a1G2D}(s_1, s_2)}{D_{a1G2D}(s_1, s_2)} \tag{2.4.29}$$

where,

$$\begin{aligned} N_{a1G2D}(s_1, s_2) &= \{g^2 s_2^2 + (g^2 L_G^2 C_G + g L_G C_G^2) s_2 + g^2 L_G C_G + g L_G C_G\} s_1^2 \\ &+ \{g^2 s_2^2 L_G^2 C_G + (L_G^2 C_G^4 + g^2 L_G^4 C_G^2 + g L_G^3 C_G^3) s_2 \\ &+ g^2 L_G^3 C_G^2 + L_G^2 C_G^3 + g L_G^3 C_G^2\} s_1 + g^2 s_2^2 L_G C_G \\ &+ (g^2 L_G^3 C_G^2 + g L_G^2 C_G^3 + L_G^2 C_G^3) s_2 + L_G^2 C_G^2 + g^2 L_G^2 C_G^2 \\ &+ g L_G^2 C_G^2 \end{aligned} \tag{2.4.30}$$

$$\begin{aligned} D_{a1G2D}(s_1, s_2) &= \{2g^2 s_2^2 + (2L_G^2 g^2 C_G + L_G C_G^2 + L_G g^2 C_G^2) s_2 \\ &+ 3L_G g^2 C_G + L_G C_G\} s_1^2 + \{2g^2 s_2^2 L_G^2 C_G + (2g^2 L_G^4 C_G^2 \\ &+ L_G^3 g^2 C_G^3 + L_G^3 C_G^3 + 2L_G^2 C_G^4) s_2 + 3L_G^3 g^2 C_G^2 + L_G^3 C_G^2 \\ &+ 2L_G^2 C_G^3\} s_1 + \{2g^2 s_2^2 L_G C_G + (3L_G^2 C_G^3 + 2L_G^3 g^2 C_G^2 \\ &+ L_G^2 g^2 C_G^3) s_2 + 3L_G^2 C_G^2 + 3L_G^2 g^2 C_G^2\} \end{aligned} \tag{2.4.31}$$

The denominator of the transfer function, $H_{a1G2D}$ can be expressed as below:

$$D_{a1G2D}(s_1, s_2) = A_{1G} s_1^2 s_2^2 + B_{1G} s_1^2 s_2 + C_{1G} s_1 s_2^2 + D_{1G} s_1^2 + E_{1G} s_2^2 + F_{1G} s_1 s_2 + G_{1G} s_1 + H_{1G} s_2 + I_{1G} \tag{2.4.32}$$

where,

$$A_{1G} = 2g^2 \tag{2.4.33}$$

$$B_{1G} = 2L_G^2 g^2 C_G + L_G C_G^2 + L_G g^2 C_G^2 \tag{2.4.34}$$

$$C_{1G} = 2g^2 L_G^2 C_G \tag{2.4.35}$$

$$D_{1G} = 3L_G g^2 C_G + L_G C_G \tag{2.4.36}$$

$$E_{1G} = 2g^2 L_G C_G \tag{2.4.37}$$

$$F_{1G} = 2g^2 L_G^4 C_G^2 + L_G^3 g^2 C_G^3 + L_G^3 C_G^3 + 2L_G^2 C_G^4 \tag{2.4.38}$$

$$G_{1G} = 3L_G^3 g^2 C_G^2 + L_G^3 C_G^2 + 2L_G^2 C_G^3 \tag{2.4.39}$$

$$H_{1G} = 3L_G^2 C_G^3 + 2L_G^3 g^2 C_G^2 + L_G^2 g^2 C_G^3) \tag{2.4.40}$$

$$I_{1G} = 3L_G^2 C_G^2 + 3L_G^2 g^2 C_G^2 \tag{2.4.41}$$

Substituting $s_2 = 1$ in $D_{a1G2D}$, it has shown that the resultant polynomial is strictly Hurwitz polynomial in $s_1$ domain (Figure 2.16).

$$\begin{aligned} D_{a1G2D}(s_1, 1) &= (A_{1G} + B_{1G} + D_{1G})s_1^2 + (C_{1G} + F_{1G} + G_{1G})s_1 + (E_{1G} + H_{1G} + I_{1G}) \\ &= a_{1G}s_1^2 + b_{1G}s_1 + c_{1G} \end{aligned} \tag{2.4.42}$$

where,

$$a_{1G} = (A_{1G} + B_{1G} + D_{1G}) \tag{2.4.43}$$

$$b_{1G} = (C_{1G} + F_{1G} + G_{1G}) \tag{2.4.44}$$

$$c_{1G} = (E_{1G} + H_{1G} + I_{1G}) \tag{2.4.45}$$

Step 1: Roots of $D_{a1G2D}(s_1, 1)$ are $T_{1G}(g) = \frac{-b_{1G} \pm \sqrt{(b_{1G}^2 - 4a_{1G}c_{1G})}}{2a_{1G}}$.

$D_{a1G2D}(s_1, 1)$ is strictly Hurwitz polynomial in $s_1$ domain for all the values of g (Figure 2.16).

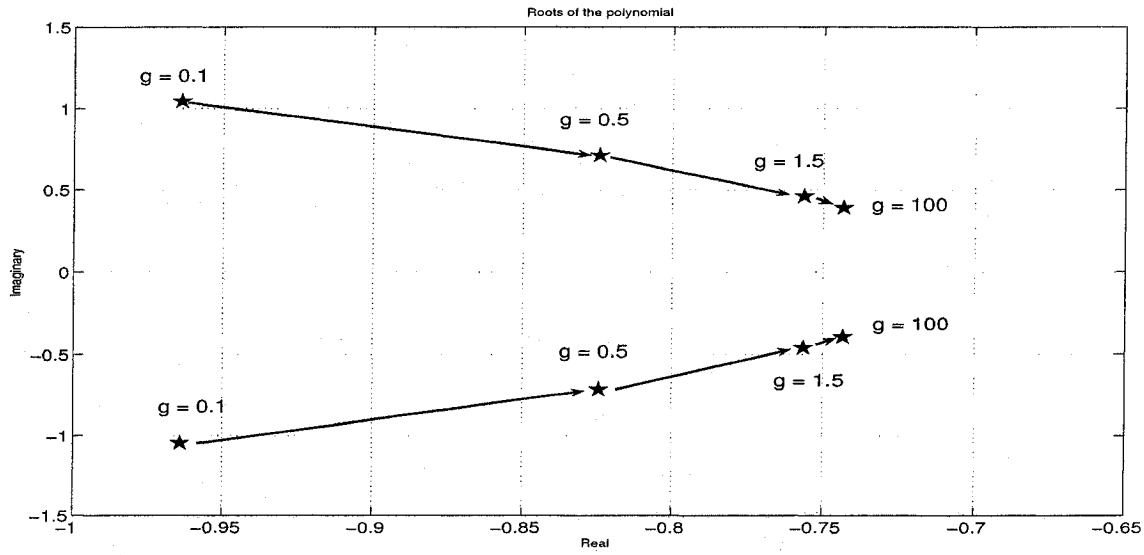


Figure 2.16: The roots of $D_{a1G2D}(s_1, 1)$ for the different values of g.

Step 2: Similar to section 2.4.1, substituting $s_1 = j\Omega_1$, $s_2 = j\Omega_2$ in $D_{a1G2D}$. The resultant equation (2.4.46) is arranged in the form of Inners [26] as below:

$$\begin{aligned} D_{a1G2D}(j\Omega_1, j\Omega_2) &= A_{1G}\Omega_1^2\Omega_2^2 - jB_{1G}\Omega_1^2\Omega 2 - jC_{1G}\Omega_1\Omega_2^2 - D_{1G}\Omega_1^2 - E_{1G}\Omega_2^2 \\ &- F_{1G}\Omega_1\Omega_2 + jG_{1G}\Omega_1 + jH_{1G}\Omega_2 + I_{1G} \end{aligned} \tag{2.4.46}$$

$$D_{a1G2D}(j\Omega_1, j\Omega_2) = (A_{1G}\Omega_2^2 - D_{1G})\Omega_1^2 - (F_{1G}\Omega_2)\Omega_1 + (-E_{1G}\Omega_2^2 + I_{1G}) + j\{(-B_{1G}\Omega_2)\Omega_1^2 + (G_{1G} - C_{1G}\Omega_2^2)\Omega_1 + H_{1G}\Omega_2\} \quad (2.4.47)$$

$$\triangle_{a1G2D} = \begin{bmatrix} (-B_{1G}\Omega_2) & (-C_{1G}\Omega_2^2 + G_{1G}) & H_{1G} & 0 \\ 0 & (-B_{1G}\Omega_2) & (-C_{1G}\Omega_2^2 + G_{1G}) & H_{1G} \\ 0 & (A_{1G}\Omega_2^2 - D_{1G}) & -(F_{1G}\Omega_2) & (-E_{1G}\Omega_2^2 + I_{1G}) \\ (A_{1G}\Omega_2^2 - D_{1G}) & -(F_{1G}\Omega_2) & (-E_{1G}\Omega_2^2 + I_{1G}) & 0 \end{bmatrix}$$

$$\triangle_{1_{a1G2D}} = A_{1G}C_{1G}\Omega_2^4 + (B_{1G}F_{1G} - A_{1G}G_{1G} - C_{1G}D_{1G})\Omega_2^2 + D_{1G}G_{1G} \quad (2.4.48)$$

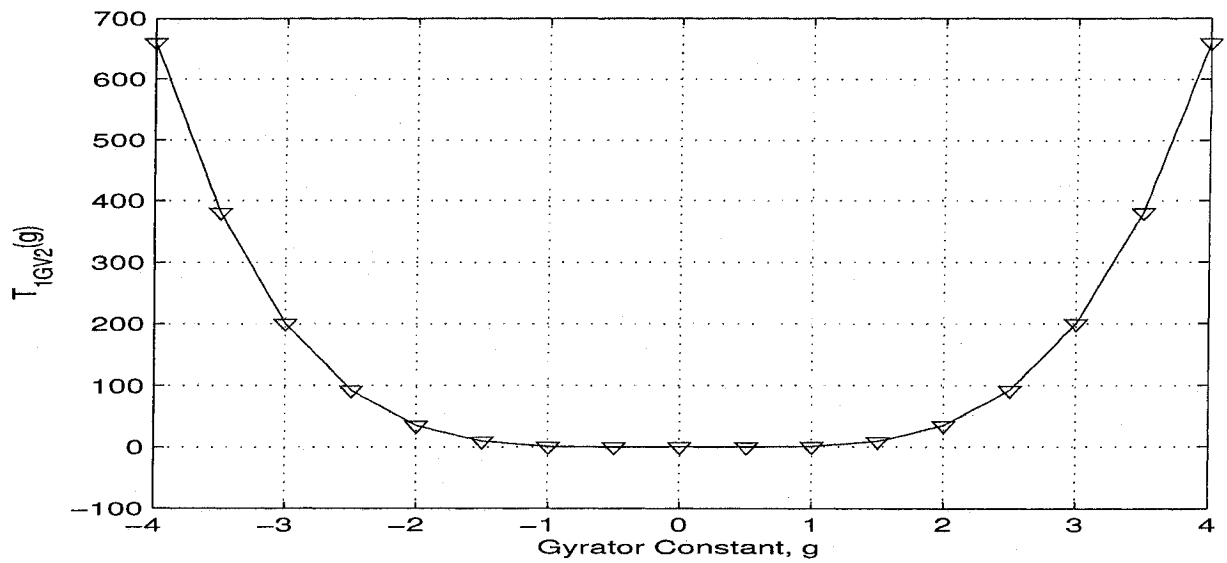


Figure 2.17: Plot of $T_{1GV2}(g)$ vs g .

Let, $T_{1GV2}(g) = (B_{1G}F_{1G} - A_{1G}G_{1G} - C_{1G}D_{1G})$. From equation (2.4.48), it is observed that $\triangle_1 \geq 0$ for all the values of $\Omega_2$ and g, which is proved in Figure 2.17. Hence it is shown that $T_{1GV2}$ always positive for the values of g.

Step 3: $D_{a1G}$ is satisfied the step 3 to be VSHP, which is shown in below:

$$D_{a1G2D}(s_1,s_2) = A_{1G}s_1^2s_2^2 + B_{1G}s_1^2s_2 + C_{1G}s_1s_2^2 + D_{1G}s_1^2 + E_{1G}s_2^2 + F_{1G}s_1s_2 + G_{1G}s_1 + H_{1G}s_2 + I_{1G} \quad (2.4.49)$$

$$D_{a1G2D}(\frac{1}{s_1},s_2) = A_{1G}\frac{1}{s_1^2}s_2^2 + B_{1G}\frac{1}{s_1^2}s_2 + C_{1G}\frac{1}{s_1}s_2^2 + D_{1G}\frac{1}{s_1^2} + E_{1G}s_2^2 + F_{1G}\frac{1}{s_1}s_2 + G_{1G}s_1 + H_{1G}s_2 + I_{1G} \quad (2.4.50)$$

$$D_{a1G2D}(s_1,\frac{1}{s_2}) = A_{1G}s_1^2\frac{1}{s_2^2} + B_{1G}s_1^2\frac{1}{s_2} + C_{1G}s_1\frac{1}{s_2^2} + D_{1G}s_1^2 + E_{1G}\frac{1}{s_2^2} + F_{1G}s_1\frac{1}{s_2} + G_{1G}s_1 + H_{1G}\frac{1}{s_2} + I_{1G} \quad (2.4.51)$$

$$D_{a1G2D}(\frac{1}{s_1},\frac{1}{s_2}) = A_{1G}\frac{1}{s_1^2}\frac{1}{s_2^2} + B_{1G}\frac{1}{s_1^2}\frac{1}{s_2} + C_{1G}\frac{1}{s_1}\frac{1}{s_2^2} + D_{1G}\frac{1}{s_1^2} + E_{1G}\frac{1}{s_2^2} + F_{1G}\frac{1}{s_1}\frac{1}{s_2} + G_{1G}\frac{1}{s_1} + H_{1G}\frac{1}{s_2} + I_{1G} \quad (2.4.52)$$

$H_{a1G2D}$ is generated from filter1 using second-order Gargour&Ramachandran polynomials and the denominator of the transfer function, $H_{a1G2D}$ is satisfied to be VSHP.

### 2.4.3 VSHP generated from filter 2 using the Butterworth polynomials

Second-order Butterworth filters are used in the transfer function, equation (2.2.10) to generate a VSHP and similarly, as in the previous sections 2.4.1 and 2.4.2, $Z_1$ and $Z_2$ are replaced by the Butterworth filter and $Z_3$ is replaced by a resistive component to satisfy VSHP. The overall transfer function.

$$Z_1 = \frac{L_BC_Bs_1^2 + L_Bs_1 + 1}{1 + C_Bs_1} \quad (2.4.53)$$

$$Z_2 = \frac{L_BC_Bs_2^2 + L_Bs_2 + 1}{1 + C_Bs_2} \quad (2.4.54)$$

$$Z_3 = 1\Omega(Resistive). \quad (2.4.55)$$

$$H_{a2B2D}(s_1, s_2) = \frac{N_{a2B2D}(s_1, s_2)}{D_{a2B2D}(s_1, s_2)} \tag{2.4.56}$$

$$\begin{aligned} N_{a2B2D}(s_1, s_2) &= \{gs_2^2 + (gL_B^2C_B + gL_BC_B^2)s_2 + 2L_BC_Bg\}s_1^2 \\ &+ \{(gL_B^2C_B + gL_BC_B^2)s_2^2 + (gL_B^4C_B^2 + 2gL_B^3C_B^3 + L_B^2C_B^4)s_2 \\ &+ 2gL_B^3C_B^2 + L_B^2C_B^3 + gL_B^2C_B^3\}s_1 + 2L_BC_Bgs_2^2 \\ &+ (2gL_B^3C_B^2 + L_B^2C_B^3 + gL_B^2C_B^3)s_2 + L_B^2C_B^2 + 3gL_B^2C_B^2 \end{aligned} \tag{2.4.57}$$

$$\begin{aligned} D_{a2B2D}(s_1, s_2) &= \{(g^2+1)s_2^2 + (L_B^2C_B + L_BC_B^2g^2 + 2L_BC_B^2 + L_B^2C_Bg^2)s_2 \\ &+ 3L_BC_B + 2L_BC_Bg^2\}s_1^2 + \{(L_B^2C_B + LC_B^2g^2 + 2LC_B^2 \\ &+ L^2C_Bg^2)s_2^2 + (4L^3C_B^3 + L^4C_B^2 + L^4C_B^2g^2 + 3L^2C_B^4 \\ &+ 2L^3C_B^3g^2)s_2 + L^2C_B^3g^2 + 5L^2C_B^3 + 3L^3C_B^2 \\ &+ 2L^3C_B^2g^2\}s_1 + (3LC_B + 2LC_Bg^2)s_2^2 + (L^2C_B^3g^2 \\ &+ 5L^2C_B^3 + 3L^3C_B^2 + 2L^3C_B^2g^2)s_2 + 8L^2C_B^2 + 3L^2C_B^2g^2 \end{aligned} \tag{2.4.58}$$

Let, the denominator of the transfer function, $H_{2B}$ is obtained in 2D domain,

$$D_{a2B2D}(s_1, s_2) = A_{2B}s_1^2s_2^2 + B_{2B}s_1^2s_2 + C_{2B}s_1s_2^2 + D_{2B}s_1^2 + E_{2B}s_2^2 + F_{2B}s_1s_2 + G_{2B}s_1 + H_{2B}s_2 + I_{2B} \tag{2.4.59}$$

where,

$$A_{2B} = (g^2+1) \tag{2.4.60}$$

$$B_{2B} = (L^2C_B + LC_B^2g^2 + 2LC_B^2 + L^2C_Bg^2) \tag{2.4.61}$$

$$C_{2B} = L^2C_B + LC_B^2g^2 + 2LC_B^2 + L^2C_Bg^2 \tag{2.4.62}$$

$$D_{2B} = 3LC_B + 2LC_Bg^2 \tag{2.4.63}$$

$$E_{2B} = (3LC_B + 2LC_Bg^2) \tag{2.4.64}$$

$$F_{2B} = 4L^3C_B^3 + L^4C_B^2 + L^4C_B^2g^2 + 3L^2C_B^4 + 2L^3C_B^3g^2 \tag{2.4.65}$$

$$G_{2B} = L^2C_B^3g^2 + 5L^2C_B^3 + 3L^3C_B^2 + 2L^3C_B^2g^2 \tag{2.4.66}$$

$$H_{2B} = (L^2C_B^3g^2 + 5L^2C_B^3 + 3L^3C_B^2 + 2L^3C_B^2g^2) \tag{2.4.67}$$

$$I_{2B} = 8L^2C_B^2 + 3L^2C_B^2g^2 \tag{2.4.68}$$

Substituting $s_2 = 1$ in the equation (2.4.59) and it has been shown in Figure 2.18 that the resultant polynomial, $D_{a2B2D}(s_1, 1)$ is a strictly Hurwitz polynomial in $s_1$ domain.

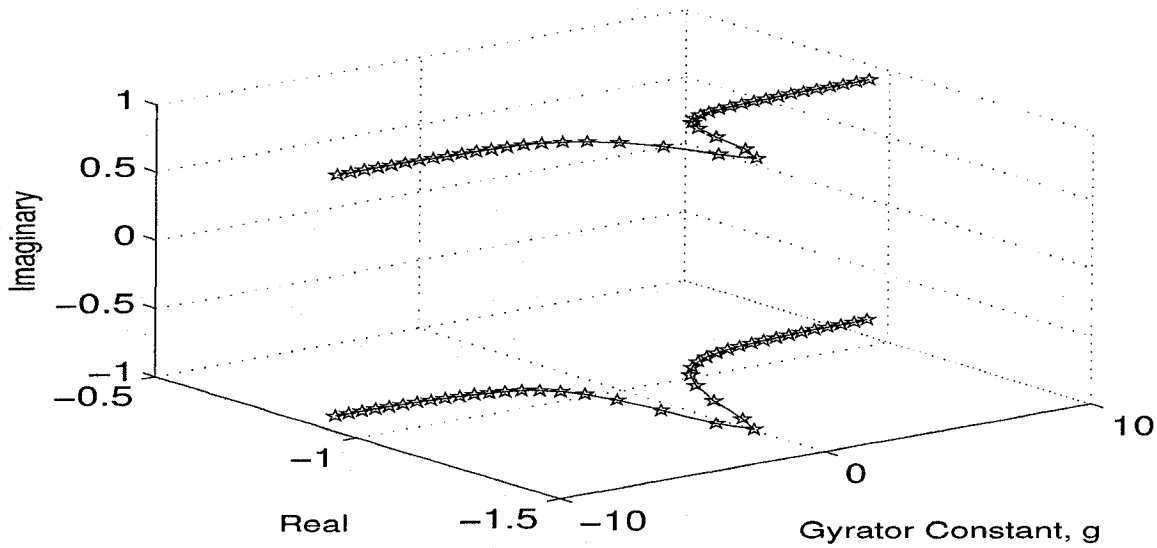


Figure 2.18: The roots of $D_{a2B2D}(s_1, 1)$ for the different values of g.

Similar to equations (2.4.48), (2.4.46), (2.4.47) and (2.4.2), it has been shown that $T_{2BV2}(g) = (B_{2B}F_{2B} - A_{2B}G_{2B} - C_{2B}D_{2B})$ is positive for the all values of g (Figure 2.19).

Similarly, from the equations (2.4.49), (2.4.50), (2.4.51) and (2.4.52), it can be shown that the denominator of transfer function, $H_{a2B2D}(s_1, s_2)$ generated using the Butterworth filters is satisfied to be VSHP.

### 2.4.4 VSHP generated from filter 2 using Gargour&Ramachandran polynomials

The second-order Gargour&Ramachandran filter is used in the transfer function, equation (2.2.10) in order to generate VSHP. In this transfer function, $Z_1$ and $Z_2$ are replaced by 'Gargour&Ramachandran' filters and $Z_3$ is replaced by a resistive component ($1\Omega$), otherwise denominator of equation (2.2.10) will not satisfy to be the VSHPs which is proven in section 2.4.5.

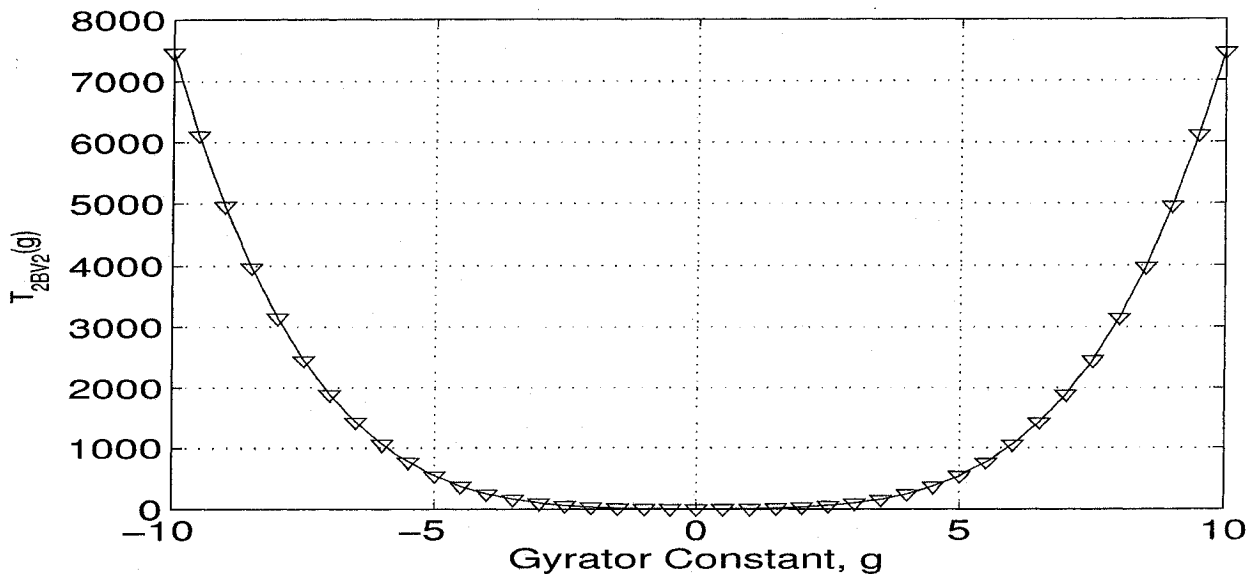


Figure 2.19: Plot of $T_{2BV2}(g)$ vs g .

It has seen that substitution $s_2 = 1$ in the resultant transfer function ($H_{a2G2D}$), the denominator ($D_{a2G2D}(s_1, 1)$) of $H_{a2G2D}$ is strictly Hurwitz polynomial in $s_1$ domain, which is shown in Figure 2.20.

Similar to equations (2.4.48), (2.4.46), (2.4.47) and (2.4.2), it has shown that $T_{2GV2}(g)$ is positive for the all values of g.

Similar to equations (2.4.49), (2.4.50), (2.4.51) and (2.4.52), it has seen that denominator of the transfer function, $H_{a2G2D}(s_1, s_2)$ is generated using Gargour&Ramachandran filters is satisfied to be VSHP.

### 2.4.5 Non VSHPs generated by filter 2

Second-order Butterworth filters are replaced by $Z_1$, $Z_2$ and $Z_3$ in the transfer function of filter2 ( equation(2.2.5) ) as shown in equations (2.4.69), (2.4.70) and (2.4.71) respectively.

$$Z_1 = \frac{L_B C_B s_1^2 + L_B s_1 + 1}{1 + C_B s_1} \tag{2.4.69}$$

$$Z_2 = \frac{L_B C_B s_2^2 + L_B s_2 + 1}{1 + C_B s_2} \tag{2.4.70}$$

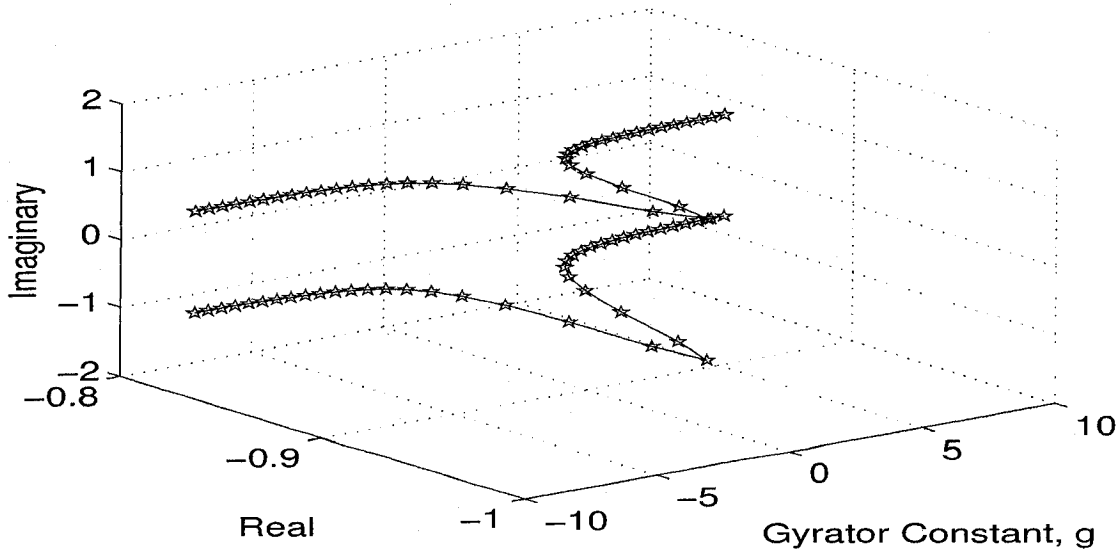


Figure 2.20: The roots of $D_{a2G2D}(s_1, 1)$ for the different values of g.

$$Z_3 = \frac{L_B C_B s_2^2 + L_B s_2 + 1}{1 + C_B s_2} \tag{2.4.71}$$

The overall transfer function of filter2 is obtained in 2D domain,

$$H_{aNB}(s_1, s_2) = \frac{N_{aNB}(s_1, s_2)}{D_{aNB}(s_1, s_2)} \tag{2.4.72}$$

where,

$$\begin{aligned} N_{aNB} &= (g + 0.753gs_1)s_2^4 + ((0.753 + 4.471g) + (4.235g + 0.506)s_1 \\ &+ 1.530gs_1^2)s_2^3 + ((2.118 + 8.353g) + (9.176g + 1.529)s_1 + 4.235gs_1^2)s_2^2 \\ &+ ((2.235 + 7.412g) + (8.353g + 1.530)s_1 + 4.471gs_1^2)s_2 + (1 + 3.176g) \\ &+ (3.647g + 0.753)s_1 + 2.118gs_1^2 \end{aligned} \tag{2.4.73}$$

$$\begin{aligned} D_{aNB} &= 1.035\{((1 + g^2) + (0.704g^2 + 0.704)s_1)s_2^4 \\ &+ ((4.204g^2 + 6.364) + (3.977g^2 + 5.568)s_1 + (1.364 + 1.364g^2)s_1^2)s_2^3 \\ &+ ((8.068g^2 + 14.773) + (13.636 + 8.523g^2)s_1 + (4.545 + 3.977g^2)s_1^2)s_2^2 \\ &+ ((15.909 + 7.045g^2) + (15.909 + 8.068g^2)s_1 + (5.682 + 4.204g^2)s_1^2)s_2 \\ &+ (3.068g^2 + 8.068) + (7.841 + 3.523g^2)s_1 + (2.045g^2 + 3.068)s_1^2\} \end{aligned} \tag{2.4.74}$$

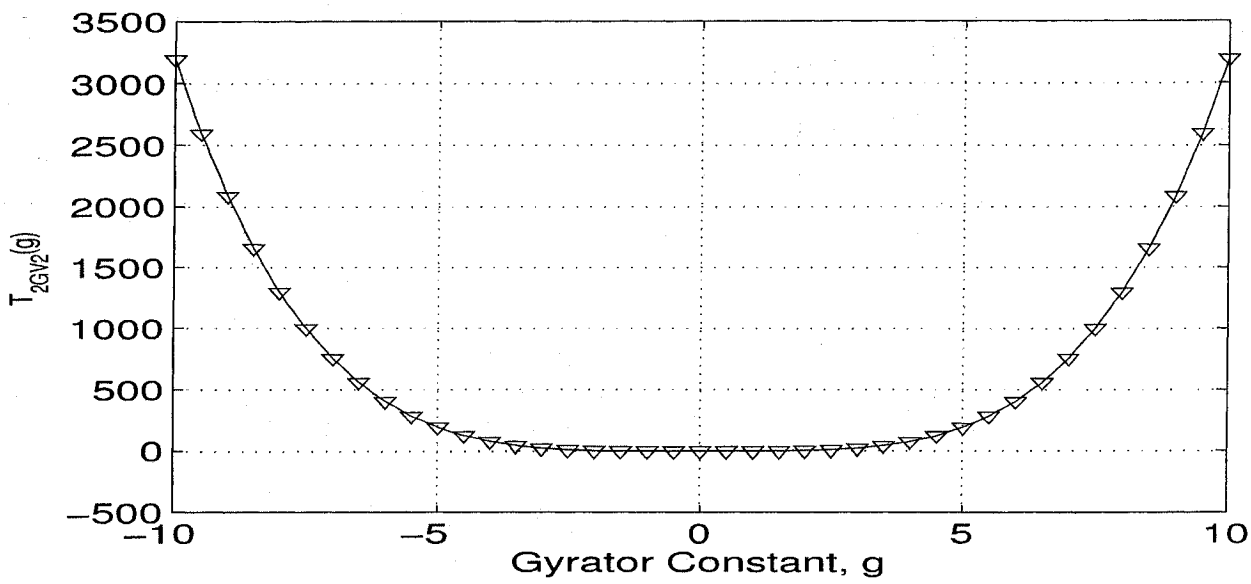


Figure 2.21: Plot of $T_{2GV2}(g)$ vs g .

For simplicity, equation (2.4.74) can be expressed as following.

$$\begin{aligned} D_{aNB}(s_1, s_2) &= A_{NB}s_1s_2^4 + B_{NB}s_2^4 + C_{NB}s_2^3 + D_{NB}s_1s_2^3 + E_{NB}s_1^2s_2^3 + F_{NB}s_2^2 + G_{NB}s_1s_2^2 \\ &+ H_{NB}s_1^2s_2^2 + I_{NB}s_2 + J_{NB}s_1s_2 + K_{NB}s_1^2s_2 + L_{NB}s_1^2 + M_{NB}s_1 + N_{NB} \end{aligned} \tag{2.4.75}$$

According to the section 2.4.1, step 3 is applied to the equation (2.4.75) and in equation (2.4.78), $D_{NB}$ becomes indeterminate when $s_1 \to 0$, $s_2 \to 0$. Hence $D_{NB}$ does not constitute a VSHP.

$$\begin{aligned} D_{aNB}(\frac{1}{s_1}, s_2) &= A_{NB}\frac{1}{s_1}s_2^4 + B_{NB}s_2^4 + C_{NB}s_2^3 + D_{NB}\frac{1}{s_1}s_2^3 + E_{NB}\frac{1}{s_1}^2 s_2^3 + F_{NB}s_2^2 \\ &+ G_{NB}\frac{1}{s_1}s_2^2 + H_{NB}\frac{1}{s_1^2}s_2^2 + I_{NB}s_2 + J_{NB}\frac{1}{s_1}s_2 + K_{NB}\frac{1}{s_1^2}s_2 + L_{NB}\frac{1}{s_1^2} \\ &+ M_{NB}\frac{1}{s_1} + N_{NB} \end{aligned} \tag{2.4.76}$$

$$\begin{aligned} D_{aNB}(s_1, \frac{1}{s_2}) &= A_{NB}s_1\frac{1}{s_2^4} + B_{NB}\frac{1}{s_2^4} + C_{NB}\frac{1}{s_2^3} + D_{NB}s_1\frac{1}{s_2^3} + E_{NB}s_1^2\frac{1}{s_2^3} + F_{NB}\frac{1}{s_2^2} \\ &+ G_{NB}s_1\frac{1}{s_2^2} + H_{NB}s_1^2\frac{1}{s_2^2} + I\frac{1}{s_2} + J_{NB}s_1\frac{1}{s_2} + K_{NB}s_1^2\frac{1}{s_2} + L_{NB}s_1^2 \\ &+ M_{NB}s_1 + N_{NB} \end{aligned} \tag{2.4.77}$$

$$
\begin{aligned}
D_{aNB}(\frac{1}{s_1},\frac{1}{s_2}) &= A_{NB}\frac{1}{s_1}\frac{1}{s_2^4} + B_{NB}\frac{1}{s_2^4} + C_{NB}\frac{1}{s_2^3} + D_{NB}\frac{1}{s_1}\frac{1}{s_2^3} + E_{NB}\frac{1}{s_1^2}\frac{1}{s_2^3} + F_{NB}\frac{1}{s_2^2} \\
&+ G_{NB}\frac{1}{s_1}\frac{1}{s_2^2} + H_{NB}\frac{1}{s_1^2}\frac{1}{s_2^2} + I_{NB}\frac{1}{s_2} + J_{NB}\frac{1}{s_1}\frac{1}{s_2} + K_{NB}\frac{1}{s_1^2}\frac{1}{s_2} + L_{NB}\frac{1}{s_1^2} \\
&+ M_{NB}\frac{1}{s_1} + N_{NB} \qquad (2.4.78)
\end{aligned}
$$

Another example is considered for the generation of VSHP using filter2. The Gargour&Ramachadran filters are replaced by $Z_1$, $Z_2$ and $Z_3$ in the transfer function of filter 2 (equation(2.2.5)) as equations (2.4.79), (2.4.80) and (2.4.81).

$$Z_1 = \frac{L_G C_G s_1^2 + L_G s_1 + 1}{1 + C_G s_1} \qquad (2.4.79)$$

$$Z_2 = \frac{L_G C_G s_2^2 + L_G s_2 + 1}{1 + C_G s_2} \qquad (2.4.80)$$

$$Z_3 = \frac{L_G C_G s_2^2 + L_G s_2 + 1}{1 + C_G s_2} \qquad (2.4.81)$$

The overall transfer function of filter2 is obtained in 2D domain,

$$H_{aNG}(s_1, s_2) = \frac{N_{aNG}(s_1, s_2)}{D_{aNG}(s_1, s_2)} \qquad (2.4.82)$$

where,

$$
\begin{aligned}
N_{aNG} &= (g + 0.35gs_1)s_2^4 + ((0.5 + 7.083g) + (4.167g + 0.167)s_1 \\
&+ 0.708gs_1^2)s_2^3 + ((3 + 18.333g) + (16.667g + 1)s_1 + 4.167gs_1^2)s_2^2 \\
&+ (5 + 20g + (24.167g + 1.75)s_1 + 7.083gs_1^2)s_2 + 2 + 6.25g \\
&+ (9.167g + 0.708)s_1 + 2.917gs_1^2 \qquad (2.4.83)
\end{aligned}
$$

$$
\begin{aligned}
D_{aNG} &= ((1 + g^2) + (0.35g^2 + 0.35)s_1)s_2^4 + ((7.083g^2 + 8.333) \\
&+ (4.167g^2 + 4.583)s_1 + (0.692 + 0.692g^2)s_1^2)s_2^3 + ((17.5g^2 + 27.5) \\
&+ (20 + 16.667g^2)s_1 + (4.25 + 4.167g^2)s_1^2)s_2^2 + ((36.667 + 18.333g^2) \\
&+ (32.5s_1 + 24.167g^2)s_1 + (8.083 + 7.083g^2)s_1^2)s_2(6.167g^2 + 16.667) \\
&+ (16.667 + 9.167g^2)s_1 + (4.417 + 2.917g^2)s_1^2 \qquad (2.4.84)
\end{aligned}
$$

Similar to the previous example , step 3 of the section 2.4.1 is applied to the equation (2.4.84) and it has been found that $D_{NB}$ does not constitute a VSHP..

From the above discussion, it is seen that $Z_1$ and $Z_2$ of filter2 are replaced by doubly terminated RLC filters, it is essential to replace $Z_3$ of filter2 by a resistive component, otherwise denominator of the resultant transfer function of filter2 will not satisfy to be the VSHPs. Even, if the $Z_3$ is replaced by an inductor or a capacitor, denominator of the resultant transfer function of filter2 will not satisfy to be the VSHPs.

## 2.5 Properties of the doubly terminated gyrator networks

From the above discussion, some properties of gyrator filter1, Figure 2.1 are briefly described in bellow.

- Frequency response is independent of frequency when g = 1.
- Denominator of the gyrator filter is independent of the sign of g.
- Numerator of the filter is controlled by the values and sign of g, as a result sharper slopes are obtained obtained by the negative values of g.
- Filter is stable for $(0 \leq |g| < \infty)$.
- Monotonic amplitude frequency response is obtained for the certain ranges of g, if and only impedances are replaced by doubly terminated RLC network which has monotonic amplitude frequency response.

Some properties of filter 2, Figure 2.2 are discussed in bellow.

- Denominator of the gyrator filter are independent of the sign of g.
- Numerator of the filter is controlled by the values and sign of g, as a result more sharp slopes are obtained obtained by the negative values of g.
- Filter is stable for $(0 \leq |g| < \infty)$.

- Monotonic amplitude frequency response is obtained for the certain ranges of g, if and only impedances are replaced by doubly terminated RLC network which has monotonic amplitude frequency response.

## 2.6 Summary and Discussion

In this chapter, two gyrator based filters are considered for the 2D digital filter design which are taken from Darlington-synthesis. The impedances in the gyrator filters are replaced by the doubly terminated RLC circuits in order to generate 2D stable transfer function. In this thesis, the second-order Butterworth and Gargour&Ramachandran filters are used as the doubly terminated RLC circuits and the both RLC filters have monotonic frequency-amplitude responses. The GBT is applied to the second-order Butterworth filter to obtain the desired digital filter. The inverse bilinear transformation is applied to the digital filter in order to obtain the corresponding modified analog filter [16]. It has shown that depending on the values of the parameters of the GBT, different kinds of filter responses are obtained, such as low-pass filters, high-pass filters, band-pass filters and band-elimination filters filter. The desired cutoff frequency and bandwidth of the filters are depend on the parameters of the GBT (section 2.3). Properties of the GBT as applied to the second-order Butterworth low-pass filter are discussed in section 2.3.6.

The 2D stable analog transfer functions are generated in section 2.4, where impedances of the doubly terminated gyrator networks (Figures 2.1 and 2.2) are replaced by the second-order RLC filters. As a result, the coefficients of the resultant transfer functions are functions of g of the gyrator networks and the g provides a wide range to obtain different kinds of filters. Properties of the doubly terminated gyrator networks (Figures 2.1 and 2.2) are shown in section 2.5.

# Chapter 3

# Proposed Design of Digital Low-pass Filter

## 3.1 Introduction

Darlington synthesis has been introduced for the realization of a driving-point impedance as lossless two-ports terminated in a resistance. The extensions of Darlington-synthesis to two-variable positive real function have been accomplished [27] and Darlington-type realization of two-variable driving-point impedance of lossless two-port network has been described [11]. Necessary and sufficient conditions for the realization of the classes of two-variable positive real function's as doubly-terminated lossless two-variable lossless ladder networks has been obtained [28] and stable 2D recursive filters have been designed by generation of Very Strict Hurwitz Polynomial (VSHP) using terminated n-port gyrator networks [29].

In [30], a 2D filter approximates the magnitude response which can be realized and then cascading it by an all-pass 2D filter to equalize the resulting group delay. A design technique of 2D recursive filters have been shown which met simultaneously magnitude and group delay specifications [30], where, they have chosen a performance index as a linear combination of three error functions for the magnitude and group delays and minimized it iteratively by the Davidon-Fletcher and Powell method. Although the technique has the advantage of always ensuring the filter stability, the difficulties to be encountered are computational complexity and convergence [31]. Later, a 2D filter design as a linear programming problem has been proposed, where

linear programming adjusts the real and imaginary parts in the filter transfer function. but, this tends to require relatively long computation time [32]. Also, a filter design has been shown using the two specifications as the problem of minimizing the total length of modified complex errors between an actual transfer function and the desired prototype over the discrete set of frequency plane and minimized it by an iterative procedure [33].

In this thesis, the 2D digital filters are designed by Darlington-type networks containing gyrator component and impedances of the gyrator network are replaced by doubly terminated RLC networks. The resultant 2D analog transfer function is stable in analog domain, if the denominator of the transfer function is satisfied to be VSHP (section 1.5). Section 2.4 has shown the generation of VSHPs using the doubly terminated gyrator networks (Figures 2.1 and 2.2). In this chapter, two filter designs are proposed for the 2D low-pass digital filter design. The proposed designs are:

1. Proposed Design - I (Regulating 'g' magnitude).

2. Proposed Design - II (Controlled Transformation).

The proposed design - I is based on the values of gyrator constant (g) of the gyrator network and various kinds of filter responses are obtained regulating the value/sign of g. For example, impedances of a gyrator network are replaced by doubly terminated RLC networks. As a consequence, the magnitude of 'g' provides a wide variation to change the filter responses; and depending on the the gyrator network and RLC filter structures, low-pass, high-pass, band-pass and band-elimination filter responses can be obtained. The proposed design-I ensures the stability of the digital filter (section 1.5); however, this design cannot ensure monotonic amplitude-frequency response in the passband regions of the digital. To overcome the problem, another design is proposed for 2D digital filter design which is called controlled transformation. The GBT plays an important role for modifying the reactive components of the RLC filters to the desired components. The desired filter responses are obtained by choosing appropriate values of the parameters of the GBT (section 2.3).

The proposed design -II satisfies the stability conditions of the digital filter and also ensures monotonic amplitude-frequency response in the passband regions. A mathematical closed form of a 1D low-pass filter with a monotonic amplitude characteristic is described in paper [17] and the mathematical closed form is extended to

two dimensional case. The extension of the paper [17] is derived from an analog filter and amplitude characteristic of an analog filter is expressed as

$$A_{1n}(\Omega) = \frac{1}{\sqrt{1+\alpha_n(\Omega^2)}} \tag{3.1.1}$$

where, $\Omega$ is analog frequency and $\alpha_n(\Omega^2)$ is a rational function of order n for $\Omega^2$. The amplitude characteristic equation (3.1.1) is low-pass filter with monotonic and arbitrary flatness in the pass-band, if and only

$$M_1(\Omega) = \frac{d\alpha_n(\Omega^2)}{d\Omega} \geq 0 \tag{3.1.2}$$

The condition for a flat characteristic in the pass-band is-

$$\frac{d^k\alpha_n(\Omega^2)}{d\Omega^k} = 0, (k = 0, 1, 2, ....2m+1) \tag{3.1.3}$$

and the amplitude characteristic $A_n(\Omega)$ is said to have m-th order flatness. Also, the slope at the cut-off frequency M is given by

$$\frac{d\alpha_n(\Omega^2)}{d\Omega}|_{\Omega=1} = M \tag{3.1.4}$$

The definition of monotonicity in the 2D amplitude-frequency response of second-order transfer function, $H(s_1, s_2)$ is in following [10]

$$\left\{ \begin{array}{l} \frac{\partial|H(\Omega_1,\Omega_2)|}{\partial\Omega_1} \leq 0, \Omega_2 = 0 \\ \frac{\partial|H(\Omega_1,\Omega_2)|}{\partial\Omega_2} \leq 0, \Omega_1 = 0 \end{array} \right\} \tag{3.1.5}$$

Transfer function of a 2D analog low-pass filter can be expressed as following [10].

$$\begin{aligned} H_{a1}(s_1, s_2) &= \frac{1}{D(s_1, s_2)} \\ &= \frac{d_{00}}{\sum_{i_1=0}^{2}\sum_{i_2=0}^{2} d_{i_1 i_2} s_1^{i_1} s_2^{i_2}} \end{aligned} \tag{3.1.6}$$

$$\tag{3.1.7}$$

Substituting $s_1 = j\Omega_1$ and $s_2 = j\Omega_2$ in the equation (3.1.6), where, $j = \sqrt{-1}$. The following necessary conditions are obtained for monotonic amplitude-frequency response of 2D analog filter:

$$\left\{ \begin{array}{l} \frac{\partial|D(\Omega_1,\Omega_2)|}{\partial\Omega_1} \geq 0, \Omega_2 = 0 \\ \frac{\partial|D(\Omega_1,\Omega_2)|}{\partial\Omega_2} \geq 0, \Omega_1 = 0 \end{array} \right\} \tag{3.1.8}$$

Therefore, the following two equations are obtained from equations (3.1.4) and (3.1.8).

$$\begin{aligned} M_2(\Omega_1) &= \frac{\partial |D(\Omega_1, 0)|}{\partial \Omega_1} \\ &= 4d_{20}^2\Omega_1^2 - 4d_{20}d_{00} + 2d_{10}^2 \geq 0 \end{aligned} \tag{3.1.9}$$

$$\begin{aligned} M_3(\Omega_2) &= \frac{\partial |D(0, \Omega_2)|}{\partial \Omega_2} \\ &= 4d_{02}^2\Omega_2^2 - 4d_{02}d_{00} + 2d_{01}^2 \geq 0 \end{aligned} \tag{3.1.10}$$

Transfer function of a 2D analog low-pass filter can be expressed [34] as below.

$$H_{a2}(s_1, s_2) = \frac{\sum_{i_1=0}^{2}\sum_{i_2=0}^{2} n_{i_1 i_2} s_1^{i_1} s_2^{i_2}}{\sum_{i_1=0}^{2}\sum_{i_2=0}^{2} d_{i_1 i_2} s_1^{i_1} s_2^{i_2}} \tag{3.1.11}$$

Substituting $s_1 = j\Omega_1$ and $s_2 = j\Omega_2$ in equation (3.1.11) and the necessary conditions of monotonic characteristic of equation (3.1.11) are obtained as below:

$$(\Omega_i - \frac{1}{2U_{1i}}\sqrt{2}\sqrt{U_{1i}(-U_{2i} + \sqrt{U_{2i}^2 - 4U_{1i}U_{3i}})}) < 0 \tag{3.1.12}$$

$$(\Omega_i + \frac{1}{2U_{1i}}\sqrt{2}\sqrt{U_{1i}(-U_{2i} + \sqrt{U_{2i}^2 - 4U_{1i}U_{3i}})}) < 0 \tag{3.1.13}$$

$$(\Omega_i - \frac{1}{2U_{1i}}\sqrt{-2U_{1i}(U_{2i} + \sqrt{U_{2i}^2 - 4U_{1i}U_{3i}})}) < 0 \tag{3.1.14}$$

$$(\Omega_i + \frac{1}{2U_{1i}}\sqrt{-2U_{1i}(U_{2i} + \sqrt{U_{2i}^2 - 4U_{1i}U_{3i}})}) < 0 \tag{3.1.15}$$

where, i = 1,2. when $\Omega_2 = 0$ in the equation (3.1.11), $U_{11}$, $U_{21}$ and $U_{31}$ define in equations (3.1.12) to (3.1.15) as below:

$$U_{11} = (2n_{20}n_{00}d_{20}^2 - 2n_{20}^2 d_{20}d_{00} - n_{10}^2 d_{20}^2 + n_{20}^2 d_{10}^2) \tag{3.1.16}$$

$$U_{21} = (2n_{20}^2 d_{00}^2 - 2n_{00}^2 d_{20}^2) \tag{3.1.17}$$

$$U_{31} = (2n_{00}^2 d_{20}d_{00} + n_{10}^2 d_{00}^2 - 2n_{20}n_{00}d_{00}^2 - n_{00}^2 d_{10}^2) \tag{3.1.18}$$

When $\Omega_1 = 0$ in the equation (3.1.11), $U_{12}$, $U_{22}$ and $U_{32}$ define as below.

$$U_{12} = (2n_{02}n_{00}d_{02}^2 + n_{02}^2 d_{01}^2 - 2n_{02}^2 d_{02}d_{00} - n_{01}^2 d_{02}^2) \tag{3.1.19}$$

$$U_{22} = (-2n_{00}^2 d_{02}^2 + 2n_{02}^2 d_{00}^2) \tag{3.1.20}$$

$$U_{32} = (-2n_{02}n_{00}d_{00}^2 + 2n_{00}^2 d_{02}d_{00} + n_{01}^2 d_{00}^2 - n_{00}^2 d_{01}^2) \tag{3.1.21}$$

Similarly, the transfer function of a 2D analog gyrator filter can be expressed as below:

$$H_{ag}(s_1, s_2, g) = \frac{\sum_{i_1=0}^{2}\sum_{i_2=0}^{2} n_{gi_1i_2}(g)s_1^{i_1}s_2^{i_2}}{\sum_{i_1=0}^{2}\sum_{i_2=0}^{2} d_{gi_1i_2}(g)s_1^{i_1}s_2^{i_2}} \tag{3.1.22}$$

where, the coefficients ($n_{gi_1i_2}(g)$ and $d_{gi_1i_2}(g)$) are function of g of the gyrator filter.

Substituting $s_1 = j\Omega_1$ and $s_2 = j\Omega_2$ in equation(3.1.22) and the necessary conditions of monotonic characteristics of equation (3.1.22) are obtained as below:

$$(\Omega_i - \frac{1}{2V_{1i}}\sqrt{2}\sqrt{V_{1i}(-V_{2i} + \sqrt{V_{2i}^2 - 4V_{1i}V_{3i}})}) < 0 \tag{3.1.23}$$

$$(\Omega_i + \frac{1}{2V_{1i}}\sqrt{2}\sqrt{V_{1i}(-V_{2i} + \sqrt{V_{2i}^2 - 4V_{1i}V_{3i}})}) < 0 \tag{3.1.24}$$

$$(\Omega_i - \frac{1}{2V_{1i}}\sqrt{-2V_{1i}(V_{2i} + \sqrt{V_{2i}^2 - 4V_{1i}V_{3i}})}) < 0 \tag{3.1.25}$$

$$(\Omega_i + \frac{1}{2V_{1i}}\sqrt{-2V_{1i}(V_{2i} + \sqrt{V_{2i}^2 - 4V_{1i}V_{3i}})}) < 0 \tag{3.1.26}$$

where, i = 1,2. when $\Omega_2 = 0$ in the equation (3.1.22), $V_{11}$, $V_{21}$ and $V_{31}$ are function of the g, which are defined in the equations (3.1.23) to (3.1.26) as below:

$$\begin{aligned} V_{11} &= 2n_{g20}(g)n_{g00}(g)\{d_{g20}(g)\}^2 - 2\{n_{g20}(g)\}^2 d_{g20}(g)d_{g00}(g) - \{n_{g10}(g)\}^2\{d_{g20}(g)\}^2 \\ &+ \{n_{g20}(g)\}^2\{d_{g10}(g)\}^2 \end{aligned} \tag{3.1.27}$$

$$V_{21} = (2\{n_{g20}(g)\}^2\{d_{g00}(g)\}^2 - 2\{n_{g00}(g)\}^2\{d_{g20}(g)\}^2) \tag{3.1.28}$$

$$\begin{aligned} V_{31} &= 2\{n_{g00}(g)\}^2 d_{g20}(g)d_{g00}(g) + \{n_{g10}(g)\}^2\{d_{g00}(g)\}^2 - 2n_{g20}(g)n_{g00}(g)\{d_{g00}(g)\}^2 \\ &- \{n_{g00}(g)\}^2\{d_{g10}(g)\}^2 \end{aligned} \tag{3.1.29}$$

When $\Omega_1 = 0$ in the equation (3.1.22), $V_{12}$, $V_{22}$ and $V_{32}$ are defined in the equation (3.1.23) to (3.1.26) as below:

$$\begin{aligned} V_{12} &= 2n_{g02}(g)n_{g00}(g)\{d_{g02}(g)\}^2 + \{n_{g02}(g)\}^2\{d_{g01}(g)\}^2 - 2\{n_{g02}(g)\}^2 d_{g02}(g)d_{g00}(g) \\ &- \{n_{g01}(g)\}^2\{d_{g02}(g)\}^2) \end{aligned} \tag{3.1.30}$$

$$V_{22} = -2\{n_{g00}(g)\}^2\{d_{g02}(g)\}^2 + 2\{n_{g02}(g)\}^2\{d_{g00}(g)\}^2 \tag{3.1.31}$$

$$\begin{aligned} V_{32} &= -2n_{g02}(g)n_{g00}(g)\{d_{g00}(g)\}^2 + 2\{n_{g00}(g)\}^2 d_{g02}(g)d_{g00}(g) + \{n_{g01}(g)\}^2\{d_{g00}(g)\}^2 \\ &- \{n_{g00}(g)\}^2\{d_{g01}(g)\}^2 \end{aligned} \tag{3.1.32}$$

The mathematical form of a monotonic amplitude characteristic [17] can be extended to 2D monotonic characteristics using a gyrator filter as below. Consider, the amplitude characteristic of a 2D analog gyrator filter is

$$A_{2n}(\Omega_1, \Omega_2, g) = \frac{1}{\sqrt{1+\beta_n(\Omega_1^2, \Omega_2^2, g)}} \tag{3.1.33}$$

where, $\beta_n(\Omega_1^2, \Omega_1^2, g)$ is a rational function of order n for $\Omega_1^2$, $\Omega_2^2$ and $g$. The amplitude characteristic equation (3.1.33) is a low-pass filter with monotonic and arbitrary flatness in the pass-band, if

$$M_4(\Omega_1, g) = \frac{\partial \beta_n(\Omega_1^2, 0, g)}{\partial \Omega_1} \geq 0 \tag{3.1.34}$$

$$M_5(\Omega_2, g) = \frac{\partial \beta_n(0, \Omega_2^2, g)}{\partial \Omega_2} \geq 0 \tag{3.1.35}$$

The proposed design-II (controlled transformation) uses the above conditions to have monotonic characteristics in frequency responses of the digital filter. In this design, the GBT is applied to equations (3.1.12) to (3.1.15), (3.1.34), (3.1.35) and limits of the parameters of the GBT are defined in order to obtain monotonic characteristics in frequency responses of the filter. Details of the two proposed designs are discussed in detail and design examples are given to illustrate the usefulness of the proposed designs.

## 3.2 Proposed Design-I

Impedances of the doubly terminated gyrator network are replaced by the doubly terminated RLC networks and stability of the resultant filter is satisfied (section 2.4). The desired filter responses are obtained by regulating the value/sign of g and double bilinear transformations are used to obtain the desired 2D digital filter response.

The block diagram of the proposed design-I is shown in Figure 3.16 and it shows the value/sign of g plays an important role for the 2D digital filter design. Design examples are given in the below to illustrate the usefulness of the proposed design.

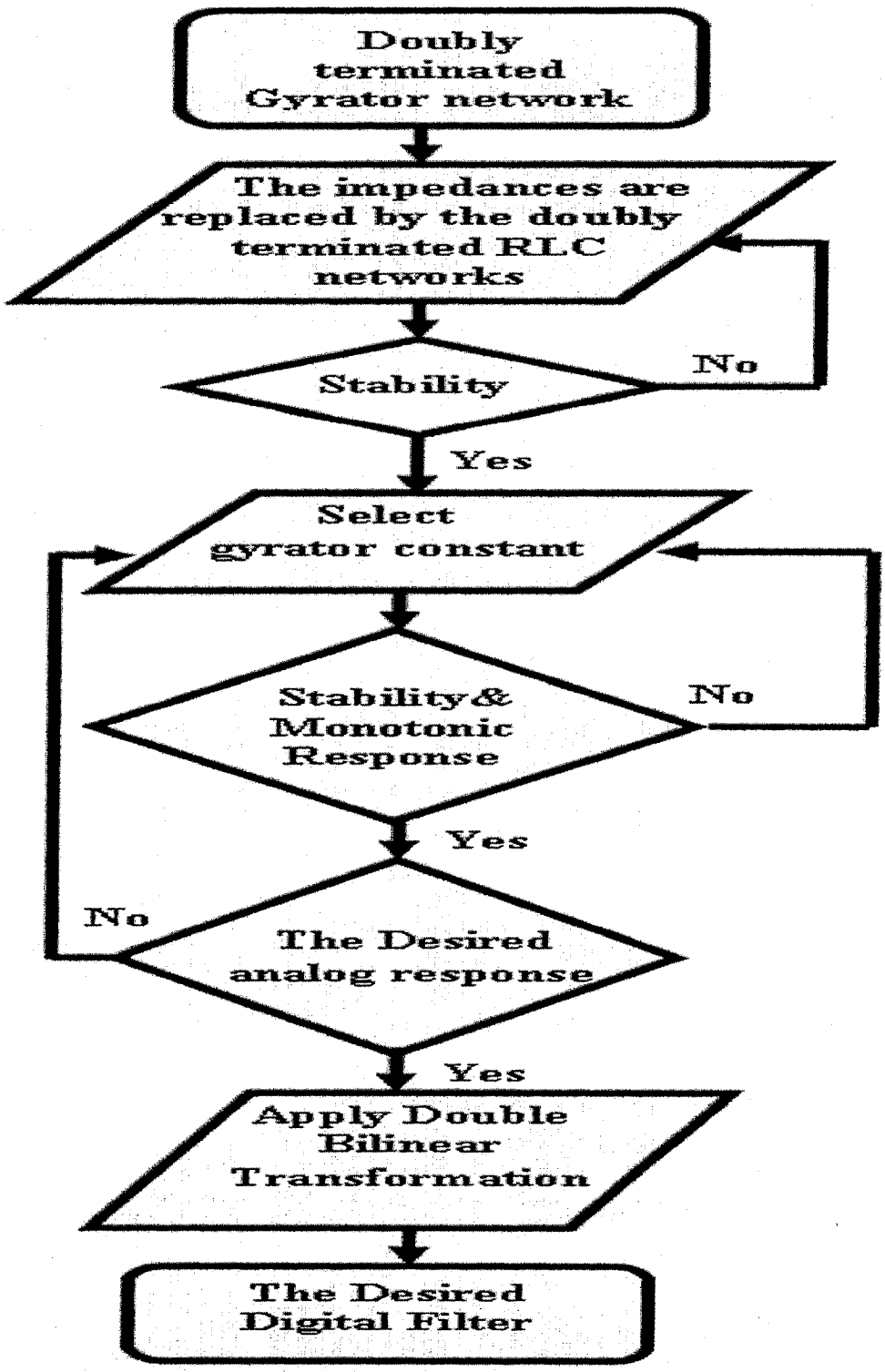


Figure 3.1: Proposed Design - I of Two-Dimensional Analog/Digital filter using Darlington-type Gyrator Networks

### 3.2.1 Filter1

Transfer function of filter1 is derived in section 2.2 and stability criteria is defined in the case of replacing the impedances of a doubly terminated gyrator network with doubly terminated second-order Butterworth and Gargour&Ramachandran filters (section 2.4). In this section, both 1D and 2D analog and digital filters are designed using proposed design-I. Some properties of the gyrator filters have to be considered before proceeding further, such as the denominator of the transfer function of filter1 is independent of the sign of g. However, the value of g can effect the magnitude response of the filter and the numerator is dependent on both sign and value of g. For example, impedances of a doubly terminated gyrator network is replaced by the doubly terminated second-order Butterworth filters. As a result, the cutoff frequency of the overall gyrator network is controlled by the value of g which is shown in the Figure 3.2 and it is also shown that a low-pass filter is transformed to a high-pass filter for the higher magnitude of g. However, both Figures 3.2 and 3.3 are not containing monotonic characteristic.

For illustration, impedances of the doubly terminated gyrator network are replaced by the doubly terminated RLC networks (second-order Butterworth and Gargour&Ramachandran filters)and different combination of the RLC network are placed in the gyrator networks and for the simplicity, each circuit is classified, such as impedances of filter1 are replaced by the second-order Butterworth filter is called case-I(filter1). Similarly, impedances of filter1 are replaced by the second-order Gargour&Ramachandran filters is called case-II(filter1) and impedances of filter1 are replaced by the second-order Butterworth and Gargour&Ramachandran filters is called case-III(filter1). Each case of filter design is discussed below.

### 3.2.2 1D case-I(filter1)

Second-order Butterworth filters are replaced with the impedances of the doubly terminated gyrator filter1 and it has seen that coefficients of the resultant analog transfer function are functions of g of filter1. The analog filter is converted to the desired digital filter by bilinear transformation.

The derived transfer function of filter1 is

$$H_1 = \frac{1 + gZ_1 + g^2 Z_1 Z_2}{2 + Z_1 + g^2 Z_1 + 2g^2 Z_1 Z_2} \tag{3.2.1}$$

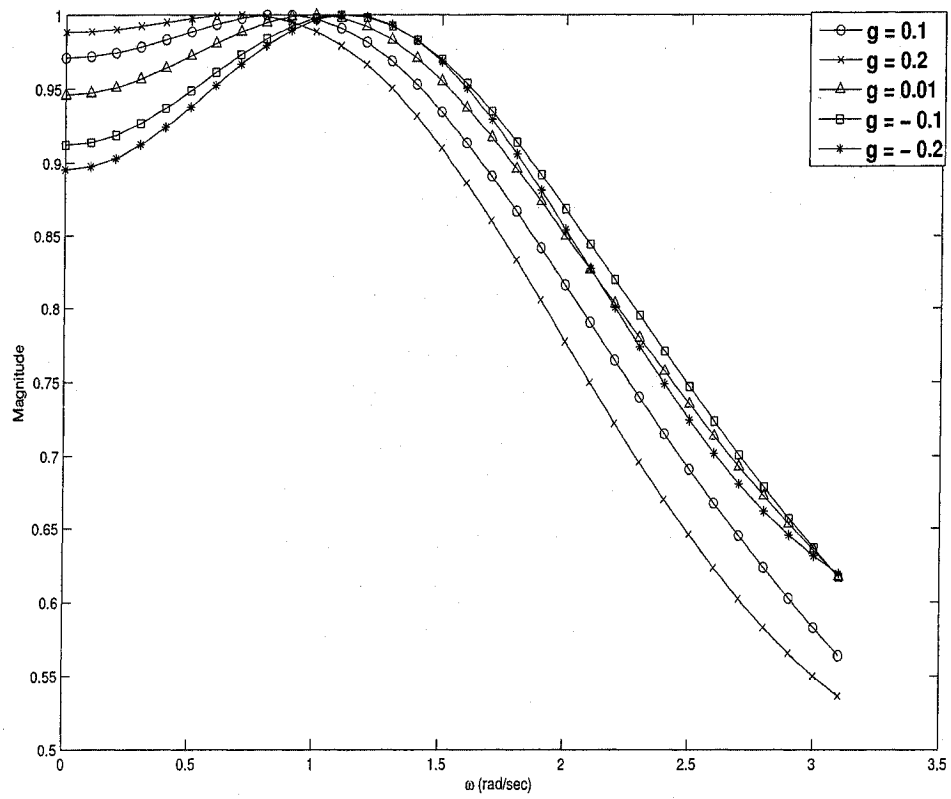


Figure 3.2: Magnitude responses of filter 1 for the different values of g

The impedances $(Z_1, Z_2)$ of the equation (3.2.1) are replaced by the impedances of Butterworth filter (equation (2.4.69)) and the overall transfer function is obtained as the following:

$$H_{a1B1D}(s) = \frac{2g^2s^4 + (5.6g^2 + 1.4g)s^3 + (1 + 4g + 8g^2)s^2 + (5.6g^2 + 4.2g + 2.8)s + 2 + 2g + 2g^2}{4g^2s^4 + (13g^2 + 1.4)s^3 + (6 + 20g^2)s^2 + (15g^2 + 9.8)s + 6. + 6g^2} \tag{3.2.2}$$

The locations of poles and zeros of the gyrator filter are dependent on the value and/or sign of g of the gyrator filter and it has been seen that the reactive behavior of the gyrator filter is changed not only for the values of resistance, capacitance and inductance of the filter, but also the value and sign of g. The system should have the property of stability that for all bounded inputs, the output is bounded [23]. To ensure the stability of 1D filter, poles should be in the left side of s-domain. Different types of monotonic responses in s-domain can be obtained by applying the proposed

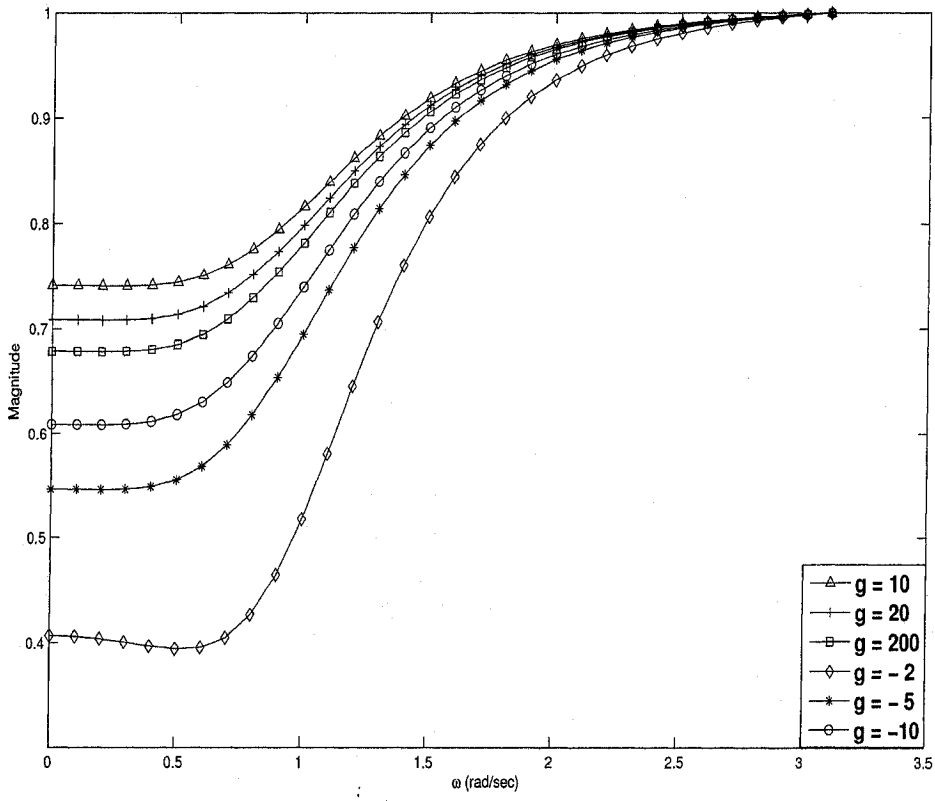


Figure 3.3: Magnitude responses of filter 1 for different values of g

filter design. It is observed that either negative real poles or complex conjugate poles having the real part greater than the imaginary part in magnitude ensures the monotonic characteristics in frequency response in the s-domain. Different filter characteristics are obtained by changing the value of g. Frequency response of the filter is inverted by regulating the value/sign of g. The locations of the poles and zeros of the filter change with the increase of the value/sign of g are shown in the in Figures 3.4 and 3.5.

Figures 3.2 and 3.3 have shown that increase of magnitude of g of the 1D analog low-pass filter turns to 1D analog high-pass filter and same types of responses are obtained for the negative value of g, because the denominator of the transfer function is independent of g's sign and the effect of the negative value of g on the numerator provides sharper slopes in the frequency responses (Figures 3.2 and 3.3).

Table 3.1 shows that the roots of the denominator do not depend on the sign of g.

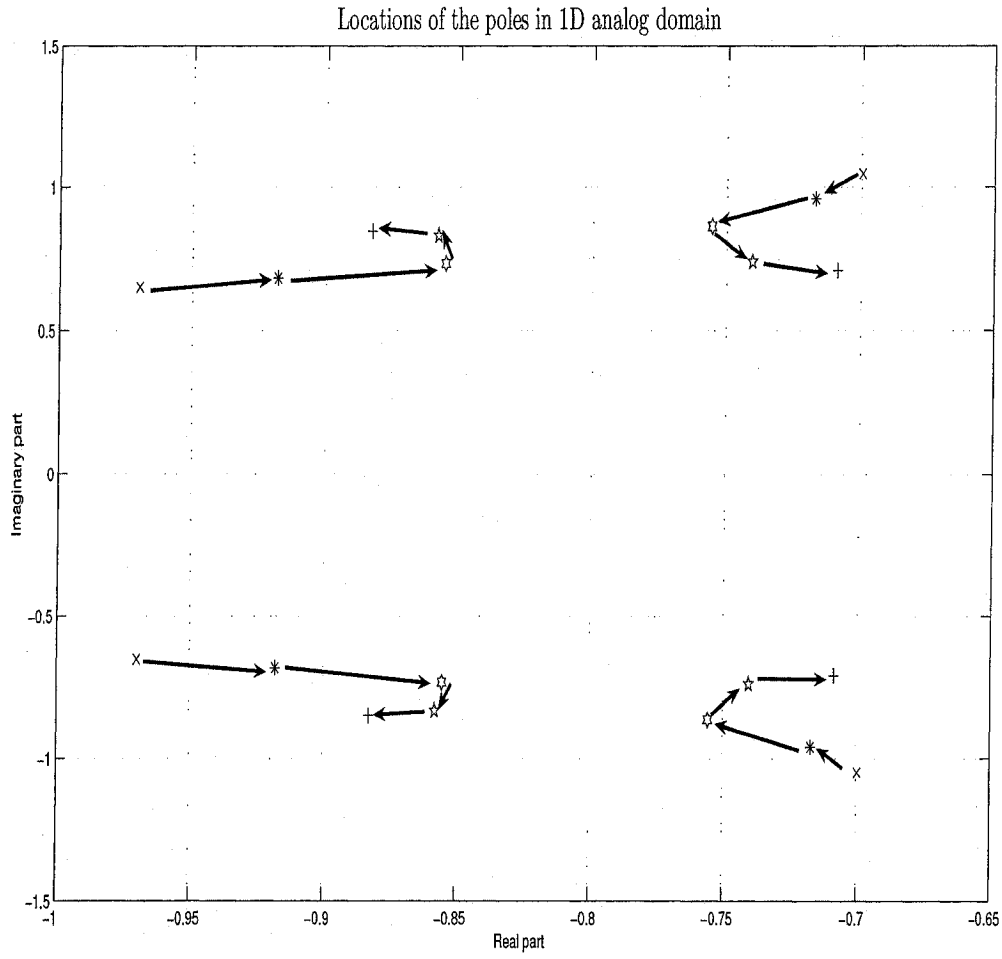


Figure 3.4: Poles locations of the case-I(filter1), g = 1.5 (x), g = 1.5(*), g = 2 (Hexagram), g = 3 (Pentagram), g = 20 (+).

So the locations of the poles are remain same for the positive and negative values of g of the filter. The lower magnitude of g provides a low-pass filter and the low-pass filter is changed to a high-pass filter by increasing the magnitude of g. It has found that the overall frequency response of the transfer function becomes a constant, when g = 1. However, the negative magnitudes of g effect on the zeros of the transfer function and sharper slopes in the frequency responses are obtained.

Transfer function of case-I(filter1) (equation (3.2.2)) can represent to the form of equation (3.1.2). Consider, in this case, equation (3.1.2) represents to $M_{1B1}(\Omega)$ and

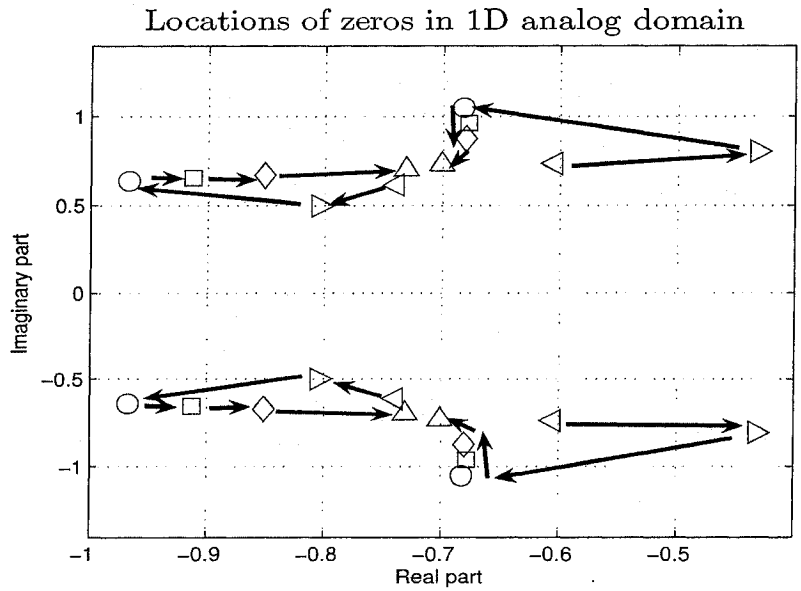


Figure 3.5: Zero locations of the case-I(filter1), g = -5 (<), g = -2(>), g = 0.1 (o),g = 3 (square), g = 5 (diamond), g = 20(triangle).

Figure 3.6 shows that $M_{1B1}(\Omega)$ does not satisfy the monotonicity in the amplitude-frequency responses of case-I(filter1). However, the GBT can bring monotonic characteristic in frequency response of the filter by modifying the reactive components, which are described in detail in the proposed design-II (controlled transformation) section 3.3.

### 3.2.3 2D case-I(filter1)

The impedances of the doubly terminated gyrator filter1 are replaced by second-order Butterworth filters and the proposed design has used the properties of positive definite matrices and their application in generating 2-variable VSHPs. The denominator of the resultant analog transfer function is assigned to VSHP in 2D analog domain which is guaranteed to generate stable 2D recursive filters and the double bilinear transformations are applied to the 2D analog filter in order to obtain stable 2D digital filter. The impedances ($Z_1$, $Z_2$) of the transfer function, equation (3.2.1) are replaced by the impedance of Butterworth filters equations (2.4.69), (2.4.70) respectively and the overall transfer function is given by

Table 3.1: Locations of the poles of the 1D analog case-I(filter1) (equation 3.2.2).

| g | Roots of the Denominator |
|---|---|
| 0.1 | $-1.4371 \pm 0.9997i, -1.4447, -34.2188$ |
| 1.5 | $-0.6997 \pm 1.0477i, -0.9699 \pm 0.6514i$ |
| 2 | $-0.7173 \pm 0.9585i, -0.9179 \pm 0.6825i$ |
| 3 | $-0.7556 \pm 0.8626i, -0.8551 \pm 0.7323i$ |
| 20 | $-0.7089 \pm 0.7089i, -0.8826 \pm 0.8470i$ |
| -0.1 | $-1.4371 \pm 0.9997i, -1.4447, -34.2188$ |
| -1.5 | $-0.6997 \pm 1.0477i, -0.9699 \pm 0.6514i$ |
| -2 | $-0.7173 \pm 0.9585i, -0.9179 \pm 0.6825i$ |
| -3 | $-0.7556 \pm 0.8626i, -0.8551 \pm 0.7323i$ |
| -20 | $-0.7089 \pm 0.7089i, -0.8826 \pm 0.8470i$ |

$$H_{a1B2D}(s_1, s_2) = \frac{\begin{bmatrix} 1 & s_1 & s_1^2 \end{bmatrix} \begin{bmatrix} 2+2g^2+2g & \sqrt{2}(1+g+2g^2) & 2g^2 \\ \sqrt{2}(2g^2+2g+1) & 1+4g^2+2g & 2\sqrt{2}g^2 \\ 2g^2+2g & \sqrt{2}(2g^2+g) & 2g^2 \end{bmatrix} \begin{bmatrix} 1 \\ s_2 \\ s_2^2 \end{bmatrix}}{\begin{bmatrix} 1 & s_1 & s_1^2 \end{bmatrix} \begin{bmatrix} 6g^2+6 & \sqrt{2}(3+5g^2) & 4g^2 \\ \sqrt{2}(6g^2+4) & 4+10g^2 & 4\sqrt{2}g^2 \\ 2+6g^2 & \sqrt{2}(1+5g^2) & 4g^2 \end{bmatrix} \begin{bmatrix} 1 \\ s_2 \\ s_2^2 \end{bmatrix}} \tag{3.2.3}$$

It is seen that the 2D analog transfer function satisfies the stability criteria (1.5) for the positive and negative values of g ($-\infty < g < \infty$), but this transfer function (equation (3.2.3)) does not satisfy the constrains of having the monotonic characteristics (equations (3.1.34), (3.1.35)), unless the second-order Butterworth filter is changed to a suitable the corresponding modified circuit.

Amplitude characteristic of the transfer function of case-I(filter1) (equation (3.2.3)) derives and similar to equations (3.1.34) and (3.1.35), $M_{4B1}(\Omega_1, g)$ and $M_{5B1}(\Omega_2, g)$ of transfer function (equation (3.2.3)) are obtained. Figure 3.8 shows that the monotonicity in the amplitude-frequency responses of case-I(filter1) do not satisfy.

Figure 3.7 shows the frequency responses of the filter and the responses do not have the monotonic characteristics. This problem can overcome using proposed design-II (controlled transformation).

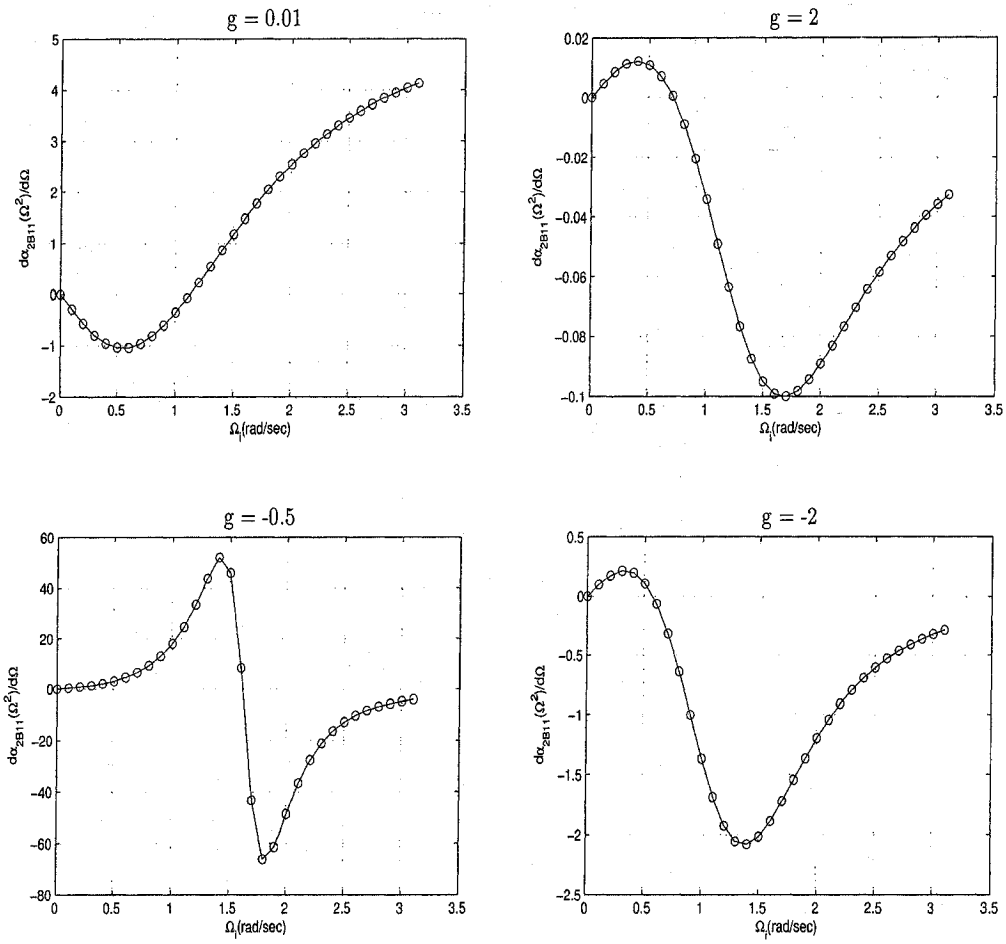


Figure 3.6: 1D analog Case-I(filter1) not satisfying monotonic characteristics.

### 3.2.4 1D case-II(filter1)

Impedances of the transfer function, equation (3.2.1) are replaced by the impedance of Gargour&Ramachandran filters equation (2.4.79) and the resultant transfer function is stable, which is proved in Table 3.2.

$$H_{a1G1D}(s) = \frac{0.5(g^2s^4 + (0.47g + 6g^2)s^3 + (0.23 + 2.8g + 11.7g^2)s^2 + (1.3 + 5g + 8.4g^2)s + 2(1 + g + g^2))}{g^2s^4 + (0.24 + 6.19g^2)s^3 + (1.6 + 13g^2)s^2 + (3.8 + 10.8g^2)s + 3 + 3g^2} \tag{3.2.4}$$

Figure 3.10 shows the amplitude-frequency responses of 1D analog case-II(filter1) with increasing of g of the gyrator network. Table 3.2 shows that the roots of the

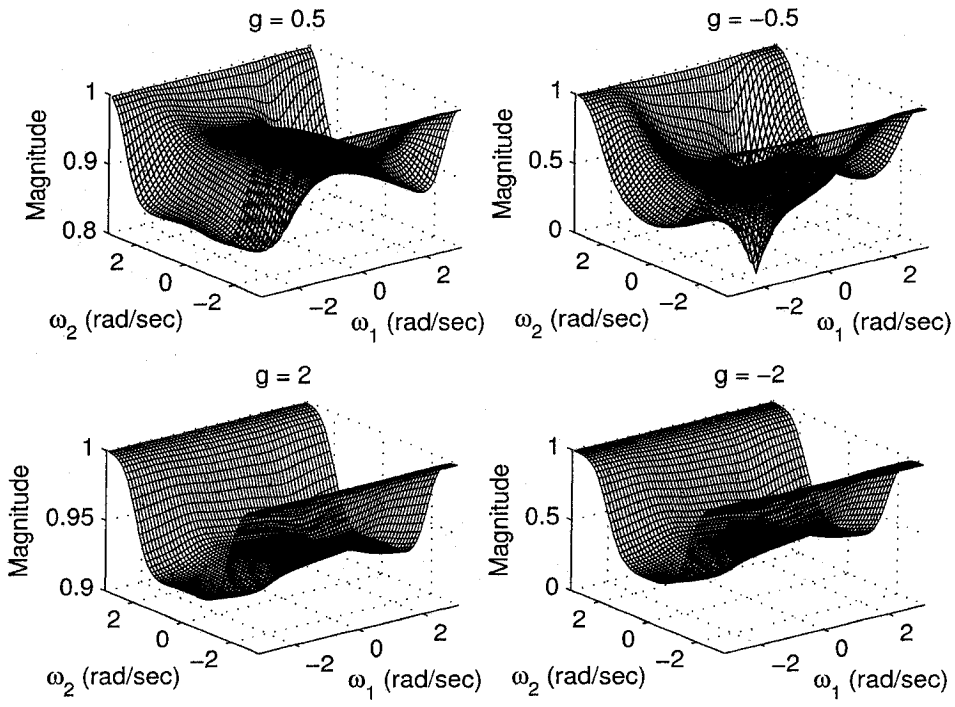


Figure 3.7: 3D magnitude plots of the 2D digital case-I(filter 1) filters

Table 3.2: Stability analysis of the 1D analog case-II(filter1) ($H_{1G1D}(s)$).

| g | Roots of Denominator |
|---|---|
| 0.1 | $-1.9781 \pm 0.6494i$, $-3.0452$, $-22.9608$ |
| 0.25 | $-2.1562 \pm 0.8631i$, $-2.8391 \pm 1.1816i$ |
| 1.5 | $-2.3416 \pm 0.1097i$, $-0.8045 \pm 0.3762i$ |
| 2 | $-2.3373 \pm 0.0762i$, $-0.7857 \pm 0.2618i$ |
| 3 | $-2.3341 \pm 0.0359i$, $-0.7724 \pm 0.1235i$ |
| -0.1 | $-1.9781 \pm 0.6494i$, $-3.0452$, $-22.9608$ |
| -0.25 | $-2.1562 \pm 0.8631i$, $-2.8391 + 1.1816i$ |
| -1.5 | $-2.3416 \pm 0.1097i$, $-0.8045 \pm 0.3762i$ |
| -2 | $-2.3373 \pm 0.0762i$, $-0.7857 \pm 0.2618i$ |
| -3 | $-2.3341 \pm 0.0359i$, $-0.7724 \pm 0.1235i$ |

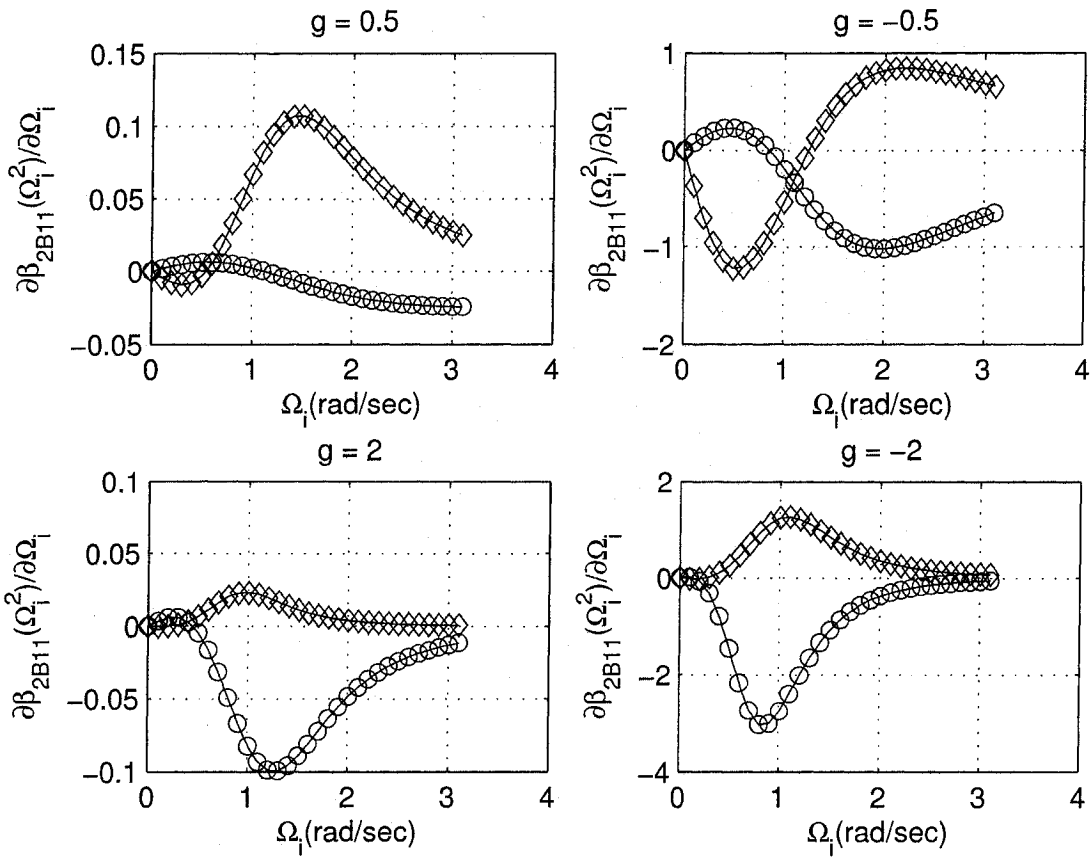


Figure 3.8: 2D Case-I(filter1) not satisfying monotonic characteristics, where, $M_{4B1}(\Omega_1, g)$ (Diamond) and $M_{5B1}(\Omega_2, g)$ (Circle).

denominator do not depend on the sign of g of the filter, as a result, poles are remained same as for the positive and negative values of g and the lower magnitude of g provides low-pass filter, but when the magnitude of g starts to increase, a 1D low-pass filter is changed to a 1D band-pass filter.

### 3.2.5 2D case-II(filter1)

Impedances of the transfer function, equation (3.2.1) are replaced by the impedance of Gargour&Ramachandran filters equations (2.4.79), (2.4.80) respectively and it has been observed in the resultant transfer function that g of the filter has less control on one dimension than another dimension (Figure 3.11).

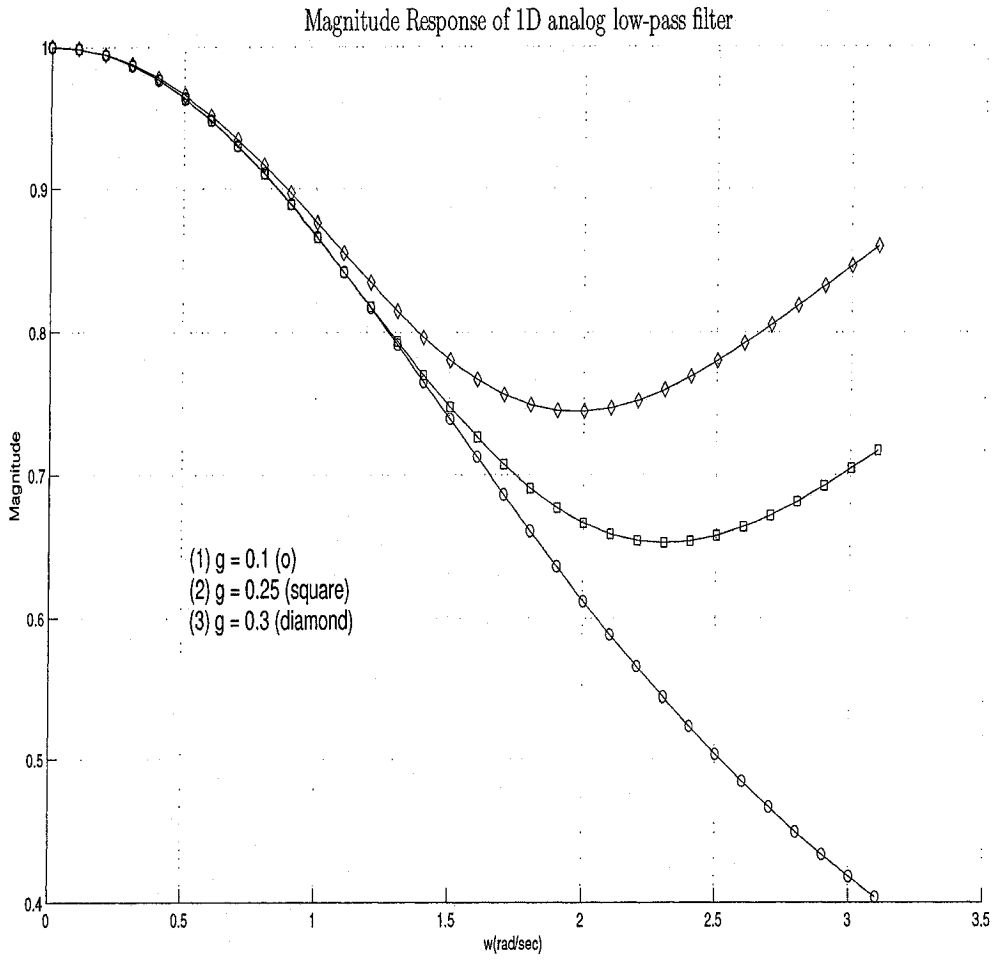


Figure 3.9: Magnitude responses of 1D case-II(filter1) for positive values of g

The overall transfer function is obtained in 2D analog domain as

$$H_{a1G2D}(s_1,s_2) = 0.48\frac{\begin{bmatrix} 1 & s_1 & s_1^2 \end{bmatrix}\begin{bmatrix} 2.1+2.1g^2+2.1g & 4.2g^2+.71g+.71 & 1.5g^2 \\ 4.2g^2+.71+4.2g & .23+9.1g^2+1.5g & 3.1g^2 \\ 1.5g^2+1.5g & 3.1g^2+.50g & g^2 \end{bmatrix}\begin{bmatrix} 1 \\ s_2 \\ s_2^2 \end{bmatrix}}{\begin{bmatrix} 1 & s_1 & s_1^2 \end{bmatrix}\begin{bmatrix} 3.0+3.0g^2 & 1.0+4.4g^2 & 1.4g^2 \\ 2.8+6.4g^2 & .92+9.6g^2 & 3g^2 \\ 2.1g^2+.72 & .24+3.2g^2 & g^2 \end{bmatrix}\begin{bmatrix} 1 \\ s_2 \\ s_2^2 \end{bmatrix}} \quad (3.2.5)$$

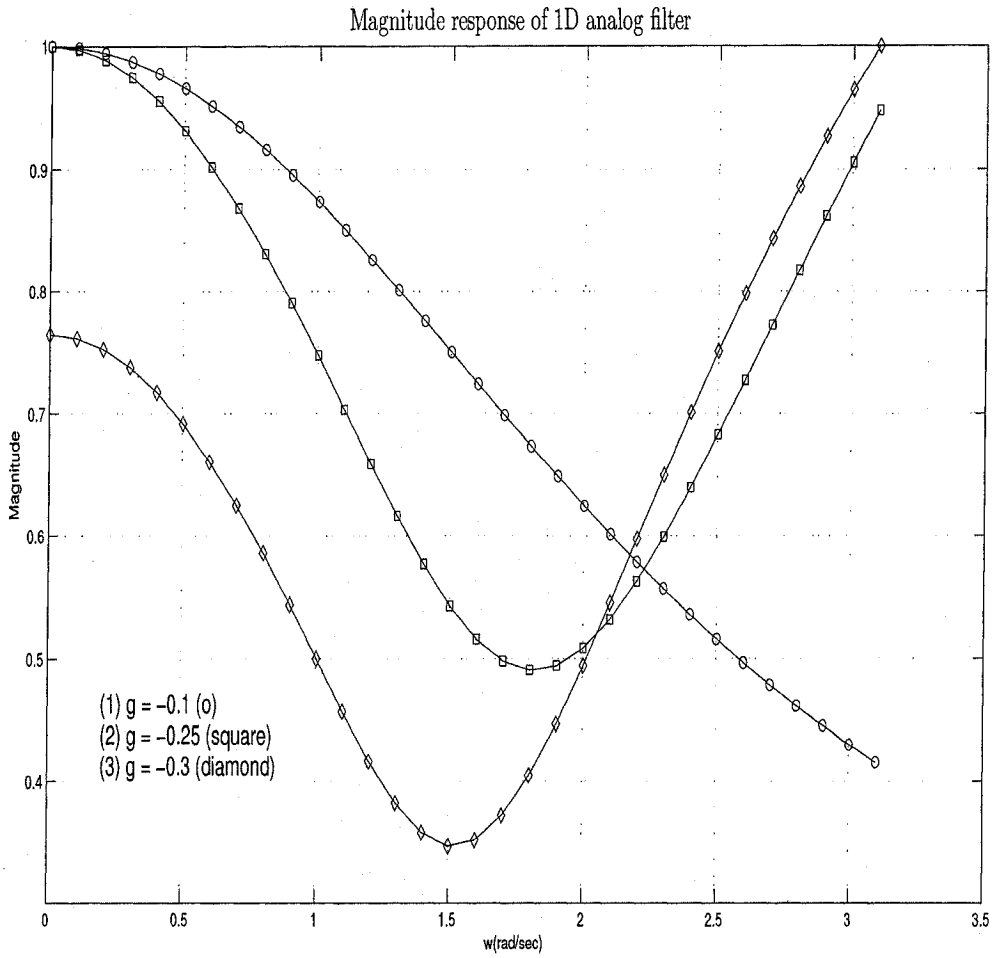


Figure 3.10: Magnitude responses of 1D case-II(filter1) for negative values of g

Figure 3.11 shows that difficulties are obtained for the specified filter design by the proposed design-I. However, the amplitude-frequency response of the filter is satisfied the monotonic characteristic, when $\mid g \mid \leq 0.1$. But the monotonic characteristic is disappeared, when the magnitude of g is started to increase.

### 3.2.6 1D case-III(filter1)

The impedances of the transfer function, equation (3.2.1) are replaced by the impedance of Gargour&Ramachandran and Butterworth filter and overall transfer function satisfies the stability condition.

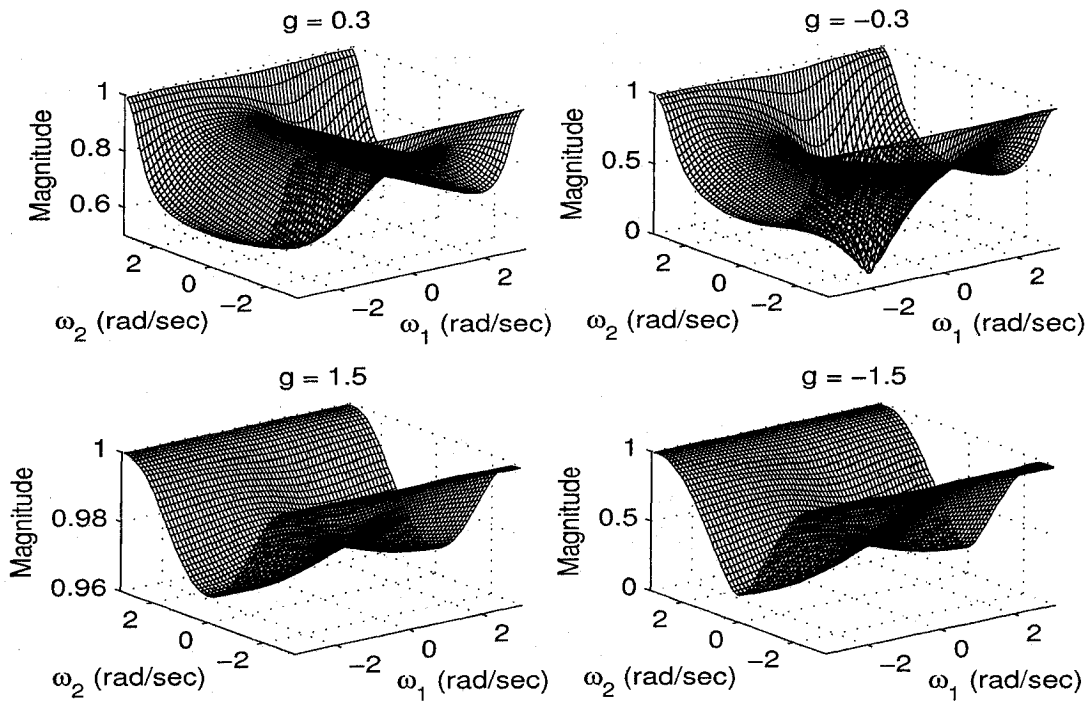


Figure 3.11: 3D magnitude plots of the 2D digital case-II(filter1) filters

$$H_{a1GB1D}(s) = \frac{g^2s^4 + (4.39g^2 + 0.7071g)s^3 + (6.62g^2 + 3.1g + 0.34)s^2 + (5g^2 + 4g + 1.4)s + 1.4(1+g)}{g^2s^4 + (0.35 + 4.7g^2)s^3 + (8.2g^2 + 1.9)s^2 + (7g^2 + 3.46)s + 2.12(1+g^2)} \tag{3.2.6}$$

Similarly, it is seen that the roots of the denominator of $H_{1BG}$ satisfy the stability condition. The bandwidth of the designed 1D low-pass filter is starts to increase and transformed to 1D high-pass filter with the increase of g's magnitude.

### 3.2.7 2D case-III(filter1)

The impedances of the transfer function (equation (3.2.1)) are replaced by the impedance of Gargour&Ramachandran filter (equation (2.4.79)) and Butterworth (equation (2.4.70)) filter. The resultant transfer function of 2D case-II(filter1) satisfies the stability criteria (section 2.4).

The overall 2D analog transfer function of the case-II(filter1) is

$$H_{a1GB2D}(s_1,s_2) = 0.50\frac{\begin{bmatrix} 1 & s_1 & s_1^2 \end{bmatrix}\begin{bmatrix} 1.4+1.4g^2+1.4g & 2g^2+.98g+.98 & 1.4g^2 \\ 3g^2+.47+3g & .34+4.2g^2+2.1g & 3g^2 \\ g^2+g & 1.4g^2+.70g & g^2 \end{bmatrix}\begin{bmatrix} 1 \\ s_2 \\ s_2^2 \end{bmatrix}}{\begin{bmatrix} 1 & s_1 & s_1^2 \end{bmatrix}\begin{bmatrix} 2.1+2.1g^2 & 1.4+2.4g^2 & 1.4g^2 \\ 4.4g^2+2.0 & 5.0g^2+1.4 & 3.0g^2 \\ 1.5g^2+.50 & .35+1.8g^2 & g^2 \end{bmatrix}\begin{bmatrix} 1 \\ s_2 \\ s_2^2 \end{bmatrix}} \quad (3.2.7)$$

It is observed that filter responses are changed with the increasing of g and the overall filter does not contain monotonic characteristics in the amplitude-frequency response. In order to overcome the problem, another design (section 3.3) is proposed which provides monotonic characteristics in the amplitude-frequency response of the desired filter.

### 3.2.8 Filter2

Transfer function of filter2 has been derived in the section 2.2 and in order to ensure the stability criteria in 2D domain, the two impedances of filter2 are replaced by second-order Butterworth and/or Gargour&Ramachandran filters and the third impendence is replaced by a resistive component, because otherwise the denominator of the transfer function will not satisfy the VSHPs (section 2.4.5). It is observed that the numerator of the transfer function depends on the value and sign of g of the gyrator filter. However, the denominator of the transfer function is independent of the sign of g. For illustration, different combinations of the RLC circuits are placed in the gyrator filter2 and for simplicity, each circuit is classified, such as the impedances of filter2 are replaced by the second-order Butterworth filters are called case-I(filter2). Similarly, the impedances of filter2 are replaced by the second-order Gargour&Ramachandran filters are called case-II(filter2) and impedances of filter2 are replaced by the second-order Butterworth and Gargour&Ramachandran filters are called case-III(filter2). Each case of the filter design is described by using the proposed design-I.

### 3.2.9 1D case-I(filter2)

The impedances of the filter2 (equation (2.2.10)) are replaced by the impedances of second-order Butterworth filters (equation (2.4.69)) and third impedance is replaced by resistive component (unit value) and the overall transfer function of the case-I(filter2) satisfies the stability condition for the different magnitudes of g which is shown in the Table 3.3. The overall transfer function of case-I(filter2) is

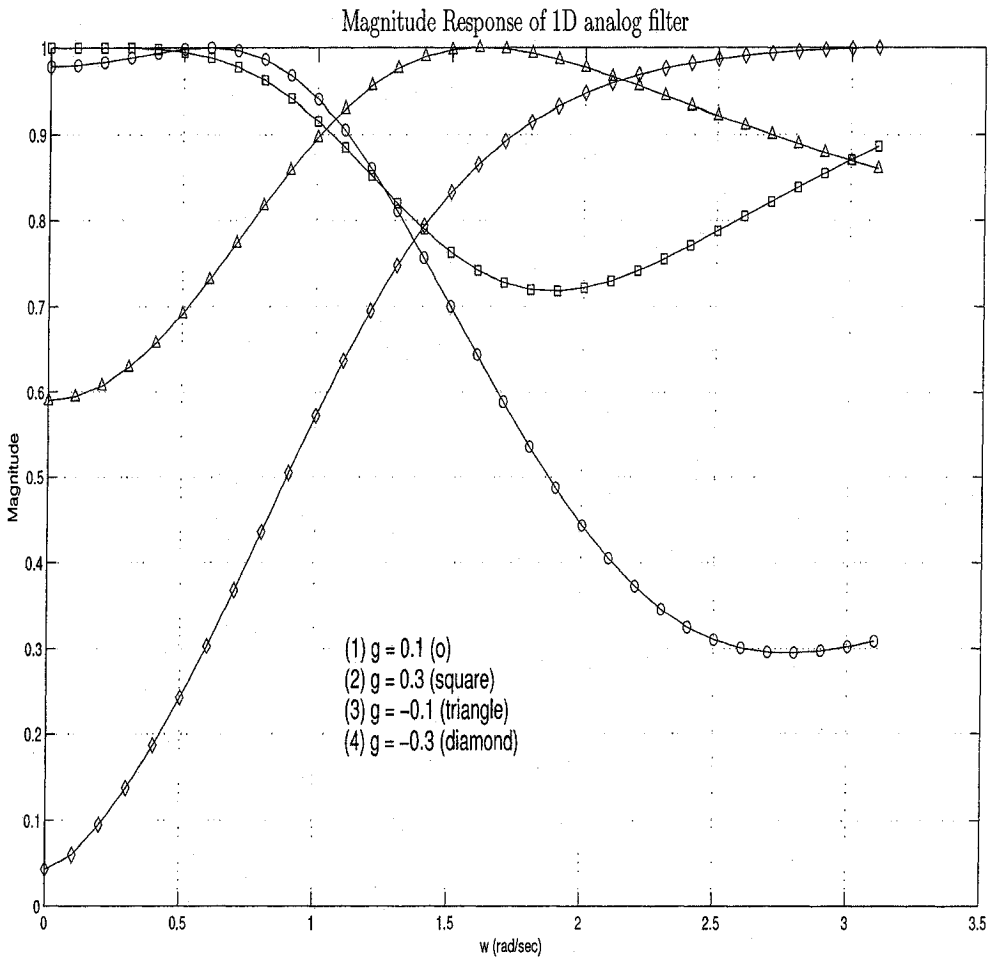


Figure 3.12: Magnitude responses of the case-I(filter2)

$$H_{a2B1D}(s) = \frac{gs^4 + 4.2gs^3 + (8g + 0.5)s^2 + (7g + 1.4)s + 3g + 1}{(1 + g^2)s^4 + (4.2g^2 + 5.6)s^3 + (13.5 + 8g^2)s^2 + (7g^2 + 15.5)s + 8 + 3g^2} \tag{3.2.8}$$

Table 3.3: The locations of poles of the case-I(filter2) ($H_{a2B1D}(s)$) in 1D analog domain.

| g | Locations of the poles of $H_{2B1D}(s)$ |
|---|---|
| 0.1 | $-1.0589 \pm 0.9347i$, $-1.7625 \pm 0.9374i$ |
| 0.3 | $-1.0451 \pm 0.9294i$, $-1.7249 \pm 0.9505i$ |
| 0.5 | $-1.0195 \pm 0.9188i$, $-1.6675 \pm 0.9674i$ |
| 1.5 | $-0.8558 \pm 0.8296i$, $-1.4831 \pm 0.9976i$ |
| 2 | $-0.8073 \pm 0.7948i$, $-1.4554 \pm 0.9992i$ |
| 5 | $-0.7273 \pm 0.7267i$, $-1.4212 \pm 1.00i$ |

Figure 3.12 shows that the amplitude-frequency responses of the 1D analog low-pass filter with the increase of g and opposite types of responses are obtained for the negative value of g. Table 3.3 ensures the stability of the 1D filter and it has been shown that poles are in the left side of s-domain and complex poles should be in complex conjugate pair.

### 3.2.10 2D case-I(filter2)

The major concern of 2D filter design is stability and the stability of filter2 is ensured when the third impendence is resistive and the rest of the two impedances of filter2 are replaced by second-order Butterworth filters (section 2.4.5). Numerator of the resulting transfer function depends on the value and sign of g. However, the denominator is independent of the sign of g. Impedances $Z_1$ and $Z_2$ are replaced by the impedances of Butterworth filter, equations (2.4.69) and (2.4.70) corresponding to $s_1$ and $s_2$ domain and $Z_3$ is independent of frequency. The overall transfer function of the 2D analog case-I(filter2) is shown below:

$$H_{a2B2D}(s_1, s_2) = \frac{\begin{bmatrix} 1 & s_1 & s_1^2 \end{bmatrix} \begin{bmatrix} 6g+2 & 0.68+8.8g & 2.8g \\ .68+8.8g & 12g+0.22 & 3.4g \\ 2.8g & 3.4g & g \end{bmatrix} \begin{bmatrix} 1 \\ s_2 \\ s_2^2 \end{bmatrix}}{\begin{bmatrix} 1 & s_1 & s_1^2 \end{bmatrix} \begin{bmatrix} 16.+6.0g^2 & 16.+8.8g^2 & 4.4+2.8g^2 \\ 16+8.8g^2 & 12g^2+15 & 3.4g^2+3.9 \\ 4.4+2.8g^2 & 3.4g^2+3.9 & g^2+1 \end{bmatrix} \begin{bmatrix} 1 \\ s_2 \\ s_2^2 \end{bmatrix}} \tag{3.2.9}$$

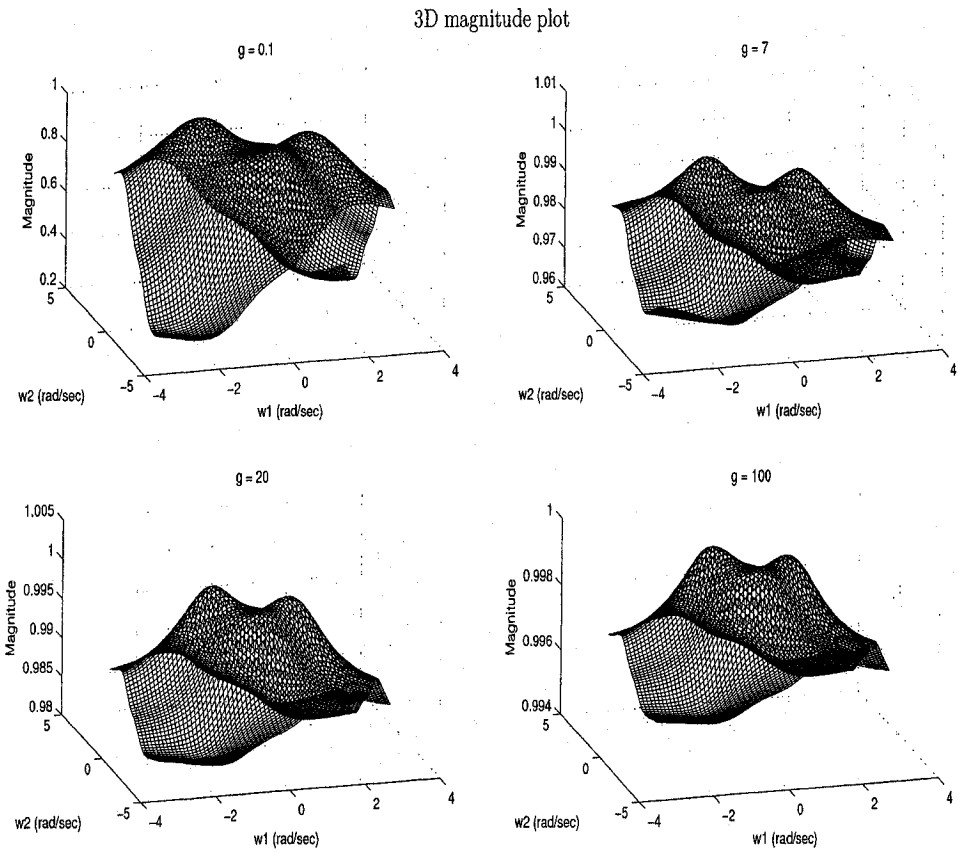


Figure 3.13: 3D magnitude responses of the case-I(filter2)

Figure 3.13 shows the frequency responses of the filter and the responses do not have satisfy the constrains of having the monotonic characteristics (equations (3.1.34, 3.1.35)).

### 3.2.11 1D case-II(filter2)

The impedances of the filter2 (equation (2.2.10)) are replaced by the impedances of Gargour&Ramachandran filters (equation (2.4.79)) and third impedance is replaced by resistive component (unit value). The overall transfer function of case-II(filter2) is given by

$$H_{a2G1D}(s) = \frac{gs^4 + 6.9gs^3 + (17.3g + 0.2)s^2 + (18.2g + 1.3)s + 6g + 2}{(g^2 + 1)s^4 + (6.9g^2 + 7.8)s^3 + (17.3g^2 + 23.7)s^2 + (23.7 + 18.2g^2)s + 16 + 6g^2} \tag{3.2.10}$$

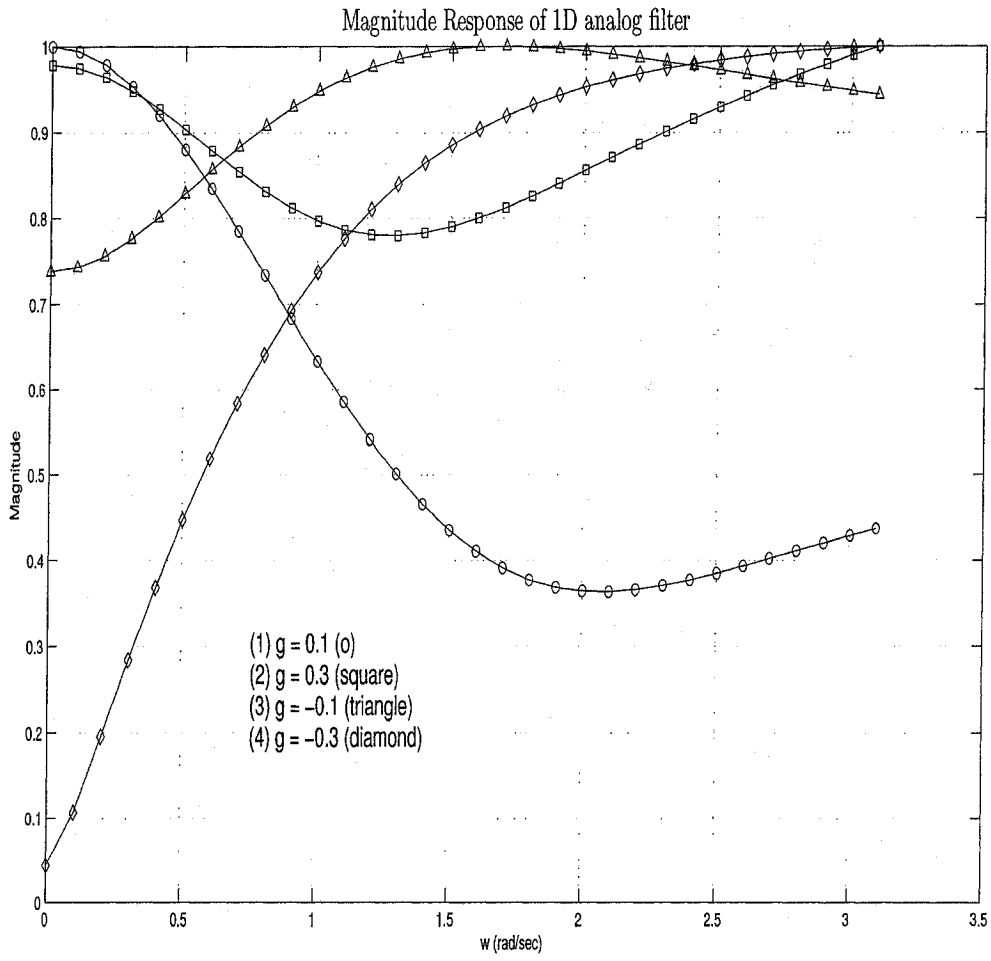


Figure 3.14: Magnitude responses of the case-II(filter2)

Table 3.4 has shown that the transfer function of case-II(filter2), $H_{2G}(s)$ satisfies the stability condition for the different values of g. Figure 3.14 has shown that amplitude-frequency responses of the 1D analog low-pass filter with the increase of g and opposite types of the responses are obtained for the negative values of g.

### 3.2.12 2D case-II(filter2)

In the filter2, two impedances ($Z_1$ and $Z_2$) are replaced by the Gargour&Ramachandran filters (equations (2.4.79) and (2.4.80)) and for the stability purpose, third impedance is replaced by resistive parameter (section 2.4.5). The overall transfer function is

Table 3.4: Stability tests of the 1D analog case-II(filter2)($H_{a2G1D}$).

| g | Poles of $H_{2G}(s)$ |
|---|---|
| 0.1 | $-1.3368, -2.1107, -2.1970 \pm 0.9000i$ |
| 0.3 | $-1.2986, -2.1304, -2.1717 \pm 0.8775i$ |
| 0.5 | $-1.2317, -2.1628, -2.1331 \pm 0.8405i$ |
| 1.5 | $-0.8731\ -2.3013, -2.009 \pm 0.6946i$ |
| 2 | $-0.7791, -2.3302, -1.9904 + 0.6679i$ |
| 5 | $-0.6306, -2.3710, -1.9674 \pm 0.6327i$ |

shown below:

$$H_{a2G2D}(s_1,s_2) = \frac{\begin{bmatrix} 1 & s_1 & s_1^2 \end{bmatrix} \begin{bmatrix} 6g+2 & 0.68+8.8g & 2.8*g \\ 0.68+8.8g & 12g+.22 & 3.4g \\ 2.8g & 3.4g & g \end{bmatrix} \begin{bmatrix} 1 \\ s_2 \\ s_2^2 \end{bmatrix}}{\begin{bmatrix} 1 & s_1 & s_1^2 \end{bmatrix} \begin{bmatrix} 16.+6.0g^2 & 16.+8.8g^2 & 4.4+2.8g^2 \\ 16.+8.8g^2 & 12g^2+15 & 3.4g^2+3.9 \\ 4.4+2.8g^2 & 3.4g^2+3.9 & g^2+1 \end{bmatrix} \begin{bmatrix} 1 \\ s_2 \\ s_2^2 \end{bmatrix}} \quad (3.2.11)$$

3D magnitude responses of case-II(filter2) are shown in Figure 3.15.

### 3.2.13 1D case-III(filter2)

The impedances of the transfer function (equation (2.2.10)) are replaced by the impedances of Gargour&Ramachandran and Butterworth filter and similarly, it is seen that the roots of denominator of the resultant transfer function satisfy the stability condition. Bandwidth of the designed 1D low-pass filter starts to increase and transformed to 1D band-pass filter with the increase of g's magnitude and opposite types of frequency responses are obtained for the negative value of g.

### 3.2.14 2D case-III(filter2)

The impedances of the transfer function (equation (2.2.10)) are replaced by the impedances of Gargour&Ramachandran filter (equation (2.4.79)) and Butterworth

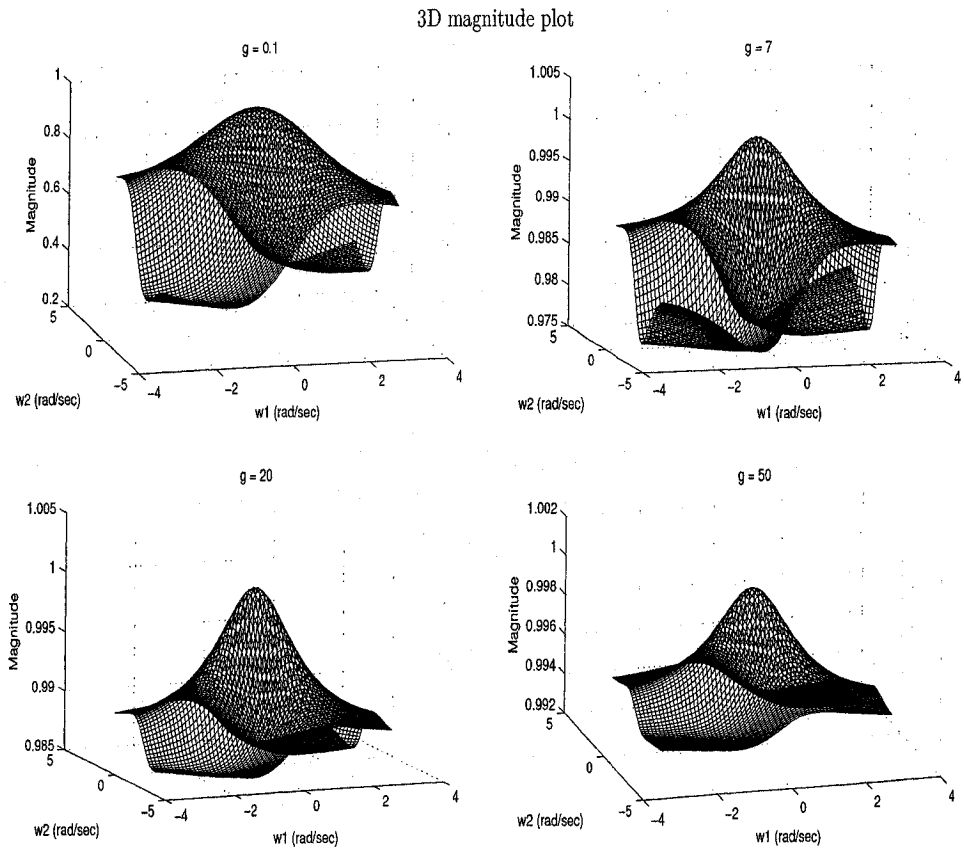


Figure 3.15: 3D magnitude responses of the case-II(filter2)

filter (equation (2.4.70)). For the stability purpose, third impedance of filter2 is replaced by resistive parameter (section 2.4.5). It has been seen that the resultant transfer function of 2D case-II(filter1) satisfies the stability criteria. It is observed that the filter responses of the transfer function are changed with the increasing of g and difficulties are encountered to achieve the monotonic characteristics in the amplitude-frequency response of the desired filter. In order to overcome the problem, another design (section 3.3) is proposed which provides monotonic characteristics in the amplitude-frequency response of the desired filter.

Overall, proposed design-I provides simpler techniques of digital filter design by choosing the appropriate doubly terminated RLC networks which are replaced by the impedances of the gyrator network. It is seen that the proposed design-I is applied to the both gyrator networks to design the 2D digital low-pass filter design. Also, the value of g of the gyrator network is kept in the lower range, because the frequency

responses are very sensitive to the magnitude of g. However, in most of the cases, the design-I has not given the monotonic characteristics in the amplitude-frequency response of the digital filter. In the following section 3.3, another filter design is proposed which can overcome the design problems created by proposed design-I.

## 3.3 Proposed Design-II

Impedances of the doubly terminated gyrator network are replaced by the impedances of doubly terminated RLC networks and the stability of the resultant analog filter is satisfied (section 2.4). The GBT is applied to the transfer function of the resultant analog filter in order to obtain the corresponding digital filter responses and some constrains have to be given to obtain the monotonic amplitude characteristic in the pass-band regions.

The desired filter response is obtained by regulating the value and sign of $g$ as well as the parameters of the GBT and some constrains (equations (3.1.12) to (3.1.15), (3.1.34) and (3.1.35)) are followed in order to obtain the monotonic characteristics in the pass-band regions.

The generalized bilinear transformation [15] in the case of 2D is shown below:

$$s_i = k_i \frac{(z_i + a_i)}{(z_i + b_i)} \tag{3.3.1}$$

where i =1,2.

To ensure stability, the conditions to be satisfied are: $k_i > 0$, $\mid a_i \mid \leq 1$, $\mid b_i \mid \leq 1$ and $a_i b_i < 0$

The desired digital filters are obtained from the analog transfer function by varying the values of $k_i$, $a_i$ and $b_i$, such as low-pass, high-pass, band-pass and band-elimination filter. It is seen that a digital low-pass filter is obtained from filter 1 and filter 2 when $k_i > 0$, $-1 \leq a_i < 0$ and $0 < b_i \leq 1$ and the overall filter satisfies monotonic characteristics. The following relations are derived from the equations (2.3.7), (3.1.9) and (3.1.10) in order to achieve the monotonic amplitude-frequency response in pass-band region.

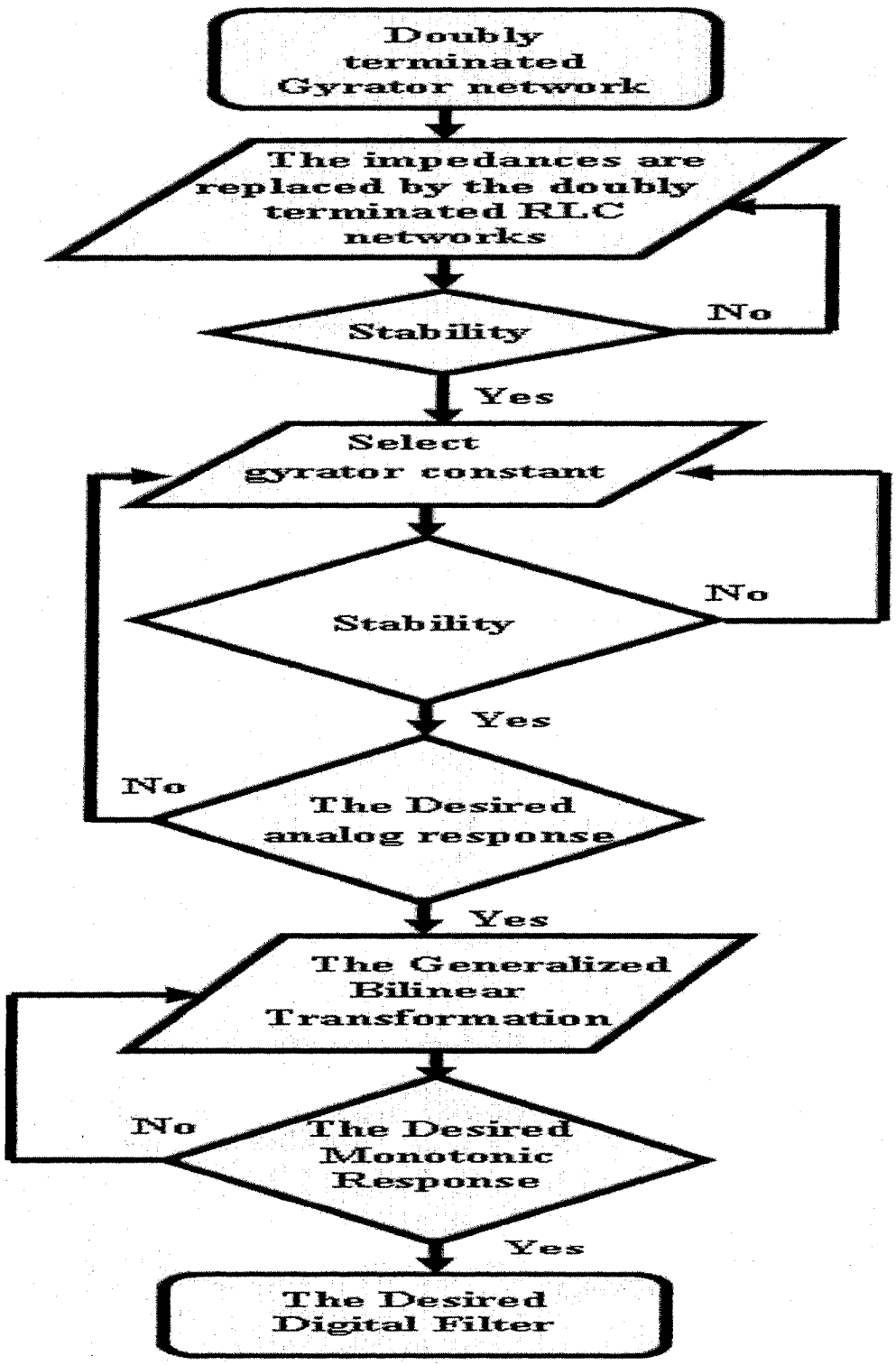


Figure 3.16: Proposed Design-II

$$M_6(\Omega_1, 0) = \{k_1 \frac{(b_1 - a_1) sin\Omega_1}{1 + (b_1)^2 + 2b_1 cos\Omega_1}\}^2 - \frac{4d_{20}d_{00} - 2d_{10}^2}{4d_{20}^2} \geq 0 \tag{3.3.2}$$

$$M_7(0, \Omega_2) = \{k_2 \frac{(b_2 - a_2) sin\Omega_2}{1 + (b_2)^2 + 2b_2 cos\Omega_2}\}^2 - \frac{4d_{02}d_{00} - 2d_{01}^2}{4d_{02}^2} \geq 0 \tag{3.3.3}$$

Similar to the equations (3.1.12) to (3.1.15), (3.1.34) and (3.1.35), the limits of the parameters of the GBT can be defined to achieve the monotonic characteristic in amplitude-frequency response of a filter. The corresponding modified analog transfer function can be obtained from the discrete transfer function by applying the inverse bilinear transformation (equation (3.3.4)).

$$z_i = \frac{(1 + s_i)}{(1 - s_i)} \tag{3.3.4}$$

where i = 1,2.

The resultant filter has the bandwidth and the cutoff frequency, which are controlled by the parameters of the GBT and $g$ of the gyrator network. This design gives freedom of choice to select any type of stable analog circuit in order design the desired digital filter. In the following, the purposed design is applied on filter1 and filter2 and illustrate the usefulness of the design.

### 3.3.1 Filter1

Previous design (proposed design-I) has shown that the impedances of filter1 are replaced by the impedances of doubly terminated RLC filters (second-order Butterworth and Gargour&Ramachandran filter) and overall filter may or may not satisfy the condition for monotonic characteristic in the amplitude-frequency response. But the proposed design-II provides the guaranteed monotonic amplitude-frequency response of the designed filter. Figures 3.2, 3.8 have shown that the overall filter responses of the case-I(filter) do not contain monotonic characteristic. However, the proposed design-II gives opportunity to obtain the monotonic characteristic from any types of analog filters.

Figure 3.8 shows that the case-I(filter1) does not contain the monotonic characteristic. But the proposed design-II can design the specified digital filter with the monotonic characteristic in the amplitude-frequency response. Figure 3.17 shows that the frequency response of the modified case-I(filter1) possesses the monotonic characteristic by applying the proposed design-II. In Figure 3.17, $g = 0.001$ and the parameters of the GBT are $a_i = -0.2$, $b_i = 0.8$ and $k_i = 1$.

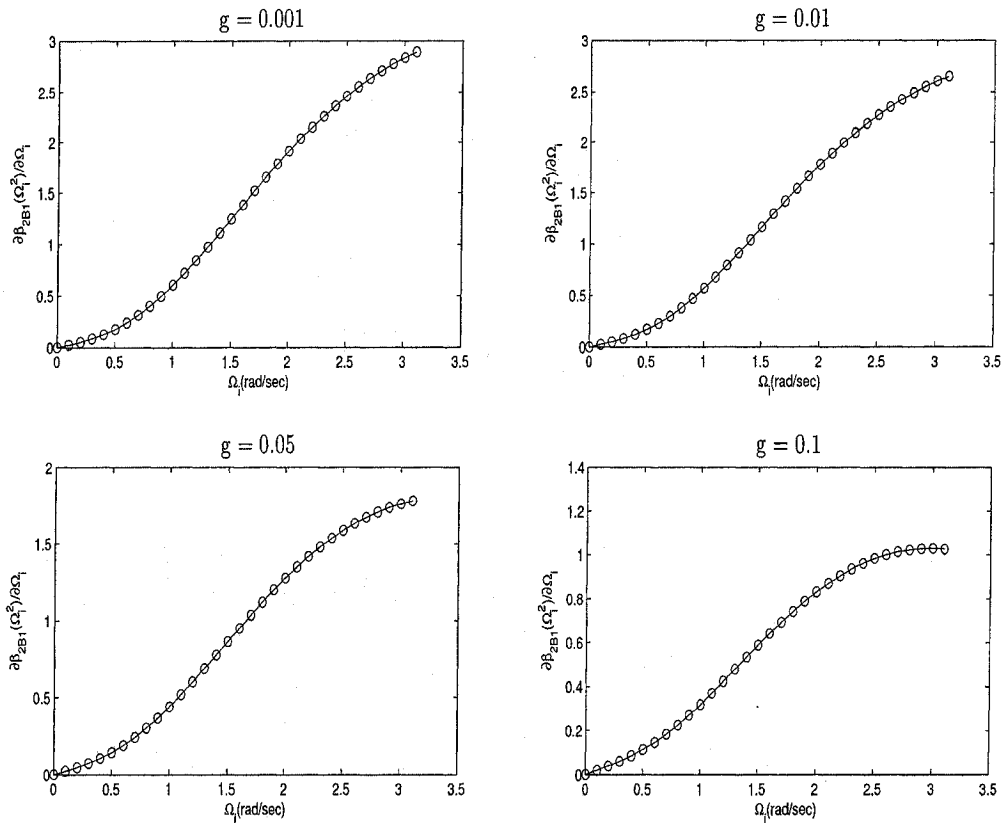


Figure 3.17: The modified case-I(filter1) satisfies the monotonic characteristic, when $g = 0.001$.

According to the proposed design-I, the impedances of the filter1 are replaced by the impedances of different combinations of the Butterworth and Gargour&Ramachandran filters. The coefficients of the overall analog transfer function (filter1) are dependent on the value and sign of $g$. The coefficients of the denominator of equation(3.2.1) are independent of the sign of $g$ and the amplitude-frequency response of the filter 1 is constant for $g = 1$. Finally, the bilinear transformation is applied in order to

obtain the desired 2D digital filter. However, the proposed method-II uses the GBT instead of using the bilinear transformation. Proposed design-II are described in the following and design examples are given to illustrate the usefulness of the proposed design.

### 3.3.2 2D case-I(filter1)

The impedances of filter1 are replaced by the impedances of second-order Butterworth filters and the GBT is applied to the overall transfer function (equation (3.2.3)). Appropriate parameters of the GBT provide the desired 2D digital low-pass filter. For example, a 2D digital low-pass filter ($g = 0.001$) is designed when the parameters of the GBT are $a_i = -0.2$, $b_i = 0.8$ and $k_i = 3$. The 3D magnitude plot and contour plot of the 2D digital low-pass filter are shown in Figures 3.18 (a) and (b) respectively. According to equations (3.1.34), (3.1.35), the response of case-I(filte1) has satisfied the monotonic characteristics ($\partial\beta_{2B12}/\partial\Omega_i \geq 0$) in the pass-band region. Figures 3.18 (c) and (d) show that the case-I(filter1) satisfies the monotonicity in the amplitude-frequency response.

Table 3.5 gives the ranges of $k_i$ for the certain values of $g$, $a_i$ and $b_i$, that satisfies the condition of monotonic characteristics in the amplitude-frequency responses of case-I (filter1).

Table 3.5: The ranges of $k_i$ satisfy the monotonic characteristics in the amplitude-frequency response of case-I(filter1)

| g | $a_i$ | $b_i$ | $k_i$ |
|---|---|---|---|
| 0.001 | −0.9 | 0.9 | $0.09 > k_i > 0$ |
| 0.001 | −0.9 | 0.5 | $0.4 > k_i > 0$ |
| 0.001 | −0.5 | 0.9 | $205 > k_i > 0$ |
| 0.001 | −0.5 | 0.5 | $10 > k_i > 0$ |
| 0.001 | −0.5 | 0.1 | Not Possible |

This 2D digital low-pass filter is turned into 2D digital high-pass filter with the increase in this value of $g$.

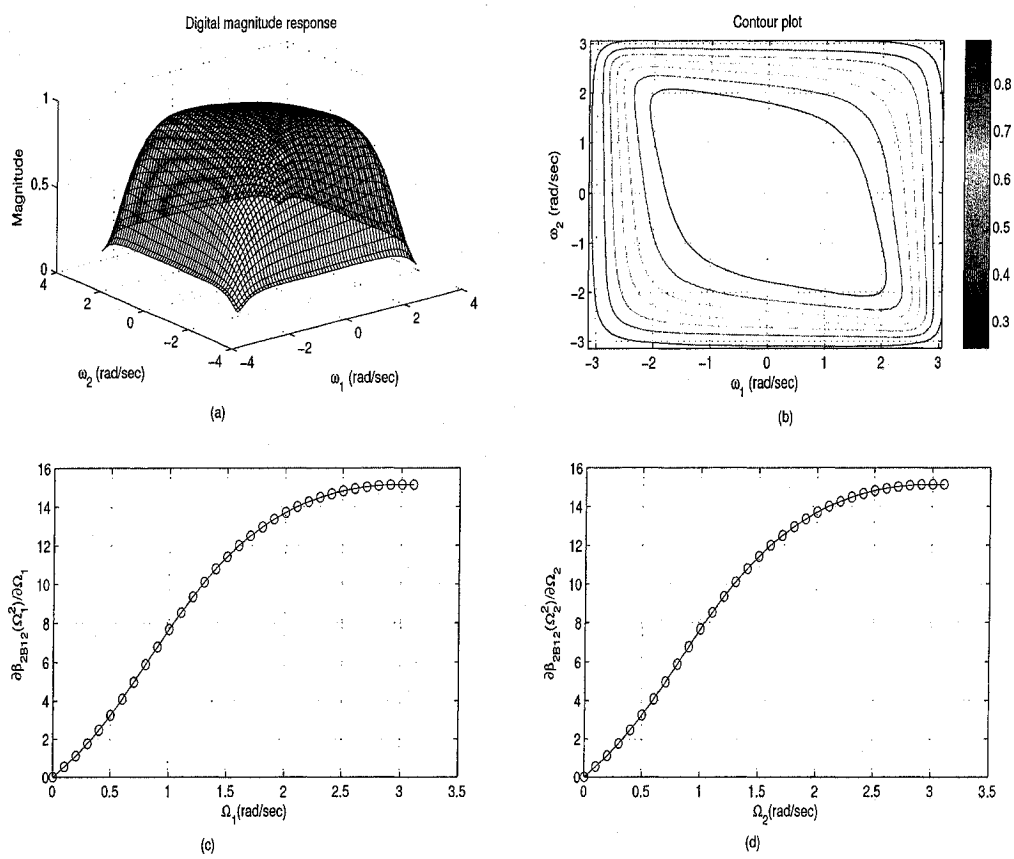


Figure 3.18: The 2D digital low-pass filter (case-I(filter1)) when g = 0.001, (a)3D magnitude plot, (b) contour plot, (c) and (d) the case-I(filter1) satisfies the monotonic characteristic.

### 3.3.3 2D case-II(filter1)

The impedances of filter1 are replaced by the impedances of second-order Gargour& Ramachandran filters and the GBT is applied to the overall transfer function (equation (3.2.5)). As a result, 2D digital low-pass filter is obtained for the appropriate parameters of the GBT and g of the gyrator network. The parameters of the GBT and g have control on the bandwidth of the designed 2D digital low-pass filter.

Figures 3.19 (a) and (b) show the 3D magnitude plot and contour plot of the 2D digital low-pass filter respectively, when $g = 0.001$, $a = -0.1$, $b = 0.7$ and $k = 1$. According to equations (3.1.34), (3.1.35), the response of case-II(filte1) has satisfied the monotonic characteristics ($\partial\beta_{2G12}/\partial\Omega_i \geq 0$) in the pass-band region. Figures 3.19

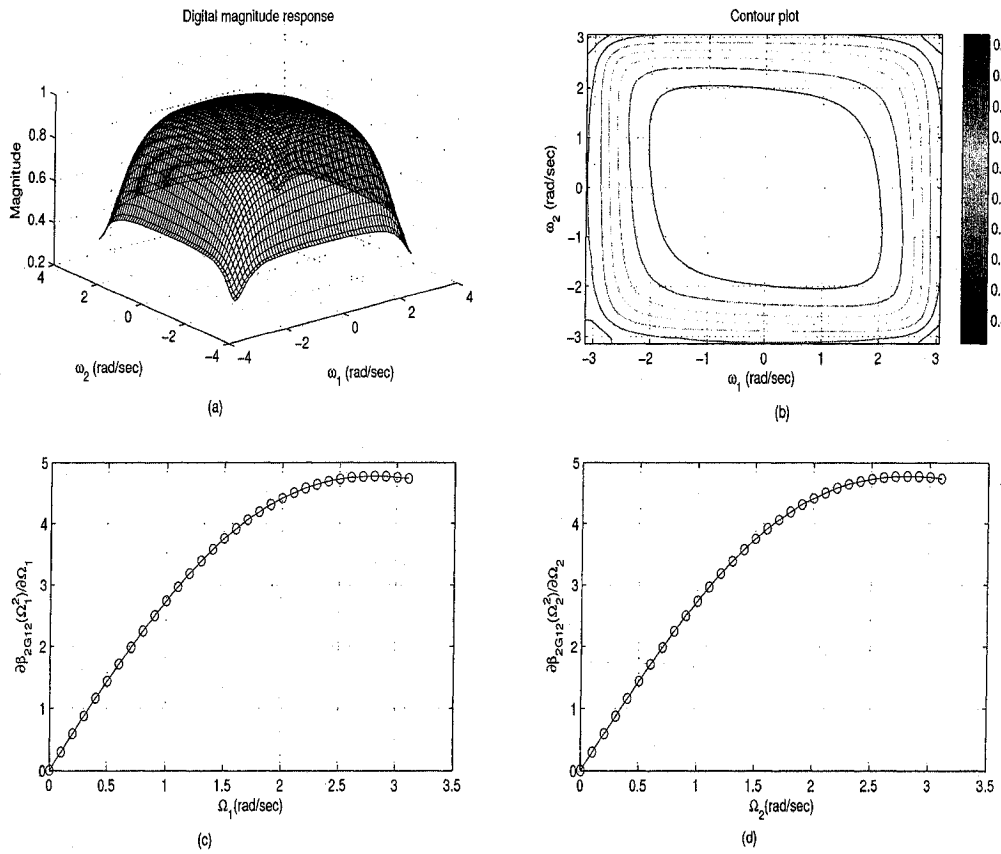


Figure 3.19: The 2D digital low-pass filter (case-II(filter1)) when g = 0.001, (a)3D magnitude plot, (b) contour plot, (c) and (d) the case-II(filter1) satisfies the monotonic characteristic.

(c) and (d) show that the case-II(filter1) satisfies the monotonicity in the amplitude-frequency response. Table 3.6 gives the ranges of $k_i$ for the certain values of $g$, $a_i$ and $b_i$, that satisfies the condition of monotonic characteristics in the amplitude-frequency responses of case-II (filter1).

### 3.3.4 2D case-III(filter1)

In this case, the impedances of second-order Butterworth and Gargour&Ramachandran filters are replaced by the impedances of the filter1 in order to design the 2D low-pass filter. In the section 3.2, It has seen that the low-pass filters are obtained for the lower values of g in equation (3.2.7). However, the proposed design-II provides the others parameters of the GBT to control the amplitude-frequency response of the filter.

Table 3.6: The ranges of $k_i$ satisfy the monotonic characteristics in the frequency response of case-II(filter1)

| g | $a_i$ | $b_i$ | $k_i$ |
|---|---|---|---|
| 0.001 | −0.9 | 0.9 | $82 > k_i > 0$ |
| 0.001 | −0.9 | 0.5 | $1.5 > k_i > 0$ |
| 0.001 | −0.5 | 0.9 | $95 > k_i > 0$ |
| 0.001 | −0.5 | 0.5 | $1 > k_i > 0$ |
| 0.001 | −0.5 | 0.1 | Not Possible |

Table 3.7: The ranges of $k_i$ allow to obtain monotonic characteristics in frequency response of the case-III(filter1)

| g | $a_i$ | $b_i$ | $k_i$ |
|---|---|---|---|
| 0.001 | −0.9 | 0.9 | $0.1 > k_i > 0$ |
| 0.001 | −0.5 | 0.9 | $100 > k_i > 0$ |
| 0.001 | −0.9 | 0.5 | $0.9 > k_i > 0$ |
| 0.001 | −0.5 | 0.5 | $0.5 > k_i > 0$ |

Figures 3.20 (a) and (b) show the 3D magnitude plot and contour plot of the 2D digital low-pass filter respectively, when $g = 0.001$, $a = -0.2$, $b = 0.9$ and $k = 10$. According to equations (3.1.34), (3.1.35), the response of case-II(filte1) has satisfied the monotonic characteristics ($\partial\beta_{2GB12}/\partial\Omega_i \geq 0$) in the pass-band region. Figures 3.20 (c) and (d) show that the case-III(filter1) satisfies the monotonicity in the amplitude-frequency response. Table 3.7 gives the ranges of $k_i$ for the values of $g$, $a_i$ and $b_i$ in order to obtain the monotonic characteristics in the amplitude-frequency responses of the case-III (filter1).

### 3.3.5 Filter2

Filter2 contains three impedances and for the stability purpose (section 2.4.5), third impedance of filter2 is replaced by a resistive component and the remaining of the two impedances are replaced by the impedances of doubly-terminated RLC filters (second-order Butterworth and Gargour&Ramachandran filter). It has determined that the denominator of the resultant 2D analog transfer function is VSHP (section 2.4)and the coefficients of the denominator are dependent on values of g of filter2. Finally, the GBT is applied to the 2D analog transfer function in order to obtain the desired 2D digital low-pass filter.

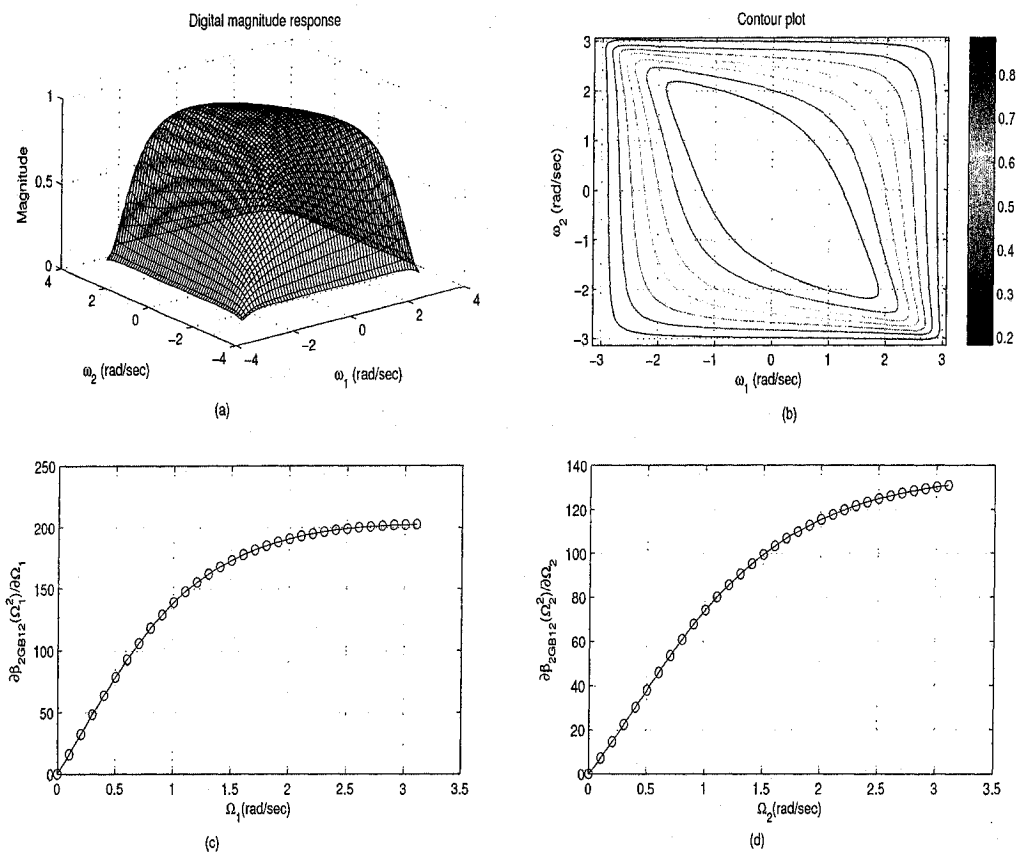


Figure 3.20: The 2D digital low-pass filter (case-III(filter1)) when g = 0.001, (a)3D magnitude plot, (b) contour plot, (c) and (d) the case-III(filter1) satisfies the monotonic characteristic.

### 3.3.6 2D case-I(filter2)

Two impedances ($Z_1$ and $Z_2$) of filter2 are replaced by the impedances of second-order Butterworth filters and the third impedance ($Z_3$) of filter2 is replaced by a resistive component. The GBT is applied to the analog transfer function (equation (3.2.9)) and the digital transfer function (equation (3.3.5)) of the case-I(filter2) is obtained, when $a_i = -0.2$, $b_i = 0.9$, $k_i = 10$. It is seen that the effect of parameters of the GBT is less for the lower values of $g$.

$$H_{d2B}(z_1,z_2)=\frac{\begin{bmatrix}1 & z_1 & z_1^2\end{bmatrix}\begin{bmatrix}0.001+9.6g & -31g+0.0085 & -0.017+25g\\ -5.5g-0.49 & -430g+8.5 & 7+65g\\ 35g-0.61 & 10+2400g & -430g+8.5\end{bmatrix}\begin{bmatrix}1\\ z_2\\ z_2^2\end{bmatrix}}{27.2\begin{bmatrix}1 & z_1 & z_1^2\end{bmatrix}\begin{bmatrix}0.033+0.47g & 35g-0.61 & -5.5g-0.49\\ -0.095-0.21g^2 & -16g^2-12 & 2.4g^2+1\\ 1.1+1.3g^2 & 100+89g^2 & -16g^2-12\end{bmatrix}\begin{bmatrix}1\\ z_2\\ z_2^2\end{bmatrix}} \quad (3.3.5)$$

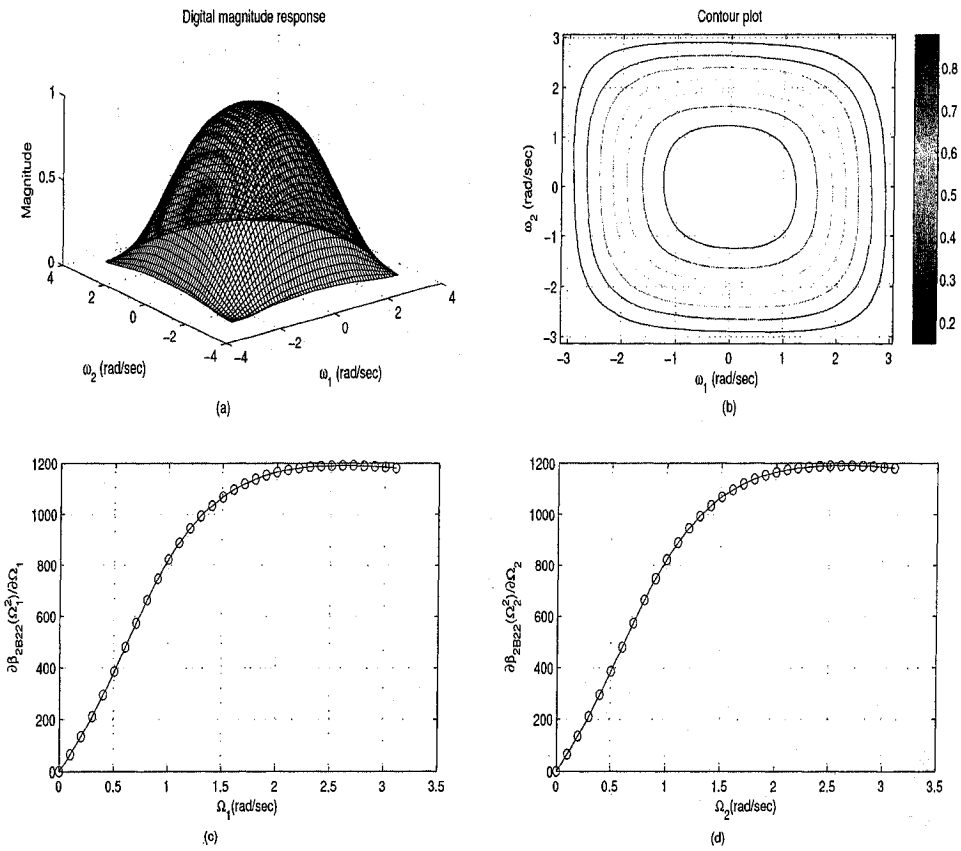


Figure 3.21: The 2D digital low-pass filter (case-I(filter2)) when g = 0.001, (a)3D magnitude plot, (b) contour plot, (c) and (d) the case-I(filter2) satisfies the monotonic characteristic.

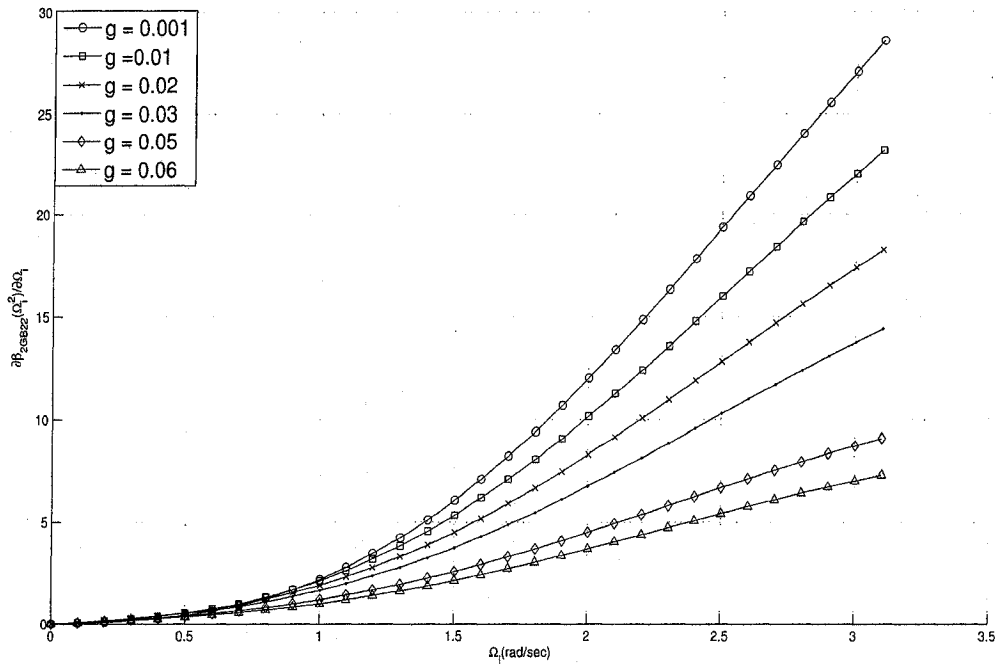


Figure 3.22: The case-I(filter2) satisfies the monotonic characteristics for the different values of $g$.

Figures 3.21 (a) and (b) show the 3D magnitude plot and contour plot of the 2D digital low-pass filter respectively, when $g = 0.001$. According to equations (3.1.34), (3.1.35), the response of case-II(filte1) has satisfied the monotonic characteristics ($\partial\beta_{2B22}/\partial\Omega_i \geq 0$) in the pass-band region. Figures 3.21 (c) and (d) show that the case-I(filter2) satisfies the monotonicity in the amplitude-frequency response. Figure 3.22 has shown the monotonic characteristics of case-I(filter2) for different values of g. Table 3.8 gives the ranges of $k_i$ for the values of $g$, $a_i$ and $b_i$ in order to obtain the monotonic characteristics in the amplitude-frequency responses of the case-I (filter2).

### 3.3.7 2D case-II(filter2)

Two impedances of filter2 are replaced by the impedances of Gargour&Ramachandran filters and third impedance of filter2 is replaced by a resistive component. The GBT ($a = -0.1$, $b = 0.9$, and $k = 0.5$) is applied to the resultant analog transfer function (equation (3.2.11)) and obtained digital transfer function, equation (3.3.6) provides

Table 3.8: The ranges of $k_i$ provide monotonic characteristics in the frequency response of case-I(filter2)

| g | $a_i$ | $b_i$ | $k_i$ |
|---|---|---|---|
| 0.01 | $-0.9$ | 0.9 | $0.2 > k_i > 0$ |
| 0.01 | $-0.9$ | 0.5 | $0.7 > k_i > 0$ |
| 0.01 | $-0.5$ | 0.9 | $4 > k_i > 0$ |
| 0.01 | $-0.5$ | 0.5 | $2 > k_i > 0$ |
| 0.01 | $-0.1$ | 0.1 | Not possible |

the variable magnitude response with the monotonic characteristics.

$$H_{d2G}(z_1,z_2) = \frac{\begin{bmatrix} 1 & z_1 & z_1^2 \end{bmatrix} \begin{bmatrix} 0.45+1.2g & 3.8g+1.1 & 0.67+3g \\ 3.8g+1.1 & 12g+2.7 & 9.1g+1.6 \\ 0.67+3g & 9.1g+1.6 & 1+7.4g \end{bmatrix} \begin{bmatrix} 1 \\ z_2 \\ z_2^2 \end{bmatrix}}{13.64 \begin{bmatrix} 1 & z_1 & z_1^2 \end{bmatrix} \begin{bmatrix} 0.25+0.087g^2 & 0.73+0.28g^2 & 0.51+0.22g^2 \\ 0.73+0.28g^2 & 0.87g^2+2 & 1.5+0.67g^2 \\ 0.51+0.22g^2 & 1.5+0.67g^2 & 1+0.54g^2 \end{bmatrix} \begin{bmatrix} 1 \\ z_2 \\ z_2^2 \end{bmatrix}} \quad (3.3.6)$$

Table 3.9: The ranges of $k_i$ for the monotonic characteristic in the amplitude-frequency response of case-II(filter2).

| g | $a_i$ | $b_i$ | $k_i$ |
|---|---|---|---|
| 0.01 | $-0.9$ | 0.9 | $0.2 > k_i > 0$ |
| 0.01 | $-0.9$ | 0.5 | $0.6 > k_i > 0$ |
| 0.01 | $-0.5$ | 0.9 | $3 > k_i > 0$ |
| 0.01 | $-0.5$ | 0.5 | $2 > k_i > 0$ |
| 0.01 | $-0.1$ | 0.1 | Not possible |

Figures 3.23 (a) and (b) show the 3D magnitude plot and contour plot of the 2D digital low-pass filter respectively, when $g = 0.01$. According to equations (3.1.34), (3.1.35), the response of case-II(filte1) has satisfied the monotonic characteristics ($\partial\beta_{2G22}/\partial\Omega_i \geq 0$) in the pass-band region. Figures 3.23 (c) and (d) show that the case-I(filter2) satisfies the monotonicity in the amplitude-frequency response. Table 3.9 gives the ranges of $k_i$ for the values of $g$, $a_i$ and $b_i$ in order to obtain the monotonic

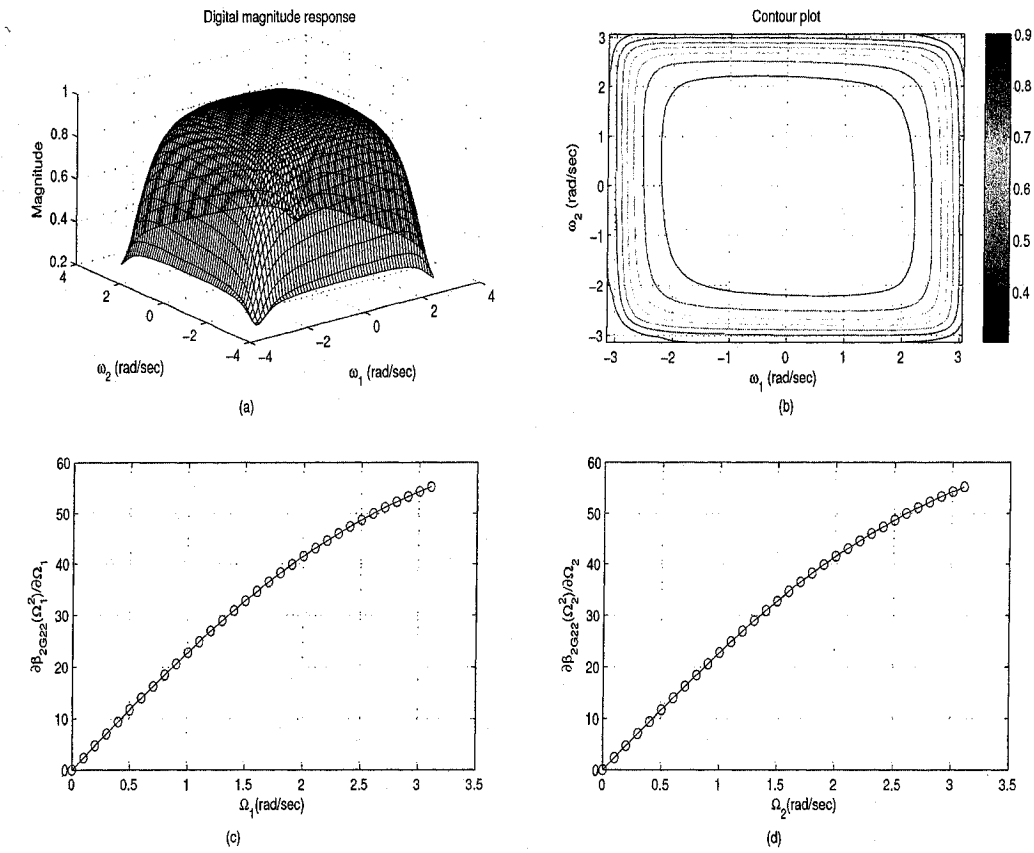


Figure 3.23: The 2D digital low-pass filter (case-II(filter2)) when g = 0.01, (a)3D magnitude plot, (b) contour plot, (c) and (d) the case-II(filter2) satisfies the monotonic characteristic.

characteristics in the amplitude-frequency responses of the case-II (filter2).

### 3.3.8 2D case-III(filter2)

The two impedances of filter2 are replaced by the impedances of doubly terminated second-order Butterworth and Gargour&Ramachandran filters and the third impedance is replaced by a resistive element. The GBT ($a = -0.3$, $b = 0.9$, and $k = 3$) is applied to the resultant analog transfer function and obtained digital transfer function (equation(3.3.7)) provides the variable magnitude response with the monotonic characteristics.

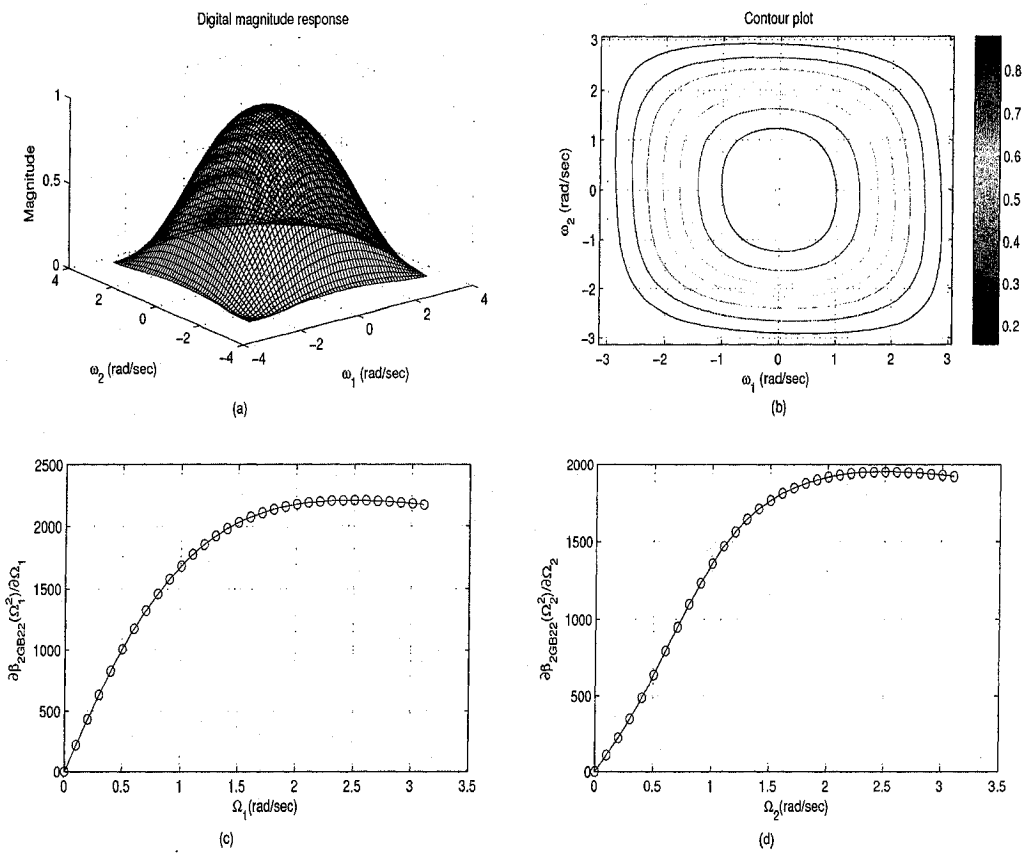


Figure 3.24: The 2D digital low-pass filter (case-III(filter2)) when g = 0.01, (a)3D magnitude plot, (b) contour plot, (c) and (d) the case-III(filter2) satisfies the monotonic characteristic.

$$H_{d2GB}(z_1,z_2)=\frac{\begin{bmatrix}1 & z_1 & z_1^2\end{bmatrix}\begin{bmatrix}1.3g+0.010 & 20g-0.44 & 0.058-8.5g\\ 37g-1.0 & 44+460g & -5.8-220g\\ -14g+130 & -560-200g & 92g+740\end{bmatrix}\begin{bmatrix}1\\ z_2\\ z_2^2\end{bmatrix}}{1.077\begin{bmatrix}1 & z_1 & z_1^2\end{bmatrix}\begin{bmatrix}1.2g^2+1.0 & 23+19g^2 & -7.9-7.9g^2\\ 38+34g^2 & 430g^2+710 & -200g^2-290\\ -11-13g^2 & -250-190g^2 & 86g^2+93\end{bmatrix}\begin{bmatrix}1\\ z_2\\ z_2^2\end{bmatrix}} \quad (3.3.7)$$

Table 3.10: The range of $k_i$ for the monotonic characteristic in the amplitude-frequency response of case-III(filter2)

| g | $a_i$ | $b_i$ | $k_i$ |
|---|---|---|---|
| 0.01 | $-0.9$ | 0.9 | $0.2 > k_i > 0$ |
| 0.01 | $-0.9$ | 0.5 | $0.5 > k_i > 0$ |
| 0.01 | $-0.5$ | 0.9 | $3.2 > k_i > 0$ |
| 0.01 | $-0.5$ | 0.5 | $1 > k_i > 0$ |
| 0.01 | $-0.1$ | 0.1 | Not possible |

Figures 3.24 (a) and (b) show the 3D magnitude plot and contour plot of the 2D digital low-pass filter respectively, when $g = 0.001$. According to equations (3.1.34), (3.1.35), the response of case-II(filte1) has satisfied the monotonic characteristics ($\partial\beta_{2GB22}/\partial\Omega_i \geq 0$) in the pass-band region. Figures 3.24 (c) and (d) show that the case-I(filter2) satisfies the monotonicity in the amplitude-frequency response. Table 3.10 gives the ranges of $k_i$ for the values of $g$, $a_i$ and $b_i$ in order to obtain the monotonic characteristics in the amplitude-frequency responses of the case-III (filter2).

## 3.4 Comparisons of the proposed designs

The two proposed filter designs are efficient in terms of computational cost, but the proposed design-II has better performance than the proposed design-I. The proposed design-I has more control on the bandwidth as well as the cutoff frequency of the 2D digital filter by regulating the single parameter (g) (sections 3.2 and 3.3). However, most of the design-I has failed to obtain monotonic characteristics in amplitude-frequency response of the digital filter. This problem is overcome by the proposed design-II (section 3.3). In the proposed design-II, impedances of the doubly terminated gyrator network are replaced by the doubly terminated RLC networks and the GBT is applied to the resultant analog transfer function in order to obtain the desired digital filter. The GBT ensures the monotonic characteristics in the pass-band regions of the digital filter. But, neither designs gives inherently stable filter nor monotonic characteristics in frequency responses. The magnitude of g of the gyrator network is kept in such ranges that denominator of the resultant transfer function is satisfied to be VSHPs and also satisfied constraints of monotonic characteristics (sections 3.2 and 3.3).

The proposed design-I provides more simple technique of digital filter design, only by choosing the appropriate doubly terminated RLC networks which are replaced by the impedances of the gyrator network. It is seen that proposed design-I is applied to the both gyrator networks to design the 2D digital low-pass filter design and g of the gyrator network is kept in lower range, because frequency responses are very sensitive to the the magnitude of g. However, proposed design-II allows to regulate seven parameters (six parameters of the GBT and g of the gyrator network) for digital filter design. As a result, other parameters allow us to choose the higher magnitudes of g in order to obtain a 2D digital low-pass filter. Bandwidths and cutoff frequencies of the desired filter are obtained by varying the seven parameters.

Comparing the two sections 3.2 and 3.3, it has seen that the proposed design-II is obviously better than the proposed design-I. However, the proposed design-I takes less computational cost than the design-II and it does not change the original analog filter structure to obtain the desire digital filter. But, proposed design-II modifies the original analog filter to the corresponding modified analog filter in order to obtain the desired 2D digital low-pass filter.

## 3.5 Summary and Discussion

The main purpose of the proposed designs are presented in this chapter is to provide an efficient design of 2D digital low-pass filter having monotonic amplitude-frequency response in pass-band region. Some constraints (equations (3.1.12) to (3.1.15), (3.1.34) and (3.1.35)) are defined on coefficients of the analog transfer function for attaining monotonic characteristics in amplitude-frequency response of the filter and it has seen the coefficients of the 2D analog transfer function are function of g of the gyrator filter. As a result, the constraints of the monotonic characteristic in the amplitude-frequency response are depend on the g.

The proposed filter design-I (section 3.2) is applied to a Darlington-type gyrator networks, where impedances of the gyrator filter are replaced by the doubly terminated RLC filters to obtain stable 2D analog transfer functions. As a result, the coefficients of the transfer function are function of g of the gyrator filter and frequency

responses of the analog filter are varied by the value/sign of g. The corresponding digital filters are obtained using the double bilinear transformations. However, proposed design-I has failed to obtain the monotonic characteristics in amplitude-frequency response of the digital filter, because g of the gyrator filter cannot control equally on the both dimensions of filter response. In order to obtain monotonic amplitude-frequency response in pass-band region of a filter, another filter design is proposed.

The proposed filter design-II (section 3.3) is applied to stable analog transfer functions. The stable analog transfers functions are generated by using Darlington-type gyrator networks. Doubly terminated RLC filters are replaced by impedances of the gyrator filter1 and filter2 in order to obtain the stable analog transfer functions. The proposed design-II uses the GBT, that is one of the powerful tool to design a digital filter. The GBT is applied to the analog transfer function and it modifies the reactive parameters of the analog filter in order to obtain the desired digital filter with monotonic amplitude-frequency response. Some constraints equations (3.1.12) to (3.1.15), (3.1.34) and (3.1.35) are defined on the design to achieve the monotonic characteristics in the filter response.

For illustration of the proposed designs, doubly terminated second-order Butterworth filters are replaced in the both impedances of the gyrator filter1 and the desired filter responses are obtained by regulating g of filter1. Similarly, doubly terminated second-order Gargour&Ramachandran filters are replaced by the both impedances and the desired frequency responses are obtained by regulating 'g' of filter1. The combination of Butterworth and Gargour&Ramachandran filter are also used in the gyrator filter1 and the desired frequency responses are obtained. Same steps are followed in the case of gyrator filter2, but for the stability concern of filter2, one impedance of gyrator filter2 is considered as resistive component (section 2.4.5). In section 3.3, the GBT is applied to the resultant analog transfer functions in order to obtain the desired 2D digital low-pass filter, however, appropriate value/sign of g of the gyrator network and parameters of the GBT have chosen to satisfy monotonic characteristics in amplitude-frequency responses of the designed filter. A comparison of the sections 3.2 and 3.3 has shown in section 3.4 and it has proven that design-II overcomes all the design problems of design-I.

# Chapter 4

# Proposed Filter Design and Digital Filter Transformation

## 4.1 Introduction

The previous chapter has shown the proposed designs for the 2D IIR digital low-pass filter and the proposed design-II. The stability and monotonic amplitude-frequency response in the passband region of the desired filter are ensured. The proposed low-pass filter design is accomplished by two steps. First, the impedances of the doubly terminated gyrator filter are replaced by the doubly terminated second-order RLC filters. As a result, the magnitude of gyrator constant (g) of the gyrator filter has control on the amplitude-frequency response. In the second step, the GBT is applied to the resultant 2D analog filter to obtain the desired 2D digital filter response which satisfies the monotonic constraints (equations (3.3.2), (3.3.3), (3.1.12) to (3.1.15), (3.1.34) and (3.1.35)) in the passband regions.

This chapter considers the proposed filter design of the 2D IIR high-pass, band-pass and band-elimination filters and the proposed digital filter transformation method. Two designs of the 2D digital low-pass filter have been proposed in the previous chapter and the proposed design-II has been shown to be more powerful than the proposed design-I, because the design-II can overcome the problems generated by the proposed design-I. This entire chapter presents the 2D digital filter design of high-pass, band-pass and band-elimination filters by the proposed design-II. The procedure of the proposed 2D high-pass filter design is quite similar to the proposed 2D digital low-pass filter design (section 3.3). However, the value and sign of g of the gyrator

networks and the values of parameters of the GBT are changed as required. The band-pass and band-elimination filters are obtained from a 2D analog low-pass or high-pass filter using a transformation (equation (4.3.2)) which is derived from the GBTs.

The locations of poles and zeros of a doubly terminated gyrator filter depends on the value and/or sign of g [35] and the proposed digital filter transformation method is based on the value and/or sign of g of a doubly terminated gyrator filter. The digital filter transformation has been done in two ways, such as considering the value of g and considering the sign of g. The constraints of the digital filter transformation imposed on the filters are outlined and details of the method are discussed in section 4.4. This thesis considers two doubly terminated gyrator filters (Figures 2.1 and 2.2) and the impedances of both the filters are replaced by the doubly terminated RLC filters. As a result, the magnitude of g of the gyrator network has control on the frequency responses of the resultant filter.

From the properties of filter1 (section 2.5), it is shown that the amplitude-frequency response of filter1 has a constant magnitude when g = 1. It is also seen that the impedances of the gyrator filter are replaced by the RLC filters and each of the RLC filters is represented by $s_1$ and $s_2$ domain respectively. As a result, the magnitude of g in the resultant 2D analog transfer function does not have control equally on the both dimensions of frequency response. In order to overcome this problem, each impedances is replaced by two cascaded connection of the RLC filters and each RLC filter is represented by $s_1$ and $s_2$ domain respectively. In such a case, it is seen that the magnitude of g can control both the dimensions equally. It is also shown that the 2D digital low-pass filters are obtained in the ranges of $0 \leq g \leq 0.03$ (approximate) and the 2D digital high-pass filters are obtained in the range of $0.99 > g \geq 0.1$ and $\infty > g > 1$ (approximate). However, the impedances of the gyrator filter2 has been replaced by the doubly terminated RLC filters and each of the RLC filters is represented by $s_1$ and $s_2$ domain respectively. The magnitude responses of the resultant 2D analog transfer function are controlled in the both dimensions equally by the magnitude of g of filter2. Approximately, the inverted filter responses of filter2 are obtained in between the range of $1 < g < \infty$ and $-\infty > g > -1$. Basically, the value or sign of g of the filter can change the total reactive property of the filter and inverts the magnitude responses of the filter to the opposite.

The magnitude responses and the inverted magnitude responses of the filters (section 4.4) are studied carefully and it is seen that the amplitude variation of the response is in between 0.9 to 1. Even though, the designed magnitude response of the filter has less variation in the amplitude, it has been used in the image processing applications and comparative improvement is achieved for the image restoration and enhancement purposes, but the computational time is longer than the other filters [10]. Considering this problem, each of the impedances of the gyrator filter is replaced by the doubly terminated higher-order RLC filters and each of the RLC filters can be represented by cascading of two or more second-order RLC filters. As a result, the inverted magnitude responses of the gyrator filters are varied in between 0.2 to 1. Details of the digital filter design are discussed below and for simplicity in this thesis, the sections 3.3.2, 3.3.3 and 3.3.4 are called as case I, case II and case III and these cases are also followed in filter2 (sections 3.3.6, 3.3.7 and 3.3.8).

## 4.2 Proposed Design of High-pass filter

The impedances of the doubly terminated gyrator network are replaced by the second-order RLC networks and the GBT is applied to the resultant analog transfer function. As a result, the desired 2D digital high-pass filter is obtained by regulating the value/sign of g and the parameters of the GBT. The proposed filter design ensures the monotonic characteristics in the amplitude-frequency responses of the 2D digital high-pass filter. The conditions of monotonic characteristics in the amplitude-frequency responses of the 2D digital high-pass filter can be defined by using the equations (3.3.2), (3.3.3), (3.1.12) to (3.1.15), (3.1.34) and (3.1.35) and the conditions of the monotonic characteristics are shown in below:

$$\frac{\partial \beta_n(\Omega_1^2, 0, g)}{\partial \Omega_1} \leq 0 \tag{4.2.1}$$

$$\frac{\partial \beta_n(0, \Omega_2^2, g)}{\partial \Omega_2} \leq 0 \tag{4.2.2}$$

The proposed 2D digital high-pass filter design is discussed in the following and design examples are also given to illustrate the usefulness of the proposed design. For illustration in this thesis, the second-order Butterworth filter and Gargour&Ramachandran

filters are used as the doubly terminated RLC networks and filter1 and filter2 (Figures 2.1 and 2.2) are used as the doubly terminated gyrator networks.

The impedances of filter1 are replaced by the second-order RLC filters and the magnitude of g of filter1 cannot control amplitude-frequency responses of the resultant analog filter equally in the both dimensions. In order to overcome this problem, each of the impedances of the doubly terminated gyrator network are replaced by the two cascaded doubly terminated RLC networks and each of the RLC networks are represented $s_1$ and $s_2$ domain. The rest of the procedure of the 2D digital high-pass filter design is quite similar to the 2D digital low-pass filter design (section 3.3). However, the value or sign of g or the values or signs of parameters of the GBT are changed to design a 2D digital high-pass filter. Bandwidth of the digital high-pass filter is controlled by the magnitude g and the parameters of the GBT. As a result, the proposed filter design provides significate amount of flexibility for the digital filter design and ensures guaranteed monotonic amplitude-frequency response of the designed 2D digital high-pass filter.

Similar to the design of low-pass filter (section 3.3), the GBT is applied to the transfer function of filter1 (equation (3.2.3)). The resultant digital filter response satisfies the constraints equations (4.2.1), (4.2.2). The inverse bilinear transformation is applied to the digital filter in order to obtain the corresponding modified analog filter [16] and Figure ?? shows that the corresponding filter satisfies the monotonic characteristics. In Figure 4.1, $b_i$ and $k_i$ regulate the response keeping the value of $a_i$ constant and in Figure ??, the value of $a_i$ and $k_i$ regulate the response keeping the values of $b_i$ constant.

It is seen that the 2D digital high-pass filter satisfies the monotonic characteristics in the amplitude-frequency response, for various values of parameters of the GBT when g =-0.5. Table 4.1 shows the ranges of g of the case-I (filter1) for the certain values of parameters of the GBT, where the 2D digital high-pass filter does not satisfy monotonic amplitude-frequency response in pass-band region (equations (4.2.1) and (4.2.2)). Avoiding those ranges of g of filter1, the 2D digital high-pass filter response is obtained in Figure 4.2(a) and this filter satisfies the monotonic characteristic as shown in Figure 4.4(a). In Figures 4.2(a) and 4.4(a), g = -0.5 and parameters of the GBT are $a_1 = -0.9, a_2 = -0.9, b_1 = 0.1, b_2 = 0.1, k_1 = 10, k_2 = 10$.

In Figure 4.2 (b), the 2D digital high-pass filter is designed similar to the 2D

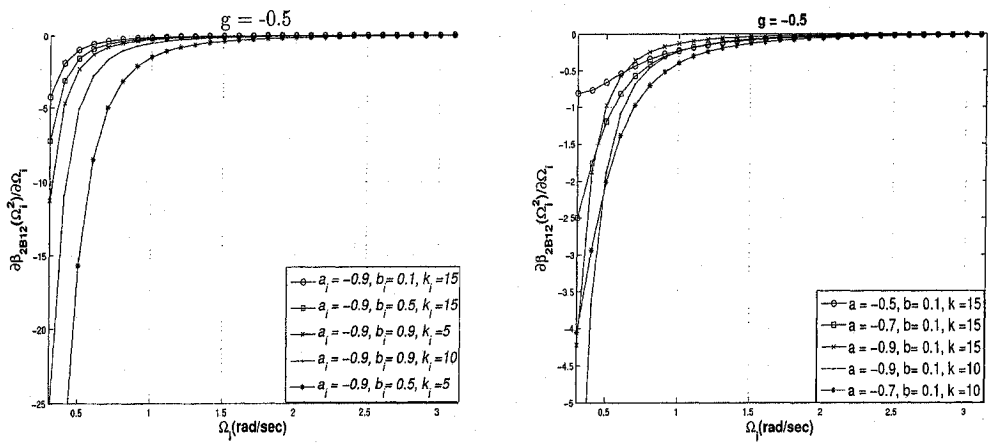


(a) (b)

Figure 4.1: The 2D high-pass filters (case-I(filter1)) satisfy the monotonic characteristics, (a) $b_i$ and $k_i$ regulate, (b)when $a_i$ and $k_i$ regulate.

Table 4.1: The ranges of g of the case-I (filter1), where the 2D digital high-pass filter does not contain monotonic characteristic in the amplitude-frequency response.

| $a_i$ | $b_i$ | $k_i$ | g |
|---|---|---|---|
| -0.1 | 0.1 | 1 | $0.3 > g \geq 0$ |
| -0.1 | 0.1 | 5 | $0.1 > g \geq 0$ |
| -0.1 | 0.1 | 10 | $0.05 > g \geq 0$ |
| -0.5 | 0.5 | 1 | $0.7 > g \geq 0$ |
| -0.5 | 0.5 | 5 | $0.4 > g \geq 0$ |
| -0.5 | 0.5 | 10 | $0.18 > g \geq 0$ |
| -0.9 | 0.9 | 1 | $\infty > \|g\| \geq 0$ |
| -0.9 | 0.9 | 5 | $4.6 > g \geq -1.5$ |
| -0.9 | 0.9 | 10 | $1 > g \geq -0.67$ |

digital low-pass filter design (section 3.3.3), only the sign of g is reversed and the values of parameters of the GBT are changed to suitable values as required. Basically, Figure 4.2(b) is the inverted amplitude-frequency response of Figure 3.19. The GBT ($a_1 = -0.9, a_2 = -0.9, b_1 = 0.1, b_2 = 0.1, k_1 = 10, k_2 = 10$) is applied to the transfer function of case II (filter1) and the overall 2D digital high-pass filter satisfies the monotonic characteristic (Figure 4.4(b)). It is seen that the bandwidth of this filter is controlled by g of filter1 and the parameters of the GBT.

In Figure 4.2(c), the 2D digital high-pass filter of case-III (filter1) with the monotonic characteristics in the amplitude-frequency responses is shown. In this case, the impedances of filter1 are replaced by the second-order Gargour&Ramachandran and

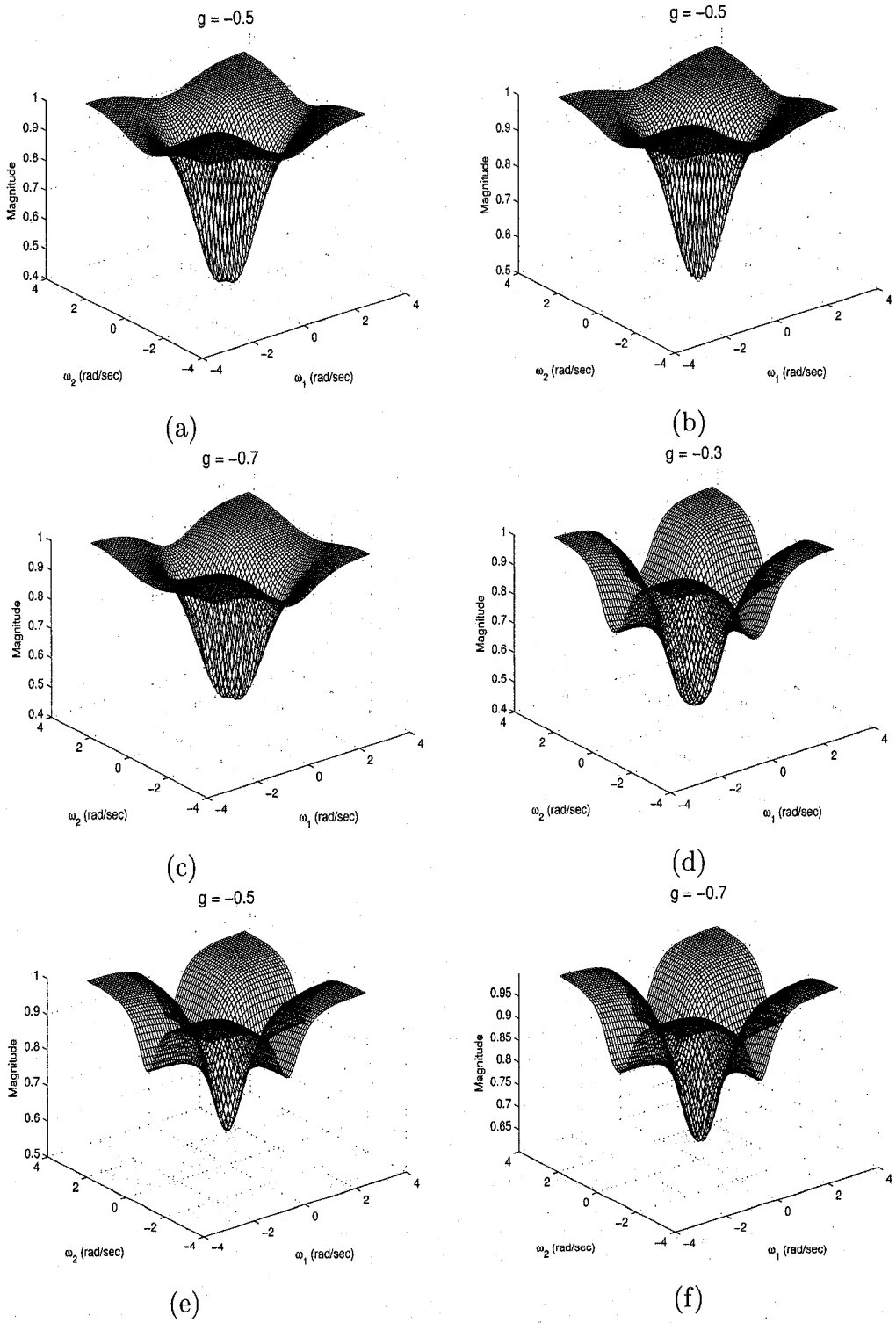


Figure 4.2: 3D magnitude plots of the 2D digital high-pass filters (a) Case-I (filter1), (b) Case-II (filter1), (c)Case-III (filter1), (d) Case-I (filter2), (e) Case-II (filter2), (f)Case-III (filter2)

Butterworth filters. The GBT ($a_1 = -0.9, a_2 = -0.9, b_1 = 0.1, b_2 = 0.1, k_1 = 5, k_2 = 5$) is applied to the resultant transfer function of case III (filter1). The overall 2D digital high-pass filter satisfies the monotonic characteristic (Figure 4.4(c)).

The impedances of doubly terminated gyrator filter2 are replaced by the second-order RLC filters and because of the stability criteria, the third impedance of the filter2 is replaced by a resistive element which is proved in the sections 2.4.3, 2.4.4 and 2.4.5. It is seen in the resultant transfer function that the magnitude of g of filter2 can control the amplitude-frequency response of the 2D high-pass filter equally in the both dimensions.

The proposed 2D digital high-pass filter design is similar to the proposed 2D digital low-pass filter design (section 3.3). However, in the case of 2D digital high-pass filter design, the value/sign of g of filter2 and/or the values of parameters of the GBT have changed. Bandwidth of the 2D high-pass filter is controlled by the g and parameters of the GBT. The proposed design ensures the monotonic amplitude-frequency response of the desired 2D digital high-pass filter. In the case-I (filter2), the impedances of doubly terminated gyrator filter is replaced by the second-order Butterworth filters and the GBT is applied to the resultant analog transfer function. As a result, the 2D digital high-pass filter satisfies monotonic amplitude-frequency response for the certain ranges of g of filter2 and these ranges of g are depend on the values of parameters of the GBT. For example, if parameters of the GBT are $a_i = -0.9$, $b_i = 0.1$ and $k_i = 1$, the ranges of g are defined as $4.1 \geq g \geq 0.32$ and $-\infty > g \geq -0.08$ in order to obtain monotonic characteristic in the magnitude response of the 2D digital high-pass filter (case-I (filter2)) (Figure 4.3).

Figures 4.3 (a) and (b) satisfy the monotonic characteristic, when the values of g are -1 and 4 respectively. However, Figures 4.3 (c) and (d) do not satisfy the monotonic characteristics, when the values of g are -0.07 and 0.1 respectively.

Table 4.2 gives the ranges of g, when case-I (filter2) does not satisfy the monotonic amplitude-frequency response in pass-band region of the 2D digital high-pass filter, while the values of parameters of the GBT are constant.

In Figure 4.2 (d), the 2D digital high-pass filter response is obtained by applying the GBT to equation (3.2.9) and regulating the value of g of filter2 so that the overall frequency response satisfies the monotonic characteristics (Figure 4.4(d)). The bandwidth of the digital high-pass filter is controlled by the g and parameters of the

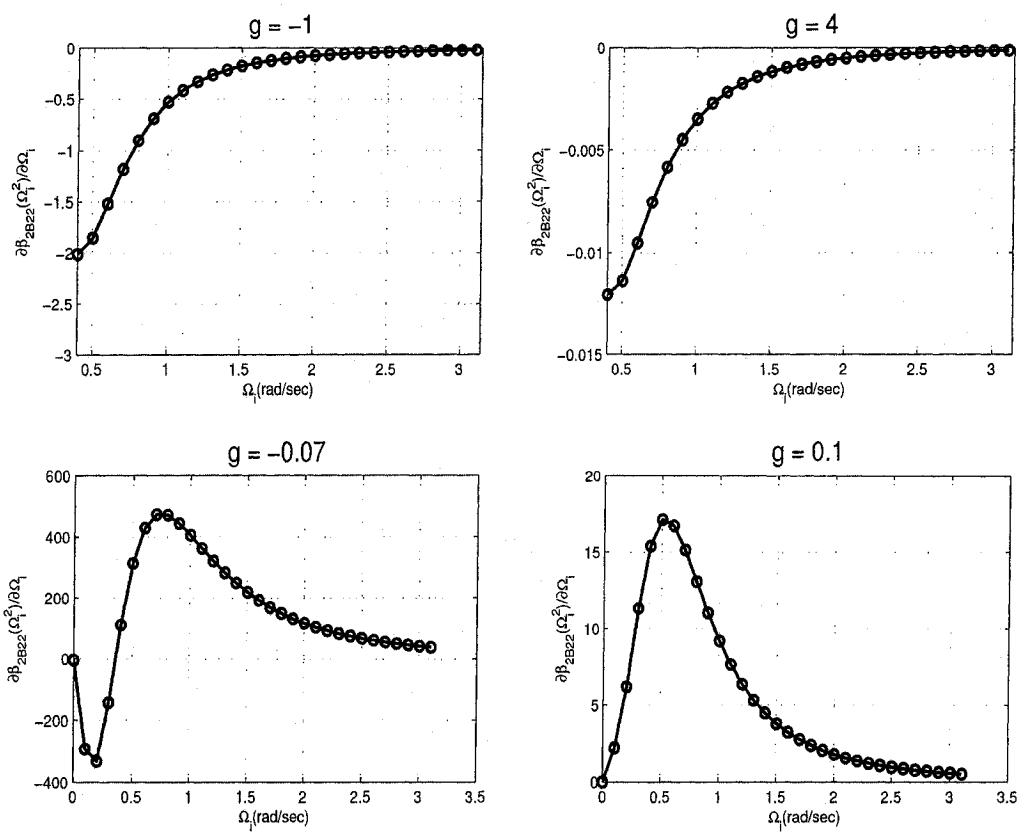


Figure 4.3: The design of digital 2D high-pass filter (case-I(filter2)), when $a_i = -0.9$, $b_i = 0.1$ and $k_i = 1$. (a) the case-I(filter2) possesses the monotonic characteristics for g = -1, (b) the case-I(filter2) possesses the monotonic characteristics for g = 4, (c) the case-I(filter2) does not possess the monotonic characteristics for g = -0.07, (d) the case-I(filter2) does not possess the monotonic characteristics for g = 0.1.

GBT.

In Figure 4.2 (e), the 2D digital high-pass magnitude response is obtained using the second-order Gargour&Ramachandran filters in the filter2 and the GBT is applied to the resultant transfer function. The values of parameters of the GBT and g of filter2 are chosen such a way that the overall frequency response satisfies the monotonic characteristics (Figure 4.4(e)).

In the filter2, the two impedances of filter2 are replaced by the Butterworth and Gargour&Ramachandran filters and third impedance is replaced by resistive element. The GBT is applied to the resultant filter and the reactive parameters of the filter

Table 4.2: The ranges of g, when case-I (filter2) does not satisfy the monotonic amplitude-frequency response in pass-band region of the 2D digital high-pass filter, while the values of parameters of the GBT are constant.

| $a_i$ | $b_i$ | $k_i$ | g |
|---|---|---|---|
| -0.1 | 0.1 | 1 | $\infty > g > 3.6,\ 0.4 > g \geq -0.1$ |
| -0.1 | 0.1 | 5 | $\infty > g > 8,\ 0.2 > g \geq -0.01$ |
| -0.1 | 0.1 | 10 | $\infty > g > 13,\ 0.08 > g \geq -0.005$ |
| -0.5 | 0.5 | 1 | $\infty > g > 3.2,\ 0.5 > g \geq -0.1$ |
| -0.5 | 0.5 | 5 | $\infty > g > 4.8,\ 0.3 > g \geq -0.04$ |
| -0.5 | 0.5 | 10 | $\infty > g > 7,\ 0.2 > g \geq -0.04$ |
| -0.9 | 0.9 | 1 | $\infty > \|g\| > 0$ |
| -0.9 | 0.9 | 5 | $\infty > g > 3.2,\ 0.5 > g \geq -0.1$ |
| -0.9 | 0.9 | 10 | $\infty > g > 3.4,\ 0.4.1 > g \geq -0.09$ |

are modified (similar to section 2.3) as required. As s result, the overall amplitude-frequency response (Figure 4.2(f)) has the monotonic characteristics (Figure 4.4(f)).

From the above discussion, it is observed that the different combinations of the doubly terminated gyrator filters and the second-order Butterworth and Gargour & Ramachandran filters provide the 2D digital low-pass and high-pass filter. But, the band-pass and band-elimination filter can be obtained by choosing the appropriate doubly terminated RLC filters.

It is seen that the impedances of the doubly terminated gyrator filter2 are replaced by the doubly terminated RLC networks which is represented by $s_1$ and $s_2$ domain respectively. As a result, the frequency responses of the resultant analog transfer function are controlled by g equally in both dimensions. The GBT is applied to the analog transfer function and the overall digital transfer function provides stable monotonic amplitude-frequency responses of the 2D digital high-pass filters (Figure 4.2(d) - (f)).

## 4.3 Proposed Design of Band-pass and Band-elimination filter

The proposed design of digital band-pass and band-elimination filter is started with a stable 2D analog filter. At first, the stable 2D analog filter is transformed to a

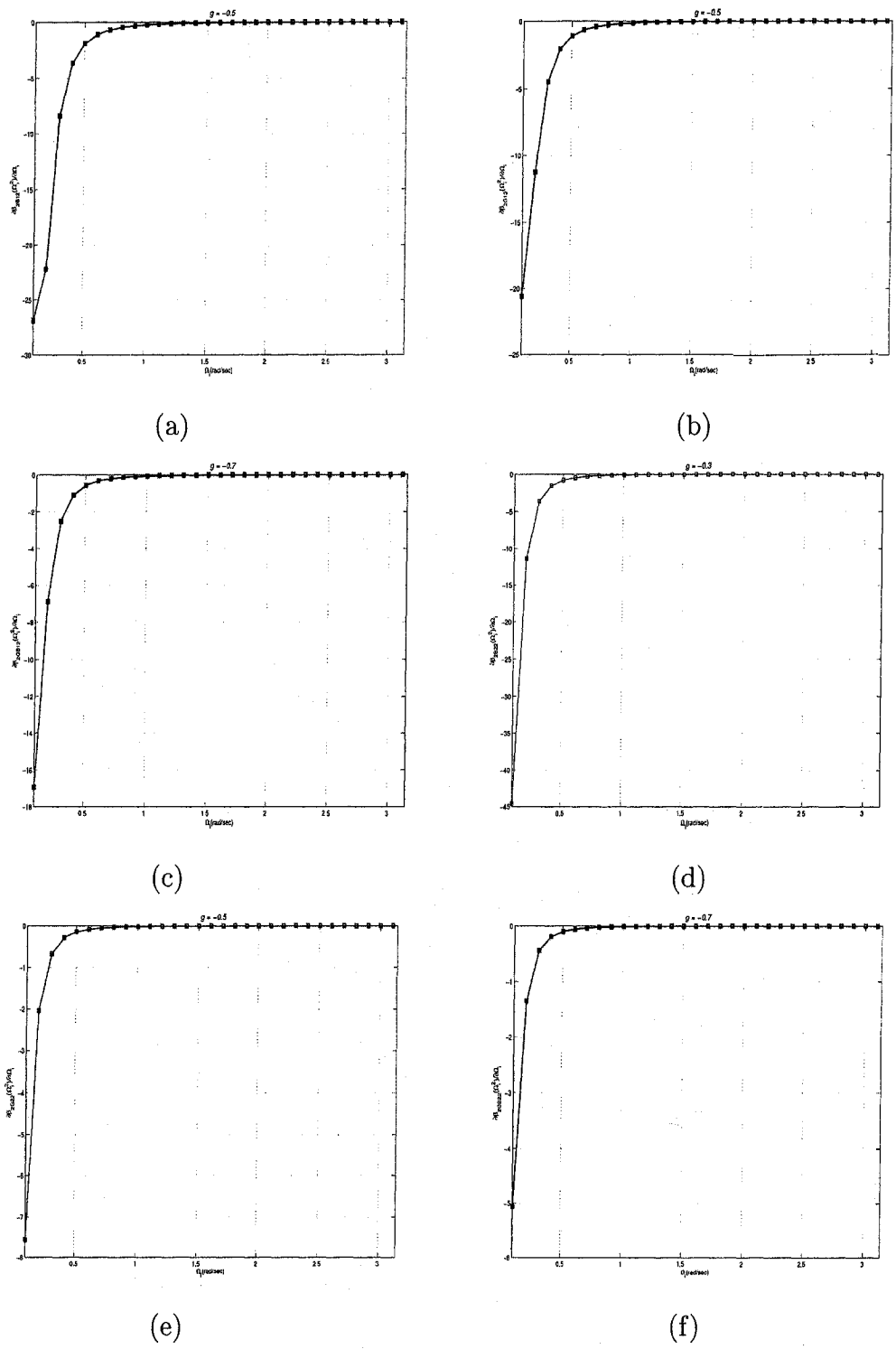


Figure 4.4: The 2D high-pass filters satisfy the monotonic characteristics, (a) Case-I (filter1), (b) Case-II (filter1), (c)Case-III (filter1), (d) Case-I (filter2), (e) Case-II (filter2), (f)Case-III (filter2)

2D digital low-pass or high-pass filter by the GBT (sections 3.3 and 4.2) and the corresponding modified 2D analog low-pass or high-pass is obtained by the inverse bilinear transformation. The modified 2D analog filter is transformed to band-pass or band-elimination filter by the summation of two GBTs (equation (4.3.1)) [36]. The overall transformation from the stable 2D analog filter to the 2D analog band-pass or band-elimination filter is shown in the equation (4.3.2). The first term in equation (4.3.1) is the original bilinear transformation that transforms the normalized analog low-pass to the discrete low-pass, and the second term transforms the normalized low-pass to the digital high-pass [37]. Block diagram of the proposed design of band-pass and band-elimination filter is shown in Figure 4.5.

Figure 4.5 shows that a stable analog transfer function is transformed to a digital transfer function by the GBT. The digital transfer function is converted to the modified analog transfer function by the double inverse bilinear transformations and the modified analog transfer function to the desired digital transfer function by equation (4.3.1).

$$s_i' = k_{i1}\frac{z_i - 1}{z_i + 1} + k_{i2}\frac{z_i + 1}{z_i - 1} \tag{4.3.1}$$

$$s_i = \frac{(a_i k_{i1} - k_{i1})k_i S_i^2 + (-1 - a_i)k_i S_i + (a_i k_{i2} - k_{i2})k_i}{(-k_{i1} + b_i k_{i1})S_i^2 + (-1 - b_i)S_i + b_i k_{i2} - k_{i2}} \tag{4.3.2}$$

Where i =1,2 and $s_i$ is laplace domain parameter of original circuit, $s_i'$ is laplace domain parameter of the modified analog low-pass or high-pass filter and $S_i$ is laplace domain parameter of the modified band-pass or band-elimination filter. In the equation (4.3.2), $a_i$, $b_i$ and $k_i$ are same as in the equation (3.3.1), which ensures the monotonic characteristic of the filter in the pass-band region, $\frac{k_{i2}}{k_{i1}}$ is defined as the center frequency of the filter and $\frac{1}{k_{i1}}$ is defined as the bandwidth of the filter. The proposed design ensures the stable 2D digital band-pass and band-elimination filter having monotonic characteristics in frequency responses.

The design is started with a stable 2D analog transfer function and the stable transfer functions are generated as in the section 2.4. The GBT is applied to the analog transfer function in order to obtain the 2D digital low-pass or high-pass filter (sections 3.3 and 4.2) and the corresponding modified analog filters are obtained by the inverse bilinear transformation (section 3.3). The equation (4.3.1) is applied to the modified analog filter in order to obtain the 2D digital band-pass filter (Figure4.6).

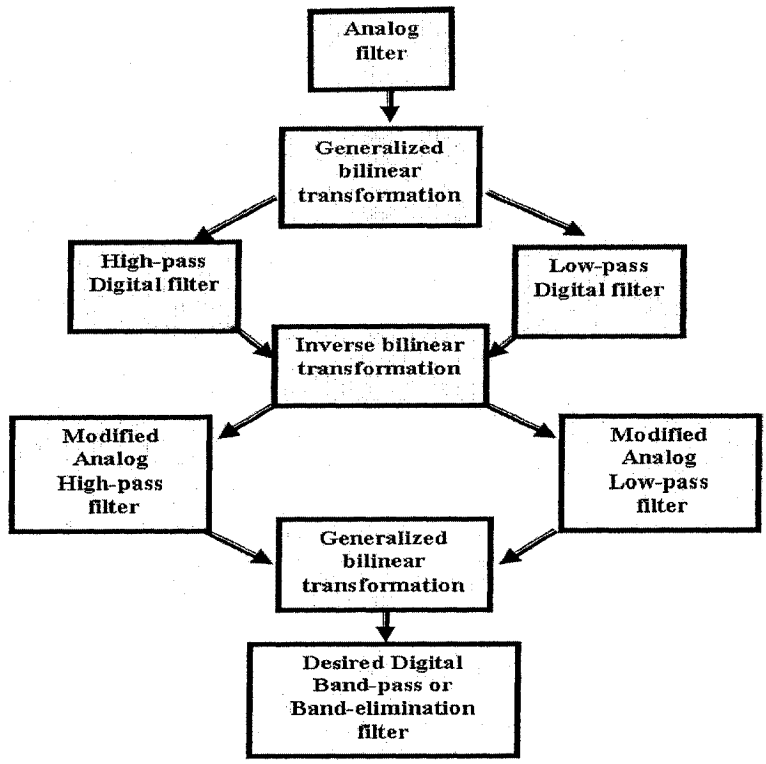


Figure 4.5: Block diagram of the the proposed design of a digital band-pass and band-elimination filter

The bandwidth and center frequencies of the 2D digital band-pass filter can be varied by $\frac{1}{k_{i1}}$ and $\frac{k_{i2}}{k_{i1}}$ respectively and the overall bandpass filter has the monotonic characteristics in the pass-band region. Similarly, the proposed design is applied on the designed filters (sections 3.3.2, 3.3.3, 3.3.4, 3.3.6, 3.3.7 and 3.3.8) and the corresponding 2D digital band-pass filters are shown in Figure 4.7.

Table 4.3: The values of parameters are used to design the 2D band-pass filter (figure 4.7)

| Filter | g | $a_i$ | $b_i$ | $k_i$ | $k_{i1}$ | $k_{i2}$ |
|---|---|---|---|---|---|---|
| Case-I(Filter1) | 0.01 | -0.5 | 0.5 | 10 | 0.15 | 0.15 |
| Case-II(Filter1) | 0.01 | -0.9 | 0.1 | 5 | 0.15 | 0.35 |
| Case-III(Filter1) | 0.01 | -0.5 | 0.1 | 10 | 0.25 | 0.15 |
| Case-I(Filter2) | 0.01 | -0.9 | 0.1 | 10 | 0.25 | 0.2 |
| Case-II(Filter2) | 0.01 | -0.9 | 0.1 | 2 | 0.05 | 0.2 |
| Case-III(Filter2) | 0.01 | -0.9 | 0.5 | 10 | 0.1 | 0.1 |

The procedure of the band-elimination filter design is similar to the band-pass

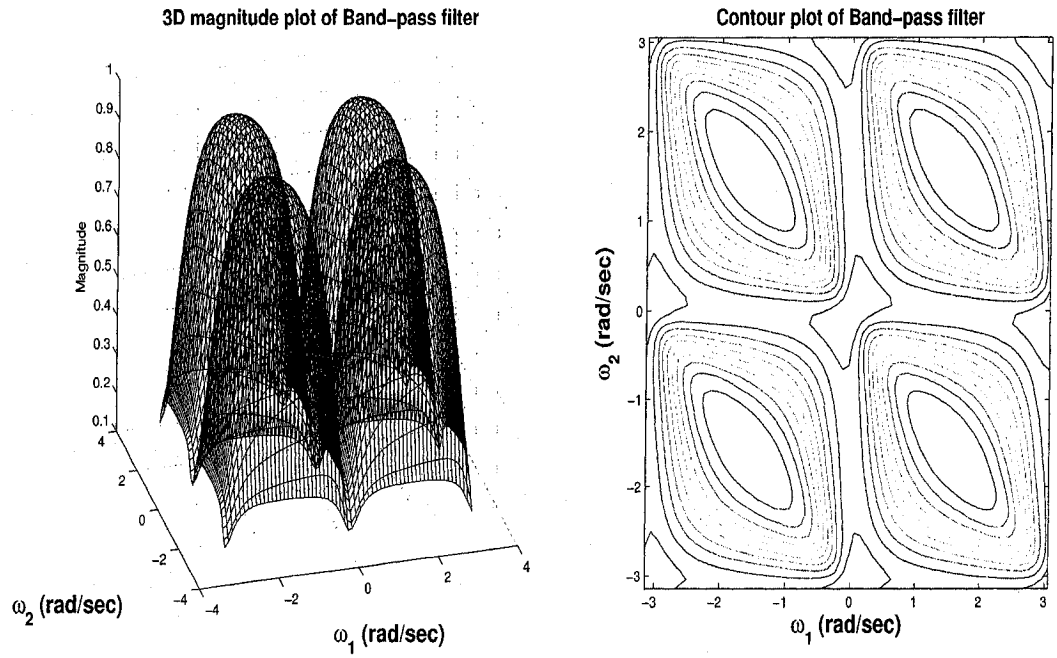


Figure 4.6: 3D magnitude plot and contour plot of the 2D digital Band-pass filter, case-I(filter1)

filter design. However, the band-pass filter is transformed to band-elimination filter by changing the value and/or sign of g of the band-pass filter.

Table 4.4 gives the values of parameters used to design the 2D digital band-elimination filters (Figure 4.8). It is observed that the monotonic characteristics in the pass-band region of the band-elimination filter are maintained by regulating the values of $a_i, b_i, k_i$, but in most of the cases, the values of parameters are kept constant as the 2D digital band-pass filters (Table 4.3). The values and sign of g of the band-pass filter filter are changed in order to obtain the opposite filter response and $k_{i1}, k_{i2}$ control the center frequencies and bandwidths of the 2D band-elimination filter.

## 4.4 Proposed Digital Filter Transformation

A digital IIR filter design is started from a continuous-time filter and it is modified to another continuous-time filter which is transformed into discrete-time filter (section 4.3). From the previous discussion, the two steps are performed for the digital filter design. First, the frequency transformation is applied to the normalized analog

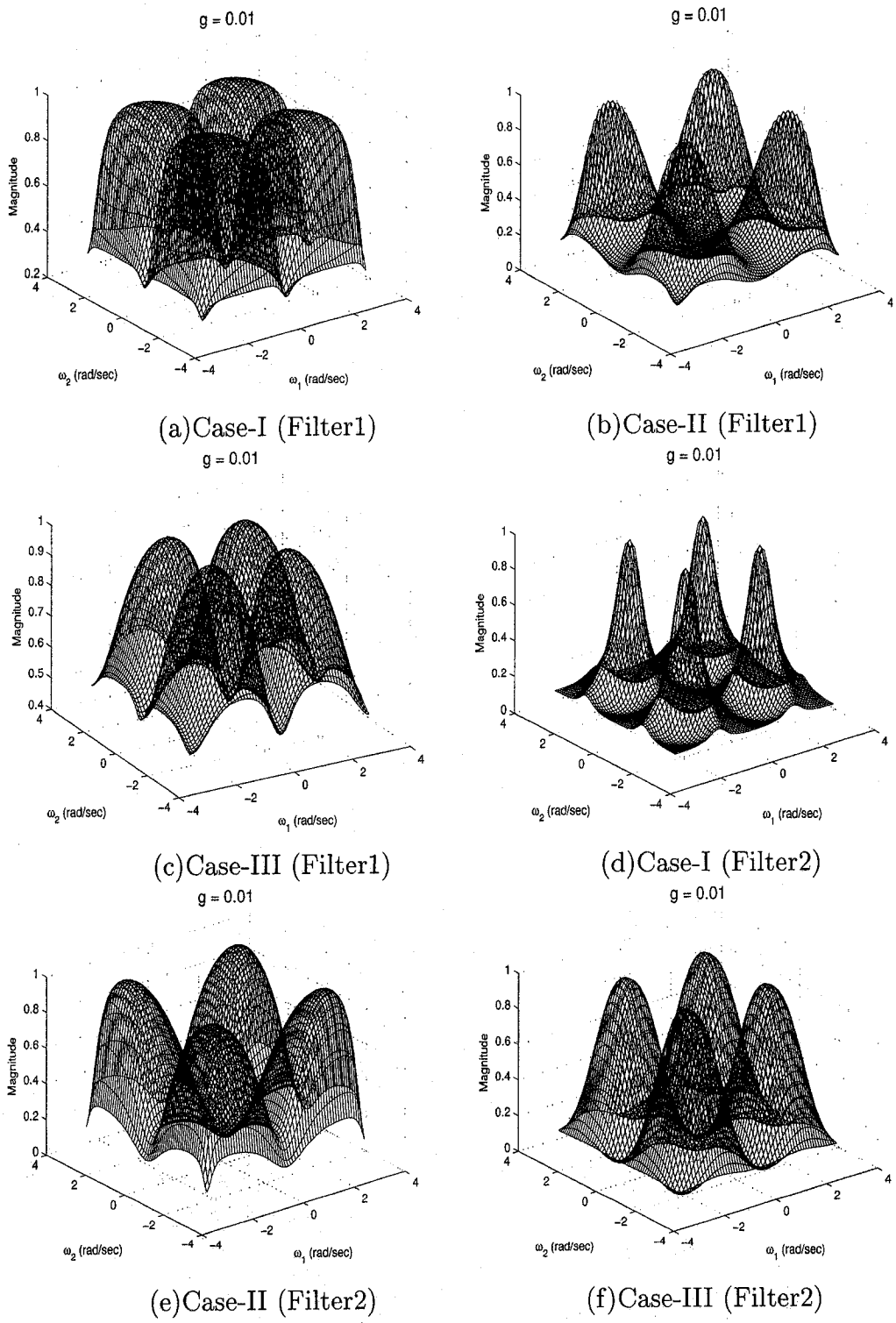


Figure 4.7: 3D magnitude plots of the 2D digital Band-pass filters (a) Case-I (filter1), (b) Case-II (filter1), (c)Case-III (filter1), (d) Case-I (filter2), (e) Case-II (filter2), (f)Case-III (filter2)

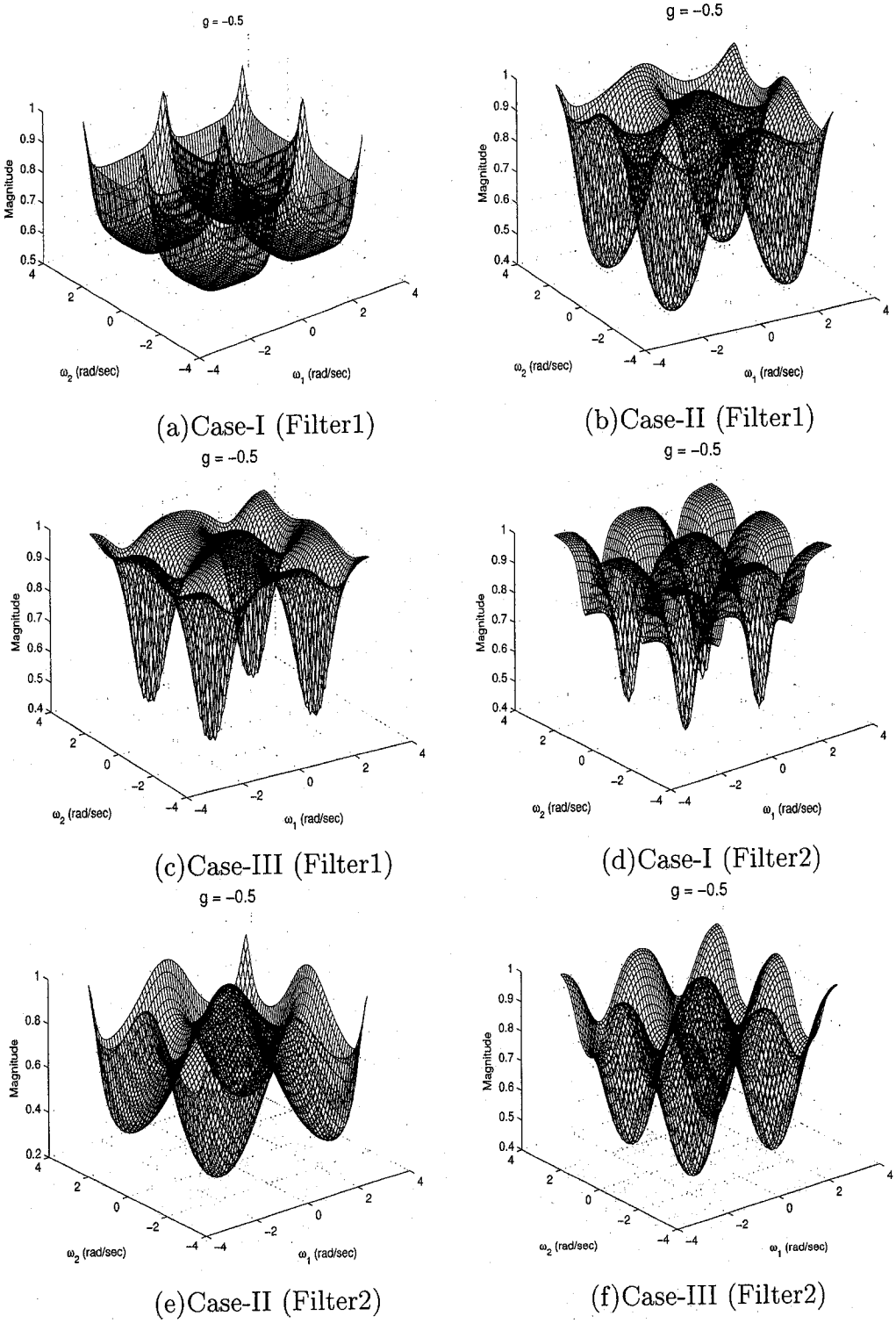


Figure 4.8: 3D magnitude plots of the 2D digital band-elimination filters (a) Case-I (filter1), (b) Case-II (filter1), (c)Case-III (filter1), (d) Case-I (filter2), (e) Case-II (filter2), (f)Case-III (filter2)

Table 4.4: The values of parameters are used to design the 2D band-elimination filters (Figures 4.8)

| Filter 4.8 | g | $a_i$ | $b_i$ | $k_i$ | $k_{i1}$ | $k_{i2}$ |
|---|---|---|---|---|---|---|
| Case-I(Filter1) | -0.5 | -0.5 | 0.1 | 2 | 0.1 | 0.1 |
| Case-II(Filter1) | -0.5 | -0.9 | 0.1 | 5 | 0.15 | 0.35 |
| Case-III(Filter1) | -0.5 | -0.9 | 0.1 | 10 | 0.3 | 0.5 |
| Case-I(Filter2) | -0.5 | -0.9 | 0.1 | 10 | 0.25 | 0.2 |
| Case-II(Filter2) | -0.5 | -0.9 | 0.1 | 2 | 0.05 | 0.2 |
| Case-III(Filter2) | -0.5 | -0.9 | 0.5 | 10 | 0.1 | 0.1 |

low-pass transfer function to obtain the modified analog low-pass transfer function. Second, the bilinear transformation is used to obtain the desired digital filter. Recently, it has been shown that Pascal matrix allows the design of digital filters from a continuous-time prototype and frequency transformations of analog transfer function is also done by matrix operation [38]. It has been proven that this digital filter design technique is better than the method of digital low-pass and high-pass filter design [37]. The method [37] has shown that Pascal matrix allows the transformation of a normalized analog transfer function from a low-pass to low-pass and high-pass discrete transfer function. Another method [36] is proposed after two years and it is shown that Pascal matrix also can be used to transform the normalized analog transfer function from low-pass to band-pass discrete transfer function. However, these methods are difficult to use in the case of transforming a normalized analog transfer function to a higher-order filter [38]. To overcome the problems, a transformation method is proposed in this thesis which is based on the GBT and the value/sign of gyrator constant (g) of a doubly terminated gyrator network.

The proposed method of the digital filter transformation is shown in the figure 4.9 and it is observed that the band-pass to band-elimination filter or the low-pass to high-pass filter or vice-versa transformation is obtained by regulating the value and/or sign of g. However, the low-pass to band-pass or the high-pass to band-elimination filter or vice versa transformation is obtained by regulating g and the parameters of the GBT as shown in equations (4.3.1) and (4.3.2). A detailed description of method is discussed in the following.

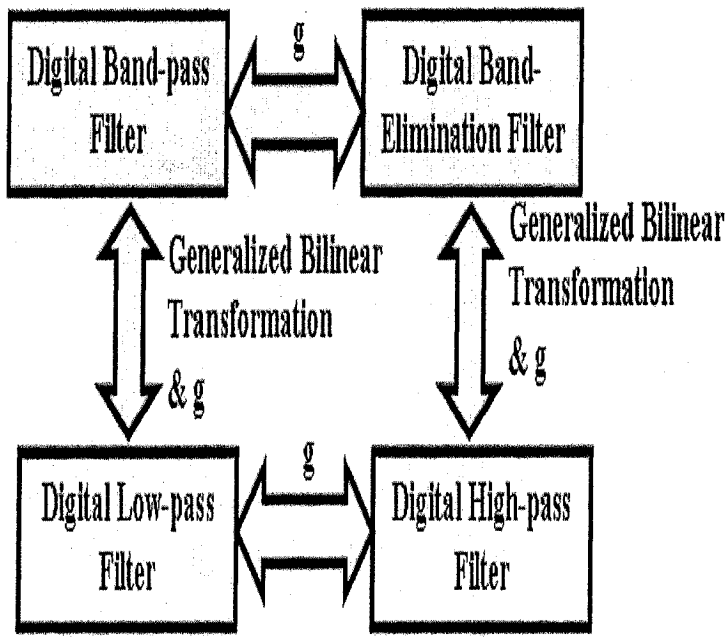


Figure 4.9: Block diagram of the Digital Filter Transformation.

### 4.4.1 Low-pass filter to High-pass filter Transformation

The digital filter transformation of a 2D digital low-pass to a 2D digital high-pass filter and vice-versa are proposed in two different ways. A detailed discussion provides the following.

It is seen that the magnitudes of g of a doubly terminated gyrator filter can change the amplitude-frequency responses of the filter (sections 4.2, 4.3, 3.2, 3.3.) and in addition, it is shown that the change of g is transformed a digital low-pass filter to a digital high-pass filter. The amplitude-frequency responses of the filter1 (sections 3.3.2, 3.3.3, 3.3.2) are studied carefully, when the value of g is changed to higher values. Approximately, it is determined that the 2D digital low-pass filters are obtained for $0 \leq g \leq 0.03$ and the 2D digital high-pass filters are obtained for $0.99 > g \geq 0.1$ and $\infty > g > 1$. But the amplitude-frequency response of the filter1 is constant for g = 1.

According to the proposed digital 2D low-pass filter design, the impedances of the gyrator filter1 are replaced by the second-order Butterworth filters and the GBT

($a_i = -0.9, b_i = 0.1, k_i = 1$) is applied to the overall 2D analog transfer function to get the 2D digital low-pass filter. The frequency response of the digital filter is dependent on the value of g and Figure 4.10 shows the transformation of filter from the 2D digital low-pass filter to the 2D digital high-pass filter by varying g of the gyrator network.

Figures 4.10 (a) and (b) show frequency response of the 2D digital low-pass and the corresponding 2D digital high-pass filter respectively. The proposed method has used different values of g in the doubly terminated gyrator filter1 for the transformation of the filters. Similarly, the proposed method is applied to case-II (filter1) for the digital filter transformation. The magnitude response of the 2D digital low-pass filter (Figure 4.10 (c)) is transformed to the 2D digital high-pass filter (Figure 4.10 (d)). Another frequency response of the 2D digital low-pass filter (Figure 4.10 (e)) is designed using the second-order Butterworth and Gargour&Ramachandran filters in the gyrator filter1 (section 3.3.3) and the proposed filter transformation method is applied to the low-pass filter to obtain the 2D digital high-pass filter (Figure 4.10 (f)).

In order to explain the filter transformation, a thorough studied has been carried out on the reactive behavior of the gyrator filter and it is found that the reactive behavior is changed not only for the parameters of the gyrator filter, but also for the value and sign of g.

It has been seen that the total reactive property of the gyrator circuit is changed using opposite sign of g [19]. As a result, the low-pass filter transforms to the high-pass filter by changing the sign of g of the gyrator filter. The amplitude-frequency responses of the sections 3.2, 3.3, 4.2, 4.3 are studied and it is shown that the inverted filter responses of the corresponding sections can be obtained for the opposite sign of g. Some examples are provided in Figure 4.11.

In Figure 4.11, the 3D magnitude responses of the several 2D digital low-pass filters are given and each of the low-pass magnitude responses is transformed to the digital high-pass magnitude responses. Figures 4.11 (a) and (b) show the frequency response of the 2D digital low-pass filter when g =10 and the corresponding 2D digital high-pass filter when g = -10 respectively. The proposed method is applied to the case-II (filter2) for the digital filter transformation and the magnitude response of the 2D digital low-pass filter (Figure 4.11 (c)) when g = 8 is transformed to the 2D digital

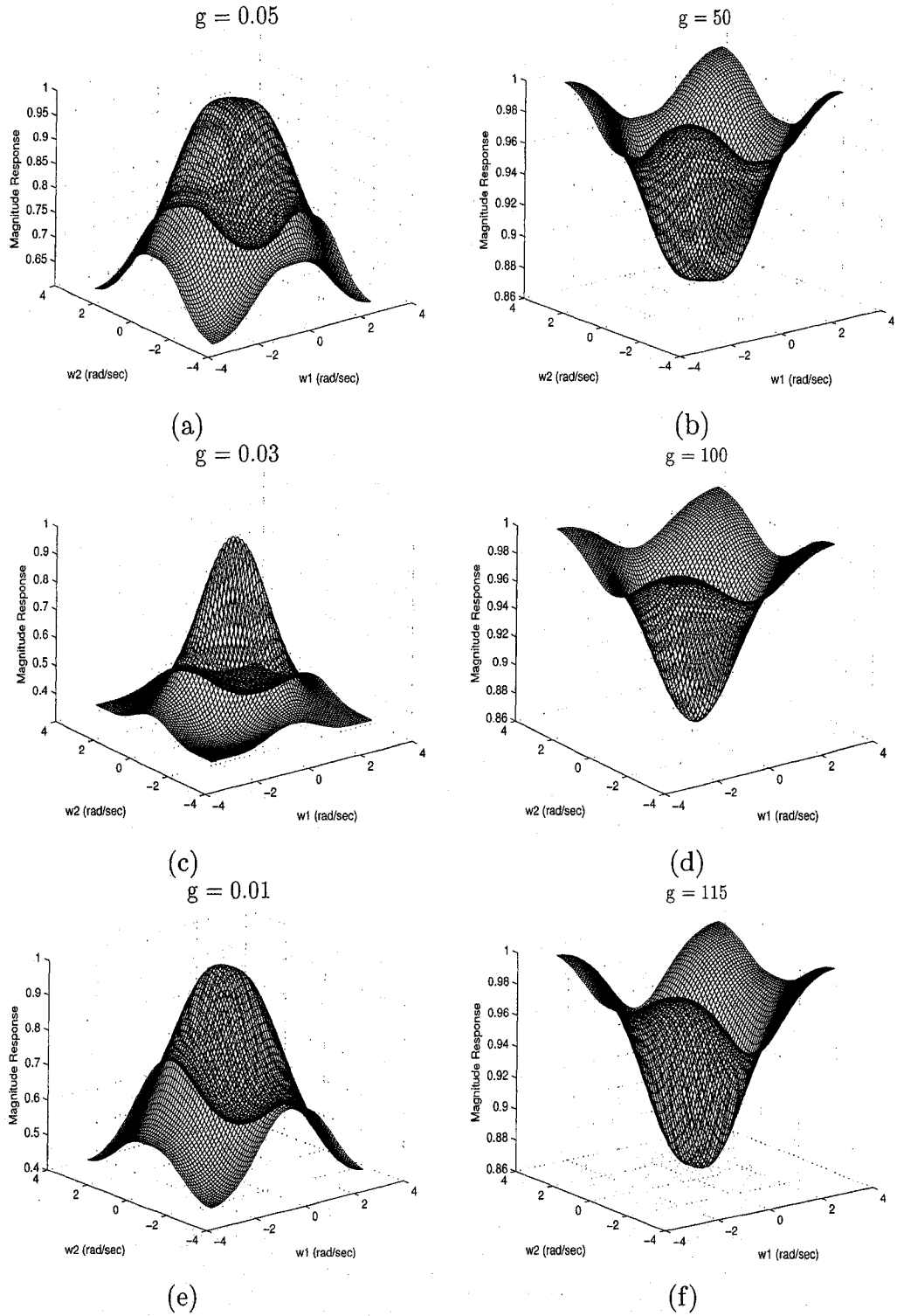


Figure 4.10: 3D magnitude responses of the several 2D digital low-pass filters and the corresponding 2D digital high-pass filter, (a) g = 0.05 in case-I(filter1), (b) g = 50 in case-I(filter1)), (c) g = 0.03 in case-II(filter1), (d) g = 100 in case-II(filter1), (e) g = 0.01 in case-III(filter1), (f) g = 115 in case-III(filter1)

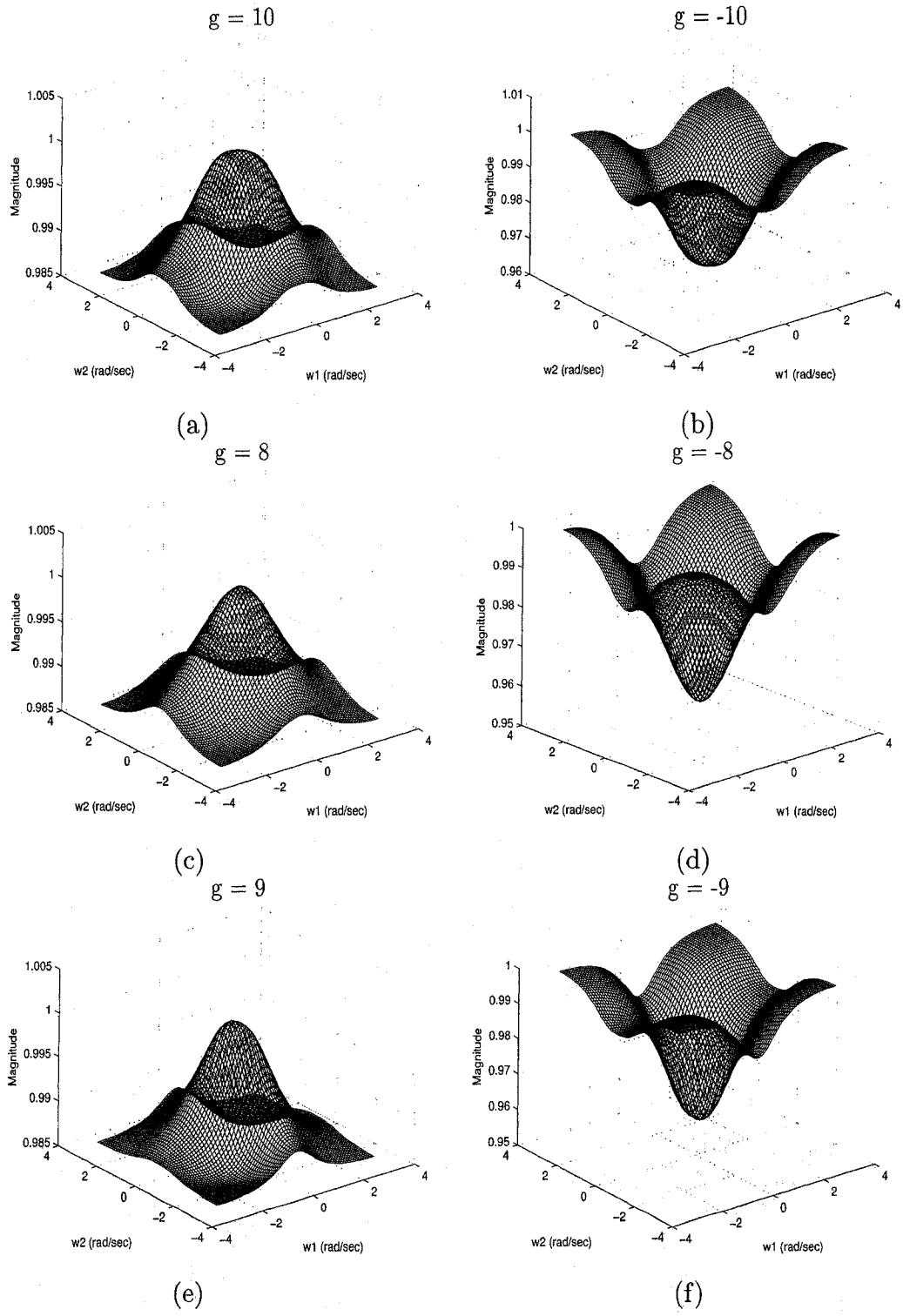


Figure 4.11: 3D magnitude responses of several 2D digital low-pass filters and the corresponding 2D digital high-pass filter, (a) Low-pass response, Case-I (Filter2); (b) High-pass response, Case-I (Filter2), (c) Low-pass response, Case-II (Filter 2), (d) High-pass response, Case-II (Filter 2), (e) Low-pass response, Case-III (Filter 2), (f) High-pass response, Case-III (Filter 2)

high-pass filter when g = - 8 (Figure 4.11 (d)). Another 2D digital low-pass filter (Figure 4.11 (e)) is obtained from the case-III(filter2) when g = 9 and this low-pass filter is transformed to the 2D digital high-pass filter when g = - 9 (Figure 4.11 (f)).

### 4.4.2 Band-pass filter to Band-elimination filter Transformation

The proposed design of 2D digital Band-pass filter and Band-elimination filter is applied to an analog doubly terminated gyrator filter, when then impedances of the gyrator filter are replaced by the doubly terminated RLC networks. As a result, g of the filter gives flexibility to obtain the desired bandwidths and center frequencies of the filter. The amplitude-frequency responses of section 4.3 are studied and it is observed that the corresponding inverted filter response can be obtained not only changing the parameters of the gyrator filter, but also for the value and sign of g of the filter.

Figure 4.12 shows the digital filter transformation from the band-pass to band-elimination filter and in this case, the effect of the values of g of the filter is considered for the filter transformation. It is also seen that the sign of g of the filter is another factor of the filter transformation (Figure 4.13).

The 2D digital band-pass filter responses (Figures 4.12 (a), (c) and (e)) are obtained from case-I(filter1), case-II(filter1) and case-III(filter1) respectively. The digital filters are transformed to the 2D digital band-elimination filter (Figures 4.12 (b), (d) and (f)) for the values of g of the filter1.

Table 4.5: The values of parameters are used for the 2D digital filter transformation from the band-pass to band-elimination filter (figures 4.12)

| Figure | $a_i$ | $b_i$ | $k_i$ | $k_{11}$ | $k_{12}$ | $k_{21}$ | $k_{22}$ |
|---|---|---|---|---|---|---|---|
| (a)-(b) | -0.5 | 0.1 | 2 | 0.25 | 0.2 | 0.25 | 0.2 |
| (c)-(d) | -0.9 | 0.5 | 1 | 0.55 | 0.02 | 0.55 | 0.2 |
| (e)-(f) | -0.9 | 0.1 | 1 | 0.6 | 0.5 | 0.6 | 0.5 |

Table 4.5 gives the values of parameters are used for the 2D digital filter transformations from the digital band-pass to the digital band-elimination filters (Figure 4.12).

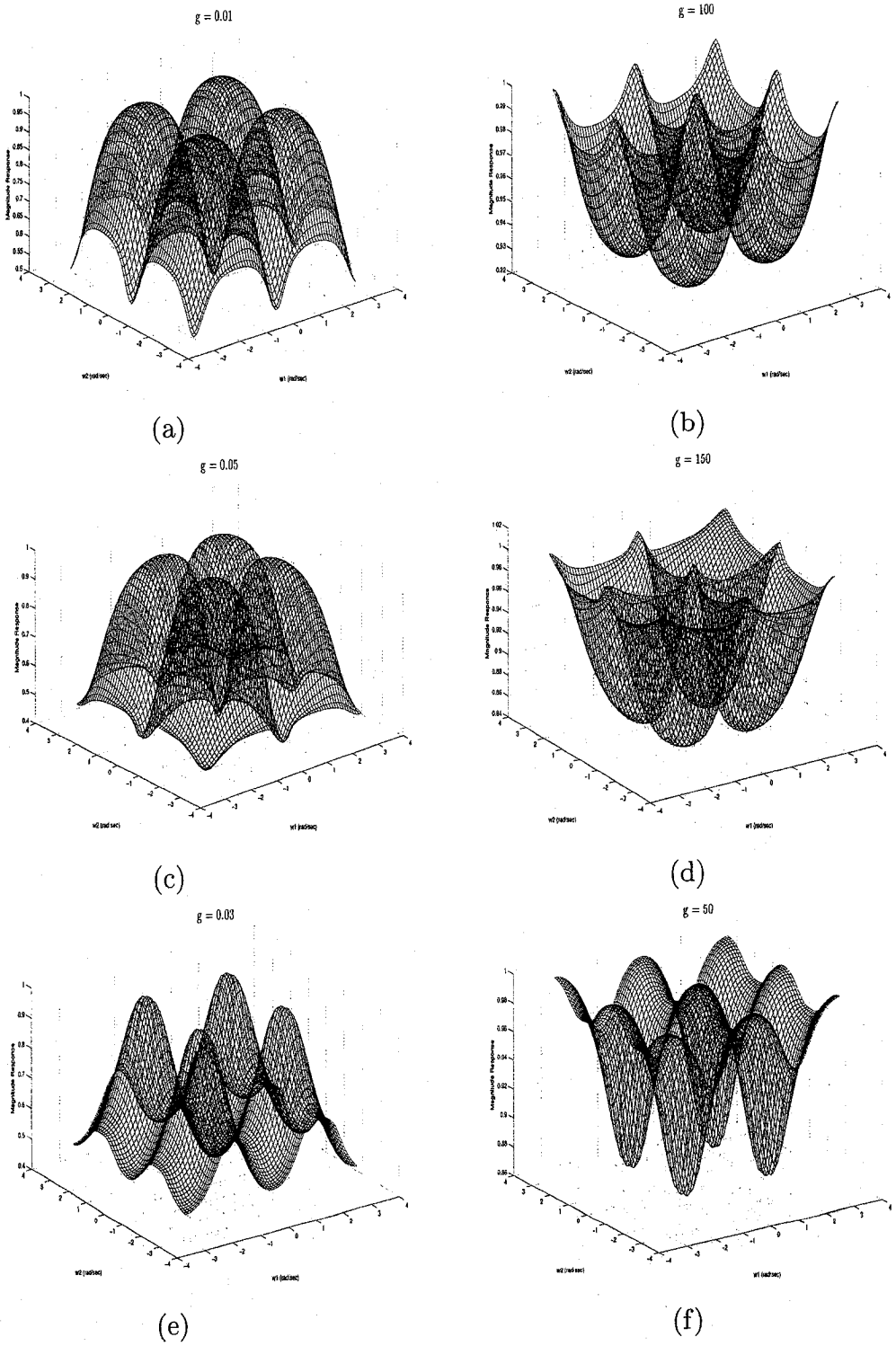


Figure 4.12: 3D magnitude plots of the several 2D digital band-pass filters and the corresponding 2D digital band-elimination filter, (a) & (b) case-I(filter1), (c) & (d) case-II(filter1),(e) & (f) case-III(filter1)

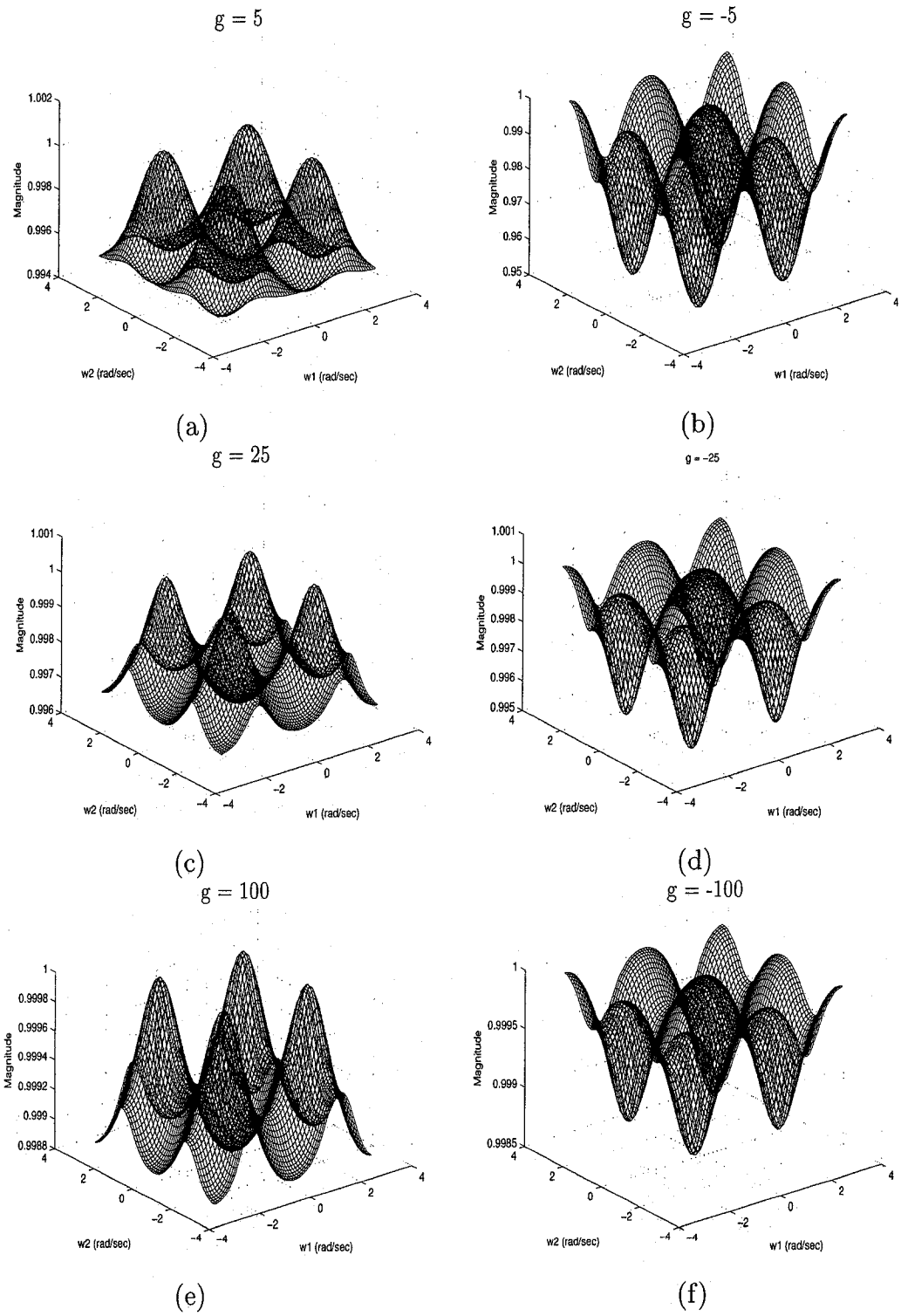


Figure 4.13: 3D magnitude plots of the digital band-pass filter to the digital band-elimination filter transformations, (a) & (b) case-I(filter2), (c) & (d) case-II(filter2),(e) & (f) case-III(filter2)

The 2D digital band-pass filter responses (Figures 4.13 (a), (c) and (e)) are obtained from case-I(filter2), case-II(filter2) and case-III(filter2) respectively. These digital band-pass filters are transformed to the 2D digital band-elimination filters (Figures 4.13 (b), (d) and (f)) by changing the sign of g of the filter2.

From the above discussion, It is seen that all the filter responses satisfy the stability conditions and the monotonic characteristics. To ensure the stability criteria in 2D domain, the two impedances of the doubly terminated gyrator filter1 are replaced by the second-order RCL filters and the denominator of the resultant transfer function is satisfied to be a VSHP (section 2.4). However, in the case of doubly terminated gyrator filter2, the two impedances of the gyrator filter2 are replaced by the second-order RCL filters and the third impendence is replaced by a resistive component; otherwise the denominator of the resultant transfer function will not be a VSHP (section 2.4.5). The GBT is applied to the overall 2D analog transfer function. As a result, in the digital domain, the frequency responses of the filters are scaled by the value of g and parameters of the GBT. It is also observed that $k_{i1}, k_{i2}$ control the center frequencies and bandwidths of the 2D digital band-pass and band-elimination filter.

In the proposed design-I, the double bilinear transformation is applied to the analog transfer function to obtain the digital transfer function. As a result, frequency distortion of the digital filters has been found in high frequencies. In order to overcome this problem, two methods are proposed in the following.

## 4.5 Frequency Prewarping

The Double bilinear transformations are an efficient technique for obtaining the 2D digital filter. The digital frequency response is expected to be the as of 2D analog counterpart; however the relation between analog and digital frequencies is non-linear, as a result distortion is introduced in high frequencies of digital domain which is commonly known as frequency warping effect [23]. The derived digital filter has the same number of pass-bands in each dimension as of the analog filter, but the center frequencies and bandwidths of higher frequency pass-bands tend to be reduced disproportionately in both dimensions of digital domain. Numbers of author have shown that the frequency warping can be reduced in one-dimensional filter design [39], [40].

But in the case of two-dimensions, no technique has been proposed until now and moreover, the 2D IIR filter design is more complicated than the 1D filter design, because of the difficulty to control stability of the 2D IIR filter. However, some approaches [41], [42], [43] have been shown in the design of 2D digital filters and those approaches have failed to meet the prescribed specifications at higher frequencies of the 2D digital filter, because double bilinear transformations have failed to provide linear relationship in between higher ranges of analog frequencies and digital frequencies and as a result, the difficulties happen in the various applications.

The objective of this section is to analyzes the problem of frequency warping in the case of two-dimensional frequency responses of the filter and propose two methods to reduce the frequency warping of 2D analog to digital filter conversion. In the first method, frequency prewarping is performed by means of the GBT and in the second method, prewarping is carried out by approximating the 2D analog gyrator filter via an optimization or 2D frequency scaling of the analog transfer function to reduce frequency warping. Finally, both methods are applied together in order to obtain the desired 2D digital filter responses.

In method-I, the GBTs are applied to a stable 2D analog filter in order to obtain the prescribed cutoff frequencies of the 2D digital filter and all the parameters $(a_i, b_i, k_i)$ of the GBT are varied to obtain the desired digital filter responses. The method-I ensures the stability and the monotonic amplitude response of the designed 2D digital filter [10] and flexibility in the filter design is achieved for the elimination of warping effect of a low-pass, high-pass, band-pass and band-elimination filter. The relation in between the analog frequencies and the digital frequencies has established (equation (2.3.7)) in chapter 2 and the frequency mappings in between two domains are studied for different values of $a_i, b_i$ and $k_i$ in order to reduce the frequency warping effect. It is found that for linear relationship in between analog frequency responses and digital frequency responses are dependent on the values of $a_i, b_i$ and $k_i$ and those values are determined from the equation (2.3.7).

For illustration, a 2D analog low-pass transfer function (equation (4.5.1)) is considered from [10] and observed for the warping effects. Frequency warping errors are calculated in term of mean-square-error (MSE) (equation (4.5.2)).

$$H_{sh}(s1,s2) = \frac{1}{\begin{bmatrix} 1 & s_1 & s_1^2 \end{bmatrix} \begin{bmatrix} 1 & 1.618 & 1 \\ 1.618 & 2.6179 & 1.618 \\ 1 & 1.618 & 1 \end{bmatrix} \begin{bmatrix} 1 \\ s_2 \\ s_2^2 \end{bmatrix}} \tag{4.5.1}$$

The analog cutoff frequency of equation (4.5.1) is 0.9 rad/sec and the double bilinear transformations are applied to equation (4.5.1) to obtain the 2D digital filter. The resultant 2D digital filter provides MSE = 0.0545 in between the 2D desired digital filter and the designed digital filter. The proposed method is applied to the equation (4.5.1) for converting the analog domain to digital domain. The resultant 2D digital filter gives the MSE = 0.0016. This method provides significant improvement for the 2D digital filter design. Frequency scaling is done on the equation (4.5.1) to obtain the different analog transfer function with the different cutoff frequency [44] and verify the MSEs and reduced MSE of the designed digital filters by the proposed method (Table 4.6)

$$MSE = \frac{\sum_{i=0}^{M}\sum_{j=0}^{N}\left(H_{ideal}(i,j) - H_{designed}(i,j)\right)^2}{M * N} \tag{4.5.2}$$

where $H_{ideal}$ is the 2D desired digital filter, $H_{designed}$ is the designed digital filter and both filters is M by N matrix.

Table 4.6: Frequency warping errors of the 2D digital filter

| $\omega_{ij}(rad/sec)$ | MSE | $k_i$ | $a_i$ | $b_i$ | Reduced MSE |
|---|---|---|---|---|---|
| 1.65 | 0.0204 | 0.385370 | -1.00 | 0.170187 | 0.005684 |
| 2.00 | 0.0257 | 0.289385 | -1.00 | 0.170180 | 0.005488 |
| 2.20 | 0.0352 | 0.240349 | -1.00 | 0.166600 | 0.004626 |
| 2.40 | 0.0425 | 0.211691 | -1.00 | 0.166599 | 0.003862 |
| 2.75 | 0.0598 | 0.153245 | -1.00 | 0.166601 | 0.002172 |
| 3.10 | 0.0718 | 0.111380 | -1.00 | 0.170185 | 0.001090 |

The second method is started with a gyrator network and impedances of the gyrator network are replaced by the doubly terminated RLC networks. The resultant 2D analog transfer function is stable (section 2.4) and coefficients of the transfer function are functions of gyrator constant (g). Equ. (4.5.3) is applied to the analog transfer

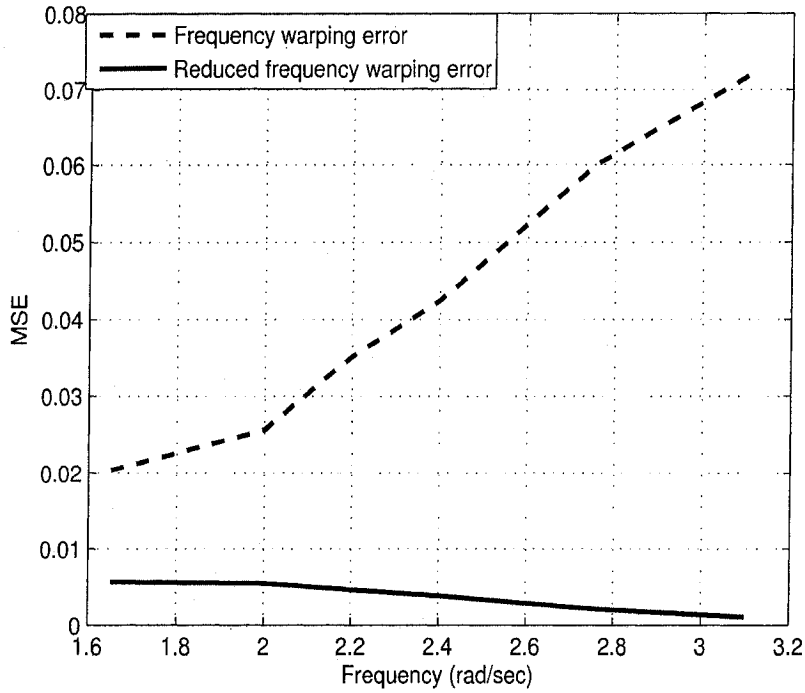


Figure 4.14: Comparison in between MSEs as generated by double bilinear transformation and reduced MSEs by the proposed method.

function in order to obtain the desired digital filter. An approximation problem of the 2D analog filter design is solved through the application of optimization method in order to obtain the analog frequencies equal to the desired digital frequencies. An error function (equation (4.5.4)) is formulated on the basis of the desired amplitude frequency response and a norm of the error function is minimized with respect to the transfer function coefficients. As the value of the norm approaches zero, the resulting amplitude or phase response approaches the desired amplitude or phase response and desired analog frequencies are achieved. Alternative technique can be followed to avoid heavy computation, that is 2D frequency scaling of the 2D analog filter and scale factors of the both dimensions are calculated as a ratio of new frequencies to old frequencies. It has found that the scale factors are function of g and judicious choice of g can obtain less warping effect in the both dimensions.

$$s_i = k_i \frac{z_i - 1}{z_i + 1} \tag{4.5.3}$$

where, i = 1,2.

$$E(\Omega_{1i_1}, \Omega_{2i_1}, g, k_i) = \sum_{i_1=0}^{M1} \sum_{i_2=0}^{M2} |H_A(j\omega_{1i_1}, j\omega_{2i_2}) - H_D(j\omega_{1i_1}, j\omega_{2i_2}, g, k_i)|^2 \qquad (4.5.4)$$

where, $H_A$ is the desired filter and $H_D$ is the designed digital filter.

For example, it is required to design a 2D digital low-pass filter to meet the following specifications:

$$H_A(z_1, z_2) = \left\{ \begin{array}{ll} 1, & \text{for} \sqrt{\omega_1^2 + \omega_2^2} \leq 1 \\ 0, & \text{for} \sqrt{\omega_1^2 + \omega_2^2} \geq 2.5 \end{array} \right\} \qquad (4.5.5)$$

A stable analog transfer function is generated in section 2.4, where impedances of a doubly terminated gyrator network (Figure 2.2) are replaced by two doubly terminated RLC networks (second-order Gargour&Ramachandran filters) and stability of the resultant transfer function (equation (4.5.6)) is satisfied (section 2.4).

$$H_{2B2D}(s_1, s_2) = \frac{\begin{bmatrix} 1 & s_1 & s_1^2 \end{bmatrix} \begin{bmatrix} 3g+1 & 0.725+3.75g & 2.05g \\ 0.725+3.75g & 4g+0.5 & 2.225g \\ 2.05g & 2.225g & g \end{bmatrix} \begin{bmatrix} 1 \\ s_2 \\ s_2^2 \end{bmatrix}}{8.25 \begin{bmatrix} 1 & s_1 & s_1^2 \end{bmatrix} \begin{bmatrix} 0.364g^2+1 & 0.454g^2+0.97 & 0.251g^2+0.364 \\ 0.454g^2+0.97 & 0.515*g^2+0.94 & 0.364+0.267g^2 \\ 0.251g^2+0.364 & 0.364+0.267g^2 & 0.127+0.127g^2 \end{bmatrix} \begin{bmatrix} 1 \\ s_2 \\ s_2^2 \end{bmatrix}} \qquad (4.5.6)$$

The error function (equation (4.5.4)) is used to minimize the error in between the desired filter ($H_A$) and the designed filter ($H_D$). It is shown that the 2D digital low-pass filter (equation (4.5.7)) with the cutoff = 1 rad/sec is obtained when g = 0.01 and k = 3.25. Figure 4.15 shows the 3D magnitude and contour plots of the

designed 2D digital low-pass filter.

$$H_{d2B}(z_1,z_2)=\frac{\begin{bmatrix}1 & z_1 & z_1^2\end{bmatrix}\begin{bmatrix}1 & -10.85 & 2.317\\ 2.317 & 69.512 & 231.7\\ -10.854 & 158.537 & 69.512\end{bmatrix}\begin{bmatrix}1\\ z_2\\ z_2^2\end{bmatrix}}{64.634\begin{bmatrix}1 & z_1 & z_1^2\end{bmatrix}\begin{bmatrix}1 & -6.038 & 13.585\\ 13.585 & -84.9 & 179.245\\ -6.038 & 35.85 & -84.9\end{bmatrix}\begin{bmatrix}1\\ z_2\\ z_2^2\end{bmatrix}} \tag{4.5.7}$$

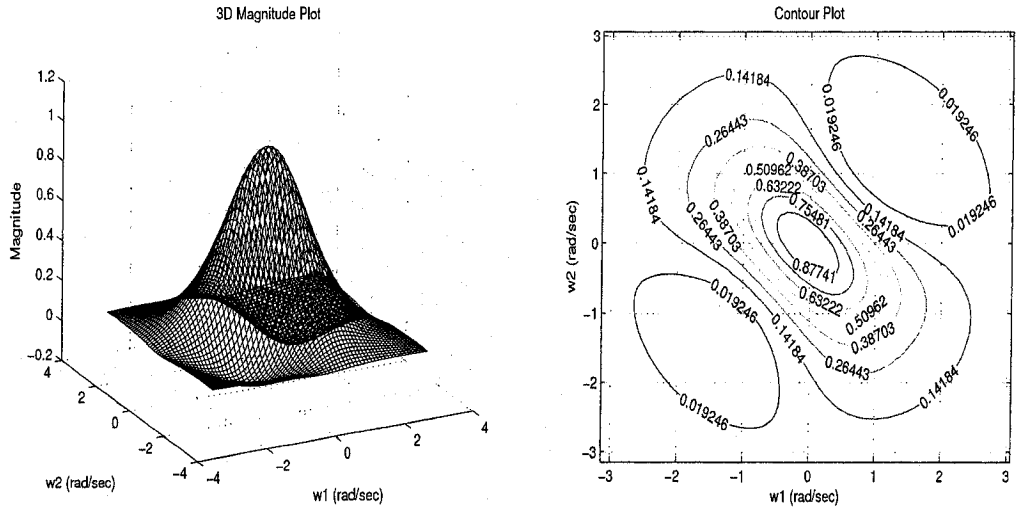


(a) (b)

Figure 4.15: 3D magnitude and contour plots of the 2D digital low-pass filter

Both the methods are efficient in the digital filter design, but the first method has more parameters than the second method for reducing the warping error. It has been shown in the chapter 3 and chapter 4 that the both methods are applied together in order to obtained the desired digital filter responses.

## 4.6 Realization of the digital filter

Realization is the process of converting the transfer function of the digital filter into a digital structure for the implementation in two forms, such as software and hardware. In a software implementation, difference equations are represented in the state-space

which is converted into a computer program that can simulate the performance of the digital filter and in the hardware implementation a digital network is converted into a piece of dedicated hardware.

Several realization methods are available that lead to a great variety of digital-filter structures [45] such as, continued fraction expansions, direct implementation, discrete state-space implementation. In 2D polynomials, there is no general factorization scheme. However under certain conditions, 2D polynomial can be expressed as a product of special type of two-variable polynomials of lower order as shown in paper [46]. Direct implementation of 2D recursive filter is realized using equation (4.6.1) in paper [47] and state-space model is developed by considering the input variable to all delay elements as state variables and applying linear transformation to the state variable, many equivalent state-space models of 2D structure can be developed. But, the direct implementation is not applicable in the case of presence of the all orders of variables and all the coefficients of all variables are not zero. In this thesis, a realization of 2D digital polynomial is proposed and the realization is suitable to implement any 2D polynomial with finite order.

A canonical realization of 2D digital polynomials is shown below:

Two-dimensional recursive filter as a ratio of two-dimensional polynomials [47] can be represented as below:

$$H_d(z_1, z_2) = \frac{\sum_{i_1=0}^{M_n} \sum_{i_2=0}^{N_n} a_{i_1 i_2} z_1^{i_1} z_2^{i_2}}{\sum_{i_1=0}^{M_d} \sum_{i_2=0}^{N_d} b_{i_1 i_2} z_1^{i_1} z_2^{i_2}} \tag{4.6.1}$$

Let, an input signal $X(z_1, z_2)$, the output of the filter $Y(z_1, z_2) = H_d(z_1, z_2)X(z_1, z_2)$ and $b_{00} = 1$ in the equation (4.6.1) and (4.6.3).

$$\begin{aligned} Y(z_1, z_2) &= [\sum_{i_1=0}^{M_n} \sum_{i_2=0}^{N_n} a_{i_1 i_1} z_1^{i_1} z_2^{i_2}] X(z_1, z_2) \\ &- [\sum_{i_1=0}^{M_d} \sum_{i_2=0}^{N_d} b_{i_1 i_2} z_1^{i_1} z_2^{i_2}] Y(z_1, z_2) \end{aligned} \tag{4.6.2}$$

For example, if $M_n = M_d = 2$ and $N_n = N_d = 2$, the equation (4.6.3) is obtained.

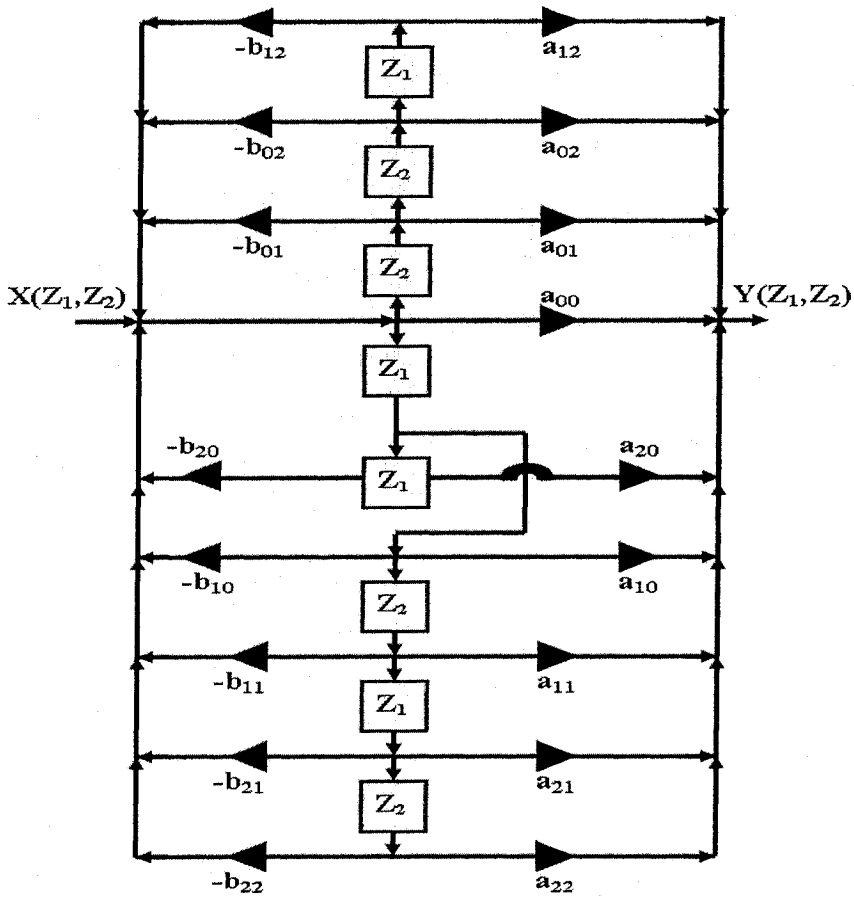


Figure 4.16: Realization of a second-order 2D Digital filter

$$H_d(z_1, z_2) = \frac{\begin{bmatrix} 1 & z_1 & z_1^2 \end{bmatrix} \begin{bmatrix} 1 & a_{01} & a_{02} \\ a_{10} & a_{11} & a_{12} \\ a_{20} & a_{21} & a_{22} \end{bmatrix} \begin{bmatrix} 1 \\ z_2 \\ z_2^2 \end{bmatrix}}{\begin{bmatrix} 1 & z_1 & z_1^2 \end{bmatrix} \begin{bmatrix} b_{00} & b_{01} & b_{02} \\ b_{10} & b_{11} & b_{12} \\ b_{20} & b_{21} & b_{22} \end{bmatrix} \begin{bmatrix} 1 \\ z_2 \\ z_2^2 \end{bmatrix}} \tag{4.6.3}$$

The digital filter can be decomposed into some building blocks and hardware implementation of the digital filter is made by interconnecting very-large-scale integrated (VLSI) circuit chips. However, it is possible to implement the entire digital filter on single chips, but complexity of the chips will be comparatively high [48].

A higher-order filter requires operation at high sampling rates and large amount of computation is done in each sampling period. As a consequence, the implementation is expected to be faster. The computation speed is increased by increasing the speed of the basic gates and reducing the propagation delays of interconnection wires. Major improvement in the computational speed is obtained by the concurrent use of processing elements. Digital filter realization allows high degree of concurrency; as a result, fast computation speed of the implementation is expected. Systolic arrays are highly regular networks and digital filter can be realized by this network [49]. In this thesis, an approach for hardware implementation of an IIR digital filter is proposed.

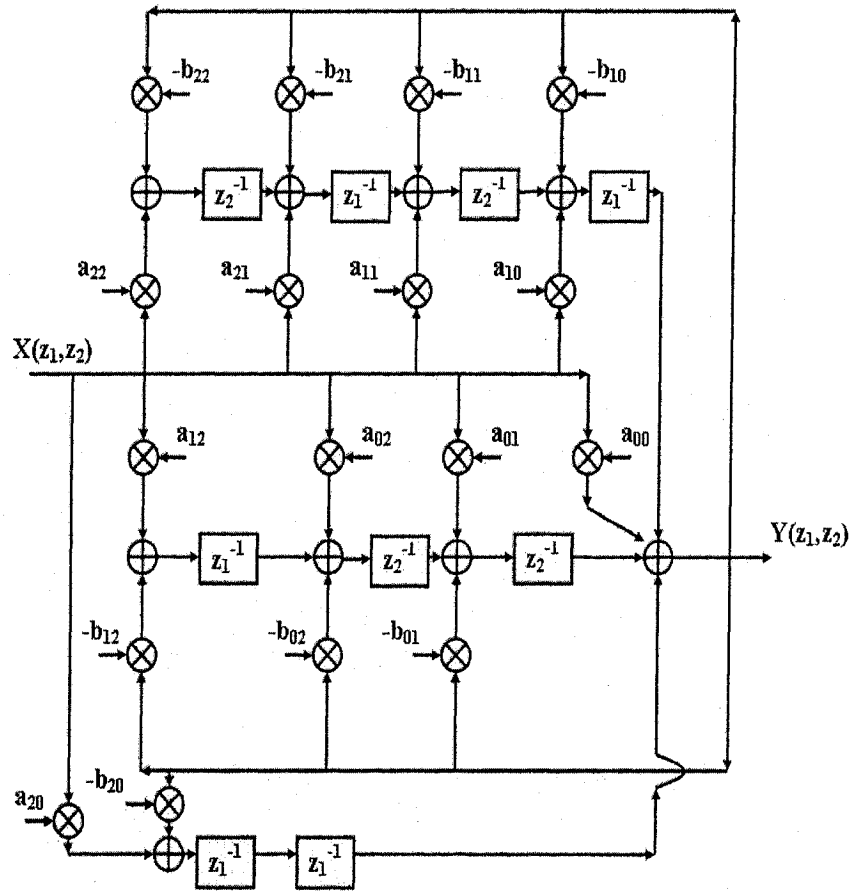


Figure 4.17: Realization of the Digital filter

The basic parameters of the digital filter implementation are created in separate programs VHDL (Very High Speed Integrated Circuit Hardware Description Language) Synopsis software [50] and interconnected those as required in the implementation [51]. The basic components are different gates, such as AND, OR, XOR,

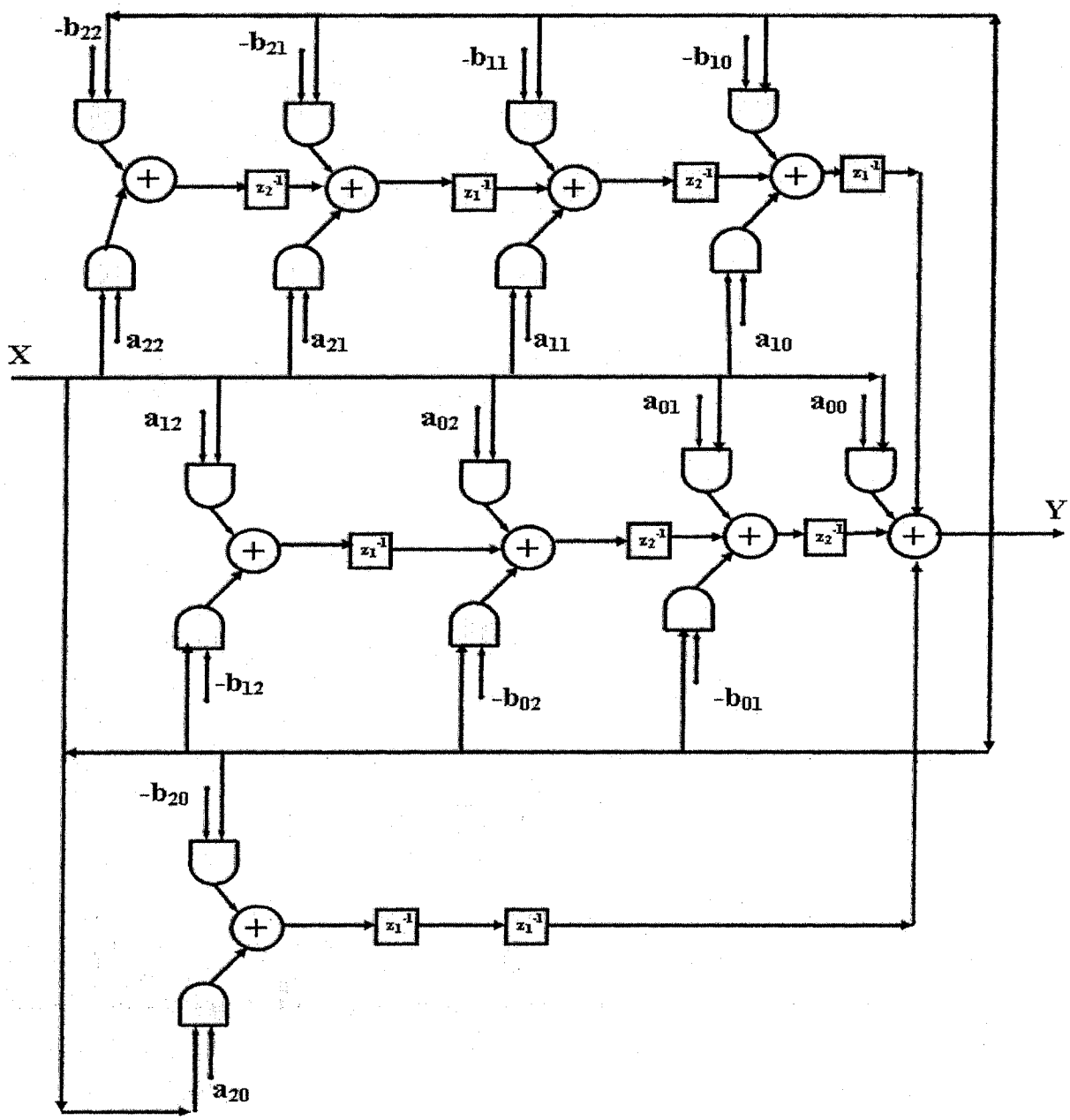


Figure 4.18: Realization of the Digital filter

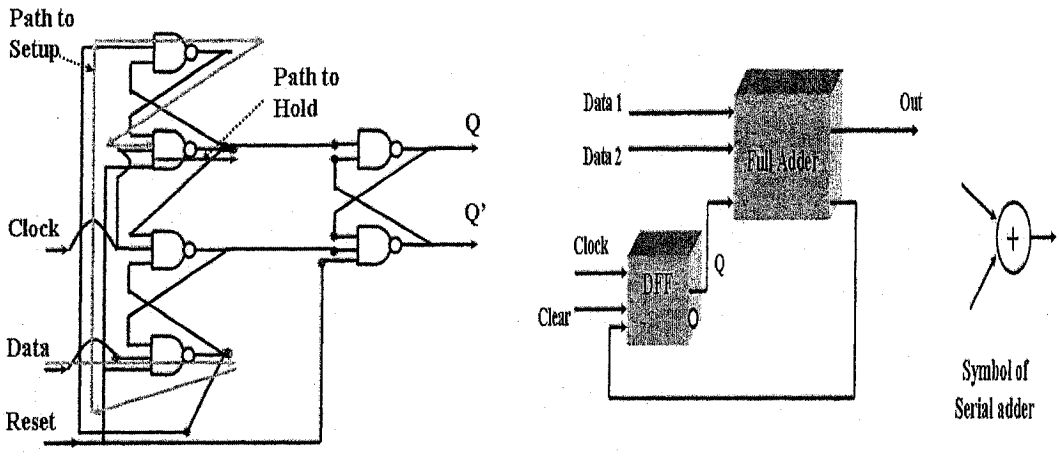


(a) (b)

Figure 4.19: (a) A D-flipflop (NAND gate based), (b) A Serial Adder and symbol of a serial adder.

Inverter and NAND. Every gates are tested in the test bench as well as VHDLDBX platform by giving different input in the gates. The delay elements (D-flip flop) are the most important components in this realization. There different kinds of D-flipflop (DFF), such as level triggered, positive edge triggered and negative edge triggered. Positive edge triggered DFF and 2 input serial adders are used for the proposed realization. The 3 input serial adder is a combination of two serial adders and a 2 input serial adder is generated by a half-adder, full-adder and DFF (Figure 5.13). A serial-in-parallel-out register is used in order to store the final result.

All basic gates have their own delays. NAND gate is a combination of AND gate and Inverter, as a result, total delay of NAND gate is (0.1+0.1) = 0.2 nanosecond (ns). The 3-input NAND gate is a combination of two NAND gate, so the delay is (0.2+0.2) = 0.4 ns. The setup time (0.6ns) and hold time (0.4 ns) of the positive edge triggered DFF (NAND gate based) is determined from Figure 5.13 and a two input serial adder has 3 ns delay. Sampling time $T_i$ (where i = 1,2) is greater than sum of delay for clock to Q of DFF (0.8 ns), maximum delay for combinational logic (0.1+ 3*0.3 = 1 ns) and setup time of the DFF (0.6 ns). Synthesis of the design can be done by FPGA (Field Programmable Gate Array) (Xilinx ISE tool) [50].

In hardware digital filter implementation, numbers are stored in finite-length

registers, but coefficients and signal values are quantized and stored in the registers. However, number quantization gives three types of errors, such as coefficient-quantization error, product-quantization error and input-quantization error. It has already been shown that there are many methods to minimize the effects of quantization [52], [53], [54], [45]. Some of the corresponding VHDL codes are given for further improvement of the hardware implementation.

```
------------------------------------------------------------------
------Nand Gate Based Positive Triggered D Flip Flop------------
------------------------------------------------------------------
library ieee; use ieee.std_logic_1164.all; entity dff is
    port(D,clk,clr: in std_logic;
        Q : out std_logic);
end dff; architecture arch_dff of dff is
    component nand_3_pac
        port(A,B,C: in std_logic;
             Z: out std_logic);
        end component;
    component nand_2_pac
        port(A,B: in std_logic;
            Z: out std_logic);
    end component;
for U1,U5: nand_2_pac use entity Work.nand_2_pac(arch_nand_2_pac);
for U2,U3,U4,U6: nand_3_pac use entity
Work.nand_3_pac(arch_nand_3_pac); signal clr1,s1,s2,s4,s3,s5,s6:
std_logic; begin clr1<= not clr; U1: nand_2_pac port map
(A=>s4,B=>s2,Z=>s1 ); U2: nand_3_pac port map
```

```
(A=>s1,B=>clk,C=>clr1,Z=>s2 ); U3: nand_3_pac port map
(A=>s2,B=>clk,C=>s4,Z=>s3 ); U4: nand_3_pac port map
(A=>s3,B=>D,C=>clr1,Z=>s4 );
        U5: nand_2_pac port map (A=>s2,B=>s6,Z=>s5 );
        U6: nand_3_pac port map (A=>s5,B=>s3,C=>clr1,Z=>s6 );
U7: Q<=s5; end arch_dff;
--------------------------------
-----------Half Adder------------
--------------------------------
library ieee; use ieee.std_logic_1164.all; entity h_adder_pac is
port (A,B: in std_logic;
    S, Ca: out std_logic);
end h_adder_pac; architecture arch_h_adder_pac of h_adder_pac is
component xor_2_pac
    port(A,B: in std_logic;
        C: out std_logic);
end component; component and_2_pac
    port(A,B: in std_logic;
        C: out std_logic);
end component; for U1: xor_2_pac use entity
Work.xor_2_pac(arch_xor_2_pac); for U2: and_2_pac use entity
Work.and_2_pac(arch_and_2_pac);--\\
begin
 U1: xor_2_pac port map
(A=>A, B=>B, C=>S); U2: and_2_pac port map (A=>A, B=>B, C=> Ca);
end arch_h_adder_pac;
```

```
-----------------------------------
-------------Full Adder------------
-----------------------------------
library ieee; use ieee.std_logic_1164.all;

entity f_adder_pac is
    port(A,B, C: in std_logic;
        S,Ca: out std_logic);
end f_adder_pac; architecture arch_f_adder_pac of f_adder_pac is
component h_adder_pac
    port(A,B: in std_logic;
        S,Ca: out std_logic);
end component; component or_2_pac
    port(A,B: in std_logic;
        C: out std_logic);
end component; signal A1,B1,s1,s2,s3: std_logic; for U1, U2:
h_adder_pac use entity Work.h_adder_pac(arch_h_adder_pac); for U3:
or_2_pac use entity Work.or_2_pac(arch_or_2_pac); --\\
begin U1: h_adder_pac port map (A=>A,B=>B,S=> s1, Ca=>s2); U2:
h_adder_pac port map (A=>C,B=>s1,S=>S, Ca=>s3); U3: or_2_pac port
map (A=>s3,B=>s2,C=>Ca); end arch_f_adder_pac;
-----------------------------------
------------Serial Adder-----------
-----------------------------------
library ieee; use ieee.std_logic_1164.all; entity adder_sr2 is
    port( X0, Y0 , clk, clr1 :in  std_logic;
```

```
          Sout: out std_logic);
end adder_sr2; architecture arch_adder_sr2 of adder_sr2 is
component dff
    port( D, clk, clr: in std_logic;
          Q : out std_logic);
end component; component f_adder_pac
    port(A,B, C: in std_logic;
        S,Ca: out std_logic);
end component; signal d1, d2, C1: std_logic; for ADDING:
f_adder_pac use entity Work.f_adder_pac(arch_f_adder_pac); for AD:
dff use entity Work.dff(arch_dff); --\\
begin ADDING: f_adder_pac port map (A=>X0,B=>Y0,C=>d1,
S=>Sout,Ca=>d2) ; --\\
AD: dff port map (d2, clk ,clr1,d1); end arch_adder_sr2;
-------------------------------------
-------------Test Bench-------------
------------Serial Adder------------
-------------------------------------
library ieee; use ieee.std_logic_1164.all;
 entity adder_2 is
    port(--A, B, C :in  std_logic;
         Sout: out std_logic);
end adder_2; architecture arch_adder_2 of adder_2 is component
adder_sr2
    port(X0, Y0 , clk, clr1 :in  std_logic;
         Sout: out std_logic);
```

```
end component; component clock1
    port(c: out std_logic);
end component; component Stimulator port(   Out1, Out2, Out3: out
std_logic); end component; component reg4
    port( D, clk, clr1 : in std_logic;
        Q: out std_logic);
end component; component df
    port( D, clk, clr: in std_logic;
          Q: out std_logic);
end component; signal clk,clr1,A,B,s5,d1: std_logic; --\\
for ST: clock1 use entity Work.clock1(arch_clock1); --\\
for ST1: Stimulator use entity Work.Stimulator(ALGORITHM); --\\
for A1: adder_sr2 use entity Work.adder_sr2(arch_adder_sr2);--
begin ST: clock1 port map(c=>clk);--\\
ST1: Stimulator port map (clr1,B,A); --\\
A1: adder_sr2 port map (A,B,clk,clr1,Sout); end arch_adder_2;
-----------------------------------------
--16-bit serial in parallel out register---
-----------------------------------------
library ieee; use ieee.std_logic_1164.all; entity reg16pr_2 is
    port( Din , clk , clr1: in std_logic;
          Dout: out std_logic_vector(15 downto 0));
end reg16pr_2; architecture arch_reg16pr_2 of  reg16pr_2 is
component dff
    port( D, clk, clr: in std_logic;
          Q: out std_logic);
```

```
end component; for AD2: dff use entity Work.dff(arch_dff); signal
C: std_logic; signal D: std_logic_vector(15 downto 0); begin C <=
clk;
        AD2: dff port map (Din, C,  clr1, D(15));
    R: for i in 14 downto 0 generate
    B1: block
    for AD1: dff use entity Work.dff(arch_dff);
            begin
            AD1: dff port map (D(i+1), C ,  clr1, D(i));
                    end block;        end generate;
        Dout <= D;
    end arch_reg16pr_2;
```

## 4.7 Summary and discussions

This chapter has introduced the proposed high-pass, band-pass and band-elimination filter design and a digital filter transformation method. The 2D digital IIR filters design is described in this chapter and the previous chapter, where a continuous-time filter is transformed into the desired discrete-time filter by applying the GBT. This design ensures the desired 2D digital filter and the corresponding modified analog filter obtained by the double inverse bilinear transformations have the monotonic amplitude-frequency response in pass-band region. The proposed 2D digital IIR filter design is started from a 2D analog doubly terminated gyrator filter and this filter is modified into another analog filter and the modified filter is then transformed into a digital filter. Two steps are performed for the digital high-pass filter design. First, the GBT is applied to an analog filter in order to obtain the desired digital filter and second, the inverse bilinear transformation is applied to the digital filter in order to obtain the modified analog high-pass filter to test the monotonic characteristic. Overall, the GBT and inverse bilinear transformation have changed the original analog filter structure to the corresponding modified analog filter (section 2.3).

The proposed high-pass filter design is discussed in section 4.2 and it is shown that the 2D digital high-pass filters (Figure 4.2) are obtained for the negative values of g of an non-symmetric filter (Figure 2.2). It is observed that sharper characteristics of a 2D digital high-pass filter are obtained for the negative values of g of a symmetric filter (Figure 2.1). However, the 2D digital high-pass filters are also obtained for the positive values of g of the both filters (Figure 4.10). Six 2D digital high-pass responses are shown in Figure 4.2 in case-I, case-II and case-III of the both doubly terminated gyrator filters. Those frequency responses are studied and it is shown in this chapter that all responses satisfy the monotonic amplitude-frequency responses (Figure 4.4).

The proposed band-pass and band-elimination filter design are shown in Figure 4.5 and first few steps of the design are similar to the design of low-pass or high-pass filter. Basically, three steps are performed for a digital band-pass and band-elimination filter design. At first, the stable 2D analog filter is transformed to a 2D digital low-pass or high-pass filter by the GBT and the corresponding modified 2D analog low-pass or high-pass is obtained by the inverse double bilinear transformation. The 2D analog modified filter is transformed to the 2D digital band-pass or band-elimination filter by the summation of two GBTs. It has been shown in this chapter that generally, the 2D digital band-pass filters are obtained for the positive values of g (Figure 4.7) and 2D digital band-elimination filters are obtained for the negative values of g (Figure 4.8). Six 2D digital band-pass filter responses are shown in Figure 4.7 in case-I, case-II and case-III of the both doubly terminated gyrator filters. In Figure 4.8, six 2D digital band-elimination filter responses are shown in case-I, case-II and case-III of the both doubly terminated gyrator filters.

A digital filter transformation method is proposed in this thesis, where the value/sign of g of a doubly terminated gyrator network provides opposite frequency responses of the filter. This method gives band-pass to band-elimination filter or low-pass to high-pass filter or vice-versa transformation by regulating the value and/or sign of g. However, low-pass to band-pass or high-pass to band-elimination filter or vice versa transformation is obtained by the regulating g and parameters of the GBT. Two techniques are applied for the digital filter transformation of low-pass to high-pass or band-pass to band-elimination or vise versa, such as the value of g and the sign of g. The concept of digital frequency transformation in the reactive behavior of a gyrator filter changes not only the parameters of resistance, capacitance and inductance of

the filter, but also the value and sign of g. Figures 4.10 and 4.12 have shown that the values of g of the doubly terminated gyrator filter can inverse the amplitude-frequency responses of the filter and Figures 4.11 and 4.13 have shown the sign of g can inverse the amplitude-frequency response. Finally, two methods are proposed to reduce frequency distortion in the high frequencies of digital domain due to the double bilinear transformation and the methods can facilitate tight tolerances over a wide frequency range. In the entire thesis, two RLC filters are considered and those are used in the gyrator filter. The RLC filters are second order butterworth filter and Gargour&Ramachandran filter, but for various applications higher order RLC filter can be used. Finally, a realization of a 2D digital filter is shown.

# Chapter 5

# Applications of The Proposed Design in Image Processing

## 5.1 Introduction

A digital image is an array of 2D data and image is divided into N row and M column, the intersection of each row and column is termed a pixel. Basically, a digital image is a 2D array of pixels which can be expressed as brightness/intensity of an image. An image is digitalized to convert in a form that can be stored in a computer's memory and it is processed by the digital computer as required [55].

An image representation is concerned about the quality that each picture element (pixel) represents. An image could present luminance of the objects in a scene (ordinary camera), the absorption characteristics of the body tissues (X-Ray image), the radar cross section of the target (radar image), temperature profile of a region (infrared imaging), gravitational field in an area (geophysical imaging). Fundamental requirements of digital image processing are sampled and quantized. The sampling rate (number of pixel per unit area) has to be large enough to present the useful information of an image which can be determined by the bandwidth of the image [1].

The 2D digital filters are used in the various image processing applications, such as image enhancement, image restoration etc. [10]. Image enhancement is appealing area of image processing and it has useful feature extraction, image analysis and visual information display. It processes a digital image to obtain a more suitable image than the original image for a specific application. For example, medical science applications are concerned with processing of chest X-Ray, cine angiogram, projection

of frame axial tomography and other medical images that occur in radiology, nuclear magnetic resonance (NMR) and ultrasonic scanning. Those images are widely used to screen and monitoring of patient or for the detection of tumor or the diseases of the patients. In the gamma-ray imaging, radioactive isotope is injected to a patient that emits gamma rays as it decays and gamma ray detector is used to collect the emission and images are produced from the collected emission. Generally it is used to locate bone pathology, such as infections or tumors. X-ray imaging is widely used in the medical science and images are generated by the X-ray tube which is a vacuum tube with cathode and anode. In the angiogram, a cathode is inserted into artery or vein in the groin and cathode is guided to the area of studied by blood vessel and cathode is heated, so free electrons strick on nucleus, as a result energy released in the form of X-radiation and collected radiation produces images. Medical astronomy uses radio wave for magnetic resonance imaging (MRI). In the ultrasound imaging, millions pulses and echoes are sent and received each second for constructing an image. For the purpose, a sound probe moves through the body and sends information for imaging [56]. Sometime in the various applications, the image is degraded by the noise and the degraded image is restored by 2D digital filter. Generally, noise arises during data acquisition or transmission and environmental conditions, such as, lightning or atmospheric disturbance cause noise added in the data. It has been seen that most of the energy of the noise is often spread across the higher frequency range and energy of the topical image located at the low frequency range, so the 2D low-pass filter has good noise removal properties [10].

In this chapter, some image processing applications are shown by using different types of 2D digital filters. In chapter 3 and chapter 4, the digital filters are designed by the proposed filter design. The applications of the 2D digital low-pass filters are shown in the case of image restoration applications, the 2D digital high-pass filter applied for the application of the image enhancement and the 2D digital band-pass filters and band-elimination filters are used to determine certain frequency elements of fourier transformation of an image. It has been shown in the previous chapter that the band-width of the digital filter can be controlled by the magnitude of g and the parameters of the GBT. As a result, in the case of image processing applications, the proposed design allows to choose the desired band-width of a 2D digital filter.

## 5.2 Image Restoration

Image restoration is removal or minimization of the known degradations of an image in order to obtain the original image. The cause of the most common degradations in an image are imperfections of the sensors, transmission etc. Mathematical model of various degradation processes is known, such as Gaussian noise, Rayleigh, Erlang (Gamma) noise, exponential noise, uniform noise, impulse (slat and pepper), periodic noise etc. and those noises can be added in the image for the analysis of image restoration [56]. Most of the common degradation is gaussian noise and this noise arises from the electronic circuit, sensor noise due to poor illumination or high temperature. Another common noise is salt and pepper noise (impulse noise) and this noise is generated in the case of fault switching during imaging.

For illustration, the standard images are corrupted by the known noises and the degraded images are passed through the 2D digital low-pass filter for de-noising purposes. The quality of the reconstructed images are measured in term of mean squared error (MSE) (equation (5.2.3)) and peak signal-to-noise ratio (PSNR) (equation (5.2.4)) in decibels (dB) for the most common gray image [10]. In the chapter 3, the 2D digital low-pass filters are designed using the proposed design and all the digital low-pass filters are designed in the section 3.3 have the monotonic amplitude-frequency response in the bandpass regions. Because of having the monotonic characteristics in the aplitude-frequency response, the significant improvement (PSNR) in the reconstructed images are obtained by the 2D digital filter.

In the filter 1, the six 2D digital low-pass filters having monotonic amplitude-frequency response are designed in the section 3.3.2, 3.3.3, 3.3.4, 3.3.6, 3.3.7 and 3.3.8. Those filters are used in this section for the image restoration. For the simplicity, the filters are categorized as case I, case II and case III corresponding to the section 3.3.2, 3.3.3 and 3.3.4 respectively. Similarly in the filter 2, the 2D digital low-pass filters are also categorized as case I, case II and case III corresponding to the section 3.3.6, 3.3.7 and 3.3.8.

Two standard images are considered for the image restoration process such as Lena (256x256) (Figure 5.1(a)) and Mriknee (256x256) (Figure 5.3(a)). The most common two types of noise are considered to degrade the images, such as Gaussian and salt&pepper noise. At first, pixels of the image are normalized in between 0

to 1 and the noises are added to the image. The effects of restoration by the 2D digital low-pass filters are studied on the reconstructed images and the quality of the reconstructed images are compared with the original image in term of MSE and PSNR [57].

MSE of the degraded image

$$MSE_{ns} = \frac{\sum_{i_1=0}^{M-1}\sum_{i_2=0}^{N-1}\left(img_{ns}(i_1,i_2)*255 - img(i_1,i_2)*255\right)^2}{M*N} \tag{5.2.1}$$

PSNR of the degraded image

$$PSNR_{ns} = 10*log_{10}\frac{255^2}{MSE_{ns}} \tag{5.2.2}$$

MSE of the reconstructed image

$$MSE_{out} = \frac{\sum_{i_1=0}^{M-1}\sum_{i_2=0}^{N-1}\left(img_{out}(i_1,i_2)*255 - img(i_1,i_2)*255\right)^2}{M*N} \tag{5.2.3}$$

PSNR of reconstructed image

$$PSNR_{out} = 10*log_{10}\frac{255^2}{MSE_{out}} \tag{5.2.4}$$

where, $img$ is the original image, $img_{ns}$ is the noisy image and $img_{out}$ is the reconstructed image and all the images contain M by N pixels. Error metrics are measured on the intensities of two images and the error pixel ranges are between black (0) and white (1).

Gaussian noise with zero mean and variance = 0.01 is added to the normalized image of Lena and Mriknee. The degraded images are reconstructed by the digital 2D low-pass filters (sections 3.3.2, 3.3.3, 3.3.4, 3.3.6, 3.3.7 and 3.3.8). Tables 5.1 and 5.2 give the values of MSE and PSNR of the degraded images and the reconstructed images of Lena by the case I, case II and case III of the both gyrator filters. Tables 5.3 and 5.4 give the values of MSE and PSNR of the degraded images and the reconstructed images of Mriknee by the case I, case II and case III of the both gyrator filters.

In Figure 5.1, Gaussian noise (mean = 0, variance = 0.01) is added to the normalized image (Lena) and restoration of the image is done by the case I (filter1) and case I (filter2) (Figures 5.1 (c)-(f)). It is observed that the presence of noise reduces (Figures (c) and (d)) from the degraded image (Figure 5.1(b)). However, the presence

Table 5.1: The restoration of an image (Lena) by filter1 when Gaussian noise with mean = 0, variance = 0.01 is added into the image

| Case | g | $MSE_{ns}$ | $PSNR_{ns}(dB)$ | $MSE_{out}$ | $PSNR_{out}(dB)$ |
|---|---|---|---|---|---|
| Case I | 0.001 | 629.9926 | 20.1374 | 257.3906 | 24.0249 |
| Case II | 0.001 | 636.2678 | 20.0944 | 257.7424 | 24.0189 |
| Case III | 0.001 | 636.3893 | 20.0936 | 273.4251 | 23.7624 |

Table 5.2: The restoration of an image (Lena) by filter2 when Gaussian noise with mean = 0, variance = 0.01 is added into the image (Lena)

| Case | g | $MSE_{ns}$ | $PSNR_{ns}(dB)$ | $MSE_{out}$ | $PSNR_{out}(dB)$ |
|---|---|---|---|---|---|
| Case I | 0.001 | 630.9419 | 20.1309 | 256.4292 | 24.0411 |
| Case II | 0.001 | 634.0169 | 20.1098 | 244.2690 | 24.2521 |
| Case III | 0.001 | 639.1828 | 20.0746 | 253.6035 | 24.0893 |

of noise reduces more (Figures (e) and (f)) from the degraded image when the values of g of the both case I (filter1) and case I (filter2) filters change. Figure 5.1 (e) has less noise than Figure 5.1(c) and PSNR of the reconstructed image (Figure 5.1(e)) is improved to 24.3337 dB. Figure 5.1(f) has less noise than Figure 5.1(d) and PSNR of the reconstructed image Figure 5.1(f) is improved from to 24.2287 dB. The corresponding MSEs are reduced by the case I (filter1) and case I (filter2) are compared in Figure 5.2. It is seen that in the both cases less MSEs in the reconstructed images are obtained for the less magnitudes of g of the filters.

Table 5.1 shows the restoration of an image (Lena) by the 2D digital low-pass filters (filter1) and the noise reduces from the degraded image (MSE = 545.4575) to the reconstructed image (MSE = 184.2213) by the case I (filter1). PSNRs of the reconstructed images are 24.0249 dB, 24.0189 dB and 23.7624 dB by using case I(filter1), case II(filter1) and case III(filter1) respectively.

Table 5.2 shows the restoration of an image by filter2 and the noise of the degraded image (Figure 5.1(b)) reduces by the 2D digital low-pass filters (filter2). MSE of the degraded image is 629.9926 and it reduces to MSE = 257.3906 by using case I (filter2) and the corresponding PSNR of the reconstructed image improves from 20.1309 dB to 24.0411 dB. Similarly, the case II (filter2) and case III (filter2) are used for denoising purposes and the corresponding PSNRs of the reconstructed images improve to 24.2521 dB and 24.0893 dB respectively. Figure 5.2 shows the filter2 has better image restoration capability than filter1.


Figure 5.1: (a) The original image of Lena (b) the noisy image with Gaussian noise (variance =0.01) (c) the reconstructed image by case I (Filter 1) when g = 0.03 (PSNR = 20.9729 dB) (d) the reconstructed image by case I (Filter 2) when g = 0.1 (PSNR = 22.6459 dB), (e) the reconstructed image by case I (Filter 1) when g = 0.001 (PSNR = 24.3337 dB), (f) the reconstructed image by case I (Filter 2) when g =0.001 (PSNR = 24.2287 dB)

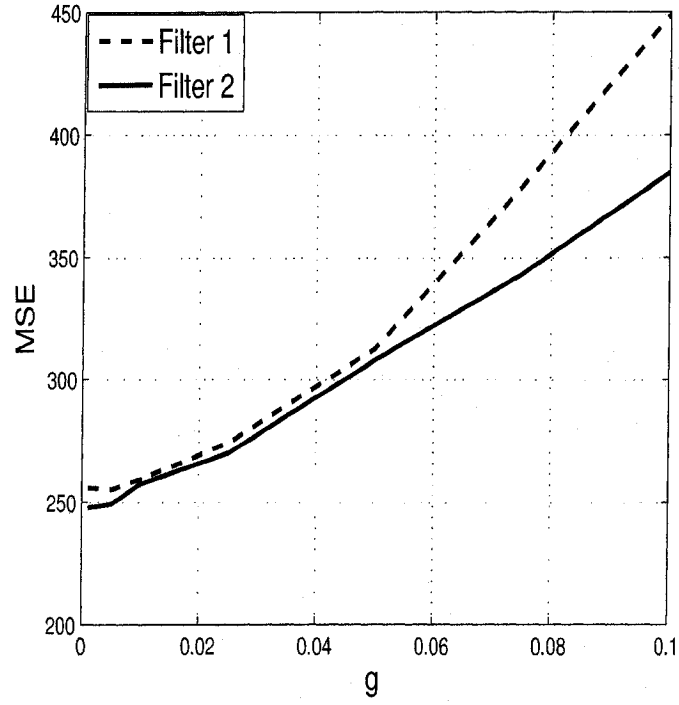


Figure 5.2: Plot of the MSE of the reconstructed Lena image vs g (when Gaussian noise with mean = 0, variance = 0.01 is added to the original image).

Another example is considered for the image restoration using the six 2D digital low-pass filters and in this case another type of image Mriknee (256x256)(Figure 5.3(a)) is used. Gaussian noise (mean = 0, variance = 0.01) is added to the normalized image (Mriknee) and restoration of the image is done by the case I (filter1) and case I (filter2) (Figures 5.3 (c)-(f)).

The noise of the degraded image is reduced by the case I (filter1) and case I (filter2). The reconstructed images are shown in Figures 5.3 (c) and (d). However, Figure 5.3 (e) has less noise than Figure 5.3 (c) and the PSNR of the reconstructed image (Figure 5.3 (e)) improves to 27.4203 dB. The value of g of filter1 is changed to a suitable value, so that a significant amount of noise in the degraded image is attenuated by the resultant 2D digital low-pass filter. For the same reason in the case of filter2, Figure 5.3(f) has less noise than Figure 5.3(d) and the PSNR of the reconstructed image (Figure 5.3(f)) improves to 27.2907 dB.

Table 5.3 gives the values of MSE and PSNR of the degraded and the reconstructed images (Mriknee). The 2D digital low-pass filters (filter1) are used for the restoration

Table 5.3: The restoration of image (Mriknee) by filter1 when Gaussian noise with mean = 0, variance = 0.01 is added to the original image

| Case | g | $MSE_{ns}$ | $PSNR_{ns}(dB)$ | $MSE_{out}$ | $PSNR_{out}(dB)$ |
|---|---|---|---|---|---|
| Case I | 0.001 | 545.4575 | 20.7632 | 184.2213 | 25.4774 |
| Case II | 0.001 | 547.6805 | 20.7455 | 202.1106 | 25.0749 |
| Case III | 0.001 | 547.2279 | 20.7491 | 222.0545 | 24.6662 |

Table 5.4: The restoration of image (Mriknee) by filter2 when Gaussian noise with mean = 0, variance = 0.01 is added to the original image

| Case | g | $MSE_{ns}$ | $PSNR_{ns}(dB)$ | $MSE_{out}$ | $PSNR_{out}(dB)$ |
|---|---|---|---|---|---|
| Case I | 0.001 | 555.7851 | 20.6817 | 191.6142 | 25.3065 |
| Case II | 0.001 | 548.8489 | 20.7363 | 189.5080 | 25.3545 |
| Case III | 0.001 | 547.7421 | 20.7450 | 205.0716 | 25.0117 |

of the image. It shows that the noise of the image reduces by the case I (filter1) from the degraded image (MSE = 545.4575) to the reconstructed image (MSE = 184.2213). PSNRs of the reconstructed images are 25.4774 dB, 25.0749 dB and 24.6662 dB by using case I(filter1), case II(filter1) and case III(filter1) respectively.

Table 5.4 gives the values of MSE and PSNR of the degraded and the reconstructed images (Mriknee). The restoration of the images are done by the 2D digital low-pass filters (filter2). It shows that noise is reduced by the case I (filter2) from the degraded image (MSE = 555.7851) to the reconstructed image (MSE = 191.6142). The corresponding PSNRs of the reconstructed images are 25.3065 dB, 25.3545 dB and 25.0117 dB by using case I(filter2), case II(filter2) and case III(filter2) respectively. Figure 5.4 shows that the both gyrator filters ( when $0.0001 \leq g < 0.02$) are equally good for the image restoration, but filter2 has better performance when g starts to increase.

From the above discussion, it is observed that filter2 can remove more noise from a degraded image with Gaussian noise (mean = 0 and variance = 0.01) than filter1. In the both examples (image Lena and Mriknee), average PSNR of the reconstructed images by filter2 is higher than filter1. However, in some cases, filter1 provides better performance than filter2. To show more comparisons, another example is considered with the different type of noise (impulse noise) and the noise is added to the same image (Lena) and reconstruction of the image is done by the both filter1 and filter2.

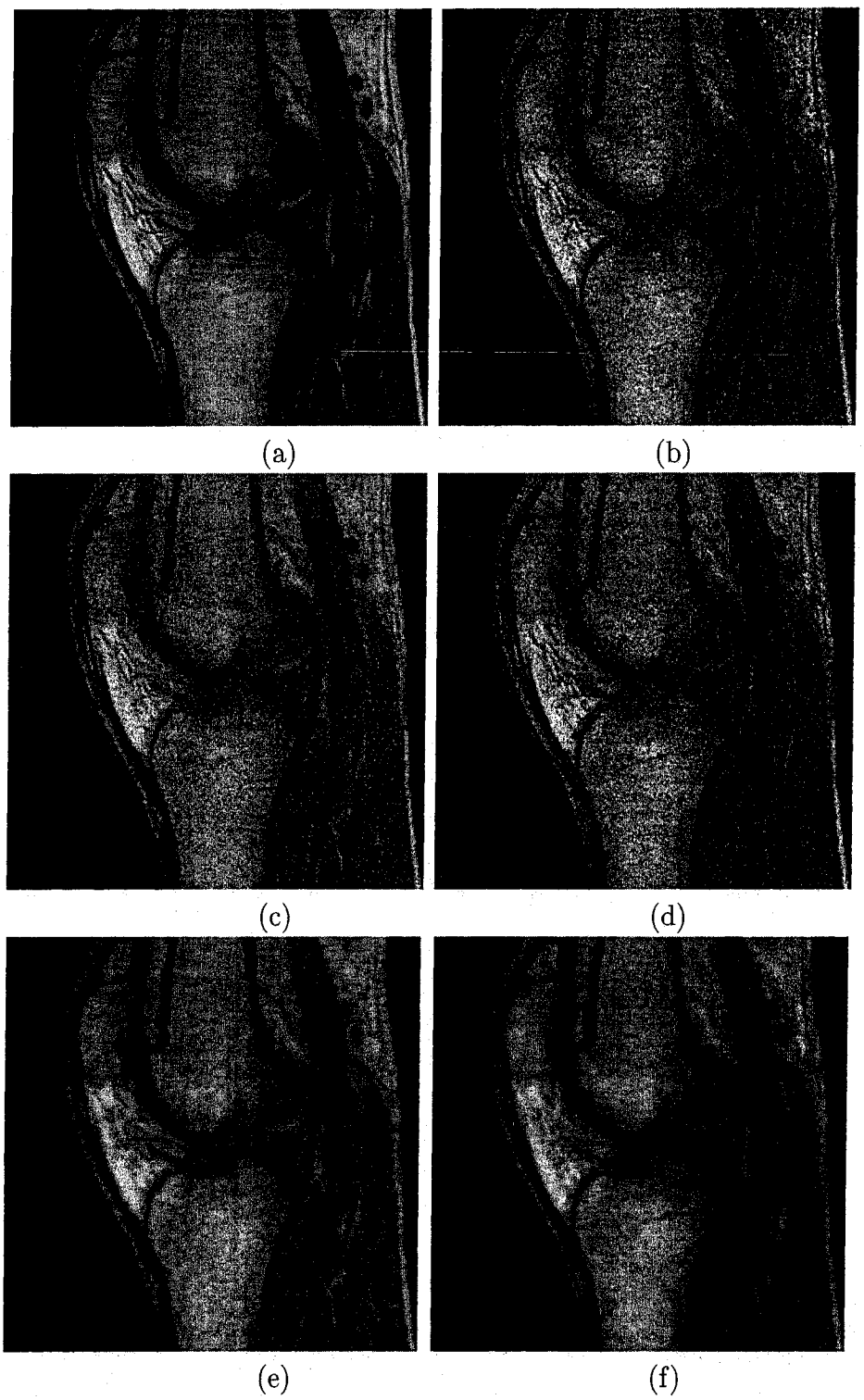


Figure 5.3: (a) The original image of Mriknee (b) the noisy image with Gaussian noise (variance =0.01) (c) the reconstructed image by case I (Filter 1) when g = 0.03 (PSNR = 21.8147 dB), (d) the reconstructed image by case I (Filter 2),when g = 0.3, (PSNR = 21.0756 dB)(e) the reconstructed image by case I (Filter 1), when g = 0.001, (PSNR = 26.9425 dB), (f) the reconstructed image by case I (Filter 2), (PSNR = 27.2907 dB)

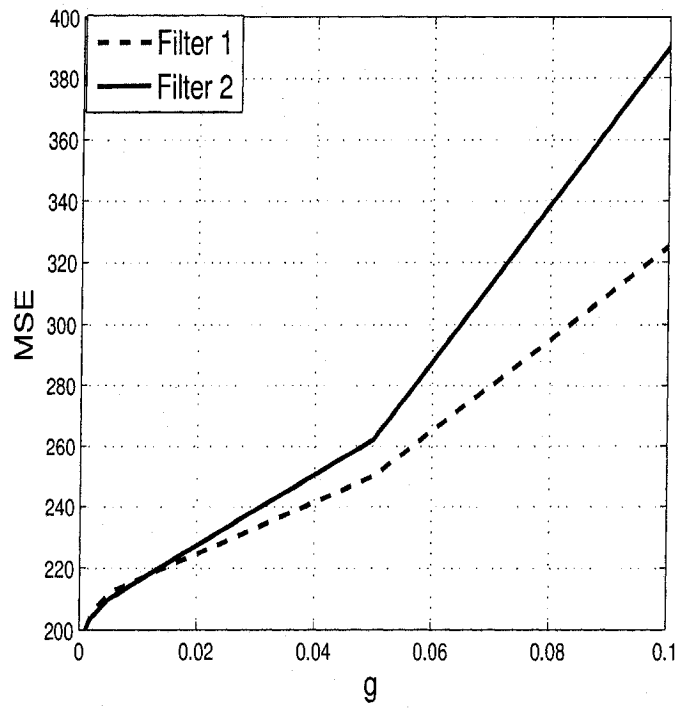


Figure 5.4: Plot of the MSE of the reconstructed images (Mriknee) vs g by the case I (filter1) and the case I (filter2) (when Gaussian noise with mean = 0, variance = 0.01 is added to the original image).

In Figure 5.5, the impulse noise with variance = 0.01 is added to the normalized image (Lena) and the restoration of the degraded image is done by the case I (filter1) and case I (filter2) (Figures 5.5 (c)-(f)). Figure 5.5 shows that the presence of noise in Figures 5.5(c) and (d) reduces from the degraded image (Figure 5.5(b)). However, more noises are reduced in Figures 5.5(e) and (f), when the values of g of the both filters change. But, blurry effect of Figure 5.5(e) is more than Figure 5.5(c). Figure 5.5 (e) has less noise than Figure 5.5(c), but Figure 5.5(e) has more blurry effect and PSNR of reconstructed image (Figure 5.5(e)) reduces to 25.8654 dB. Figure 5.1(f) has less noise than Figure 5.1(d), but Figure 5.1 (f) has more blurry effect. As a result, the PSNR of the reconstructed image (Figure 5.1(f)) reduces to 25 dB.

Table 5.5 show the restoration of the degraded image (Lena) by the 2D digital low-pass filters (filter1) and the noise reduces from the degraded image (MSE = 190.5210) to the reconstructed image (MSE = 128.5301). The corresponding PSNRs of the reconstructed images are 27.0408 dB, 27.2000 dB and 27.1226 dB by using case


Figure 5.5: (a) The original image of Lena (b) the noisy image with salt&pepper noise (variance =0.01) (c) the reconstructed image by case I (Filter 1) when g = 0.05 (PSNR = 27.040 dB), (d) the reconstructed image by case I (Filter 2) when g=0.05 (PSNR = 27.4203 dB) (e) the reconstructed image by case I (Filter 1) when g = 0.001 (PSNR = 25.8654 dB),(f) the reconstructed image by case I (Filter 2) when g = 0.001, (PSNR = 25.000 dB)

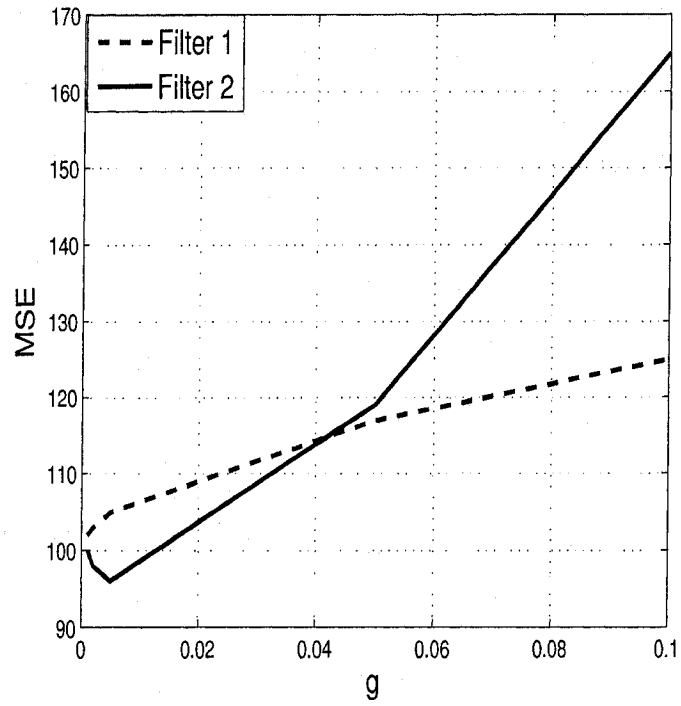


Figure 5.6: Plot of the MSE of the reconstructed images (Lena) vs g by the case I (filter1) and the case I (filter2)(when salt&pepper noise (variance =0.01) is added to the original image).

I (filter1), case II (filter1) and case III (filter1) respectively.

Table 5.6 shows the restoration of the degraded image (Lena) by the filter2 and the noise reduces from the degraded image (MSE = 173.8383) to the reconstructed images. The MSEs of the reconstructed images are 117.7736, 123.3094 and 126.6066 by using case I (filter1), case II (filter1) and case III (filter1) respectively. The PSNRs of the reconstructed images are 27.4203 dB, 27.2208 dB and 27.1062 dB by using case I (filter1), case II (filter1) and case III (filter1) respectively. From the above discussion, it is observed that filter2 can remove more noise from a degraded image with impulse

Table 5.5: The restoration of the image (Lena) by filter1 when impulse noise with variance = 0.01 is added in the image

| Case | g | $MSE_{ns}$ | $PSNR_{ns}(dB)$ | $MSE_{out}$ | $PSNR_{out}(dB)$ |
|---|---|---|---|---|---|
| Case I | 0.05 | 190.5210 | 25.3314 | 128.5301 | 27.0408 |
| Case II | 0.05 | 176.9348 | 25.6527 | 123.9032 | 27.2000 |
| Case III | 0.05 | 178.8236 | 25.6066 | 126.1320 | 27.1226 |

Table 5.6: The restoration of the image (Lena) by filter2 when impulse noise with variance = 0.01 is added in the image

| Case | g | $MSE_{ns}$ | $PSNR_{ns}(dB)$ | $MSE_{out}$ | $PSNR_{out}(dB)$ |
|---|---|---|---|---|---|
| Case I | 0.05 | 173.8383 | 25.7293 | 117.7736 | 27.4203 |
| Case II | 0.05 | 189.4831 | 25.3551 | 123.3094 | 27.2208 |
| Case III | 0.05 | 195.1364 | 25.2274 | 126.6066 | 27.1062 |

noise (variance = 0.01) than filter1. Figure 5.6 shows that the both gyrator filters (when $0.0001 \leq g < 0.02$) are equally good for the image restoration, but filter2 has better performance when g is starts to increase.

Average PSNR of the reconstructed images are obtained by filter2 is higher than filter1, but, some cases, filter1 provides better performance than filter2. Overall, it is seen that the significant amount of noise is reduced from a degraded image by the both filters. So the proposed design is quite useful in the case of image processing applications, such as the restoration of images. Another application of the proposed design in the image processing is shown in below.

## 5.3 Image Enhancement

Image enhancement interprets the image for better visualization. The 2D high-pass filter manipulates the digital pixel values of an image and can modify the visual interpretation according to the specific application. In the previous section, blurry effect in the image is found, because of high frequency components of fourier transformation of the image is attenuated and the high frequency components are edges and abrupt changes in the gray label. In this section, the 2D digital high-pass filters enhance the high frequency components of fourier transformation of a image and attenuate the low frequency components, as a result, better visualization of the image is obtained.

For the image enhancement purpose, Cerebral image (512x512) (Figure 5.7) is considered and the 2D digital high-pass filters are used for the enhancement of Cerebral image. Those high-pass filters are designed in the previous chapter using the proposed method. Figure 5.7 has shown a normal Cerebral MRA of a patient, where, visualization of the cerebral vessels is poor. Figures 5.8(a), (b), (c), (d), (e) and (f) show the enhanced images of Cerebral by using the case I (filter1), case II (filter1),

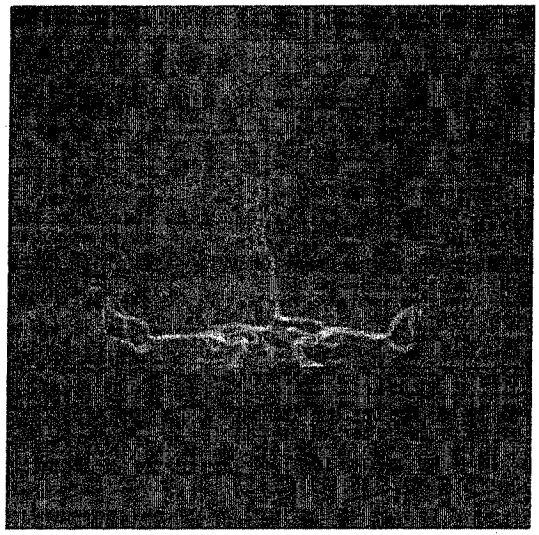

Figure 5.7: Original Cerebral image (512x512)

case III (filter1), case I (filter2), case II (filter2) and case III (filter2) respectively and the significant amount of enhancements are obtained in these cases. The bandwidths of the each 2D digital high-pass filters can be changed by varying the magnitudes of g of the both filters. As a result, the proposed design could be suitable for the enhancement of any kinds of images.

## 5.4 Different Frequency Bands Filtering

The band-pass and band-elimination filters can attenuate the selected frequency regions in between low and high frequencies of the fourier transformation of an image. Section 4.3 has described the designs of six band-pass filters and six band-elimination filters. This section shows the applications of the band-pass filters and band-elimination filters. It has been shown in the previous chapter that the bandwidth of a band-pass and band-elimination filter can be controlled by the magnitudes of g of the filter and the parameters of the GBT. As a result, in the case of image processing applications, the proposed design allows to choose the desired bandwidth of a 2D digital band-pass and band-elimination filter.

For illustration, Baboon image (256x256) is considered (Figure 5.9) and pixels of the image is normalized is between 0 and 1. The normalized image passes through

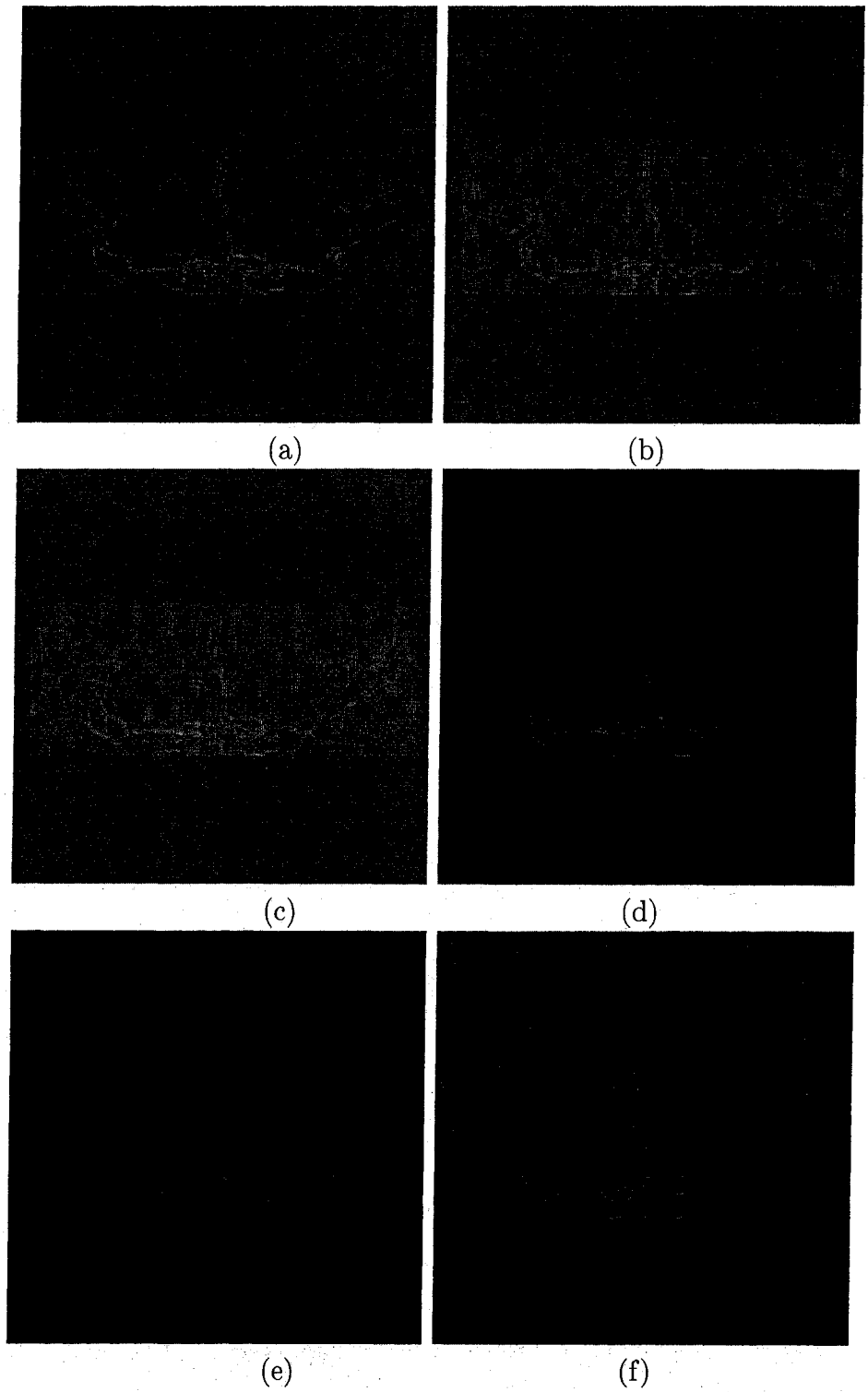


Figure 5.8: (a)The enhanced Cerebral image by case I (Filter 1) (b) the enhanced Cerebral image by case II (Filter 1), (c) the enhanced Cerebral image by case III (Filter 1), (d) the enhanced Cerebral image by case I (Filter 2), (e) the enhanced Cerebral image by case II (Filter2), (f) the enhanced Cerebral image by case III (Filter2)

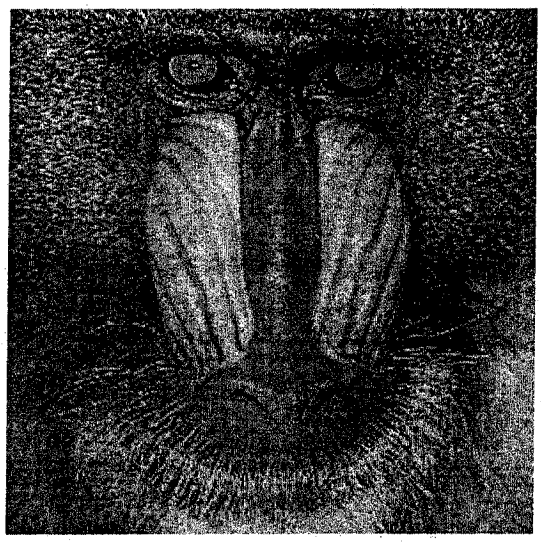

Figure 5.9: The original Baboon image (256x256)

the 2D digital band-pass filters to determine different frequency bands of the fourier transformation of the image. Figure 5.10 shows the output images of the 2D digital band-pass filters in the case of both filter1 and filter2. Figures 5.10(a), (b), (c), (d), (e) and (f) show the output images of Baboon by using the case I (filter1), case II (filter1), case III (filter1), case I (filter2), case II (filter2) and case III (filter2) respectively.

The application of band-elimination filters is shown by degrading an image with sinusoidal noise [58] and the reconstruction of the image is done by the band-elimination filters (section 4.3). For this application an image Pepper (256x256) is considered and pixels of the image are normalized in between 0 and 1. Maximum value of pixels of the image is 227 and each of the pixels are divided by 227 in order to normalize the pixels in between 0 and 1. A sinusoidal noise (equation (5.4.1)) is added to the normalized image and the reconstruction of the degraded image is done by the 2D digital band-elimination filters. The quality of the reconstructed images is calculated in term of MSE(equations (5.2.1), (5.2.3)) and PSNR (equations (5.2.2), (5.2.4)).

$$img_{ns}(i_1, i_2) = \frac{50}{227} sin(0.5 * pi * i_1 + 0.5 * pi * i_2) + img(i_1, i_2); \qquad (5.4.1)$$

where, $(0,0) \leq (i_1, i_2) \leq (255, 255)$, $img$ is original image (Figure 5.11(a)) and $img_ns$ is degraded image (Figure 5.11(b)).

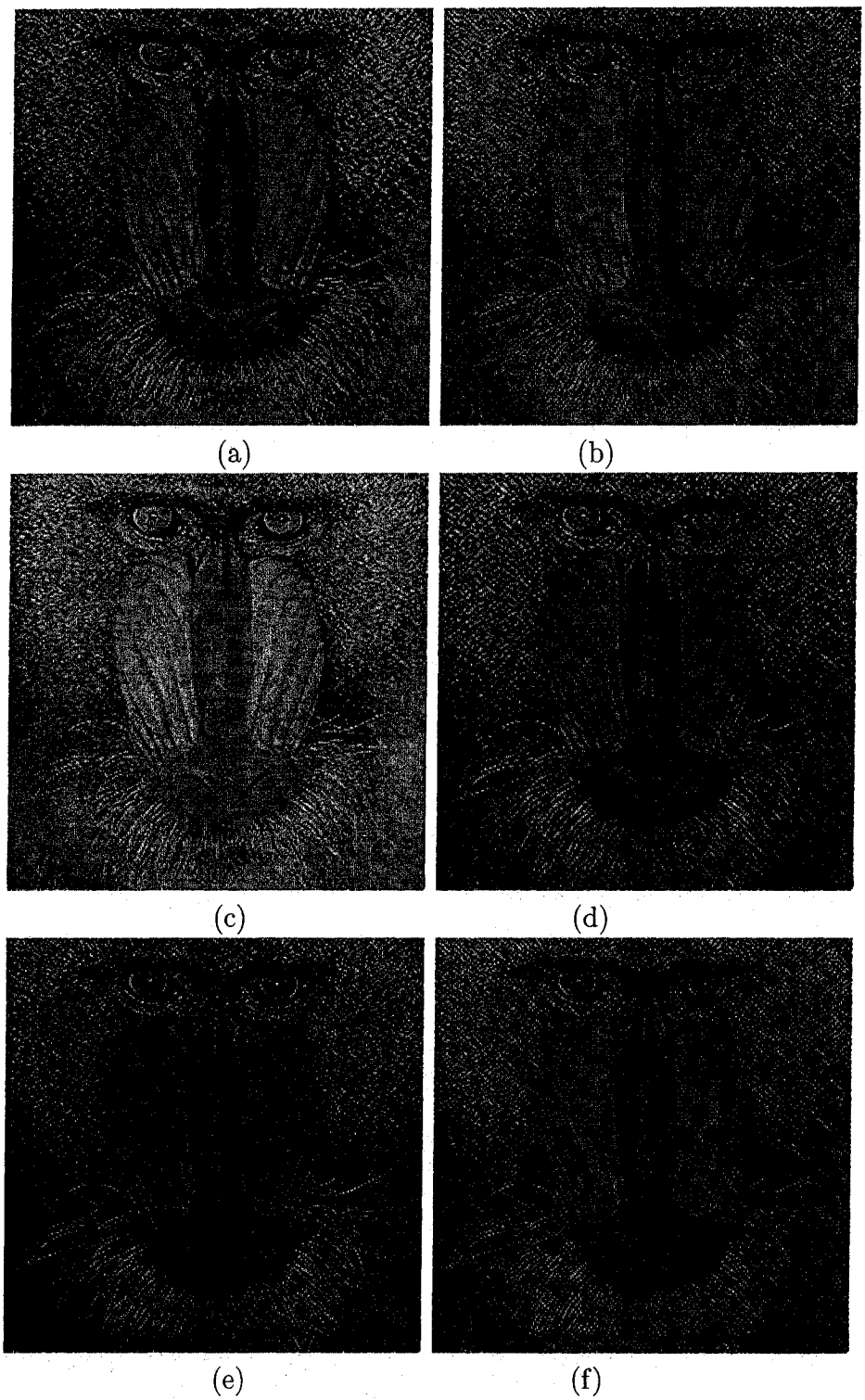


Figure 5.10: The output images of the designed 2D digital Band-pass filters (a) the output image of case I (Filter 1), (b) the output image of case II (Filter 1), (c) the output image of case III (Filter 1), (d) the output image of case I (Filter 2), (e) the output image of case II (Filter 2), (f) the output image of case III (Filter 2)

(a) (b)

Figure 5.11: (a) Original image of Pepper, (b) Degraded image of Pepper.

Table 5.7: The restoration of image (Pepper) by filter1 when sinusoidal noise is added to the image

| Case | $MSE_{ns}$ | $PSNR_{ns}(dB)$ | $MSE_{out}$ | $PSNR_{out}(dB)$ |
|---|---|---|---|---|
| Case I | 1577.3885 | 16.1514 | 639.4489 | 20.0727 |
| Case II | 1577.3885 | 16.1514 | 858.8890 | 18.7914 |
| Case III | 1577.3885 | 16.1514 | 659.7376 | 19.9371 |

The effect of the 2D digital band-elimination filters on the image is shown in Figure 5.12. Figures 5.12(a), (b), (c), (d), (e) and (f) show the output images of Pepper by using the case I (filter1), case II (filter1), case III (filter1), case I (filter2), case II (filter2) and case III (filter2) respectively. Tables 5.7 and 5.8 give the values of MSE and PSNR of the degraded images and the reconstructed images. The reconstruction of images have been done by the different 2D digital band-elimination filters (filter1 and filter2). It is observed that filter2 has better PSNRs of the reconstructed images

Table 5.8: The restoration of image (Pepper) by filter2 when sinusoidal noise is added to the image

| Case | $MSE_{ns}$ | $PSNR_{ns}(dB)$ | $MSE_{out}$ | $PSNR_{out}(dB)$ |
|---|---|---|---|---|
| Case I | 1577.3885 | 16.1514 | 457.4738 | 21.5271 |
| Case II | 1577.3885 | 16.1514 | 470.4074 | 21.4061 |
| Case III | 1577.3885 | 16.1514 | 300.6090 | 23.3508 |

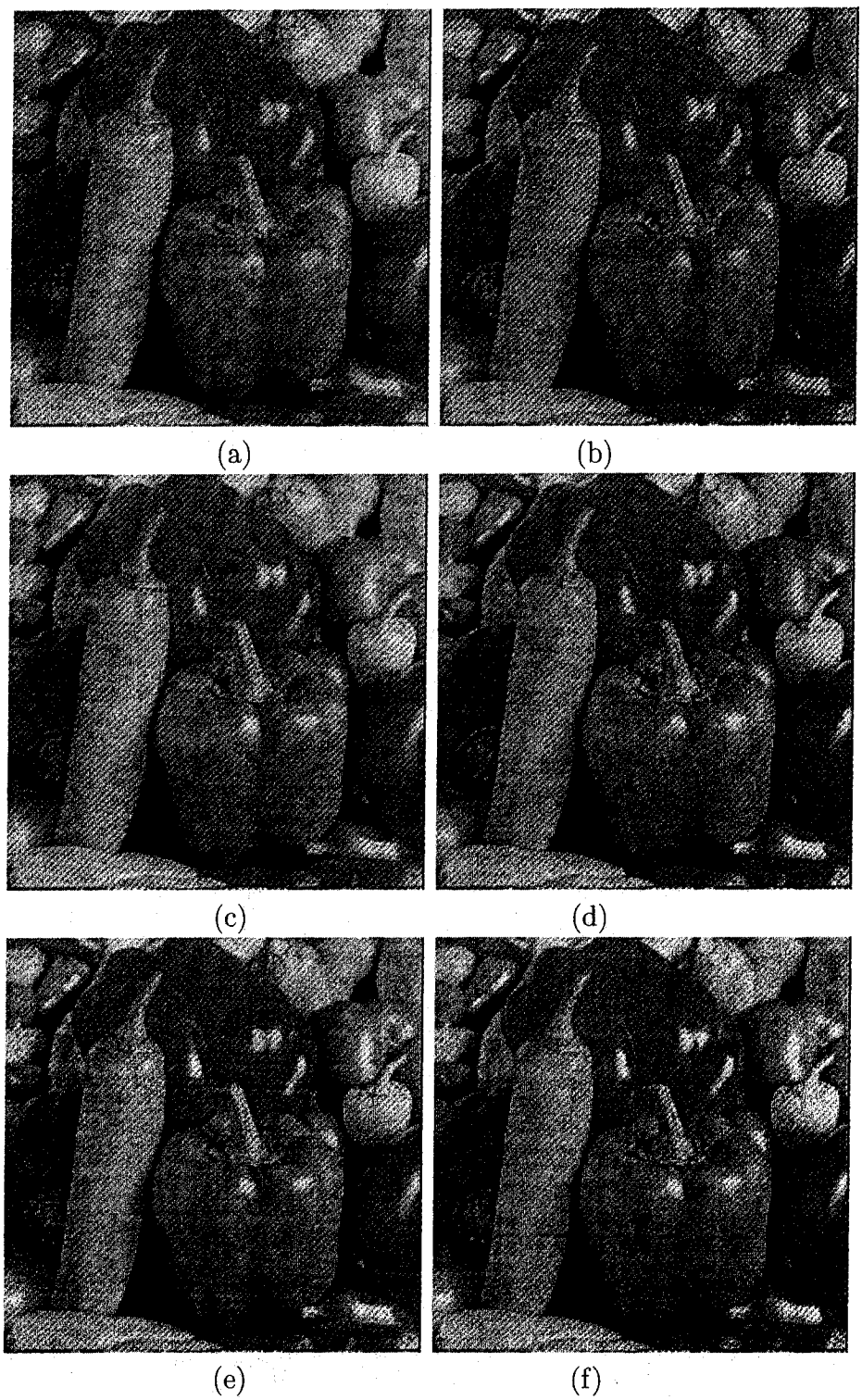


Figure 5.12: The output images of the designed 2D digital Band-elimination filters (a) the output image of case I (Filter 1), (b) the output image of case II (Filter 1), (c) the output image of case III (Filter 1), (d) the output image of case I (Filter 2), (e) the output image of case II (Filter 2), (f) the output image of case III (Filter 2)

than filter1.

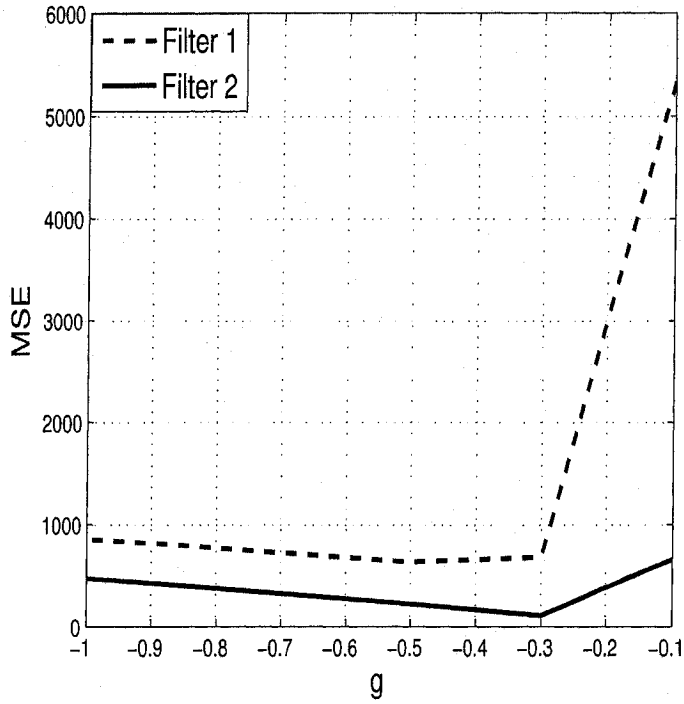


Figure 5.13: Plot of the MSE of the reconstructed Pepper images vs $g$ by the Band-elimination filters (when sinusoidal noise is added to the original image).

Overall, it is observed that a certain bands of frequencies elements of the fourier transformation of the image is attenuated by the band-pass and band-elimination filter. The advantages of the proposed design provide the facility to obtain the desired 2D digital filter as required in the applications. Moreover, the magnitudes of g of the filter provides more flexibility in the filter design purpose and the magnitude of g can be chosen as required for the applications.

## 5.5 Summary and Discussion

An image is digitized to be stored in a computer's memory and it can be operated upon by various image processing operations [55]. Most of the energy of the image is located at the low frequencies, however, the sharp edge information of the image is located at the high frequencies. Various kind of noise can be generated in the

image and the energy of the common noises are located at the higher frequency range, but energy of the white noise will be spread across the frequency axis. The 2D digital low-pass filter is commonly used to reduce the noise from a degraded image. Section 5.2 has described the noise reduction processes, where the 2D digital low-pass filters attenuate high frequency components of the fourier transformation of the degraded images. As a result, the corresponding PSNR of the reconstructed image has improved, but the blurry effect in the reconstructed image has arisen. The image restoration process has been done by degrading an image with the known noise and the reconstruction of the images by applying the 2D digital low-pass filters. The MSE and PSNR of the degraded images and the reconstructed images are studied and different comparisons are shown. Section 5.3 has described the image enhancement application by 2D digital high-pass filters. The digital high-pass filters have attenuated low-frequency components of the fourier transformation of the image and allowed the high-frequency components (sharp edges) and better visualization of the image is obtained. Finally, the effects of the 2D digital band-pass and band-elimination filters on the images are illustrated in Figures 5.10 and 5.12. Basically, the band-pass and band-elimination filters have attenuated certain range of frequency components of the fourier transformation of the image. The filters are used in this chapter to attenuate the different bands in different applications and those filters are designed by the proposed filter design. The design provides flexibility to design any types of filter as required for the applications.

# Chapter 6

# Conclusions

Because of recent growth in the 2D signal processing activities, a significant amount of research work has been done on the 2D filter design and it is seen that monotonic characteristics in frequency response of a filter is getting more popular. This is because the filters with the monotonic characteristics are one of the best filters for the digital image, audio and video (enhancement and restoration) [10].

This thesis proposes the designs of 2D digital filter having monotonic amplitude-frequency responses using Darlington-type gyrator networks. To the best of our knowledge, the design of 2D monotonic amplitude-frequency responses using Darlington-type gyrator networks have not been done till now. According to the proposed design, the 2D digital filters are designed by Darlington-type networks containing gyrators and the impedances of the gyrator network are replaced by doubly terminated RLC networks. As a result, the overall 2D analog transfer function is stable in analog domain, if the denominator of the transfer function is satisfied to be VSHP (section 2.4). The coefficients of the 2D analog filter are functions of g of the gyrator filter and the ranges of g are defined for attaining the stable monotonic characteristics in amplitude-frequency responses, because g has control over the frequency responses of the filter. The GBT is applied to the stable 2D analog transfer function in order to obtain the digital transfer function and the corresponding modified analog filter structure is obtained by the inverse bilinear transformation. All the parameters of the GBT are varied to obtain the desired filter responses which satisfy the stability conditions and also ensure the monotonic amplitude-frequency response in the passband region. As a result, more flexibility is achieved for the low-pass, high-pass, band-pass and band-elimination filter design purposes. The locations of poles and zeros of the

gyrator filter depend on the value and/or sign of g and it is seen that the reactive behavior of the gyrator filter is changed not only for the values of resistance, capacitance and inductance of the filter, but also for the value and sign of g. The digital filter transformation method is proposed considering the value and sign of g of the gyrator filter. The constraints of the proposed digital filter transformation method is imposed on the gyrator filters.

For illustration, the symmetrical doubly terminated gyrator network and the nonsymmetric doubly terminated gyrator network are taken from Darlington synthesis. The doubly terminated second-order Butterworth and Gargour&Ramachandran filters are taken as the doubly terminated RLC networks. The impedances of the gyrator network are replaced by the impedances of doubly terminated RLC networks and it is found that the denominator of the overall 2D analog transfer function is satisfied to be VSHP. Higher order of the transfer function is generated by cascading the two RLC networks or using stable higher order doubly terminated RLC networks. The GBT ($k_i > 0, -1 \leq a_i < 0, 0 < b_i \leq 1$ and $|a_i b_i| < 0$) is applied to the transfer function in order to obtain the digital transfer function and the coefficients are functions of g of the gyrator filter. It has been shown in the case of symmetric and nonsymmetric gyrator networks that the stable 2D digital low-pass filters are obtained due to lower values of g. When the value of g is started to increase, the 2D digital low-pass filters are changed into the 2D digital high-pass filters. In the symmetrical doubly terminated gyrator network, the effect of negative values of g on the denominator of the transfer function are same as positive values of g, but more sharp slopes in the frequency responses are obtained due to the effect of the negative value of g on the numerator. The negative values of g of the nonsymmetric doubly terminated gyrator network have inverted the frequency responses of the filter as of the positive values of g. The proposed design of digital band-pass and band-elimination filter can be continued from the 2D digital low-pass/high-pass filter which can be transformed to a 2D analog low-pass/high-pass filter by the inverse bilinear transformations. The 2D analog filter is transformed to the 2D digital band-pass or band-elimination filter by the summation of two GBTs and the bandwidths and center frequencies of the 2D digital band-pass and band-elimination filter are controlled by the parameters of the GBTs. Finally, in the proposed digital filter transformation, it is found that the 2D digital low-pass to high-pass filter or 2D digital band-pass to band-elimination

filter or vice-versa transformation is obtained by regulating the value and/or sign of g. However, the low-pass to the band-pass or the high-pass to the band-elimination filter or vice versa transformation is obtained by regulating the value and/or sign of g and the parameters of the GBTs.

In Chapter 2, the doubly-terminated gyrator networks are introduced and the transfer function of each filter is derived. For the frequency transformation of the filter, the GBT [15] is introduced and the relation between the analog domain to the digital domain as well as the digital domain to the modified analog domain [16] are obtained. For example, a simple filter structure is considered and the modifications of the filter are shown. The generation of VSHPs have been done using VSHP generation method I (section 1.7) and this method is applied to the doubly-terminated gyrator networks. For the generation of VSHPs, the impedances of doubly terminated second-order RLC filters are replaced with the impedances of the doubly terminated gyrator networks and properties of the overall filters are outlined.

In the chapter 3, two filter designs are proposed for the 2D digital low-pass filter design and the several examples are illustrated by the numerical examples. In the section 3.2, 1D and 2D low-pass filter designs have shown and each of the responses of the filters ensure the stability criteria. Another design is proposed for the low-pass filter design which has much control on the transformation of a filter from analog to digital domain and this design can overcome the drawbacks of the previous design. The proposed design can modify the filter structure to the desired filter structure. The GBT and the magnitudes of g of the filter are used together to obtain the desired digital filter response. The proposed method ensures the monotonic amplitude-frequency response [17] of the desired filter. In the section 3.3, the proposed method is applied to a transfer function and the transfer function is generated by replacing impedances of the doubly terminated networks with second-order RLC filters.

In Chapter 4, a method is proposed to design a 2D digital high-pass filter having monotonic amplitude-frequency response in the pass-band. In the section 4.2, the method is applied to the doubly terminated networks and impedances of the gyrator network are replaced with the different combinations of second-order RLC filters and the corresponding 2D digital high-pass filter responses are shown. Another important method is proposed for the frequency transformation and the method ensures the

monotonic amplitude-frequency response and stability of the desired filter. In the section 4.4, the proposed method is applied to the doubly terminated networks as before and the low-pass to high-pass filter transformations as well as the band-pass to band-elimination filter transformations are shown.

In Chapter 5, some applications of the image processing are shown using the various digital filters and those digital filters are obtained by the proposed design. The 2D digital low-pass filters are used for the image restoration purposes. The 2D digital high-pass filters are used for the image enhancement purposes. The 2D band-pass filters are used to attenuate some frequency bands of fourier transformation of an image. The 2D digital band-elimination filters are used for the image restoration purposes. Overall, it is shown that the proposed design is quite useful in the case of image processing applications, such as restoration and enhancement of images.

The overall goal of the thesis is the design of 2D digital filter having monotonic amplitude-frequency responses using Darlington-type gyrator network. The proposed filter design and the proposed filter transformation constitute powerful techniques for the 2D digital filter design. It is useful for the design of a digital filter with the specified frequency response and it can facilitate tight tolerances over a wide frequency range or when the frequency response of an existing system is known.

## 6.1 Scope for Future Work

This thesis has shown the 2D digital filter design and the filter transformation method of a Darlington-type doubly terminated gyrator network. However, this thesis can be extended by considering n-port gyrator networks and it has been shown long time ago (1983) that a 2-variable VSHP is generated without associating the various partial derivatives and conditions are derived regarding the gyrator matrix ensuring that the resulting polynomial is VSHP in nature [29]. Those polynomials can be used for the 2D digital filter.

An important area noted for future work involves choosing other types of filter structures from Darlington-synthesis and apply the proposed design and the filter transformations. As a result, flexibilities of the design will be increased depending on the structures.

The proposed design has demonstrated that impedances of the gyrator filter are replaced by the doubly terminated second-order RLC networks. But it is possible to increase the order of the RLC filter and in such case accuracy of the filter design will be increased. The numbers of resistance, inductance and capacitance values of the filter give more flexibility in the filter design. Again impedances of a gyrator filter can be replaced by the another gyrator filters and impedances of the second gyrator filter are replaced by the doubly terminated second-order RLC networks. As a result, two or more gyrator constants will have to be used in the design of a 2D digital filter.

Further knowledge of the GBT properties would be valuable in the digital filter design. A comparative investigation of impulse invariance method would be effective in the analog to digital filter transformation and the modifications of impulse invariance method can be used instead of using the double bilinear transformation or the GBT.

An extension of this work is to develop a filter design which can approximate an arbitrary phase response.

Further investigation of the 2D digital frequency response will be necessary in order to obtain monotonic characteristics in the passband regions of the filter.

Finally, the implementation of the 2D digital filter would be valuable in the digital signal processing applications. Systolic implementation of the 2D digital filter can be effective in the application, its operation can be realized to the rhythmical systolic operation of the heart and arteries by which blood is pumped forward from one artery to the next. This realization is not always suitable in the signal processing applications. However, a useful technique could be pipelining of the system. The total computation will be divided into small part and it can be assigned to a series of different concurrent processing elements such a way that processing speed is improved.

# Bibliography


[1] A. K. Jain, *Fundamentals of digital image processing.* Englewood Clifffs, NJ: Prentice-Hall, 1989.

[2] M. P. Inc., *http://www.microphotonics.com/skymto.html*, Irvine, CA 92618., 2006.

[3] J. Leng, J. Brooke, T. Hewitt, and H. Davies, "Visualization of seismic data in geophysics and astrophysics," *SGI Users' Conference, Krakow, Poland*, 11-14th October, 2000.

[4] W. Sandham and M. Leggett, *Geophysical Applications of Artificial Neural Networks and Fuzzy Logic.* Texas, USA: Springer, 2004.

[5] D. E. Clark, I. Tena-Ruiz, Y. Petillot, and J. Bell, "Multiple-target tracking and data association in sonar images," *Target Tracking: Algorithms and Applications, 2006. The IEE Seminar on (Ref. No. 2006/11359)*, pp. 147– 154, 2006.

[6] B. F. Burke and F. Graham-Smith, *An introduction to radio astronomy.* UK: Cambridge University Press; 2 edition, April 4 2002.

[7] C. Hentschel, "Generic method for 2d image resizing with non-separable filter," *International Conference on Image Processing, IEEE*, pp. 1653– 1656, 2004.

[8] T. S. Huang, *Two-Dimensional Digital Signal Processing, Vol.2.* Applied Optics IP, vol. 20, Issue 16, p.2867, 1981.

[9] V.Ramachandran and C.S.Gargour, *Generation of Very Strict Hurwitz Polynomials and Applications to 2-D Filter Design, Multidimensional Systems: Signal*

*Processing and Modeling Techniques.* Los Angeles, U.S.A: Academic Press Inc. Vol.69, 1995.

[10] A. S. Sandhu, *Generation of 1-D and 2-D analog and digital lowpass filters with monotonic amplitude-frequency response.* Concordia University, Montreal, QC: M.A.Sc. Thesis, 2005.

[11] A. Bhumiratana and S. K. Mitra, "On darlington-type realization of two-variable driving-point functions," *Int. J. Electron*, vol. 39, pp. 545–550, 1975.

[12] M. . Ahmad, H. C. Reddy, V. Ramachandran, and M. N. S. Swamy, "Cascade synthesis of a class of multivariable positive real functions," *IEEE Trans. Circuits Systems*, vol. CAS-2.5, pp. 871–878, 1978.

[13] M. O. Ahmad, K. V. V. Murthy, and V. Ramachandran, "Doubly-terminated two-variable lossless ladder networks," *Journal of the Franklin Institute*, vol. 314, Issue 6, pp. 381–392, 1982.

[14] D. Hazony, *Elements of network synthesis.* New York: Reinhold Pub.,, 1963.

[15] C. S. Gargour, V. Ramachandran, R. P. Ramachandran, and F. Awad, "Variable magnitude characteristics of 1-d iir filters by a generalized bilinear transformation," *43 1d Midwest Symposium on Circuits and Systems, Michigan State University, U.S.A.*, vol. Session FAP-2, p. Four pages, August 8-11, 2000.

[16] C. S. Gargour, V. Ramachandran, and R. P. Ramachandran, "Modification of filter responses by the generalized bilinear transformations and the inverse bilinear transformations," *IEEE Canadian Conference on Electrical and Computer Engineering*, pp. 2043–2046, May 47, 2003.

[17] T. Ueda, N. Aikawa, and Masamitsu, "Design method of analog low-pass filters with monotonic characteristics and arbitary flatness," *Electronics and Communications in Japan*, vol. Vol. 82, No.2, pp. 21–29, 1999.

[18] B. D. H. Tellegen, "The gyrator, a new electric nework element," *Philips Res. Rep.*, vol. vol. 3, pp. 81–101, 1948.

[19] A. Antoniou, "Novel rc-active-network synthesis using generalized-immittance converters," *IEEE Transactions on Circuit Theory*, vol. Vol. CT-17 No.2, pp. 212–217, MAY 1970.

[20] S. Franco, *Design with operational Amplifiers and Analog Integrated Ciruits, Third Edition.* NY, New York: Mac Graw Hill, 2002.

[21] M. Ahmadi and V. Ramachandran, "New method for generating two-variable vshps and its application in the design of two-dimensional recursive digital filters with prescribed magnitude and constant group delay responses," *Proc. Inst. Elect. Eng.*, vol. 131, Pt.G, pp. 151–155, Aug. 1984.

[22] B. Nauta, *Analog CMOS Filters For Very High Frequencies.* Massachusetts, USA: Kluwer Academic Publishers, 1964.

[23] A. Oppenheim and Schafer, *Discrete-Time Signal Processing.* Englewood Clifffs, NJ: Prentice-Hall, 1989.

[24] V. K. Aatre, *Network Theory and Filter Design.* India: A Halsted Press Book, 1986.

[25] A. Sadkowski, "Unusual electrochemical immittance spectra with negative resistance and their validation by kramerskronig transformation," *Institute of Physical Chemistry of the Polish Academy of Sciences, Kasprzaka 44/52, 01-224 Warszawa, Poland*, 10 August 2004.

[26] E. I. Jury, *Inner and Stability of Dynamic System.* New York: John Wiley and Sons, '1974.

[27] M. O. Ahmad, H. C. Reddy, V. Ramachandran, and M. N. S. Swamy, "Cascade synthesis of a class of multivariable positive real functions," *IEEE Trans. Circuits Systems*, vol. CAS-2.5, pp. 871–878, 1978.

[28] M. O. Ahmad, K. V. V. Murthy, and V. Ramachandran, "Doubly-terminated two-variable lossless ladder networks," *Journal of the Franklin Institute*, vol. 314, pp. 381–392, 1982.

[29] V. Ramachandran and M. Ahmadi, "Design of stable 2-d recursive filters by generation of vshp using terminated n-port gyrator networks," *Journal of the Franklin Institute*, vol. 316, pp. 373–380, 1983.

[30] G. A. Maria and M. M. Fahmy, "$l_p$ approximation of the group delay response of one and two-dimensional filters," *IEEE Trans. Circuits Syst.*, vol. CAS-21, pp. 431–436, May 1974.

[31] S. A. H. Aly and M. M. Fahmy, "Design of two-dimensional recursive digital filters with specified magnitude and group delay characteristics," *IEEE Trans. Circuits Syst.*, vol. CAS-25, pp. 908–916, Nov. 1978.

[32] A. T. Chottera and G. A. Jullien, "Design of two-dimensional recursive digital filters using linear programming," *IEEE Trans. Circuits Syst.*, vol. CAS-29,, pp. 417–826, Dec. 1982.

[33] S. Fallah, *Generation of polynominal for application in the design of stable 2-D Filter.* Concordia Unversity,QC: Ph.D Thesis, June 1988.

[34] V.Ramachandran and C.S.Gargour, *Generation of Stable 2-D Transfer Functions having Variable Magnitude Characteristics, Multidimensional Systems: Signal Processing and Modeling Techniques.* Los Angeles, U.S.A: Academic Press Inc. Vol.69, 1995.

[35] T. Kagisawa, "Constant-resistance network using a three-port gyrator," *PROCEEDINGS OF THE IEEE.*, pp. 836–837, MAY 1970.

[36] B. Psenicka and F. Garcia-Ugalde, "Z transform from lowpass to bandpass by pascal matrix," *IEEE Signal Processing Lett.*, vol. 11, no. 2, pp. 282–284, 2004.

[37] B. Psenicka, F. Garca-Ugalde, and A. Herrera-Camacho, "The bilinear z transform by pascal matrix and its application in the design of digital filters," *IEEE Signal Processing Lett.*, vol. 9, no. 11, pp. 368–370, 2002.

[38] J. Konopacki, "The frequency transformation by matrix operation and its application in iir filters design," *IEEE Signal Processing Lett.*, vol. 12, no. 1, pp. 5–8, 2005.

[39] R. M. Golden and J. F. Kaiser, "Design of wideband sampled-data filters," *Bell Syst. Tech. J.*, vol. 43, pp. 1533–1546, 1964.

[40] R. M. Golden, "Digital filter synthesis by sampled-data transformation," *IEEE Trans. Audio Electroacoust.*, vol. AU-16, pp. 321–329, 1968.

[41] K. C. Lavu and V. Ramachandran, "Study of elliptical symmetry in two-dimensional iir butterworth digital filters," *The 7th IEEE International Midwest Symposium on Circuit and Systems*, pp. II–77 – II–80, 2004.

[42] M. Ahmadi and V. Ramachandran, "A method for the design of stable n-dimensional analog and digital filters," *IEEE Int. Conf. Acoust., Speech, Signal Processing, Atlanta, Georgia*, pp. 704–707, 1981.

[43] S. Erfani and B. Peikari, "Digital design of two-dimensional lc structures," *IEEE Trans. On circuits and systems*, vol. As-28, no. 1, pp. 75–77, 1981.

[44] L. P. Huelsman, *Active and Passive Analog Filter Design - An Introduction.* McGrawHill, Inc., 1993.

[45] A. Antoniou, *Digital Filters: Analysis, Design, and Applications.* New York: McGraw-Hill, 1993.

[46] S. Chakrabarti, N. K. Bose, and S. K. Mitra, "Sum and product separabilities of multivariable functions and applicationd," *Franlin Institute*, pp. 53–66, 1975.

[47] S. K. Mitra, A. D. Sagar, and N. A. Pendergrass, "Realizations of two-dimensional recursive digital filters," *IEEE Trans. Circuits Syst.*, vol. CAS-22,, pp. 177–184, 1975.

[48] H. T. Kung, "Why systolic architectures," *IEEE Computer*, vol. 15, pp. 37–46, 1982.

[49] M. J. Smith, *Application Specific Integrated Circuits.* Boston, MA: Addison Wesley, '1997.

[50] E. O. Hwang, *Digital Logic and Microprocessor Design with VHDL.* Los Angeles, CA: Thomson-Engineering, '2006.

[51] N. Weste and K. Eshraghian, *Principles of CMOS VLSI Design.* Reading, MA: Addison wesley, '1985.

[52] E. Avenhaus, "On the design of digital filters with coefficients of limited word length," *IEEE Trans. Audio Electroacoust.*, vol. AU-20, pp. 206–212, 1972.

[53] Abu-El-Haija and A. M. Peterson, "An aproach to eliminate roundoff errors in digital filter," *IEEE Trans. Circuits Syst.*, vol. ASSP-27, pp. 195–198, 1979.

[54] T.-L. Chang, "Supression of limit cycles in digital filters with one magnitude-truncation quantizer," *IEEE Trans. Circuits Syst.*, vol. CAS-28, pp. 107–111, 1981.

[55] I. Pitas, *Digital Image Processing Algorithms and Applications.* Wiley-IEEE, '2000.

[56] R. C. Gonzalez and R. E. Woods, *Digital image processing.* Saddle River, NJ: Prentice-Hall, 2002.

[57] A. Netravali and B. Haskell, *Digital Pictures: Representation, Compression, and Standards (2nd Ed).* New York, NY: Plenum Press, 1995.

[58] T. Hinamoto, N. Ilceda, S. Nishimura, and A. Doi, "Design of two-dimensional adaptive digital notch filters," *Signal Processing Proceedings, 2000, WCCC-ICSP 2000, 5th International Conference*, vol. 1, pp. 538–542, 2000.